



HUNGARIAN UNIVERSITY OF AGRICULTURE AND LIFE SCIENCES

Efficiency improvement of the hybrid solar collector systems

DOI: 10.54598/004330

PhD Dissertation

by

Ahssan M. A. Alshibil

Gödöllő

2024

Doctoral school

Denomination: Doctoral School of Mechanical Engineering

Science: Mechanical Engineering

Leader: Prof. Dr. Gábor Kalácska, DSc
Institute of Technology
Hungarian University of Agriculture and Life Sciences, Gödöllő,
Hungary

Supervisor: Prof. Dr. István Farkas, DSc
Institute of Technology
Hungarian University of Agriculture and Life Sciences, Gödöllő,
Hungary

Co-Supervisor: Dr. Piroska Víg, PhD
Institute of Mathematics and Basic Science
Hungarian University of Agriculture and Life Sciences, Gödöllő,
Hungary

.....
Affirmation of supervisor

.....
Affirmation of head of school

CONTENTS

NOMENCLATURE AND ABBREVIATION	6
1. INTRODUCTION, OBJECTIVES	9
1.1. Introduction	9
1.2. Objectives.....	10
2. LITERATURE REVIEW.....	12
2.1. Concept of photovoltaic thermal PV/T systems.....	12
2.2. Air-cooled PV/T module.....	13
2.3. Water-cooled PV/T module	19
2.4. Bi-fluid-cooled PV/T module	27
2.5. Summary of literature review.....	29
3. MATERIALS AND METHODS	31
3.1. Experiment's location	31
3.2. Methodology approaches	32
3.3. Methodology of the conventional PV/T module.....	34
3.3.1. <i>Hybrid PV/T system schematic</i>	34
3.3.2. <i>TRNSYS model</i>	35
3.4. Methodology of the created PV/T module.....	37
3.4.1. <i>Creation of the new absorber with tube and novel fins</i>	37
3.4.2. <i>Adhering the new absorber to the conventional PV module</i>	42
3.4.3. <i>Air channel and insulation</i>	42
3.4.4. <i>Air and water streams</i>	43
3.4.5. <i>Creation of the heat exchanger tank</i>	44
3.4.6. <i>Comparison modules</i>	45
3.4.6.1 <i>Verticals fins-based air-cooled PV/T module</i>	45
3.4.6.2 <i>Water-cooled PV/T module via serpentine tube</i>	45
3.5. Nanotechnology assessments	46
3.5.1. <i>Actual statement</i>	46
3.5.2. <i>Creation of the fluid thermal equilibrium tester</i>	46
3.5.3. <i>Ternary and binary nanoparticles synthesis</i>	49
3.5.4. <i>Nanofluids preparation</i>	49
3.5.5. <i>Thermodynamic model of the fluid thermal equilibrium tester</i>	51
3.6. Instrumentations	54
3.7. Heat transfer-thermal nodes equations	57

3.8. Performance assessment and exergy analysis	62
3.9. Sustainability contribution of the new PV/T module.....	64
3.10. Uncertainty analysis	66
3.11. Experiments summary.....	66
4. RESULTS	68
4.1. Multi-functional platform of the PV/T module toward performance evaluation.....	68
4.1.1. Performances comparison of the PV/T with PID controller	69
4.1.2. Assessment of adding an ON-OFF controller	71
4.1.3. Daily profile of the hot water usage	72
4.1.4. Performance summaries of the five TRNSYS models.....	73
4.1.5. New contribution to the PID controller.....	73
4.1.6. Model validation.....	74
4.2. Effect of the louvered fins.....	75
4.3. Design of the louvered fins and serpentine tube	79
4.3.1. Temperature profile of the created PV/T module	79
4.3.2. Performance achievement.....	83
4.3.3. Thermal camera investigation	83
4.4. Correlation between solar cell temperature and solar intensity of the new PV/T.....	85
4.5. Quantifying the wasted heat toward sustainability contributions	90
4.6. Effect of ternary nanofluid as a heat transfer fluid	94
4.7. Thermal conductivity of the ternary nanofluids.....	106
4.8. Flowrate influence.....	108
4.9. Water-cooled PV/T module	109
4.10. New scientific results	112
5. CONCLUSION AND SUGGESTIONS	115
6. SUMMARY	116
7. ÖSSZEFOGLALÁS (SUMMARY IN HUNGARIAN).....	117
8. APPENDICES.....	118
A1: Bibliography.....	118
A2: Publications related to the dissertation.....	138
A3: Graphical summary of air-cooled PV/T configurations.....	140
A4: Summary of recent studies conducted on the PV/T modules	141
A5: Graphical summary of water-cooled PV/T configurations	143
A6: Summary of exergy efficiency obtained from previous studies.....	144
A7: Graphical summary of bi-PV/T configurations.....	145

Contents

A8: Hierarchical chart of the classification of the PV/T modules	146
A9: Description of TRNSYS model elements	147
A10: TRNSYS model of the PV system	148
A11: Summary of exergy efficiency and sustainability index obtained in the previous studies and current research	149
9. ACKNOWLEDGEMENT	150

NOMENCLATURE AND ABBREVIATION

Abbreviations

AC-PV/T	Air-cooled Photovoltaic-thermal module
ALF-PV/T	Photovoltaic thermal collector using louvered fins without water circulation
BiF	Bilateral fluid
BNF	Binary nanofluid
BN	Boron Nitride
DW	Distilled water
EPDM	Ethylene propylene-diene material
Ex	Experimental
FPC	Flat plate collector
FTET	Fluid thermal equilibrium tester
LFS-PV/T	Photovoltaic thermal collector using louvered fins and serpentine tube
MgO	Magnesium Oxide
MWCNT	Multi-walled carbon nanotubes
NF	Nanofluid
Nu	Numerical
NZEBs	Net-zero energy buildings
NZEBs	Net-zero energy buildings
PCM	Phase change material
PID	Proportional integral derivative controller
PV	Photovoltaic module
PV/T	Photovoltaic thermal module
PV/T-ID	PV/T module with PID controller
PV/T-O	PV/T module with ON-OFF controller
PV/T-Wd	PV/T module without using a daily profile of hot water
R^2	Coefficient of determination
SEM	Scanning electron microscopy
SI	Sustainability index
STC	Standard test condition
TET	Thermal equilibrium time
TNF	Ternary nanofluid
WC-PV/T	Water-cooled Photovoltaic-thermal module
ϵ_P	Exergy power (W)

Symbols

ΔKE	Kinetic energy change (J)
ΔPE	Potential energy change (J)
ΔX	Thickness (m)
A	Area (m ²)
cp	Specific heat (J/kg K)
E	Energy (J)
h	Heat transfer coefficient (W/m ² K)
I	Current (A)
K	Thermal conductivity (W/m K)

m	Mass (kg)
\dot{m}	Mass flowrate (kg/s)
P	Power (W)
Q	Thermal power (W)
S	Global radiation (W/m ²)
T	Temperature (°C)
t	Time (s)
U	Internal energy (J)
Un	Uncertainty
V	Voltage (V)
V _w	Velocity (m/s)
Wh	Wasted heat (W)
x	Variables of uncertainty function

Greek symbols

~	Between two layers
Δ	Change
β	Temperature coefficient (%/K)
δ	Thickness (m)
ε	Emissivity
ρ	Density (kg/m ³)
σ	Constant of Stefan–Boltzmann, 5.6704×10^{-8} (W/m ² ·K ⁻⁴).
φ	Volume concentrations (%)
η	Efficiency (%)

Subscripts

a	Air
af	Airflow
a-in	Inlet air
am	Ambient
a-out	Outlet air
B	Back
bf	Base fluid
c	Collector
ca	Copper absorber
cd	Conduction
cfi	Copper fins
ct	Copper tube
cv	Convection
d	Duct
el	Electrical
ep	Electrical production
Eq	Equilibrium
f	Fluid
F	Front
gs	Glass surface

in	Inlet
in	Inlet
mx	Max
NF	Nanofluid
o	Reference to the standard test condition
out	Outlet
rd	Radiation
sc	Solar cell
th	Thermal
tn	Ternary nanofluid
u	Useful
w	Water
wf	Water flow
w-in	Inlet water
w-out	Outlet water
ex	Exergy

1. INTRODUCTION, OBJECTIVES

The research work's background, significance, and principal research goals are discussed in this chapter.

1.1. Introduction

The global energy demand has experienced an increase in various places across the world due to factors such as population expansion, industrialisation, and economic advancement.

As the need for energy continues to grow, the fundamental sources of energy, particularly fossil fuels, are gradually depleted due to their excessive usage (Alshibil et al., 2022). The alteration of climatic conditions, including the greenhouse effect, ozone layer degradation, and polar ice caps melting, can be attributed to human activities related to energy consumption and pollution (Raza et al., 2016). Eliminating contamination of the environment, with a specific focus on decreasing ozone layers and utilising energy, stands out as a paramount global concern (Bel Haj Jrad et al., 2017). The mitigation of environmental degradation and the associated challenges of global warming afterwards can be achieved through the use of renewable and clean energy sources (Alshibil et al., 2023b). Academic researchers worldwide have initiated efforts to enhance the proportion of energy derived from renewable sources. There is an ongoing study aimed at increasing the proportion of solar photovoltaic PV energy production via refinements to current technologies or the introduction of new methods.

Solar energy derived from the sun is often regarded as a highly efficient option among renewable energy resources due to its inherent cleanliness, unrestricted accessibility, and abundant availability (Alshibil et al., 2023c; Sathe and Dhoble, 2017). Terrestrial solar radiation encompasses the infrared, ultraviolet, and visible wavelengths (Joshi et al., 2016). Most photovoltaic (PV) cell materials have a restricted response to a percentage of solar energy originating from the Earth's surface. The photovoltaic (PV) cell harnesses electrical energy only from radiation that aligns with its response spectrum, while any surplus radiation is converted into thermal energy inside the PV cell. The efficiency and performance of the PV system are negatively impacted by thermal losses resulting from heat dispersion. Hence, maintaining the solar cells' reduced operational temperature is crucial (Alshibil et al., 2023d; Bódi et al., 2018).

A photovoltaic thermal collector (PV/T) is an apparatus that concurrently converts solar radiation into electrical and thermal energy simultaneously. Essentially, the PV/T is an open solar collector that has been incorporated into a flat surface and connected to a PV module (Yazdanifard and Ameri, 2018). The thermal collector is positioned underneath the PV module and has a mechanism for circulating a cooling fluid. This fluid captures the surplus heat generated by the module and collector, enhancing the PV cell's electrical efficiency. During this process, the fluid undergoes heating and may be used in low-temperature applications such as space heating, domestic hot water supply, industry preheating, agricultural drying, etc (Ibrahim et al., 2011).

Wolf (1976) first proposed the idea of PV/T to increase PV conversion efficiency by lowering its surface temperature. Throughout the preceding decade, other experimental and theoretical investigations (Kern, Jr., 1978; Florschuetz, 1975, 1979) on PV/T were documented in the academic literature, elaborating upon the previous work conducted by Wolf (1976).

Over the last three to four decades, investigators have increasingly recognised the importance of energy production by utilising PV/T systems. This prompted the researchers to engage in extensive theoretical, experimental, and computation investigations aimed at enhancing the performance of the PV/T module through the optimisation of its configuration parameters, flow patterns within the collector, energy generation characteristics across various climates, and the impact of glazing and unglazing, among other factors. However, it is worth noting that there is currently a limited availability of efficient PV/T modules on the market. Based on the previous information, the leading solar energy applications are illustrated in Fig. 1.1.

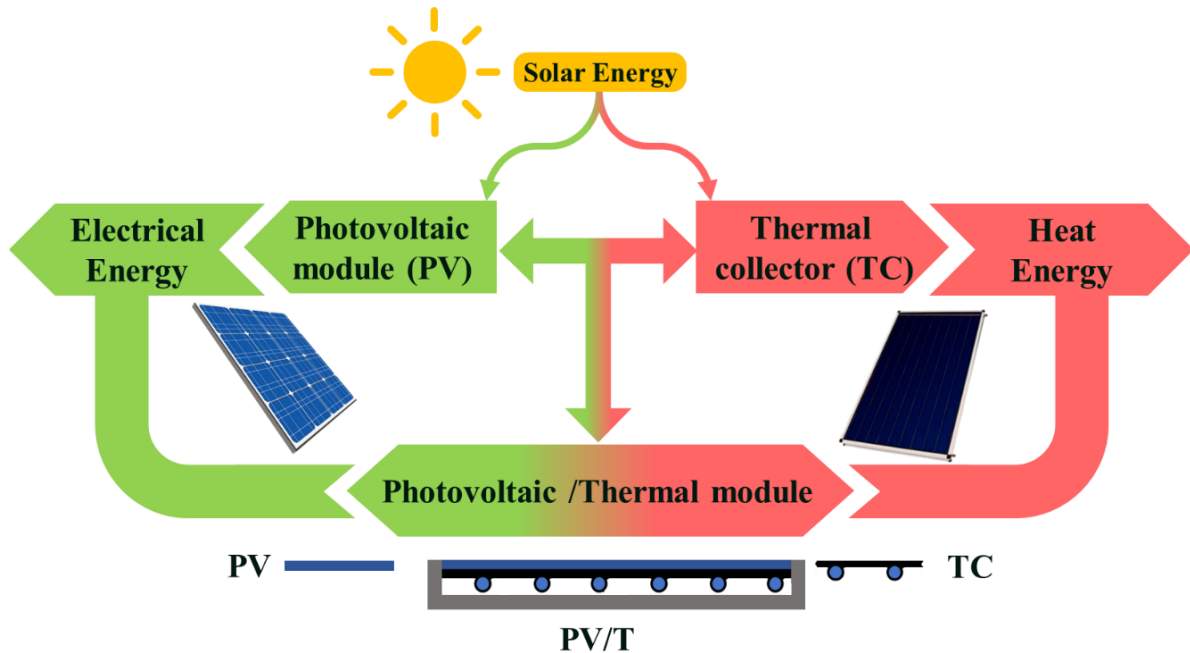


Fig. 1.1. solar energy applications

1.2. Objectives

A comprehensive review of experimental and theoretical studies examined how various factors affect PV/T module electrical and thermal performance. There is currently no comprehensive standardised approach for modelling and evaluating the PV/T performance. Most of the works mentioned above focused on the different fin configurations in the PV/T field; no study reported louvered fins in the PV/T field. Additionally, there has been no experimental study on copper absorbers with copper fins and tubes in the bilateral unit of the PV/T. This research essentially intends to consider the performance of a novel experimental design of an air-water-cooled PV/T collector, which mounts louvered fins and serpentine tubes to the copper absorber adhered to the PV module. Also, no study calculates the amount of wasted heat that the solar PV panels transfer to the surroundings, which negatively affects the environment, contributes to global warming, and reduces the desired sustainability of net-zero energy buildings (NZEBS). Besides, no study utilised ternary multi-walled carbon nanotubes (MWCNTs)-magnesium oxide (MgO)-boron nitride (BN) nanofluids in the thermal and electrical enhancement of the PV/T module. This research aimed to fulfil and considering the previously mentioned experimental and numerical issues, the major objectives of the current research are as follows:

- To build and validate a new multi-controller platform of PV/T units within the common functional tools in the simulation of the solar system TRNSYS tool environments to be a base-tool for further performance enhancement.
- Develop a new configuration of copper fins, louvered fins and examine their effects on the PV/T module performances.
- Develop a new design of bi-fluid PV/T utilising the design of louvered fins and serpentine tube.
- To study the effect of the solar cell temperature and how it decreased using a developed PV/T module via a new correlation.
- To assess the sustainability contribution by calculating the wasted heat removed by solar cells compared to the developed PV/T module.
- To study the potentiality of ternary MWCNTs-MgO-BN nanofluid as a high thermal conductivity fluid to improve PV/T performance.
- To experimentally develop a new correlation of thermal conductivity of the chosen nanofluid as a base equation for further investigations.

2. LITERATURE REVIEW

This chapter aims to provide a comprehensive overview of the conceptualization and development efforts undertaken consequently concerning the integration of heat exchangers with air- and liquid-based photovoltaic thermal collector PV/T systems. The objective is to present a detailed comparative analysis of the investigated designs, highlighting their respective characteristics and features.

2.1. Concept of photovoltaic thermal PV/T systems

This section provides coverage of the fundamental aspects of PV/T modules, including cooling systems, heat transfer rates, and conversion performance metrics. The PV/T module is designed to serve a dual purpose, functioning not only as an electricity generator but also as a heat absorber. In this manner, thermal and electrical energy generation occurs concurrently (Tyagi et al., 2012). Incorporating dual functionalities inside the PV/T module leads to a superior solar conversion rate compared to a singular photovoltaic PV or solar collector. This enhanced efficiency allows for more efficient utilisation of solar energy resources. Given the frequently complementary nature of the need for solar heat and electricity, it appears to be an intellectual proposition to pursue the development of a device capable of satisfying both requirements simultaneously. PV cells harness some of the incoming solar radiation to produce electrical energy.

In contrast, the remaining energy is predominantly dissipated as waste heat within the cells and substrate, reducing the module's overall efficiency. The PV/T technology effectively harnesses this portion of the thermal energy and applies it to practical uses. The concurrent cooling of the PV module ensures that its electrical efficiency remains acceptable. Consequently, the PV/T collector presents a more practical approach to harnessing solar energy since it exhibits superior overall efficiency. Significant investments in research and development have been undertaken in recent years to improve PV/T technology, with a notable increase in activity levels.

In addition, the PV/T system possesses catchy characteristics (Hasan and Sumathy, 2010):

- It is dual-purpose: the same system can be used to produce electricity and heat output,
- it is efficient and flexible: the combined efficiency is always higher than using two independent systems and is especially attractive in building integrated PV when roof spacing is limited,
- it has a wide application: the heat output can be used both for heating and cooling (desiccant cooling) applications depending on the season and practically being suitable for domestic applications,
- it is cheap and practical: it can be easily retrofitted/integrated into the building without any significant modification and replacing the roofing material with the PV/T system can reduce the payback period.

Various types of PV/T modules were utilised based on the heat transfer fluid, including air-cooled, liquid-cooled (Kalogirou, 2014), and hybrid configurations, which utilise liquid and air simultaneously; it is called bi-fluid PV/T modules (Abu Bakar et al., 2014) as presented in Fig. 2.1a-c. The next section of this chapter focuses on the development conducted on the major types of PV/T collectors.

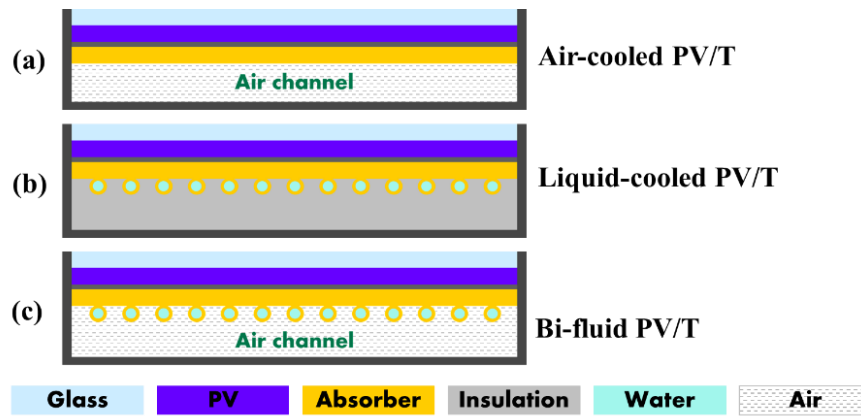


Fig. 2.1. Major types of PV/T modules: a) air-cooled PV/T module, b) liquid-cooled PV/T module, and c) bi-fluid PV/T module

2.2. Air-cooled PV/T module

Air exhibits lower viscosity and density in comparison to water, resulting in a lower pressure drop during intake, therefore providing it with a leverage advantage (Tiwari and Sodha, 2006b, 2007). In regions characterised by cold climates and the occurrence of freezing water, the utilisation of air as a cooling medium for PV/T modules becomes a viable option. Moreover, air can also serve the purpose of space heating in such contexts. PV/T modules have gained significant popularity due to their uncomplicated construction and efficient integration into building structures (Hussain et al., 2013). Several attempts have been undertaken to enhance the efficiency of the conventional PV/T module, employing numerical, theoretical, and experimental analyses. Several studies have examined the influence of design aspects (Farshchimofared et al., 2015; Joshi et al., 2009; Sarhaddi et al., 2010; Singh et al., 2015), weather aspects (Agrawal and Tiwari, 2011; Kamthania et al., 2011; Pathak et al., 2014), glazed and unglazed (Agrawal and Tiwari, 2013, 2015; Bambrook and Sproul, 2012; Farshchimofared et al., 2015; Slimani et al., 2016), single and double pass flow (Garg and Adhikari, 1997; Hegazy, 2000; Vivek Raman, 2009), etc. Nevertheless, in this section, an endeavour is undertaken to provide an overview of the research completed on AC-PV/T thus far, incorporating specific alterations or innovative approaches pertaining to a heat exchanger to enhance the heat transfer surface area.

The incorporation of fins in AC-PV/T systems has considerable potential to enhance power production efficiency within a given surface area of the PV cell (Alshibil et al., 2023a; Fan et al., 2018). A preliminary model of a double-pass AC-PV/T module with rectangle-shaped fins was created, manufactured, and subjected to investigation (Othman et al., 2005, 2006), Fig. 2.2.

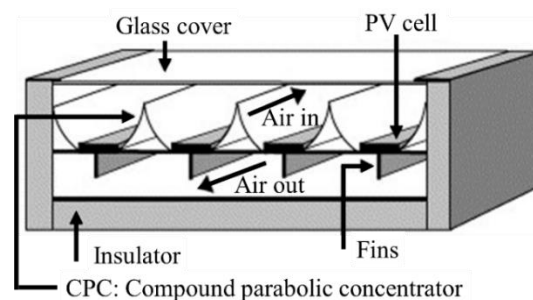


Fig. 2.2. Double-pass AC-PV/T module (Othman et al., 2005, 2006)

Incorporating fins on the back side of an absorber plate was designed to augment the amount of heat transferred to the airflow (Othman et al., 2005). At a solar radiation intensity of 500 W/m^2 , the overall efficiency experiences a transition from 39% to 70% within the range of flow rates of 0.015 to 0.16 kg/s. Alfegi et al. (2009) investigated the fins' cooling influence through an experimental study. In their research, the fins were integrated with the absorber plate, which was mounted to the rear of the photovoltaic (PV) module. The influence of varying airflow rates on the effectiveness of the AC-PV/T was investigated through a spectrum of operational parameters. The study found that the finned AC-PV/T increased total efficiency from 49.1% to 62.8% when the airflow rate was adjusted from 0.0316 kg/s to 0.009 kg/s. These observations were made under specific conditions: a solar radiation of 600 W/m^2 and an input air temperature of $35 \text{ }^\circ\text{C}$. Othman et al. (2007) constructed an air-cooled photovoltaic/thermal (PV/T) module, wherein air was introduced through the upper channel inlet and exited through the lower channel outlet, circulating in a counter-parallel path (see Fig. 2.3). The test was achieved at steady state procedure in an indoor condition. A set of 23 lights (500 W tungsten halogen) was employed to facilitate solar radiation during the experiment. The study noted that using fins led to an electrical efficiency of 2.1% when operating at a flow rate of 0.181 kg/s. The study's findings indicated that the double-pass flow exhibited superior performance compared to the single-pass flow.

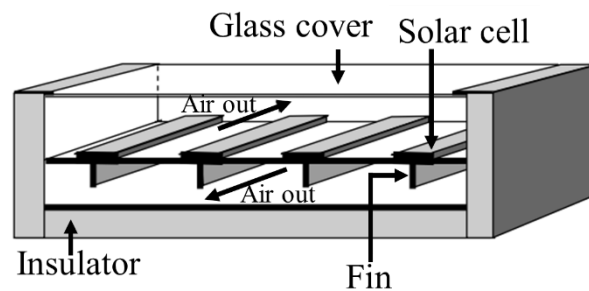


Fig. 2.3. Counter-parallel path channel (Othman et al., 2007)

Gopi et al. (2022) established and evaluated an adapted double-pass AC-PV/T system and conducted a comparative analysis with the conventional AC-PV/T system. They investigated their study at the National Institute of Technology, Calicut, India. Solar radiation intensities between 200 and 1000 W/m^2 were used in the tests. Vertical slats were installed in the lower channel of their unit. The slats were affixed in a vertical orientation to the lower surface of the absorber plate to enhance the thermal dissipation process, facilitating the transfer of heat to the air. The cell temperature decreased by 13.4% of the slatted module compared to the un-slatted module. The study results indicate that the modified AC-PV/T system exhibits a significantly improved electrical efficiency of 20.4-28.3% and energy efficiency of 44.6-46.8% compared to the conventional system. An innovative AC-PV/T was created by Arslan et al. (2020) at the Energy Systems Engineering Laboratory at Gazi University in Ankara, Turkey. Using the glass facing a side airflow, they attached 12 copper fins see Fig. 2.4.



Fig. 2.4. Air channel of the novel fin shape (Arslan et al., 2020)

The study was carried out using both numerical and experimental approaches, indicating a strong concurrence between their findings. The studies used two distinct air flow rates

(0.031087 kg/s and 0.04553 kg/s) while manipulating solar radiation levels within the range of 600-1069 W/m² and the surrounding temperatures between 19.3-24 °C. At 0.04533 kg/s, the temperature of a PV module was found to be 40 °C, a value 27.2% below what was attained at 0.031087 kg/s. The cooling influence emanating from the fins enhanced the PV module's electrical efficiency by 0.42%. Özakın and Kaya (2020) conducted research at Ataturk University on the frequency and sparsity of fin arrangements throughout the air duct of the AC-PV/T employing copper, brass, and aluminium (see Fig. 2.5). The results indicated that the optimal number of fins, which provided the highest levels of thermal and electrical performance, was determined as 27 for brass fins and 55 for aluminium and copper fins.

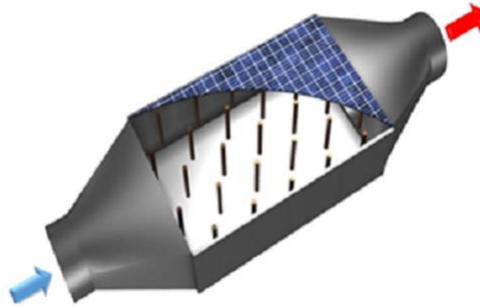


Fig. 2.5. Frequency and sparsity of fin arrangements (Özakın and Kaya, 2020)

Tonui and Tripanagnostopoulos (2007b) conducted a theoretical investigation to assess three unglazed AC-PV/T modules. The initial model utilised typical AC-PV/T modules and was classified as a referred (REF) unit. In contrast, the subsequent model incorporates a flat, thin metallic sheet (TMS) positioned inside the middle portion of the air duct. In the third design, the fins were affixed to the posterior surface wall of an air channel to enhance heat transfer. Both passive and active forms of cooling were included in the investigation. When comparing the TMS module and the finned module to the REF system, it was reported that the former reduced the backside of the PV module temperature by 3–5 °C and the latter by 2 °C. When the flow rate was set at 1 m³/min, the finned module outperformed the TMS and REF modules by 7.1% and 20%, respectively. This research encompasses an expansion to evaluate the performance of unglazed and glazed AC-PV/T modules (Tonui and Tripanagnostopoulos, 2007a). The research findings indicate that the glazed technique exhibits superior thermal efficiency compared to the unglazed structure, mostly due to reduced heat losses. However, the glazed module demonstrates poorer electrical efficiency due to increased absorption and reflection losses resulting from the presence of a glass cover. The module equipped with TMS, and fins exhibited a 1% and 6% increase in electrical efficiency compared to the REF module. Alfegi et al. (2008) conducted an experimental evaluation of a single-pass double-duct AC-PV/T module. The experiment occurred in an indoor environment and utilised a solar simulator. The dual duct layout was designed by positioning the absorber plate centrally within the duct, with a series of 29 vertical fins positioned below the absorber plate throughout its entire length. The airflow occupies both sides of the absorber plate in a parallel direction, effectively removing additional heat generated by the collector and the PV module via the outlet. At steady solar radiation of 400 W/m², the finned module's overall efficiency increased from 27.5 to 40% at a flow rate of 0.09 kg/s. Tonui and Tripanagnostopoulos (2008) presented two low-cost arrangements approaches to implement air conditioning in a commercial photovoltaic (PV) module. TMS suspended in the middle of the air duct and fins placed in the air duct's back wall were two of the techniques under consideration. The effectiveness of these two adjustments

over various design and operating characteristics was studied using a parametric analysis. There was a positive correlation between collector length and thermal efficiency; however, a negative correlation was reported between collector length and electric efficiency. The research indicated that the modified systems conserve more energy during heating.

Researchers looked at glazed and unglazed AC-PV/T modules to determine how the hanging TMS in the centre of the duct affected how energy and exergy were made (Shahsavari et al., 2012; Shahsavari and Ameri, 2010). The rationale for incorporating the TMS was to function as a significant means of enhancing heat augmentation. The researchers conducted experiments on the AC-PV/T module in both passive and active convection conditions. However, a separate study focused solely on utilising natural ventilation modes. The research conducted by Shahsavari and Ameri (2010) focused on determining the optimal number of fans based on the system's electrical performance. Additionally, Shahsavari et al. (2012) investigated the optimal design characteristics related to the system. Both investigations reported that the glazed AC-PV/T system exhibited superior energy performance, while the unglazed AC-PV/T system showed more extraordinary energy performance. Franklin and Chandrasekhar (2019) introduced an innovative configuration for an AC-PV/T module, whereby the staves (a vertical metal sheet of TMS) were incorporated exclusively in the trailing section of the air channel. A comparison was made between the findings of the AC-PV/T module with and without staves. The recorded highest exit air temperatures were 34 °C and 30.7 °C for the cases with and without staves, respectively, while the inlet air temperature was 29 °C. Kumar and Rosen (2011) investigated a double-pass flow arrangement. They compared the effect of vertical fins in the air duct of the AC-PV/T module, as depicted in Fig. 2.6. The surface temperature of the photovoltaic (PV) system experienced a significant reduction, decreasing from 82 °C to 66 °C as a result of the increased surface area of the fins. The incorporation of fins resulted in a notable enhancement of the electrical and thermal efficiency, with an increase of 10.5% and 15.5%.

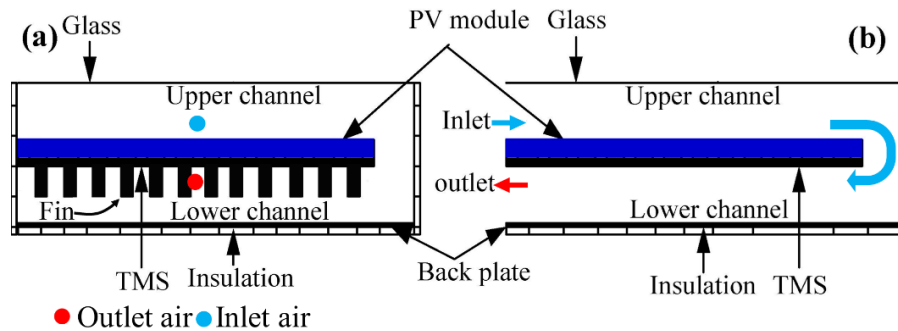


Fig. 2.6. AC-PV/T module, a) with, b) without vertical fins (Kumar and Rosen, 2011)

Elsafi and Gandhidasan (2015) performed a comparison study involving traditional double-pass finned and unfinned AC-PV/T modules. This research investigated the impact of different design parameters, including channel depth (ranging from 0.02 to 0.035 m), length (ranging from 1.5 to 6 m), and flow rate (ranging from 0.06 to 0.2 kg/s), on the overall effectiveness under different operating circumstances. The finned collector exhibited an annual thermal productivity of 1% greater and an electrical productivity greater than 3% compared to the conventional model.

Another study compared the effect of fins on the AC-PV/T was approved by Çiftçi et al. (2021). They relied on both computational and experimental approaches. ANSYS software

environment was used for the numerical method. According to the results, the finned and unfinned AC-PV/T had appropriate thermal efficiencies of 47.2% to 54.8% and 50.2% to 58.1%. Chandra et al. (2016) presented the integration of four slim rectangular fins in a single-pass AC-PV/T module to enhance heat dissipation. Under optimal circumstances, the AC-PV/T module with four fins demonstrated a maximum PV cell efficiency of 13.7%. This was achieved by maintaining the most minor reported solar cell temperature of 43.7 °C. Under identical conditions, the thermal efficiency was 56.1% in both cases. Fan et al. (2017) made a dynamic model of an AC-PV/T module with lengthwise fins to determine how fins' numbers and lengths affect the outcomes. The computational model was verified by comparing with experimental findings obtained according to actual operating circumstances. It has been shown that the augmentation of fin numbers and reduction of fin heights can improve thermal and electrical performance. The range of 20–40 mm exhibited the optimal fin length, resulting in a slight decrease in pressure with an increase in the overall efficiency. Zohri et al. (2018a) employed a theoretical methodology to assess the efficiency of an AC-PV/T module, comparing configurations with and without vertical fins. The finned module is 1% more efficient in terms of exergy than the unfinned module. An additional kind of heat exchanger, called multi-pins and offset-pins, was implemented within the flow channel of the AC-PV/T module to enhance its overall efficiency (Elsayed, 2018; Tabatabaian et al., 2012) (see Fig. 2.7).

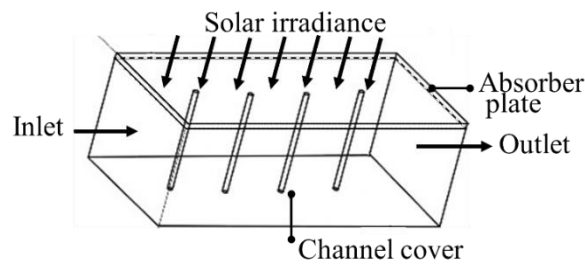


Fig. 2.7. AC-PV/T module of Elsayed, (2018)

Tabatabaian et al. (2012) introduced a design for an AC-PV/T module utilising computational fluid dynamics (CFD) software, namely the COMSOL tool. The design was subsequently experimentally confirmed. Two variants of AC-PV/T modules were developed, including the regular AC-PV/T and the AC-PV/T utilising offset pins integrated into the rear wall of the duct. The study's findings indicated that implementing the new design enhanced the system's efficiency by approximately 30–40%. Othman et al. (2013) conducted an experimental investigation to assess the effectiveness of three distinct heat exchanger shapes, including steel wool fabric, honeycomb, and V-groove, in improving the total efficiency of AC-PV/T (see Fig. 2.8). The performance evaluation of all AC-PV/T modules was carried out at an indoor laboratory facility in Malaysia. The solar simulator utilised 23 halogen lights to provide a consistent solar radiation intensity of 828 W/m². The thermal efficiency of the steel wool, honeycomb, and V-groove configurations reached 71%, 87%, and 86%, respectively. Regarding electrical efficiency, the corresponding values were 7.04%, 7.13%, and 6.89%, respectively. These results suggest that the honeycomb configuration outperformed the other designs regarding heat exchanger performance.

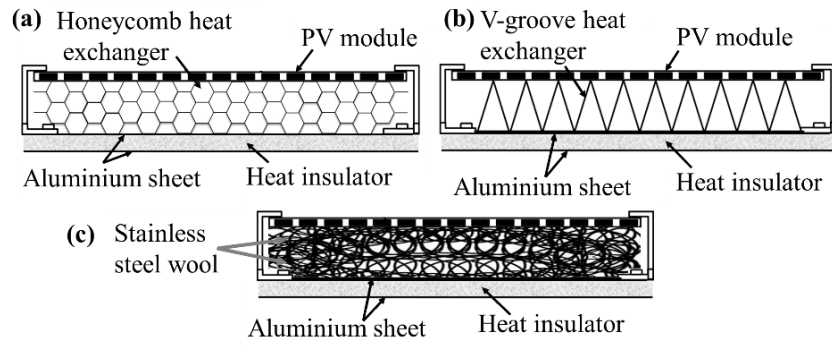


Fig. 2.8. Configuration study of Othman et al., (2013), a) Honeycomb, b) V-groove, c) Stainless steel wool

Shrivastava et al. (2022) investigated various air-cooling configurations for AC-PV/T modules. The configurations include ducts without fins, ducts with totally and partially crosswise fins and horizontal fins equipped with straight and sloping baffles. The study found that horizontal fins and sloped baffles had the highest energy and exergy efficiency due to their ability to generate an increased friction factor, consequently leading to an improved heat transfer rate. Zhao et al. (2020) investigated the thermal effectiveness of an AC-PV/T incorporating a heat exchanger in a hexagonal (honeycomb) configuration in indoor conditions. The study aimed to assess the impact of solar radiation and the coverage area of the PV module on the system's thermal efficiency. The research discovered that within the boundaries of the experimental evaluation, an optimal instant thermal efficiency of 64% was attained when the solar radiation reached 600 W/m^2 , and the photovoltaic coverage area was set at 45%. Slimani et al. (2019) investigated a baffles-based AC-PV/T (see Fig. 2.9) and conducted numerical simulations and experimental tests to validate the performance in the specific climate of Bouzareah, Algeria. The primary aim of this investigation was to examine the impact of altering the quantity of baffle lines on thermal and electrical efficiency. The experiment revealed that as the number of rows ranged from 6 to 24, there was a notable gain of 7% in thermal efficiency. Additionally, a marginal improvement of 0.3% was detected in electrical efficiency.

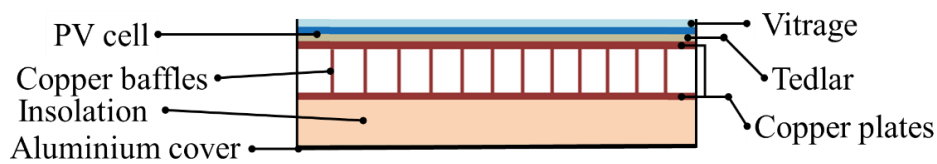


Fig. 2.9. Configuration study of Slimani et al., (2019)

Zohri et al. (2018b) conducted an exergy study of an AC-PV/T, including a V-groove absorber, utilising the matrix inversion approach. A theoretical exergy assessment was undertaken to pursue this purpose, considering various amounts of solar radiation $385, 575, \text{ and } 875 \text{ W/m}^2$ for flow rates of $0.01 \text{ and } 0.05 \text{ kg/s}$. The V-groove absorber demonstrated its highest exergy value of 86.32 W and associated system efficiency of 17.80% under certain conditions, namely a solar radiation level of 875 W/m^2 and a flow rate of 0.05 kg/s . Fudholi et al. (2019) performed an experimental and analytical exergy investigation of AC-PV/T using a V-corrugated absorber plate. The tests used two specific solar radiation levels, $520 \text{ and } 820 \text{ W/m}^2$. The investigation was carried out across various flow rates and solar radiation levels. The results indicated a significant and comprehensive concurrence between the empirical and theoretical data. The exergy efficiency of the technique utilising a V-corrugated plate was determined to be 13.36%

and 12.89% for theoretical and experimental calculations, respectively. In their study, Fterich et al. (2021) altered the flow path of AC-PV/T by incorporating aluminium square tubes of 40×40 mm. The constructed system successfully attained the maximum temperature of 59 °C and 75 °C for the PV module, corresponding to airflow velocities of 2 m/s and 0.5 m/s, respectively. Additionally, the outcome yielded the most elevated mean thermal efficiency of 42.5%, corresponding to the most significant airflow velocity.

A group of researchers conducted a study involving the modelling, creation, and experimentation of an AC-PV/T equipped with a flat transpired plate (see Fig. 2.10) (Gholampour et al., 2014; Maysam Gholampour and Ameri, 2016a). The effects of the location of PV modules, suction speed, solar radiation, and PV coverage ratio (fraction of plate covered by PV) on module efficiency were studied. According to the findings, the location of the PV modules had a minor effect on the overall system efficiency. In contrast, the percentage of PV coverage played a significantly more important role.

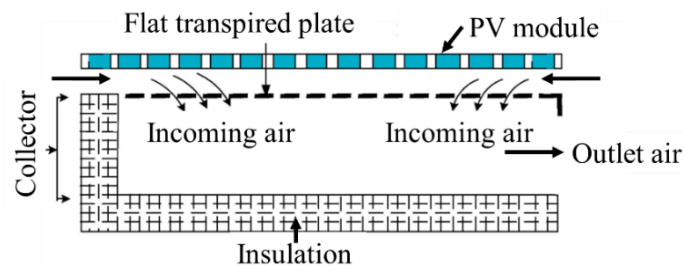


Fig. 2.10. Principle of the solar dryer of Gholampour and Ameri, (2016a)

In recent years, a wavy plate has been implemented as a heat exchanger within the flow channel of an AC-PV/T module (Jha et al., 2019, 2020, 2022). In their study, Jha et al. (2019) conducted an experimental comparison between two AC-PV/T models. One of them was equipped with a wavy absorption plate, as depicted in Fig. 2.11, while the other model included a flat absorption plate. According to the comparison investigation, it was found that the system equipped with a wavy plate achieved a solar panel temperature of 62 °C during the noon hour, which was 3 °C lower compared to the system utilising a flat plate. The utilisation of wavy plate-based photovoltaic thermal air collectors AC-PV/T leads to an increase of 1.2% in total electrical production.

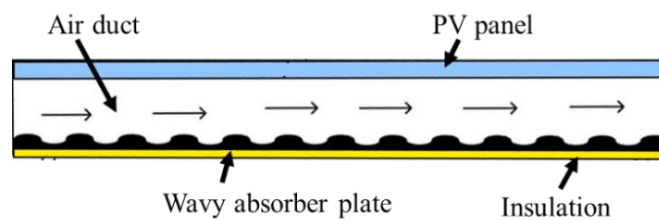


Fig. 2.11. Wavy plate-based AC-PV/T module (Jha et al., 2019)

Graphically, Appendix A3 represents the main most used configurations of the air-cooled photovoltaic thermal module focused on the literature.

2.3. Water-cooled PV/T module

The most common PV/T modules utilise water as a working fluid owing to higher thermal ability than air, allowing for more uniform cooling of PV cells (Herrando et al., 2014). A flat plate absorber coupled with tube loops within the flow channels is the most common

configuration for a water-cooled photovoltaic thermal module (WC-PV/T). This module generates steaming hot water and electrical current at the same time (Diwania et al., 2019).

Numerous scholarly publications have documented a multitude of experimental and theoretical inquiries focused on improving the performance of the conventional WC-PV/T. Several studies have examined the influence of glazing (Nualboonrueng et al., 2012; Santbergen et al., 2010) and unglazing (Bilbao and Sproul, 2015; Huang et al., 2012; Yazdanifard et al., 2016), the influence of design aspects and weather circumstances (Dubey and Tiwari, 2008; Hazi et al., 2014; Zhao et al., 2011), and wholly and partly wrapped collectors with PV modules (Dubey and Tiwari, 2009; Shyam et al., 2016), flow attempts (Tiwari and Sodha, 2006a), etc. However, given the aim of this chapter to provide a comprehensive overview of the literature about advancements in the heat transfer field through the utilisation of modern heat exchangers, only pertinent studies will be addressed in the subsequent discussion.

In early 1986, (Lalović et al., 1986) conducted a study including the creation and assessment of a solar thermal collector that incorporated flat fins and an aluminium tube. The model was experienced through sunny and cloudy days. The system exhibited superior performance as a solar thermal collector, raising the water temperature to 65 °C. Conversely, the electric behaviour of the PV module showed minimal variation. The outcomes show that it is possible to manufacture simple, affordable hybrid systems with improved electrical and thermal efficiency.

The idea of incorporating fins into the WC-PV/T module flow channel became popular, and scientists eventually adopted it through various studies (Gomaa et al., 2022; Jaiganesh and Duraiswamy, 2013; Kalogirou, 2001; Rahman et al., 2017). Jaiganesh and Duraiswamy (2013) conducted a study to investigate the efficacy of the WC-PV/T module. In their research, they affixed a photovoltaic (PV) module onto a glass absorber equipped with six full-length copper fins. To remove the heat generated by the finned absorber mounted beneath the PV module, a water channel with a thickness of 95 mm was employed. The thermal efficiency of the system was determined to be 44.37%. The electricity production from WC-PV/T was 0.7% higher than a single photovoltaic PV system of comparable dimensions. A study was conducted by Rahman et al. (2017) to experimentally investigate the characteristics of WC-PV/T, a system consisting of a rectangular plate containing tubes and a semi-circle finned sheet. The placement of the heat exchanger occurred at the rear of the photovoltaic (PV) module. According to the findings of the study, it was observed that there is a decline in photovoltaic PV efficiency by 5.8% when the temperature of the PV surface rises from 33.8 to 59.9 °C. Xu et al. (2015) incorporated a novel configuration of a WC-PV/T with a very thin absorber, resulting in a significantly enhanced relative output compared to traditional photovoltaic (PV) modules. The utilisation of this novel design resulted in a significant increase in electricity produced and thermal efficiency, with improvements of around 5% and 65%, respectively. Bakker et al. (2005) conducted a comparison between a typical roof-sized system and a model of rooftop-sized WC-PV/T. The WC-PV/T model featured a loop-shaped tube serving as the heat exchanger located at the back surface of the PV module, as depicted in Fig. 2.12. According to the researchers, a system measuring 25 m² fulfilled 100% of the hot water demand for a typical single-family residence while also satisfying a significant portion of its electricity requirements. In comparison, the conventional system required 32 m² to achieve similar results.



Fig. 2.12. Rooftop-sized WC-PV/T of Bakker et al., (2005)

Experiments were done by Touafek et al. (2013) on a WC-PV/T with a new absorber system comprising a galvanised steel tube and a galvanised steel tank. The system exhibits a straightforward design and is economically advantageous compared to alternative contemporary systems. The findings indicate that the temperature of the output water observed an approximate increase of 10 °C compared to the initial inflow temperature. The photovoltaic (PV) efficiency and PV temperature were 12.2% and 58 °C, respectively, through 0.05 kg/s of water flow rate. Dubey and Tay (2013) conducted a study on two distinct variations of WC-PV/T utilising two different PV modules within the climatic context of Singapore. Module -I is comprised of a WC-PV/T module that is combined with monocrystalline (m-Si) solar cells. This configuration includes a tube and sheet absorber, as depicted in Fig. 2.13a. On the other hand, Case II involves using multi-crystalline (mc-Si) solar cells together with a parallel plate-type absorber, as illustrated in Fig. 2.13b. Module-I has 3.3% greater thermal and 2.6% higher electrical productivity than module-II as a result of PV module temperature of the module I that was 38–72 °C instead of 47–76 °C in module II.

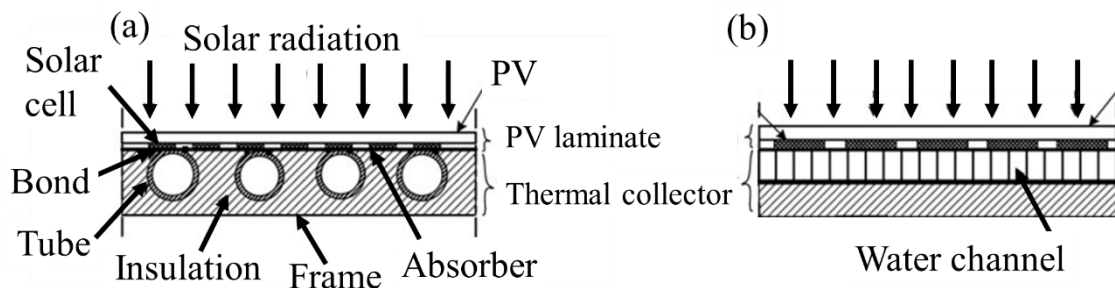


Fig. 2.13. PV/T modules of (Dubey and Tay, 2013)

Amid seven new absorber configurations based on the water flow tube design for WC-PV/T, as illustrated in Fig. 2.14a-g suggested by Ibrahim et al. (2009), the spiral configuration (Fig. 2.14e) demonstrated superior performance as it covers an entire surface area of the WC-PV/T module. The spiral flow arrangement showed a maximum thermal efficiency of 50.2% and an electrical efficiency of 11.98% at a flow rate of 0.01 kg/s. In contrast, the serpentine flow configuration exhibited the lowest thermal efficiency of 32.35% and electrical efficiency of 11.94%.

The three different designs based on the tube configuration u, serpentine, and spiral shape through different water mass flow rates from $5 \cdot 10^{-4}$ kg/s to $5 \cdot 10^{-3}$ kg/s were carried out by Afzanizam et al. (2018). Additionally, the findings indicated that the WC-PV/T with a spiral flow channel exhibited a thermal efficiency of 9.2% and 1.5% greater than the u-shaped and serpentine flow channels, respectively, when operating at the most significant mass flow rate. However, while considering electrical efficiency, it was seen that the u-shaped flow channel

exhibited a greater electrical efficiency of 0.95% compared to the other two flow channel designs. Abdullah et al. (2020;2019) constructed a WC-PV/T module, including a dual oscillatory flow channel. The purpose of this design was to conduct a comparative analysis of the electrical performance between the WC-PV/T module and a conventional PV module that lacks a cooling mechanism. The study revealed that the selected configuration had the highest electrical efficiency of 11.5% when operated at a flow rate of 6 litres per minute and an irradiance level of 500 W/m^2 . Conversely, the optimal thermal efficiency of 58.64% was attained when the system operated at a flow rate of 5 litres per minute and an irradiance level of 1000 W/m^2 .

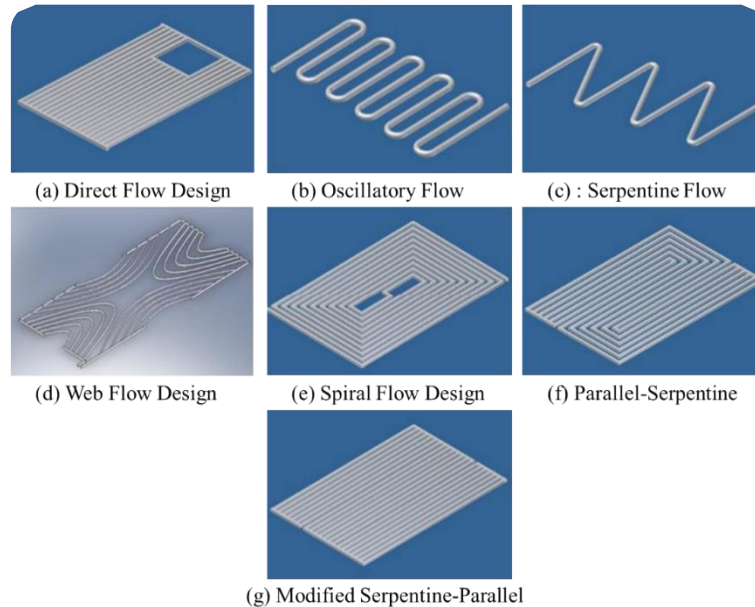


Fig. 2.14. Water flow tube design of Ibrahim et al. (2009)

Another comparative analysis concerning direct water flow, spiral, and finned box-type WC-PV/T was examined by Sardouei et al. (2018). The numerical findings indicated that the spiral flow type design demonstrated consistent temperature distribution over a PV module. Conversely, the direct flow type design exhibited the most significant temperature gradient. Moreover, the finned box type and spiralling flow type designs of a water-cooled photovoltaic/thermal system (WC-PV/T) showed the highest electrical efficiency when subjected to various operational conditions. Hossain et al. (2021) incorporated a novel parallel serpentine flow tube into a WC-PV/T system. A comparative analysis was conducted between classical water-based solar collectors and a WC-PV/T module, yielding findings that indicate a thermal efficiency of 74.62% for the WC-PV/T module and 82.5% for the classical solar collectors, both operating at a flow rate of 0.034 kg/s . Kazem et al. (2021) created a hybrid flow-based (oscillatory and direct) WC-PV/T system to address the non-uniform heat distribution problem in the thermal collector and PV module. Researchers devised a hybrid WC-PV/T system to mitigate these concerns, including a flow channel that supports oscillatory and direct. They compared their new rig with single patterns of flow design oscillatory, direct, and web flow. The research showed that the hybrid pattern WC-PV/T is 9.1% more efficient at using electricity than the oscillatory flow type, 9.9% more efficient than the straight flow type, and 15.2% more efficient than the web flow type.

Boumaaraf et al. (2020) conducted a study that involved a numerical and experimental analysis of the WC-PV/T system equipped with a serpentine-shaped heat exchanger. The investigation

was conducted in the weather of Ghardaia city, Algeria. The research also found that the WC-PV/T with the serpentine heat exchanger has the potential to provide 61% thermal efficiency, 7% electrical efficiency, and 79.43% overall energy efficiency. Gelis et al. (2022) designed and analysed a unique WC-PV/T by affixing 12 cooling cubes to the back of a PV module. The maximum thermal efficiency of 17.7% was attained when the flow rate was set at 1.65 litres per minute and the sun radiation reached 900 W/m^2 . The unique WC-PV/T system demonstrated a significant increase of 4.67% in electrical efficiency compared to the uncooled PV module. The lower surface of the photovoltaic (PV) module was attached with a distinctive water tube configuration (see Fig. 2.15) that was developed by Nahar et al. (2017) to configure the WC-PV/T module. Increasing the value of water inlet velocity from 0.0009 to 0.05 m/s led to a decrease in the surface temperature of the photovoltaic (PV) system by $42 \text{ }^\circ\text{C}$. Consequently, this temperature reduction yielded a 2% increase in PV efficiency.

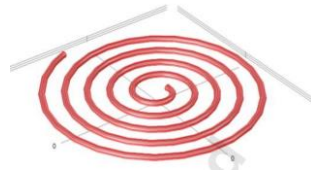


Fig. 2.15. Distinctive water tube configuration (Nahar et al., 2017)

Besides, roll bond absorbers have been investigated in several studies and compared with other types (Aste et al., 2015; Bombarda et al., 2016; Dupeyrat et al., 2011). Han et al. (2021) conducted an experimental and theoretical investigation on a flow channel utilising a roll bond design, examining its performance with and without water cooling in varying weather situations, including clear and cloudy skies. The study findings indicate that their unit's photovoltaic (PV) conversion efficacy achieved 14% and 10% during sunny and cloudy conditions, respectively. The observed improvement in performance was 14.8% and 3.1%, as in the case of uncooled units. Barbu et al. (2021) conducted a study on a roll-bound-based WC-PV/T system, employing a parametric approach to ascertain the optimal channel width of the absorber. The experiment revealed that when the width of the channel was increased from 5 to 10 mm while maintaining a constant flow rate of 0.05 kg/s, the wider channel exhibited a greater surface area for heat transfer between the absorber and the working fluid.

One study in the literature focused on the heat exchanger utilising the half-tube coil to remove the heat from the PV module. Kianifard et al. (2020) conducted a study that combined theoretical and experimental approaches to investigate the impact of cooling on the performance of poly-crystalline PV panels. They utilised a serpentine half-pipe configuration for this purpose, as shown in Fig. 2.16. They verified that efficiency was enhanced by 11.5 % with the related cooling system.

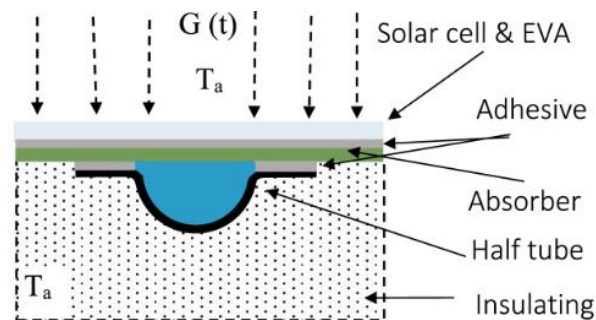


Fig. 2.16. Configuration of the half-tube coil (Kianifard et al., 2020)

Other studies on the flat-box and sheet-and-tube types were also conducted to contribute to the PV/T performance enhancement (Zhou et al., 2020). Herrando et al. (2019) presented 26 distinct absorber-exchanger designs, each characterised by unique geometrical dimensions and materials. Their study aimed to examine the potential enhancements in heat transfer efficiency while concurrently reducing the collector's overall weight and associated expenses. Numerical comparisons were conducted between the replaced designs and the conventional WC-PV/T system. The flat box design with rectangular channels has been noted as a potentially viable alternative to commercial WC-PV/T. This design exhibits a 4% increase in optical efficiency and a 15% decrease in linear heat loss coefficient compared to the cited example.

Widyolar et al. (2020) found that replacing the sheet-and-tube heat exchanger with an aluminium mini rectangular channel increased system efficiency. According to the results, the selected configuration of the WC-PV/T, which is 1.2 m², can generate a thermal efficiency of 57.4% and an electrical efficiency of 12.3%. Additionally, it was approximated that the system has the capability to produce 226 kWh of electricity and 603 kWh of heat energy per square metre annually, based on a solar energy potential of 5.5 kWh per square metre per day.

Recently, in a study conducted by Kalateh et al. (2022), twisted tapes were utilised as heat exchangers and placed within the flow channel of a WC-PV/T system. The twisted tapes were arranged in both clockwise and counterclockwise directions. Implementing twisted tapes enhanced the photovoltaic (PV) module's surface temperature and the overall energy efficiency of the WC-PV/T system. From an exergy perspective, using twisted tapes in WC-PV/T systems led to a 14.8% increase in total efficiency compared to traditional WC-PV/T systems.

Water and air are the most common heat transfer fluids utilised in the realm of photovoltaic thermal modules, and several techniques are conducted utilising water and air to cool the PV module. Appendix A4 illustrates some recent studies conducted using various methods.

Nanofluids significantly influence the facilitation and management of thermal energy transfer and storage in several energy-related applications. The choice of adequate nanoparticles in these applications is a significant factor, especially regarding thermophysical properties. The progress in the nanotechnology field has resulted in enhanced operational speeds, necessitating the development of novel cooling methods that offer improved performance. Recently, there has been a growing interest in utilizing colloidal dispersions composed of particles at the nanoscale scale (nanoparticles) inside conventional heat transfer liquids. These dispersions, commonly called nanofluids, are being explored as a novel category of engineering fluids (Singh, 2020; Yang et al., 2020). A nanofluid is a colloidal mixture formed by combining a base fluid with a specific type of nanoparticle. This particular fluid exhibits significant value in thermal control and cooling, augmentation, and fluid temperature reduction (Alktranee et al., 2023; Hajatzadeh et al., 2019). Extensive investigation of this fluid has revealed the presence of two distinct types of nanoparticles that have exhibited a significant degree of integration with the underlying liquid medium. Consequently, this fluid can be classified as a hybrid nanofluid.

Research has demonstrated that PV/T collectors that use water as the working fluid are more effective than those that use air. However, the efficiency of these devices can be further enhanced by substituting water with nanofluids (Kazem, 2019). Due to the superior thermal conductivity of dispersed nanoparticles, contemporary coolants can extract a more significant amount of heat from PV units than purified water (Gelis et al., 2023).

This concern has been substantiated throughout several investigations. The effect of utilising 3.0 wt% SiC/deionised H₂O nanofluid for cooling 120 W PV module as polycrystalline at rates of flow 0.068-0.170 kg/s was investigated experimentally by Al-Waeli et al. (2017a). They stated that the efficiency was elevated by 24.1% compared to the PV system, whereas thermal efficiency was elevated by 100.19% compared to the water-based PV/T collector system.

Al-Waeli et al. (2018) utilized silicon carbide (SiC) nanofluid in the cooling system of the PV/T module. They assessed the performance of the PV/T collector when utilizing a SiC nanoparticle-infused water-dispersing fluid in both outdoor and indoor settings. The results were close for both systems, proposing an enhancement to the performance and rising incremental efficiency. Shahirah et al. (2019) used titanium/water nanofluid (TiO₂/water) as a coolant in two concentrations of TiO₂ in H₂O to study the system of PV/T under different values of solar radiation and the rate of mass flow. Exergy and energy are analysed, and energy outputs were higher at a low TiO₂ concentration value. Besides, efficiencies would elevate if the rate of mass flow elevated. Abbas et al. (2019) have critically reviewed the enhancement systems of PV/T performance. They analysed the influences of size, nanoparticle type, concentration ratio, and volume fraction on PV/T systems' performance, where nanofluid inclusion enhances the PV/T system's overall efficiency. Al-Waeli et al. (2020) suggested mathematical linear models and neural models for the PV/T system. They were validated by the results of experiments mathematically investigated to enhance the PV/T power production performance according to three cooling models utilising SiC-H₂O, nano-PCM, and nanofluid, which elevated its outputs as electrical and thermal efficiency.

Hissouf et al. (2020) examined the influence of dispersing Cu and Al₂O₃ nanoparticles in pure H₂O on hybrid system performances using a mathematically applied model derived from the application of energy balance equations. Furthermore, by utilising 2% volume and copper fraction as nanoparticles, the electrical and thermal efficiency of the Cu-H₂O nanofluid was enhanced by 1.9% and 4.1%, respectively, compared to pure H₂O. A study conducted by Ahmadinejad et al. (2022) utilised numerical methods to examine the effects of a newly designed staggered collector on the performance of a photovoltaic/thermal module based on nanofluids nf-PV/T. The coolant under consideration was an aqueous suspension containing nano additives of single-walled carbon nanotubes (SWCNT). The utilisation of a staggered collector and nanofluid (NF) has been verified to enhance the effectiveness of the gadget. Aboueiian and Shahsavari (2022) conducted a numerical analysis of the effects of using an aqueous silver nanofluid on the sheet with a grooved tube nf-PV/T module. An increase in system productivity was observed when employing NF.

Gelis et al. (2022) conducted an experimental study to evaluate the effectiveness of a nf-PV/T module using an aqueous solution of silicon dioxide SiO₂ NF. The study revealed that the intensity of solar radiation has the most significant effect on the device efficacy, while the nanoparticle volume concentration has the slightest influence. Kouravand et al. (2022) conducted an experimental examination of the results produced by a concentrating nanofiltration-based photovoltaic/thermal (PV/T) device equipped with a finned phase change material (PCM) heatsink. An observable impact of NF on the performance of the apparatus was clearly apparent. In their study, Kazem et al. (2021) developed a PV/T module with two configurations, utilising water-based and SiC nanoparticles. The objective was to assess the thermal and electrical performance of the modules by computational simulations and laboratory testing. The observation was made that nf-PV/T behaved better than the WC-PVT

module. The electrical and thermal efficiency of the nf-PV/T reached 20.21% and 43.3%, respectively, whereas the WC-PV/T improved by 8.51% and 29.0%, respectively. Al-Waeli et al. (2017b) conducted a comprehensive assessment of the research undertaken on PV/T systems and provided an overview of the various implementations of this equipment.

The exceptional effectiveness of NFs in numerous applications has prompted research efforts to enhance their thermodynamic characteristics. The researchers aimed to determine whether incorporating nanoparticles (consisting of two or more particles) may improve the thermophysical properties of the NFs. The results revealed an excellent answer to this issue. Subsequently, a novel set of NFs was created, referred to as hybrid (two particles) and ternary (three particles) NFs (Adun et al., 2021; Maleki et al., 2021; Vallejo et al., 2022).

Following the successful development of hybrid nanofluids (NFs) and the demonstration of their superior effectiveness compared to mono NFs, several researchers examined the performance of PV/T systems utilising these NFs. Hooshmandzade et al. (2021) conducted an experimental study to compare the performance of PV/T devices using mono and hybrid NFs. They used SiO₂ and Al₂O₃ with water through mono and hybrid composite. The utilisation of hybrid NF, as opposed to mono NF, results in a significant increase of 19.55% and 12% in the total efficiency of PV/T systems.

Hooshmandzade et al. (2021) attempted to increase the electricity generated by PV panels and achieve enough heating by integrating a PV/T module coupled with a solar thermal collector and utilising a hybrid NF as the coolant. Aqueous suspensions of Gr/GO, Gr/SiC, MWCNT-SiC, and MWCNT/Al₂O₃ nano additives were used as hybrid NFs. The water-SiC NF demonstrated the highest performance throughout the cases that were evaluated. Ahmadinejad and Mousavi (2023) conducted a theoretical evaluation of the effectiveness of a baffled nf-PV/T module. The NFs that were analysed comprised water-CuP and water-CNT. The best results were seen when a baffled channel was used in conjunction with water-CNT NF.

The effectiveness of the nf-PV/T module was simulated using the water-Cu NF by Ahmadinejad et al. (2023). It was found that the system's first and second thermodynamical law performances may be improved by 2.24% and 7.55%, respectively, when NF is employed.

Ternary hybrid nanofluid (THNF) studies have recently attracted much attention. Few studies have looked into the behaviour of THNFs. To the authors' knowledge, there are only four studies on using ternary nanofluid for solar PV/T technologies. Adun et al. (2021) employed a ternary nanofluid in the nf-PV/T module and examined the module's exergy output numerically. The NF that was analysed consisted of an aqueous solution of CuO–MgO–TiO₂ nanoparticles. A 4.2% enhancement in the exergetic efficiency of the nf-PV/T module was documented in comparison to the WC-PV/T module. Adun et al. (2022) conducted a numerical study on utilising Al₂O₃/Fe₃O₄/ZnO-water ternary NFs in the nf-PV/T system. The study aimed to examine the heat transfer efficiency of the nanofluids to enhance the productivity of the PV/T module.

The performance of a ternary nanofluid-based PV/T system based on GO-TiO₂-Fe₃O₄ was experimentally investigated by Abdalla and Shahsavari (2023). They assessed the influences of flow rate and nanoparticle volume fraction. At a mixing ratio of 1:1:1, a flow rate of 80 kg/h, and a volume fraction of 1%, their results verified superlative total energy (88.23%) and exergy (15.36%) efficiency. Kenfack et al. (2023) introduced an improved design of an air/water PV/T utilised three particles of CuO, MgO and TiO₂ collector. The goal was to find the most effective

arrangement of construction factors to enhance energy production. A system is subjected to study of its energy and exergy, which is implemented using MATLAB to do multiple goals standardisation.

Graphically, Appendix A5 represents the main most used configurations of the water or nanofluids-cooled photovoltaic thermal module focused on by the literature.

2.4. Bi-fluid-cooled PV/T module

Bi-fluid PV/T modules are a modern term that uses air and water as coolants with an absorber plate (Assoa et al., 2007; Tripanagnostopoulos et al., 2000; Tripanagnostopoulos, 2007). This type, in addition to producing electricity, also produces hot water and hot air in parallel, and it is more efficient than air-cooled and water-cooled types. The primary objective of their module is to overcome the weaknesses encountered in the PV/T units in the water and air heat exchanger modes when each was operated independently (Abu Bakar et al., 2014; Hamid et al., 2014). Studies with this type conducted several configurations to improve heat transfer. Tripanagnostopoulos (2001; 2002) suggested a primary idea for such systems. Assoa et al. (2007) designed a new configuration for BiF-PV/T modules. They inserted a water tube with an absorber between the two PV modules in a unique groove. They studied three solar modules, 20, 10, and 2.7 meters. Their innovation indicated that the highest electrical and thermal efficiencies were more than 11.5 and 85 %, respectively, for the module with a 2.7 m length. Jarimi et al. (2013) performed a simulation analysis of BiF-PV/T, and they validated their model with the experimental research of Joshi et al. (2009). They attached the tube loop to the backside of the PV module without using an absorber by using an air channel with fins at the bottom parallel to the air direction. Their results showed the efficient behaviour of a dual fluid system (water and air). The design's overall efficiency reached more than 55%. The average cell temperatures of their module decreased by 6 °C and 4 °C, respectively, compared to the air and water units.

Bakar Abu et al. (2014) conducted a design analysis of the BiF-PV/T concepts, and they modelled a serpentine tube mounted directly to the rear side of the PV module inside a single-pass air channel (see Fig. 2.17). They simulated their system using different mass flow rate values for water and air in a two-dimensional steady state. The validated simulation results showed that the efficiency of the water flow rate was 0.0247 kg/s with 78.8 % total efficiency at a constant airflow rate, and the efficient value of the airflow rate was 0.051 kg/s with 76.3% total efficiency at a constant water flow rate.

Othman et al. (2016) experimentally created a dual-pass air channel BiF-PV/T collector with a transparent solar PV module. The absorber plate was secured in the middle of the air channel, and a water-tube coil was attached to the top and back sides of the absorber. Their system reached the best value when the flow rates for water and air were 0.02 and 0.05 kg/s. Jarimi et al. (2016) conducted an indoor experimental condition on the BiF-PV/T module. A serpentine-shaped tube with fins inside a single-pass air channel was used beneath the PV module. They examined the PV/T module in three modes based on the coolant used: air, water, or air-water. According to the data, studies found that total efficiency and primary energy savings efficiency had risen by 13.82% and 13.88%, respectively, and by 4.13%, the electrical module efficiency increased.

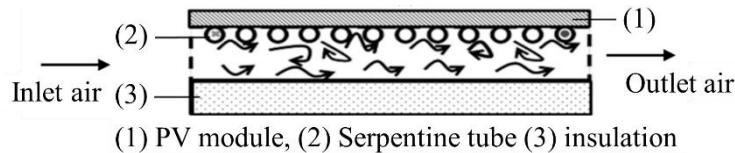


Fig. 2.17. Configuration of the Bi-fluid PV/T of Bakar Abu et al., (2014)

Othman et al. (2016) experimentally created a dual-pass air channel BiF-PV/T collector with a transparent solar PV module. The absorber plate was secured in the middle of the air channel, and a water-tube coil was attached to the top and back sides of the absorber. Their system reached the best value when the flow rates for water and air were 0.02 and 0.05 kg/s. Jarimi et al. (2016) conducted an indoor experimental condition on the BiF-PV/T module. A serpentine-shaped tube with fins inside a single-pass air channel was used beneath the PV module. They examined the PV/T module in three modes based on the coolant used: air, water, or air-water. According to the data, studies found that total efficiency and primary energy savings efficiency had risen by 13.82% and 13.88%, respectively, and by 4.13%, the electrical module efficiency increased.

A stainless steel serpentine-shaped tube loop was used in a novel design of a dual-pass BiF-PV/T module by Baljit et al. (2017). They also used concentrators above the solar cells for radiation investigation. According to what they found, BiF-PV/T got an electrical harvest of 13.02%, which was a significant improvement over single-flow units by about 25% in terms of thermal performance. Daghigh and Khaledian (2017) investigated a novel BiF-PV/T module experimentally and numerically. They used a spiral-shaped aluminium tube connected directly to the absorber sheet under the PV module. They used water flow, airflow, or non-flow into the module channel to compare their performance. The maximum temperature of the PV as an absorber was decreased by 17.5 and 15 °C for water flow and airflow cases, respectively. The water case had a 20 % higher maximum efficiency than the air case.

Atmaca and Pektemir (2019) conducted an experimental comparative study of a BiF-PV/T module and classical water-PV/T and PV modules. Their model consisted of hexagonal fins connected to a sheet-and-tube absorber placed under the PV module. They concluded that it was more efficient than the traditional PV and PV/T units, where the total efficiency of the module was 78 %. Manssouri et al. (2020) conducted a simulation study using the same design as in Ref. (Jarimi et al., 2013). They validated this result using the experimental results from Ref. (Jarimi et al., 2016). They determined the energy improvement of the water-air mode. The thermal powers of the BiF-PV/T module were 200 and 400 W higher than those of the water and air modes, respectively. Baljit et al. (2020) investigated Fresnel lens technology on a new BiF-PV/T design to improve incident radiation (see Fig. 2.18). They used a square cross-section water tube connected to the aluminium absorber under the PV module that also acted like fins when put through the air channel. They showed that the thermal efficiency of their module was achieved at 73.8% under fixed airflow and 73% under fixed water flow.

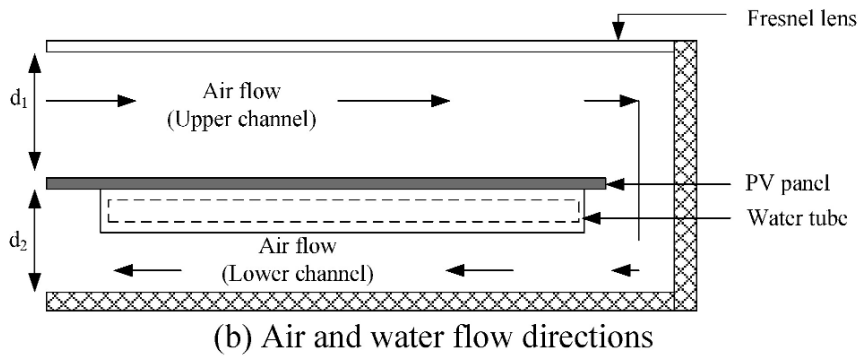


Fig. 2.18. Configuration of the Bi-fluid PV/T of Baljit et al. (2020)

Using water nuzzling, Lebbi et al. (2021) cooled the front surface of solar cells within a BiF-PV/T module. They compared it with a classical PV unit. The novel hybrid BiF-PV/T system succeeded in maintaining the electrical efficiency of the PV module at its highest level, which is equivalent to the base case. Additionally, the findings indicate that the total average energy efficiency was 85.3 %.

Manssouri et al. (2021) attached a roll-bond-absorber with fins under a PV module to create a novel BiF-PV/T module and compared it with another module without fins in the air channel. Their simulation results showed that BiF-PV/T was superior to a standard PV/T collector, and their design produced 15.3 % more overall energy. Slimani et al. (2021) created a new module of BiF-PV/T. A copper radiator with a copper tube was adhered to the backside of the monocrystalline-PV module. Their results showed that the overall efficiency of their configuration reached 94.53%.

Some studies focused on the exergy enhancement of the bi-fluid PV/T modules. Appendix A6 lists the recent experimental and numerical studies on the exergy analysis of that type.

Besides, graphically, this chapter represents the main most-used configurations of the bi-fluid-cooled photovoltaic thermal module focused on the literature. Appendix A7 illustrates the most focused configurations.

2.5. Summary of literature review

The first outstanding and most promising energy source is renewable energy, especially solar energy. Photovoltaic-thermal (PV/T) modules are a promising technology because they have a dual energy source, thermal and electrical. This chapter offers an extensive review of the scientific literature regarding PV/T modules, which will be highly beneficial to investigators in this field. This research focused on the latest research on the PV/T systems currently employed in air and water collectors. It examined the impact of different factors on the efficiency of the PV/T module. Additional significant enhancements that enhance PV/T systems involve the incorporation of nanoparticles in the channel alongside water as the working fluid, implementing bi-fluid circulation. Collectively, these improvements contribute to the overall enhancement of system performance. The different uses of solar photovoltaic, for example, building PV/T systems as integrated solar PV/T heating systems, liquid collector PV/T, concentrator PV/T systems, and nanofluid-based PV/T collectors, are also presented. Based on the literature, the most focused PV/T modules are described in the hierarchical chart in Appendix A8, which is a graphical summary of the reviewed literature.

Insignificant amounts of simulation and modelling literature were conducted in the evaluation of the PV/T module's performances; accordingly, there is a lack of investigations that build a uniform simulation platform to evaluate the PV/T module.

Several heat exchanger fin configurations were evaluated experimentally and theoretically to enhance the heat transfer of the air-cooled PV/T module through natural and forced air circulation. One of the most effective fin types in the heat exchanger, louvered fins, hasn't been utilised in the PV/T module.

Among the many studies on PV/T modules, there have been no significant experimental studies on bi-fluid-based PV/T. Additionally, there is no study combining louvered fins and serpentine tubes within a copper absorber through a bi-fluid PV/T module.

Literature experiments focused on most parameters like solar radiation, cell temperature, heat transfer fluids, and modifications that influence efficiency improvements through reviews of all aspects and concepts related to conceptual and performance issues. However, there is a lack of studies that give a dependent relationship between solar radiation and solar cell temperature based on particular modifications.

Besides, no study developed a new mathematical model to estimate the amount of wasted heat eliminated from the PV module by the design of the PV/T modules, leading to a high sustainable contribution in the urban area.

Many nanofluid-based PV/T module studies have been performed. Nanofluids, a high-thermal conductivity fluid, can improve PV/T module performance. Most nanofluids used were mono, binary, and ternary types. However, a few investigations use ternary nanofluids as PV/T module coolants. Few studies used ternary nanofluids in bi-fluid PV/T modules, especially no study used MWCNTs in a ternary composite. Additionally, no new study has correlated the thermal conductivity of ternary nanofluids using MWCNT composites with temperature and volume concentrations.

Based on the research analysis, it could be concluded that the present research fulfils the intended goal of addressing the existing knowledge gap. Therefore, the current research has been carried out both experimentally and theoretically focused on the parametric evaluation of various photovoltaic thermal module configurations, including building a new simulation platform, creating a new fin confirmation, utilising a combination of copper fins and serpentine tubes, assessing the effect of solar radiation, developing a thermodynamic model of estimating the wasted heat extracted from solar cells by PV/T modules, investigating ternary nanofluids, and presenting a new correlation of thermal conductivity of ternary nanofluids.

3. MATERIALS AND METHODS

This chapter provides a comprehensive overview of the materials, techniques, and equipment utilised in the experimental measurements, along with the scientific approaches implemented to achieve the research objectives. It outlines the procedures for conducting the examination, acquiring data, and performing visual analysis.

3.1. Experiment's location

The location of the study is one of the most essential factors that renewable energy research depends on because each area has its weather properties based on its site within the world. The experiments were conducted at the Hungarian University of Agriculture and Life Sciences (MATE) (former Szent Istvan University), Gödöllő, Hungary, at the institute of Technology, Solar Laboratory. The geographical latitude and longitude of the Gödöllő are 47° 35' 39" N and 19° 21' 59" E, as shown in Fig. 3.1. The experiment works were conducted during clear days in June-August 2022 and July- August 2023, and the numerical works were performed based on metrological data 2021.

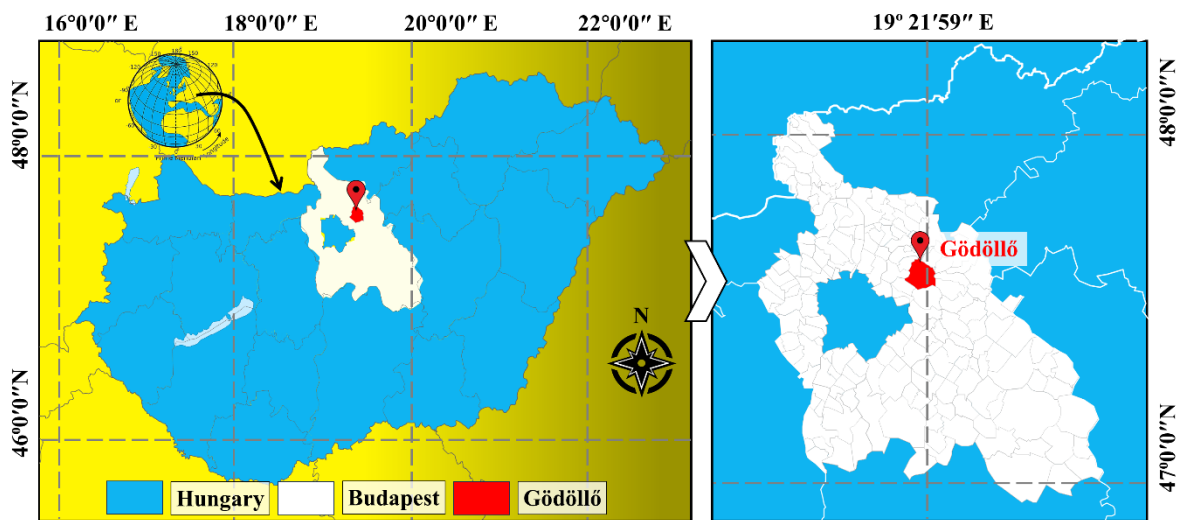


Fig.3.1. Study area and location of the setup (Source: hand made by PowerPoint using Google pictures)

The solar systems should be positioned squarely facing the sun to achieve optimal performance. For optimal performance, it is imperative for the sun to directly illuminate the surface of the solar system at an optimal angle, without any hindrance from shadows. Nevertheless, solar systems employed in this experiment remain stationary and do not actively track the sun's movement. Fig. 3.2 and Table 3.1 illustrate the exact orientation characteristics of the experimental rigs of this research.

Table 3.1. Characteristics of study location

	Value
Country	Hungary
City	Gödöllő
P-code	2100
Plus-code	H9V8+QJ
Coordinates	@47.5941467, 19.3664471



Fig. 3.2. The topographical information of the study location (Source: Google Maps)

3.2. Methodology approaches

To study and evaluate the performance of the PV/T module, the experiment methodology of this research was conducted through two solar modules belonging to the Solar Lab at the Hungarian University of Agriculture and Life Sciences, Institute of Technology; each module has a different methodology.

The first assessments were conducted on a conventional PV/T module installed at a Solar Lab of the MATE university (see Table 3.2), and the second experiments were conducted on a novel PV/T module by utilising a conventional PV module (see Table 3.3) available in the Solar Lab.

Table 3.2. Details of conventional PV/T module

	Unit	Value
Dimensions	m	$0.870 \times 1.640 \times 0.105$
Gross surface	m ²	1.474
Absorber surface	m ²	1.270
Type of cells	-	Monocrystalline
Cells	Number	72
Cell length and width	m	0.125×0.125
Nominal power	W	180
Short circuit current	V	5.55
Nominal current	A	5.12
Open circuit voltage	V	43.39
Absorber	-	Copper alloy
Internal tube	-	Copper alloy
Model	-	Power-Volt / MA-0013

The methodology of the first module (conventional PV/T) is focused on the evaluation and comparison based on the TRNSYS tool. The methodology flow chart is illustrated in Fig. 3.3.

Table 3.3. Conventional PV module details based on Standard Test Condition (STC)

	Symbol	Value
Solar cells type	-	Poly-crystalline
Current (at Short-circuit)	Isc	3.8 A
Temperature coefficient of Isc	-	(0.065 ±0.015) % / °C
Voltage (at open circuit)	Voc	21.1 V
Temperature coefficient of Voc	-	− (80 ±10) mV / °C
Maximum power	Pmx	60 W
The current at Pmx	Imx	3.5 A
The voltage at Pmx	Vmx	17.1 V
Temperature coefficient/power	-	− (0.5 ± 0.05)% / °C
Nominal Operating Cell Temperature	NOCT	47 ± 2 °C
Dimensions of PV module		
Length	Lm	1.108 m
Width	Wm	0.502 m
Height	Hm	0.05 m
Cells number	-	36
Cell dimensions	Lc×Wc	0.0114 × 0.0114 m
Model	-	Solarex MSX-60

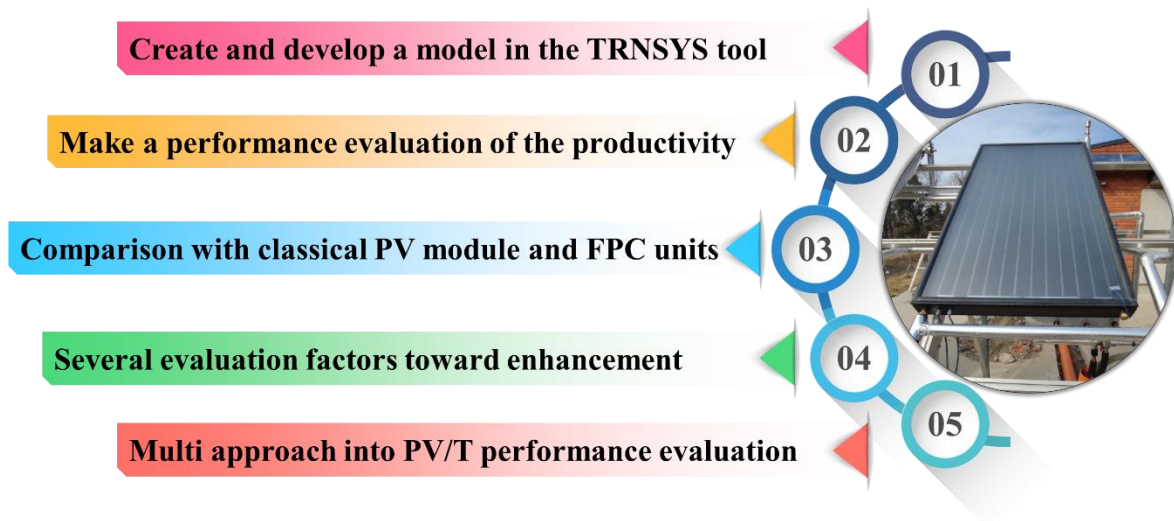


Fig.3.3. Flow chart of the first module (conventional PV/T) (Source: hand-made by PowerPoint)

Besides, the main methodology of the experiments conducted on the created PV/T module is based on crucial methods mainly addressed in the literature to improve conversion efficiency by enhancing heat extraction from solar cells integrated into PV/T cells. These methods first depend on the geometry modifications on the PV/T layers and second on improving the thermal conductivity of the heat transfer fluids utilising hybrid nanoparticles. Fig. 3.4 illustrates the procedures of the evaluation methodology of the created PV/T module.

- 1 Fabricating a novel bi-fluid PV/T module as a primary device
- 2 Develop a thermodynamic mathematical model for performance behaviours
- 3 Fabricating an air-cooled PV/T with and without fins for comparison
- 4 Fabricating a water-cooled PV/T for comparison
- 5 Develop a thermodynamical model for sustainability contribution evaluation
- 6 Synthesis of a hybrid ternary and binary nanoparticles
- 7 Fabricating a novel instrument for nanoparticle comparison, evaluation and choosing
- 8 Evaluations of the performance improvement

Fig.3.4. Methodology procedures of the new PV/T (Source: hand-made by PowerPoint)

3.3. Methodology of the conventional PV/T module

3.3.1. Hybrid PV/T system schematic

Several parts and components are configured in the PV/T system, as indicated in Fig.3.5. The suggested system involves a PV/T module, a thermal storage part for hot water, a pump, a differential controller as a thermostat, and output parts for electric power and hot water consumption.

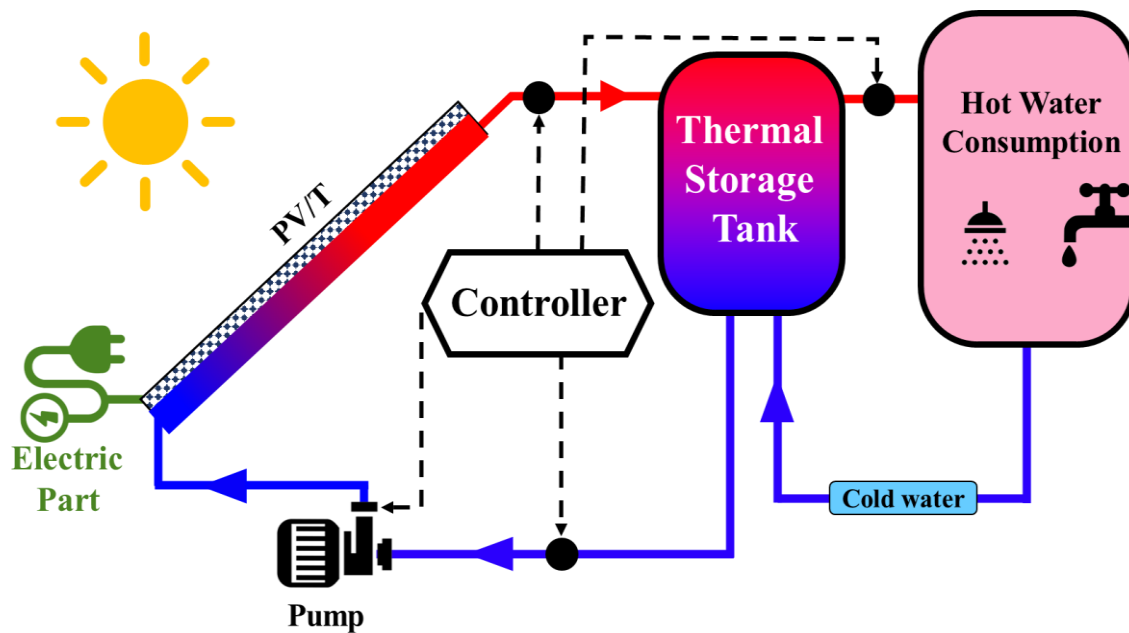


Fig. 3.5. The complete arrangement of the proposed system of PV/T (Source: hand-made by PowerPoint)

This analysis utilised PV/T module specifications that consist of a copper absorber and a monocrystalline PV module with a glass cover. The system is part of the solar laboratory at the Hungarian University of Agriculture and Life Science. As listed before, Table 3.2 presents the conventional PV/T module specifications. This research used the actual module illustrated in

Fig. 3.6a. Additionally, Fig. 3.6b shows all the parts of the PV/T module installed in the laboratory.

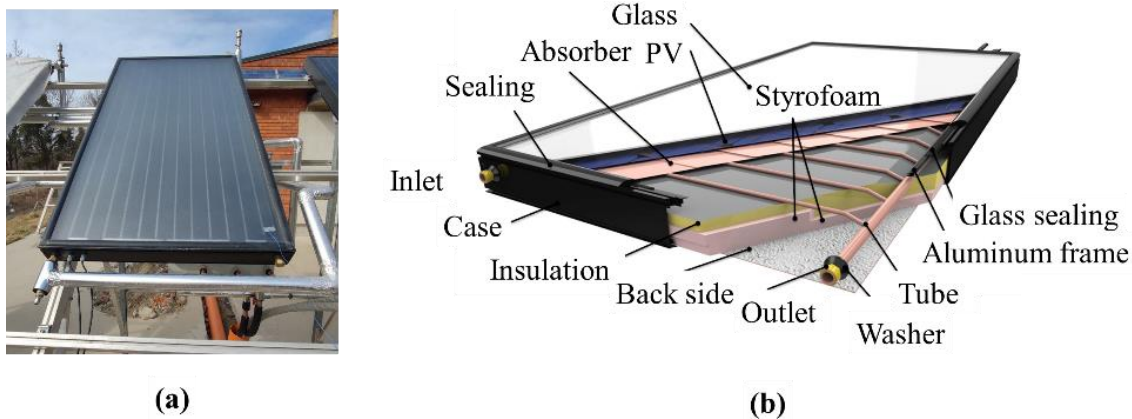


Fig. 3.6. a) actual view and b) parts of the conventional PV/T module

3.3.2. TRNSYS model

This subsection describes the dynamic and mathematical model of the presented PV/T system. The models in this section utilised the specifications and characteristics mentioned in section 3.3.1. As a functional tool used to evaluate solar systems, TRNSYS software was used in this research to build a concrete model of the PV/T system, which can chart the behaviour of the outputs throughout various components in TRNSYS environments. As this tool depends on the Fortran programming language to hold the model in run mode, this research created a new element representing the experiments conducted in the laboratory module. TRNSYS characteristically includes several approaches and structures bound together by using subroutines. The building of simulation process lines of such systems, or any solar system, starts by adding objects to represent a user's feedback. A unique icon representing each component was specified to exchange the parameters and variables for inputs and outputs with another element. Fig. 3.7 shows the linked components and particular types used to build the hybrid system parts. Appendix A9 lists the description of all icons used to construct the final model of this research. A proportional integral derivative controller (PID- Type23) was used as a temperature controller to control the outlet water temperature of the PV/T system and the storage tank temperature. The pump worked at a variable flow rate with the PID controller, and the difference between these two temperatures remained constant at 5 °C. The basis system of this research is PID-controlled (PV/T-ID), which was fixed at a tilt angle of 45°.

This research uses a TMY meteorological year (a component of Type109-TMY2) condition. The Type500 was created in Fortran's programming language as a new TRNSYS component to represent the study module of the PV/T system based on the proposed specifications for building a whole model. The thermal losses of this type of PV/T were measured according to the operating temperature, wind velocity, surface cell temperatures, and collector structure information. The thermal storage tank was thoroughly mixed using Type4c with no stratification impact (Klein et al., 2006). Type 65a represents the electronic monitoring display of model outputs. The Type110 represents the pump with a flow rate of 0.138 kg/s, and several other auxiliary components are added necessarily.

Several modifications and aspects were examined and tested in the original model PV/T-PID to assess the electrical and thermal behaviour. The first experiment examined the effect of non-

use of the daily consumption profile of hot water on the entire model. The red dashed line in Fig. 3.7 represents the consumption profile. The second model modification replaced the PID controller in the original model PV/T-PID with an ON-OFF controller (Type2b). Unlike PID, at the ON-OFF controller, the pump worked at a constant flow rate when the difference between the temperature of stored water and the outlet temperature of the collector was higher than 5 °C. As reported in the literature, the tilt angle varies depending on the location of the study (Yadav and Chandel, 2013; Yunus Khan et al., 2020). Besides, most studies did not report how the PV/T outputs change through various title angles. Therefore, the third model modification was introduced to change the tilt angle of the module from 0° to 90° with a 5° interval. Besides, the azimuth angle of the modules was constant at -20°.

Generally, to follow the main path of the model developed and illustrated in Fig. 3.7, the PV/T module (Type500) produces electrical energy that proceeds to the result monitoring processor (Type65a). At the same time, it produces hot water that goes to the storage tank (Type4c). Hot water will be exploited by the daily profile components selected by the dashed red line in Fig. 3.7. Then the water will leave the tank for the pump (Type110), which circulates the water again to the PV/T module (Type500).

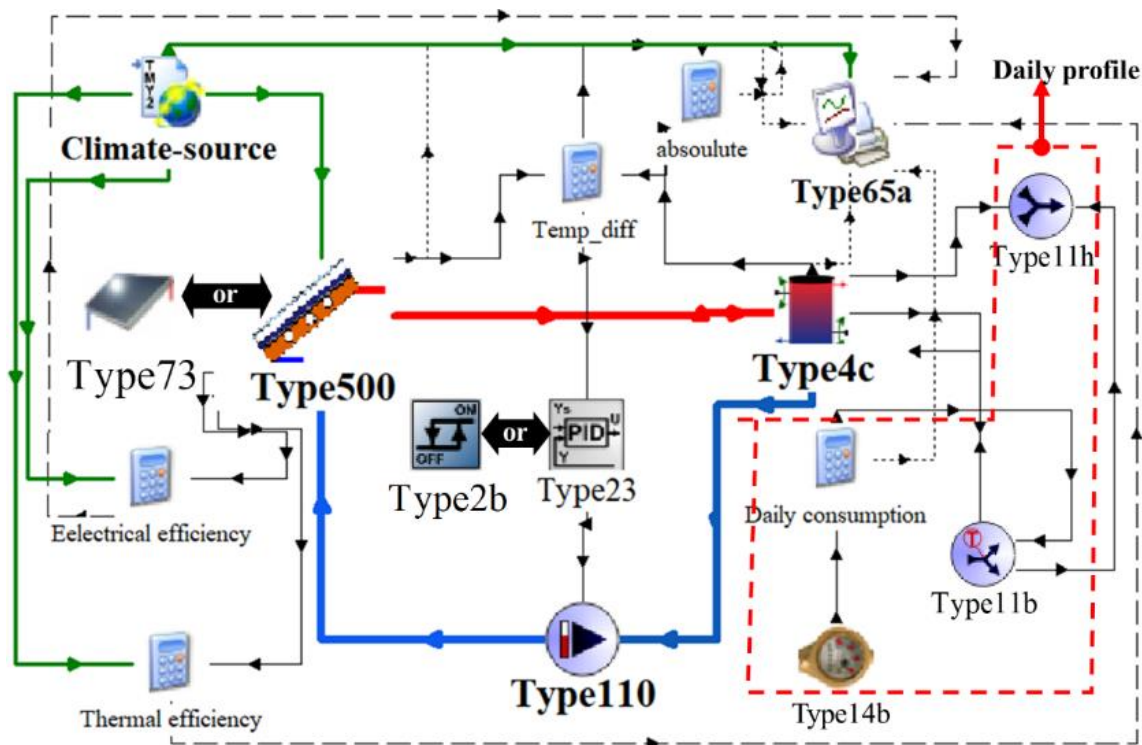


Fig. 3.7. TRNSYS model of proposed PV/T system

Apart from the PV/T system model, this research established two additional models for analysis and comparison in the TRNSYS system. These systems are a photovoltaic PV module and flat-plate collector FPC using the same meteorological weather data source, exact dimensions, and specifications as those in the original PV/T model. The PV model built in TRNSYS is demonstrated in Appendix A10, which was used to compare it with the PV/T model. Besides, the flat plate collector system was also conducted for domestic hot water as a TRNSYS model, similar to the PV/T model in Fig. 3.7, but the FPC icon replaced the PV/T icon. Table 3.4 represents the above systems used in this research to simplify the systems models.

Table 3.4. Tested systems of the current research

No.	System description	Symbol
1	PV/T with PID controller, 45° as a tilt angle, basis system with the daily water profile	PV/T-ID
2	PV/T with PID controller, 45° as a tilt angle, without the daily water profile	PV/T-Wd
3	PV/T with an ON-OFF controller, 45° as a tilt angle with the daily water profile	PV/T-O
4	Flat plate collector system with the equivalent specifications of PV/T-ID	FPC
5	PV system with the equivalent specifications of PV/T-ID	PV

All models mentioned in Table 3.4 were examined and compared to evaluate the systems regarding electrical and thermal proficiency.

3.4. Methodology of the created PV/T module

The geometry modification is the first attempt conducted in this research to enhance heat extraction from the PV module. The conventional PV module that is available at the solar lab of the MATE University is employed to manufacture the new design of the utilised PV/T module to fulfil the objectives of this research. The manufactured PV/T module comprises a PV module, copper absorber, novel fins, water serpentine tube, and air channel.

Besides, the manufacturing process starts with creating the absorber, serpentine tube, fins, new absorber, adhering the absorber to the PV module, air channel, insulation, air flow ducts, and heat exchanger tank. The following subsections will detail the manufacturing process of each part.

The modification works conducted on the PV module were to create three PV/T modules: classical air-cooled PV/T without fins, classical water-cooled PV/T, and the novel bi-fluid PV/T employing a novel absorber with fins and a serpentine tube.

3.4.1. Creation of the new absorber with tube and novel fins

This laboratory experiment created a new design of an absorber by using louvered fins in contact with a copper plate between a serpentine tube fixed to the PV module to configure a new design for the BiF-PV/T module.

Several studies on heat exchangers focused on the use of the louvered fins (LF) (see Fig. 3.8); it was widely used in heat exchangers, especially with automotive radiators and various heat exchangers, to enhance thermal behaviour (Atkinsonam et al., 1998; Leu et al., 2001; Okbaz et al., 2018). In addition to the interrupted air flow due to the louvered fins, this configuration has high thermal performance at the end of the flow thanks to the louvered fins that enhance the heat transfer from the inlet to the outlet of the air duct (Erbay et al., 2017).

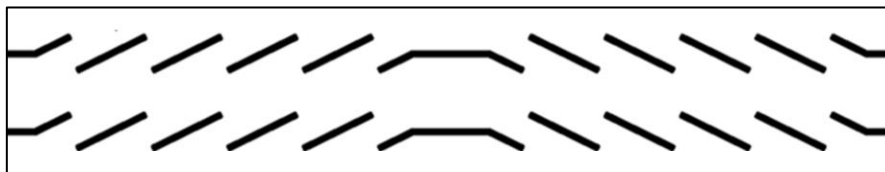


Fig. 3.8. Louvered fins (Erbay et al., 2017)

Mao et al. (2013) studied how the distribution of airflow rate affects the thermohydraulic performance of a louvered finned tube heat exchanger. They confirmed that the thermal gain from the airflow distribution positively affected their model's performance. Liang et al. (2015) used different louvered fins to test and calculate the thermal behaviour of automotive condenser condensing and evaporating units. Their result showed that the short louvered fins gave the condenser a high heat capacity. Karthik et al. (2015) numerically and experimentally investigated the influence of geometrical factors and inlet airflow conditions on the louvered fin heat exchanger. The result indicated that the thermo-hydraulic performance was enhanced with a louvered fin and flat tube. A variety of numerical simulations were performed by Okbaz et al. (2020) for a variety of louvered fin angles and lengths. They concluded that the louvered fin heat exchanger had higher friction factors than the wavy fin.

Previous studies confirmed that the louvered fin heat exchanger provides the highest performance due to the interruption caused by the louvered fins to the airflow inside the channels, which increases the heat transfer rate; this research exploits the shape of these fins to form a hybrid solar collector.

Additionally, as reported in recent studies, there has been no experimental study on copper absorbers with copper fins and tubes in the bilateral unit of the PV/T. This research essentially intends to experimentally consider the performance of a novel design of an air-water-cooled PV/T collector, which mounts louvered fins to the copper absorber and adheres to this new absorber under the PV module.

The absorber plate utilised to create the research modules is a pure copper alloy plate with a thickness of 1.5 mm. First, two absorber plates were cut based on the exact area of the solar cells of the examined PV module (see Fig. 3.9) for the new PV/T and air-cooled unit. The area of the copper plates is 0.49 m².



Fig. 3.9. Copper absorber of the research modules

Different areas of 50 louvered fins at a fixed height of 50 mm and thickness of 1.5 mm were cut with and bent through several specialist machines at the mechanical workshop of MATE University, as illustrated in Fig. 3.10.

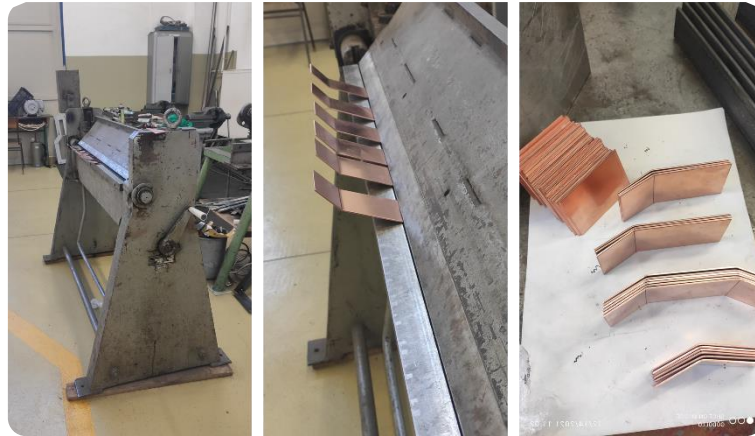


Fig. 3.10. Louvered fins at the mechanical workshop

The distribution of the louvered fins on the absorber plate was first clarified in the sketch illustrated in Fig. 3.11. The dimensions of the distributed louvered fins were extracted based on several studies (Erbay et al., 2017; Atkinsonam et al., 1998; Leu et al., 2001; Okbaz et al., 2018) to get the final configuration of the research absorber.

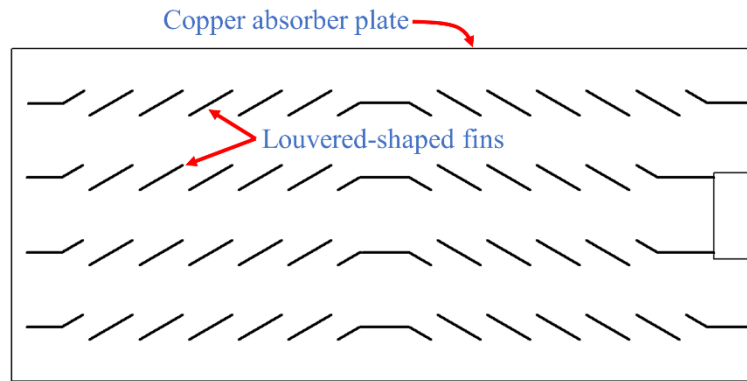


Fig. 3.11. Distribution of the louvered fins on the copper absorber

In addition to the louvered fins fixed to the absorber plate, a segment of the serpentine tube was also connected to the absorber. The final sketch of the absorber with the exact dimensions of all parts that configure the new shape of the proposed absorber is clarified in Fig. 3.12.

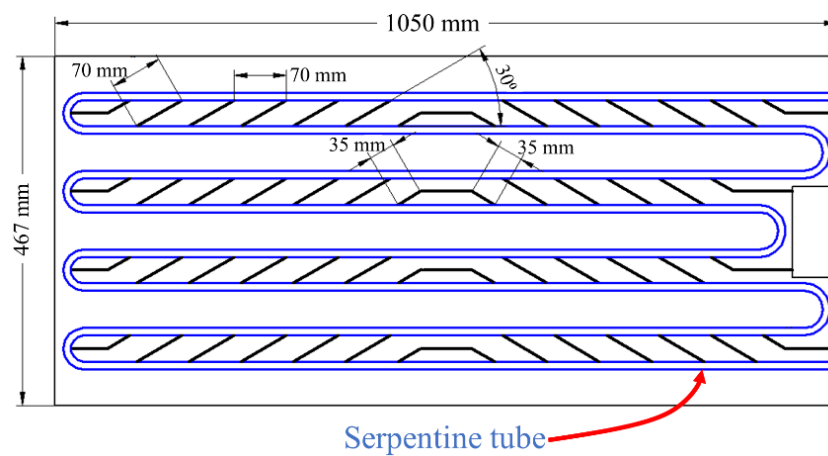


Fig. 3.12. Final sketch of the new absorber

3. Materials and methods

Based on the previous theoretical procedure, the creation process was started. Fig. 3.13 illustrates the drawing of the exact positions of the fins on the absorber plate. Additionally, the serpentine tube was created using the twisting manual machine (see Fig. 3.14).



Fig. 3.13. Drawing of the exact positions of the fins



Fig. 3.14. Creation of the serpentine tube

The first work was soldering the louvered fins and serpentine tube configurations. Sn99Cu1 soldering wire was selected for the soldering process. First, the fins were fixed in the direction of the airflow. Fig. 3.15 describes the steps of the soldering until reaching the final shape of the louvered fins designed on the absorber.

3. Materials and methods

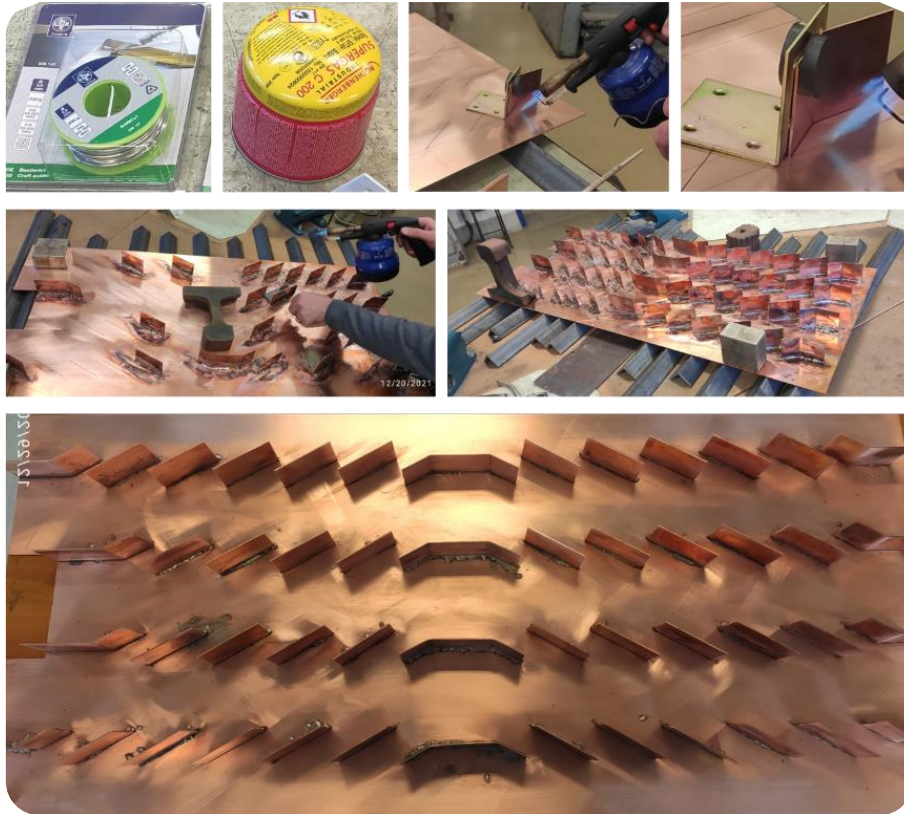


Fig. 3.15. The creation process of the fins soldering

Then, the serpentine tube was welded to the absorber plate among the louvered fins using the same soldering wire. Fig. 3.16 describes the soldering steps of the tube fixing and the final configuration of the novel absorber with louvered fins and serpentine tube.

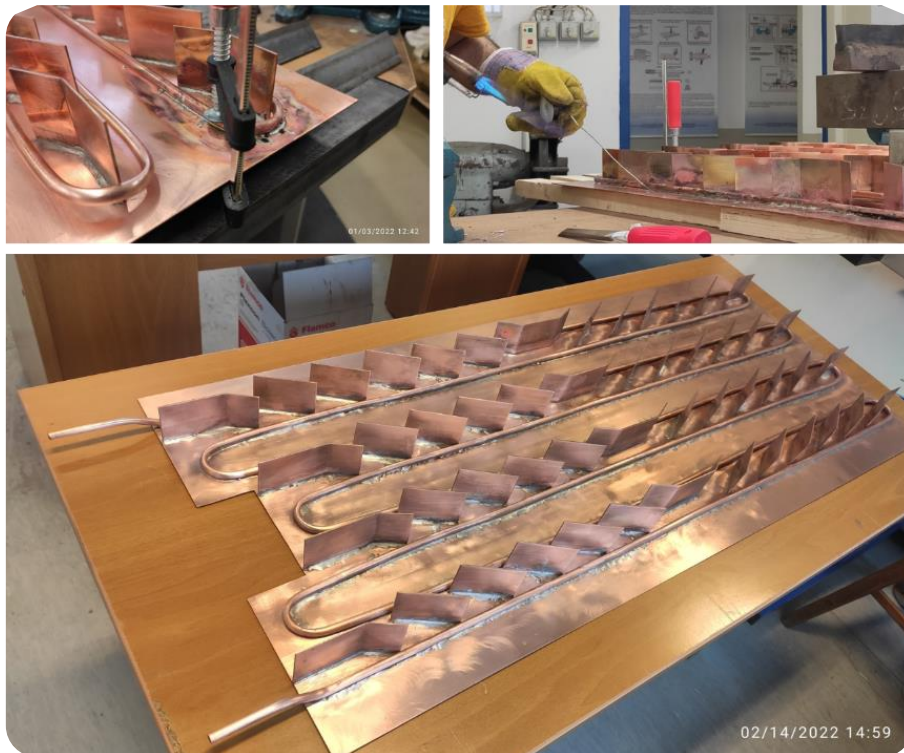


Fig. 3.16. The final configuration of the new absorber.

3.4.2. Adhering the new absorber to the conventional PV module

The PV module utilised in this research is disassembled to be used for this process, as illustrated in Fig. 3.17. The area of the PV module is 0.56 m^2 . The adhesive material (Tedlar) used to hold the new absorber behind the SolarexMSX-60 module was GHAFFARI acetoxy silicone. It is a high thermal resistor material with excellent thermal conductivity, as tested in this research (see Fig. 4.27 in the Results section). Fig. 3.18 describes the adhering process of the PV module and the absorber.

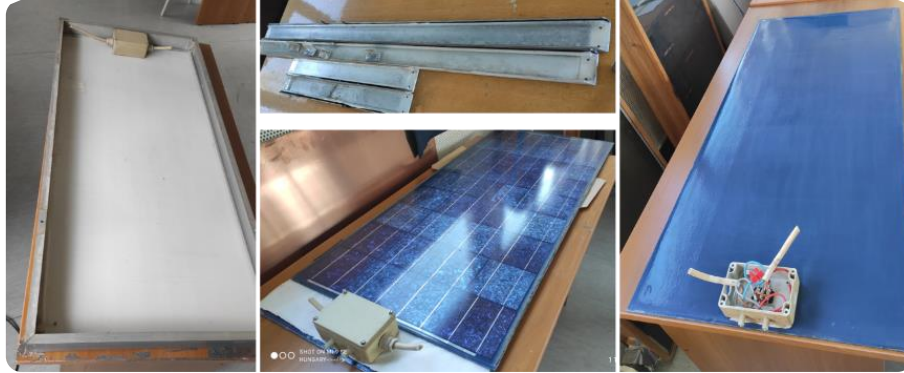


Fig. 3.17. Disassembly of the PV module



Fig. 3.18. Adhering process of the PV module

This copper combination configures the novel design presented in this research as a PV/T module with two coolant fluids (air and water).

3.4.3. Air channel and insulation

In this process, the frames of the PV module are used as air channel walls and supported by wood bars formed as insulated walls. The back side sheet of the module consists of a wood sheet of 4 mm in thickness, a bio-ceramic fibre with a 0.1 W/mK thermal conductivity as an insulation layer, and cross-linked polyethene foam with metal-film coating as the last cover. In addition, wood bars were formed as an insulated wall on the right and left sides of the module. Fig. 3.19 illustrates the process of air channel creation and insulation and the last view of the PV/T modules that were created. Additionally, the air channel dimensions are 0.05 m for the height and 0.443 m for the width.

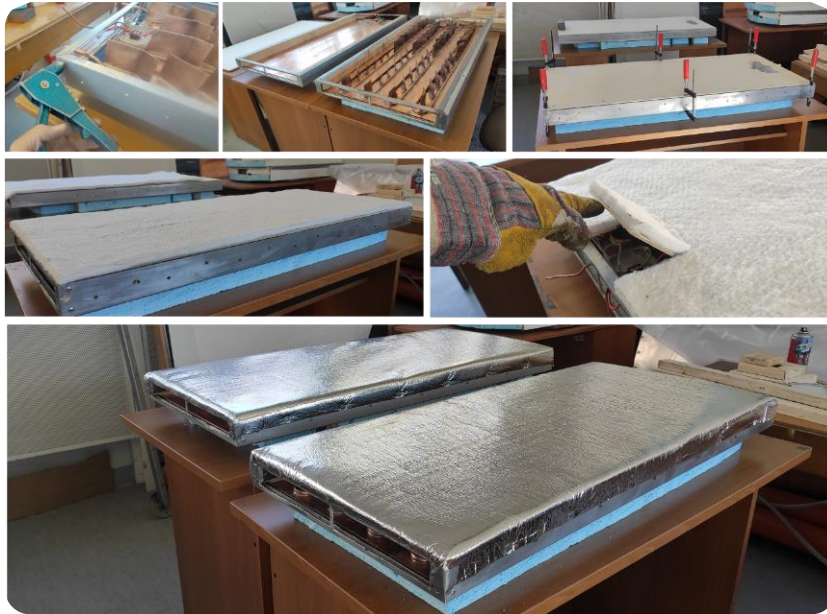


Fig. 3.19. The creation of the air channel and the insulation

3.4.4. Air and water streams

A controlled axial AC fan (Xpelair XIM-100+) was used to flow the air in modules of this research; the fan was positioned in the outlet of the PV/T modules utilising air ducts created manually via cardboard plastic plate 100 mm PVC plastic pipes. Fig. 3.20 illustrates the creation process of the airflow ducts and pipes. Besides, a controlled DC pump (MSW-M-WPP) circulated the water through the serpentine tube using water fittings and silicon pipes.

Based on the previous creation process, Fig. 3.21 illustrates the final actual view of the experimental setup. It shows standalone photovoltaic modules, air-cooled photovoltaic thermal modules, and bi-fluid photovoltaic thermal modules; these units illustrated in Fig. 3.21 are mostly used in this research.



Fig. 3.20. Airflow ducts and pipes of the systems

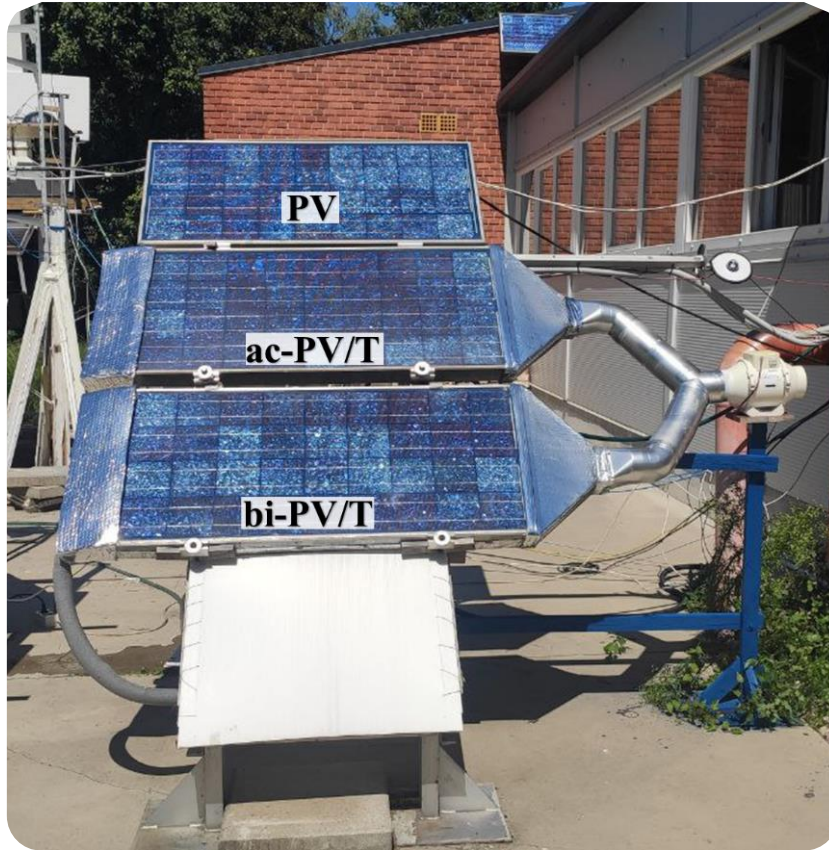


Fig. 3.21. Actual image of an experimentation systems

3.4.5. Creation of the heat exchanger tank

The warm water that exits from the PV/T modules goes to the heat exchanger tank for cooling and exits the tank to the inlet of the PV/T module. This tank is made of plastic, and a copper helical tube was manufactured and inserted inside this tank. Additionally, bio-ceramic fibre and polyethene foam were used for the tank insulation. Fig. 3.22 illustrates the manufacturing steps of the heat exchanger tank.

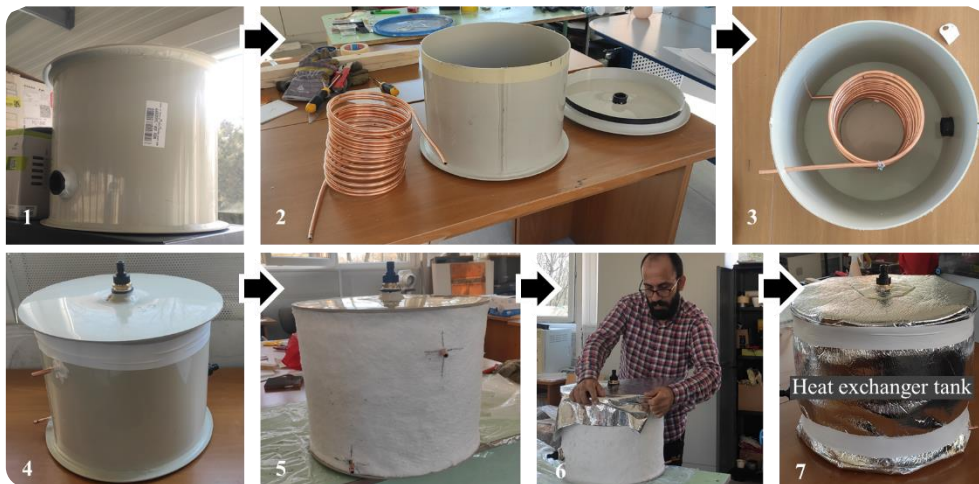


Fig. 3.22. Manufacturing steps of the heat exchanger tank

3.4.6. Comparison modules

This research manufactured two more PV/T modules to utilise them to evaluate the novel design and developed in this research, which is detailed in the previous subsections.

3.4.6.1 Verticals fins-based air-cooled PV/T module

In order to evaluate the performance of the louvered fins, the most commonly used vertical fins were utilised and fixed to the copper absorber air-cooled PV/T module, as illustrated in Fig. 3.23. To make an appropriate comparison, the area of the vertical fins was the same as that of the louvered fins. The insulation process completed in the previous module was also repeated in this module.

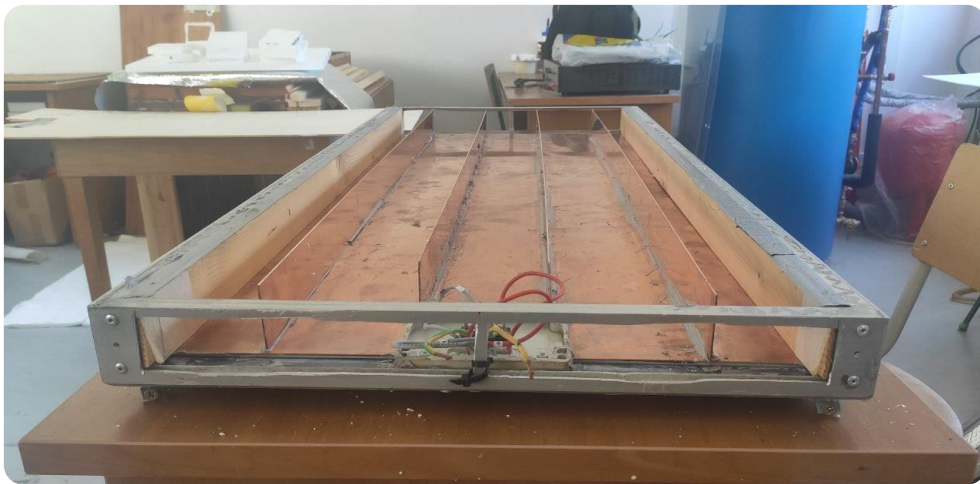


Fig. 3.23. Vertical fins of the air-cooled PV/T module

3.4.6.2 Water-cooled PV/T module via serpentine tube

A water-cooled PV/T module is another classical type of this realm of PV/T. In this experiment, a serpentine tube was created again and fixed directly to the back side of the PV modules using the same thermal Tedlar that was used to adhere the PV module to the absorber. Bio-ceramic fibre, white cork, wood bars, and wood sheets were used to insulate and form the water-cooled PV/T module. Fig. 3.24 illustrates the creation process of the new water-cooled module.

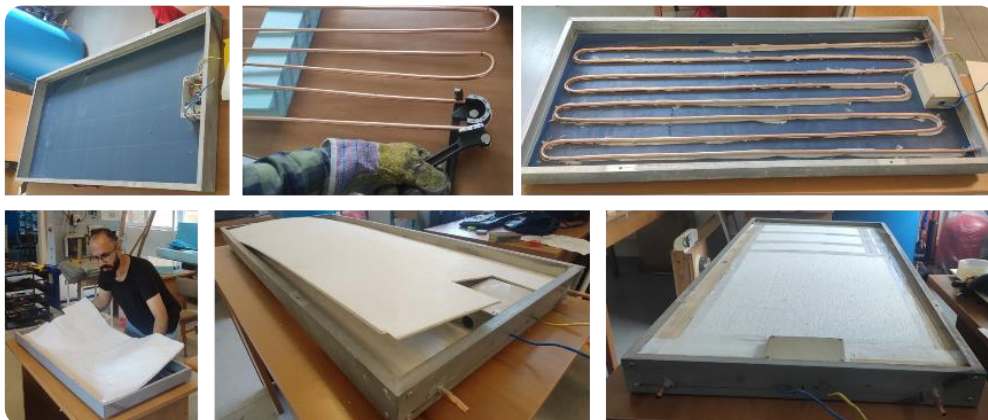


Fig. 3.24. Creation steps of the water-cooled PV/T module

3.5. Nanotechnology assessments

Another efficiency enhancement factor in the solar systems field is the heat transfer fluid, and the most common and widely used in solar systems are nanofluids, which are used as a heat transfer fluid. Consequently, this research considered MWCNTs and homogenised them with magnesium oxide (MgO) and boron nitride (BN) – first used- to make ternary and binary hybrid nanofluids in different ratios and volume concentrations.

Based on the above and the difficulty of conducting thermal conductivity tests, this research designed a novel instrument to generate a new characteristic, especially for nanofluids and generally for all fluids. This device depends on the time required for the nanofluid to reach thermal equilibrium status.

3.5.1. Actual statement

Energy researchers, mainly focusing on comparing and evaluating heat transfer rates of nanofluids, need to measure the thermal conductivity of such fluids. The point worth mentioning in this research is the limitations that impede conducting the thermophysical examinations of nanofluids, especially the hybrid types, because of the creation of a new liquid based on previously specified materials, and the researcher needs thermal conductivity to compare among them and choose the best thermally. Especially if the researchers have more than one hybrid nanofluid type at various concentrations and thus generate many samples of nanofluids, the limitations of the above statement could be listed as follows:

- The thermal conductivity analyser is unavailable at the institution to which the researcher belongs.
- The thermal conductivity analyser is unavailable in the country where the researcher is studying.
- If the analyser is available, in that case, the test fees may be high when the researcher needs to examine a large number of concentrations of nanofluids.
- The cost of purchasing the device is extremely high.

All these restrictions lead to the researcher's delay in choosing the appropriate fluid if the study involves more than three types and different concentrations, which makes it difficult and expensive. From this standpoint and to avoid these restrictions, this research proposes a new property for liquids based on the time it takes to reach a state of thermal equilibrium. This research designed a new and straightforward device through which it is possible to calculate the time required for the nanofluid to reach thermal equilibrium. This research called this device a "Fluid Thermal Equilibrium Tester" (FTET). Knowing that time allows for thermally comparing and evaluating various types of nanofluids at various concentrations. Based on thermodynamic science, fluids with less thermal equilibrium time have a high heat transfer rate (Cengel, 2011).

3.5.2. Creation of the fluid thermal equilibrium tester

Thermodynamic equilibrium refers to the state of a system in which all pertinent forms of equilibrium are duly fulfilled. When the systems are isolated from their environment, they remain in an equilibrium state without facing any changes. Thermal equilibrium is achieved inside systems when the temperature is uniform. Based on the state of Zeroth's law of

thermodynamics, “Two bodies are in thermal equilibrium if both have the same temperature reading even if they are not in contact”(Cengel, 2011).

From this point, the idea behind creating the fluid thermal equilibrium tester (FTET) is generated. The importance of the device is to create two thermodynamic systems, apply a heat source to one, and the other will be in thermal equilibrium in a while. The design idea is to make two cylinders, one inside the other, to form the two thermal systems. Fig.3.25a illustrates the sketch of the FTET instrument. Cylinder B is filled with boiling distilled water (DW), which is the highest heat source in the device. Thermodynamically, heat moves from the high-temperature system to the lower one. Through temperature sensors inserted in the two cylinders, as shown in Fig. 3.26a, which are connected to the data logger system, the time of heat transfer from the initial state when the boiling water is put in until the equilibrium state is calculated.

The A cylinder was firmly fixed to the B cylinder with a special adhesive. Then, cylinders A and B were combined into the C cylinder. After that, compressed sawdust was filled into the C cylinder, as clarified in Fig. 3.25b, which illustrates all the configuration steps. The cost of the device components was very low, estimated at 20 euros.

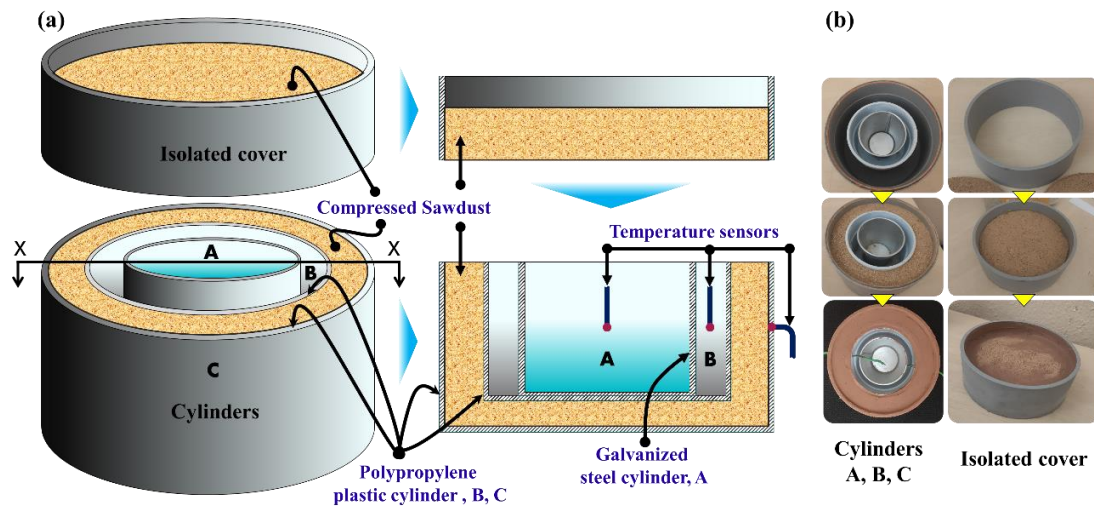


Fig. 3.25 a) 3-D configuration of the FTET instrument, b) experimental step of the FTET configuration

The steps of the test are as follows and as described in Fig. 3.26:

1. Turn on the data logger.
2. Boil the distilled water.
3. Fill in cylinder A with nanofluids.
4. Fill in the cylinder B with a boiling water.
5. Close the system perfectly with the isolated cover.
6. Monitoring the temperatures on the data logger display until the $T_A=T_B$.
7. Turn off the data logger.
8. Now, the equilibrium time is ready by computer data analysis.

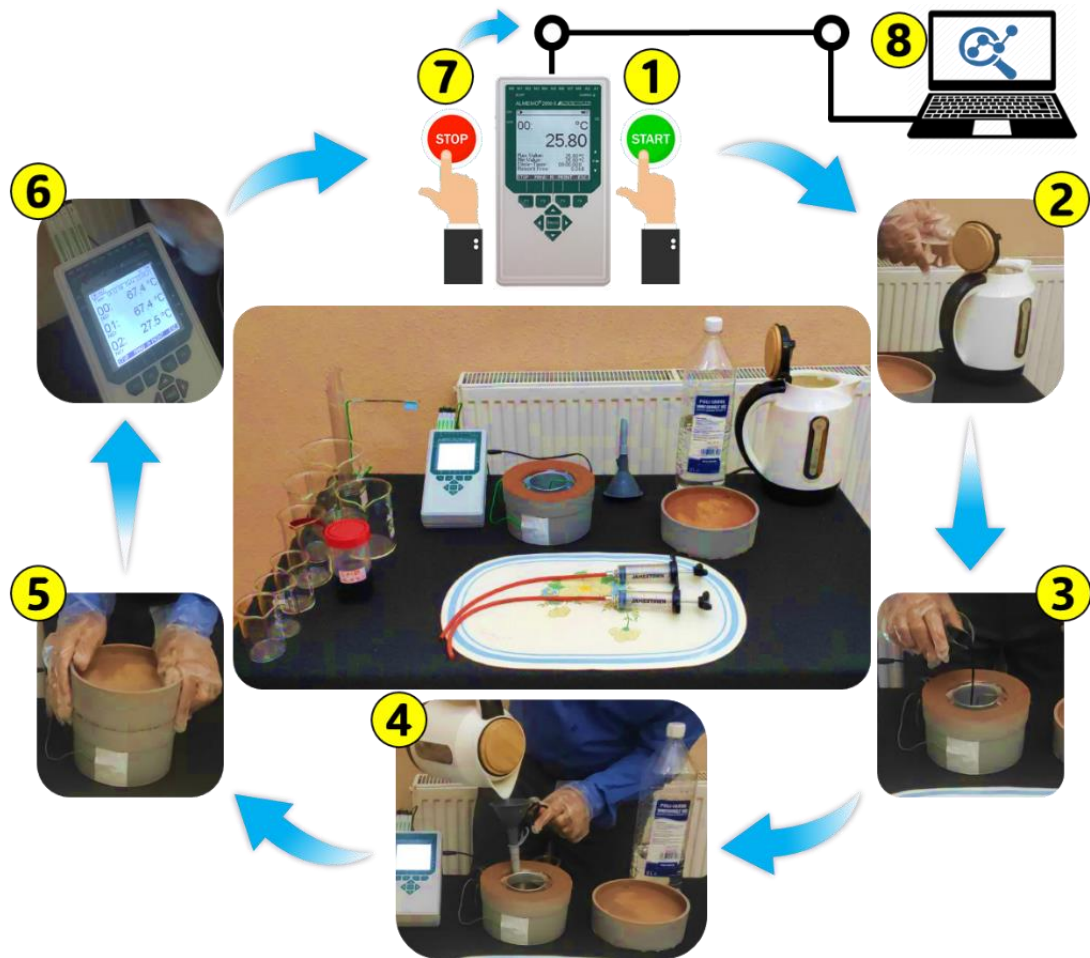


Fig. 3.26. The experimental steps of the FTET with an actual steps view

The following easy points are crucial to consider by the investigator to pass the test successfully:

- Ensure that the test cylinders are well isolated from all sides,
- Ensure that the water is replaced before boiling because the properties of water, change after the boiling process. Repeat water replacement for each test,
- To do the second test, after completing the first test, wait until the device and its parts reach room temperature to ensure the same circumstances for each test,
- Strictly ensure that the procedure time is the same for the all-sample tests to ensure the same circumstances for each test,
- Ensure the same values of the initial temperature of the boiling water and nanofluids.

Besides, the test provides the following parameters:

- Equilibrium temperature,
- The thermal equilibrium time,
- Nanofluids specific heat,
- The transferred heat to the nanofluids.

3.5.3. Ternary and binary nanoparticles synthesis

This research uses multi-walled carbon nanotubes (MWCNTs), magnesium oxide (MgO), and boron nitride (BN) nanoparticles to create four nanoparticles' composites based on different weight ratios as follows:

- 1- Ternary hybrid nanoparticles comprised of 50% MWCNTs, 25% MgO, and 25% BN.
- 2- Binary hybrid nanoparticles comprised of 50% MWCNTs and 50% MgO.
- 3- Binary hybrid nanoparticles comprised of 50% MWCNTs and 50% BN.
- 4- Binary hybrid nanoparticles comprised of 50% MgO and 50% BN.

The four nanoparticle composites were mixed and homogenised using an electrical pre-shaker and ball milling (see Fig. 3.27).

3.5.4. Nanofluids preparation

This research prepared the nanofluids of each nanoparticle's composites mentioned in section 3.5.3 through six volume concentrations, 0.05, 0.1, 0.2, 0.3, 0.4, and 0.5%. Table 3.5 describes and lists all information on the proposed nanoparticles. Distilled water is the base fluid used during the experiment of nanofluid preparation with the FTET instrument. Table 3.5 lists the properties of the distilled water used.

Table 3.5. Specification of proposed nanoparticles





Nanoparticles	BN	MgO	MWCNTs
Actual view			
Morphological shape	hexagonal	polyhedral	cylindrical
Purity	99%	99%	97%
Density	2.29 g/cm ³	3.58 g/cm ³	2.1 g/cm ³
Size	70 nm	20 nm	outer diameter: 60-100 nm length: > 5 μm
Specific surface area	19.4 m ² /g	20.3 m ² /g	40-70 m ² /g
Colour	white	white	dark black
Appearance	powder	powder	powder

Table 3.6. Specification of the base fluid

	Base fluid	Distilled water
Brand		POLI-FARBE
Density		997 kg/m ³
pH		4
TDS, total dissolved solids		40 ppm
Boiling temperature		98.5 °C








Two pre-steps were conducted before the most commonly used method (two-step) to prepare nanofluids in this research. An electrical shaker and ball milling devices were used to homogenise the proposed ternary and binary hybrid nanoparticles to achieve homogeneity. The instruments used in this research to prepare study nanoparticles and the time spent by each

3. Materials and methods

device to finish the sample preparation are illustrated in Table 3.7. Fig. 3.27 describes the detailed steps of preparing ternary and binary nanofluids while four DW-based-nanofluids have been prepared as follows:

- Ternary hybrid nanofluids, MWCNTs–MgO- BN (A).
- Binary hybrid nanofluids, MWCNTs–MgO (B).
- Binary hybrid nanofluids, MWCNTs–BN (C).
- Binary hybrid nanofluids, MgO–BN (D).

Table 3.7. Purposes and details of preparation devices.

Device	Actual view	Brand/Model	Purpose	Time
Precision scale		SUPERIOP /SCL-i-2000	Nanoparticle weighing	-
Electrical Shaker		VORTEX / QL-861	Pre-shaker of nanoparticles	15 minutes
Ball milling		TMAX /MQM-0.4	Mill and homogenizes the ternary and binary nanoparticles	2 hours
Magnetic stirrer		VEVOR /SH-2	- Mixing the surfactant Arabic gum with base fluid.	30 minutes
			- Mix the nanoparticles with base fluid (with surfactant).	1 hour
Ultrasonic		ELMA /E-60-H	Sonication of nanoparticles	2 hours

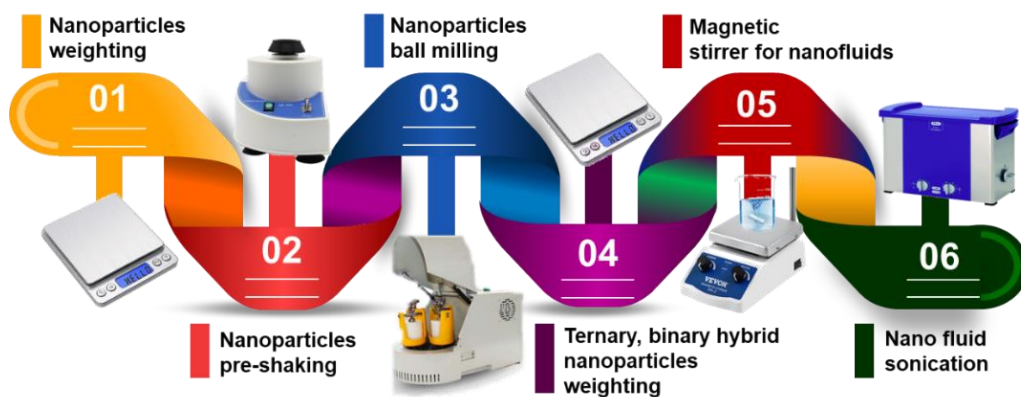


Fig. 3.27. Experimental steps of nanofluid preparation

Regarding the characterization of ternary and binary nanofluids, as this research proposes, three nanoparticles are utilised to synthesize four nanoparticles investigated to prepare four hybrid nanofluids (ternary and binary) with six volume concentrations (ϕ). As presented by (Nanda et al., 2023; Sundar et al., 2017), the formulas of the volume concentrations of ternary and binary are as given in Eqs. (3.1) and (3.2), respectively.

$$\phi_{\text{TNF}} = \frac{\frac{m_1}{\rho_1} + \frac{m_2}{\rho_2} + \frac{m_3}{\rho_3}}{\frac{m_1}{\rho_1} + \frac{m_2}{\rho_2} + \frac{m_3}{\rho_3} + \frac{m_{\text{DW}}}{\rho_{\text{DW}}}} \quad (3.1)$$

$$\phi_{\text{BNF}} = \frac{\frac{m_1}{\rho_1} + \frac{m_2}{\rho_2}}{\frac{m_1}{\rho_1} + \frac{m_2}{\rho_2} + \frac{m_{\text{DW}}}{\rho_{\text{DW}}}} \quad (3.2)$$

Besides, the density and specific heat for the ternary (TNF) and binary (BNT) nanofluids are calculated based on the following equation, respectively.

$$\rho_{\text{TNF}} = \rho_1\phi_1 + \rho_2\phi_2 + \rho_3\phi_3 + (1 - \phi_{\text{TNF}})\rho_{\text{DW}} \quad (3.3)$$

$$C_{\text{TNF}} = \frac{\rho_1\phi_1C_1 + \rho_2\phi_2C_2 + \rho_3\phi_3C_3 + (1 - \phi_{\text{TNF}})\rho_{\text{DW}}C_{\text{DW}}}{\rho_{\text{TNF}}} \quad (3.4)$$

$$\rho_{\text{BNF}} = \rho_1\phi_1 + \rho_2\phi_2 + (1 - \phi_{\text{BNF}})\rho_{\text{DW}} \quad (3.5)$$

$$C_{\text{BNF}} = \frac{\rho_1\phi_1C_1 + \rho_1\phi_1C_1 + (1 - \phi_{\text{BNF}})\rho_{\text{DW}}C_{\text{DW}}}{\rho_{\text{BNF}}} \quad (3.6)$$

It is worth noting that nanofluids significantly affect heat transfer, as they have a high thermal conductivity compared to traditional fluids. However, it still has some issues that need solutions to be more reliable. One of these problems is stability, which is related to sedimentation. The ternary nanofluid used in this research gives good results in stability and sedimentation thanks to the surfactant utilised to dissolve the base fluid nanoparticles. Gum Arabic was used as a surfactant as it has the ability to stabilise the nanofluids (Ding et al., 2006). Another issue is the corrosion of the nanofluid that affects the pipes. The nanofluid used in this research has the potential for corrosion resistance, as stated by Joseph and Thomas (2022).

Besides, nanofluids could be disposed of nano-fluids after use in solar panels after use in solar systems by treatment or neutralization via chemical or physical processes to break down or neutralize the nanoparticles. These processes may be employed to mitigate any potential environmental impact.

3.5.5. Thermodynamic model of the fluid thermal equilibrium tester

Before going through the thermodynamic model, the following points are the assumptions of the FTET instrument circumstances.

- Both distilled water and nanofluids are incompressible substances.

- Specific heat (C) of the distilled water and the nanofluids are constant at room temperature.
- Since the system is stationary, there is no change in the kinetic (ΔKE) or potential (ΔPE) energy, so their values are zero.
- No mechanical or other form of work is implicated.
- The system is adequately insulated; thus, there is no transfer of mass and heat.

Fig. 3.28 clarifies the entire contents of the FTET device as a schematic thermodynamic system. The system under consideration can be classified as closed due to the absence of any mass transfer across its boundary throughout the procedure.

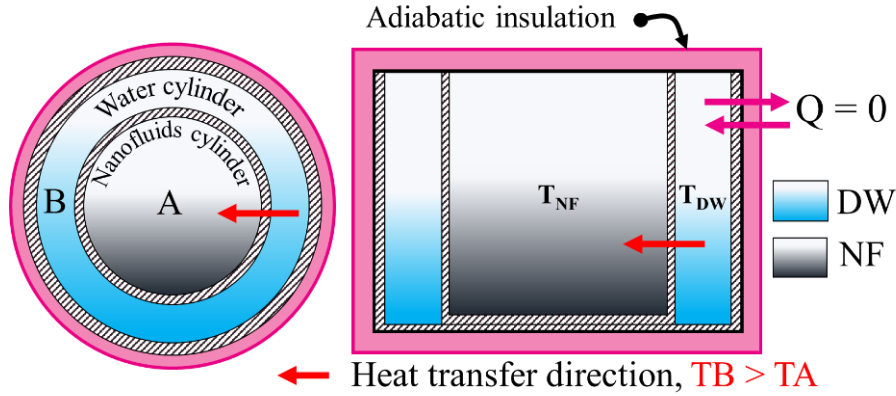


Fig. 3.28. Schematic thermodynamic system of the FTET instrument

As depicted in Fig. 3.28, it is evident that the volume of a system remains constant, hence resulting in no indication of boundary work. The energy E balance of the entire system can be mathematically represented in the following equations:

$$E_{in} - E_{out} = \Delta E_{System} \quad (3.7)$$

$$E_{in} - E_{out} = \Delta U + \Delta KE + \Delta PE \quad (3.8)$$

Because of no transfer in mass and heat in the system, then $E_{in} - E_{out} = 0$, and because the system is stationary, then $\Delta KE = \Delta PE = 0$, Eq. (3.7) could be expressed as just an internal energy change ΔU :

$$0 = \Delta U \quad (3.9)$$

The overall internal energy U is an extensive thermodynamic characteristic; consequently, it could be evidenced as the totality of the water and nanofluid internal energy. So, Eq. (3.9) can be articulated as the following equations:

$$\Delta U_{sys} = \Delta U_{DW} + \Delta U_{NF} = 0 \quad (3.10)$$

$$m_{DW}C_{DW}(T_{Eq} - T_{DW}) + m_{NF}C_{NF}(T_{Eq} - T_{NF}) = 0 \quad (3.11)$$

where m , C , and T are the mass, specific heat, and temperature of distilled water DW and nanofluid NF , and T_{Eq} is the equilibrium state temperature.

Based on Eq. (3.11), Eq. (3.12) describes the specific heat of the hybrid nanofluids.

$$C_{NF} = \frac{m_{DW}C_{DW}(T_{DW} - T_{Eq})}{m_{NF}(T_{Eq} - T_{NF})} \quad (3.12)$$

The heat transferred to the nanofluid Q_{NF} until the system reaches the thermal equilibrium state could be expressed by Eq. (3.13).

$$Q_{NF} = m_{NF}C_{NF}(T_{Eq} - T_{NF}) \quad (3.13)$$

Based on the test conducted by the FTET instrument, the study computes the thermal equilibrium time (t_{Eq}). Based on that, the heat transfer per unit of time during the process from the initial state until the thermal equilibrium state could be determined using the following equation:

$$\dot{Q}_{NF} = \frac{Q_{NF}}{t_{Eq}} \quad (3.14)$$

Besides, the most significant thermodynamical factor of the fluids is the heat transfer coefficient, which is considered an indicator to evaluate the heat transfer fluids. Based on the thermodynamic schematic model in Fig. 3.29 and its mathematical heat transfer model, it could be possible to calculate the heat transfer coefficient of nanofluids in the FTET instrument as the properties of water are already known. This methodology is first used to calculate the overall heat transfer coefficient by the effect of the nanofluids.

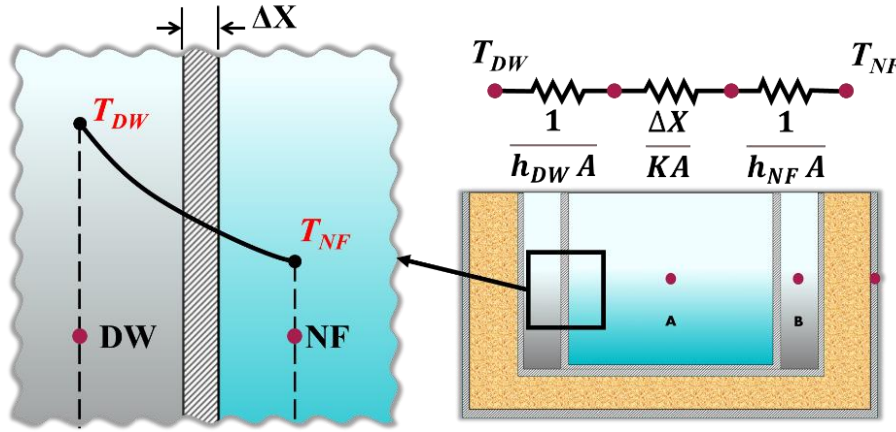


Fig. 3.29. Thermodynamic schematic of heat transfer coefficient

Based on the schematic in Fig. 3.29, the heat transfer rate could be calculated by the following equation (Cengel, 2003):

$$\dot{Q}_{DW \rightarrow NF} = \frac{T_{DW} - T_{NF}}{\frac{1}{h_{DW} A} + \frac{\Delta X}{KA} + \frac{1}{h_{NF} A}} \quad (3.15)$$

where h , A , ΔX , and K are the heat transfer coefficient, convective area, thickness, and thermal conductivity.

The overall heat transfer coefficient (h) of the system is described by the Eq. (3.16):

$$h_{\text{overall}} = \frac{1}{\frac{1}{h_{\text{DW}}} + \frac{\Delta X}{K} + \frac{1}{h_{\text{NF}}}} \quad (3.16)$$

Then, Eq. (3.15) could be written as:

$$\dot{Q}_{\text{DW} \rightarrow \text{NF}} = h_{\text{overall}} A (T_{\text{DW}} - T_{\text{NF}}) \quad (3.17)$$

Then, the overall heat transfer coefficient of the system is:

$$h_{\text{overall}} = \frac{\dot{Q}_{\text{DW} \rightarrow \text{NF}}}{A (T_{\text{DW}} - T_{\text{NF}})} \quad (3.18)$$

Based on the results obtained from the FTET instrument, the optimum nanofluids were chosen and used in the research experiments through the new bi-PV/T module and compared with the module used the DW as a heat transfer fluid through the serpentine tube fixed to the copper absorber.

3.6. Instrumentations

Numerous instruments and sensors are employed to acquire data during the experimental phases of this research. Two data loggers were used to gather several parameters during the experiments. Additionally, a desktop computer was used to run the display moods to monitor the sensor values. VOLTcraft-1602-Pro was the DC power supply. Fig. 3.30 shows a view of the data logger with the computer during the measurement time. Table 3.8 describes the specifications of data loggers. Besides, the data measured for all experiments are as follows:

- Input and output temperatures of air and water
- Solar cell temperatures
- Module backside temperatures
- Ambient temperature
- Solar radiation
- Currents and voltages

This research employed several sensors to sense the actual data during the experiments. Besides, Fig. 3.31 shows the positions of the sensors through the experimental set-up and Table 3.9 lists all sensor types, functionalities, photos, and the associated uncertainties.

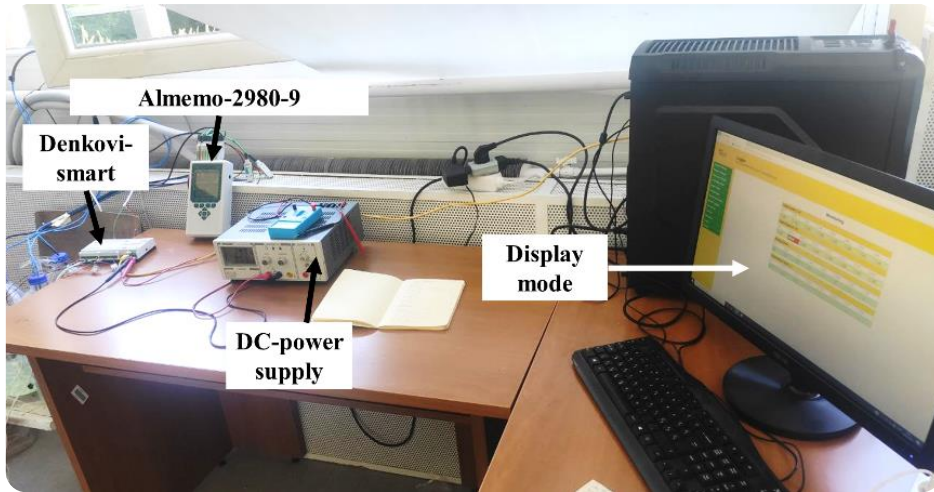


Fig. 3.30. Data logging system of an experiments

Table 3.8. Specifications of data loggers used

No.	Data logger	Measurement purpose	Photo of the device
1	Almemo-2980-9	<ul style="list-style-type: none"> • Solar radiation • Inlet and outlet water temperature • Inlet and outlet air temperature • Solar cell surface temperature 	
2	Denkovi-smart-32in	<ul style="list-style-type: none"> • Current and voltage • Ambient temperature • Module backside temperatures 	

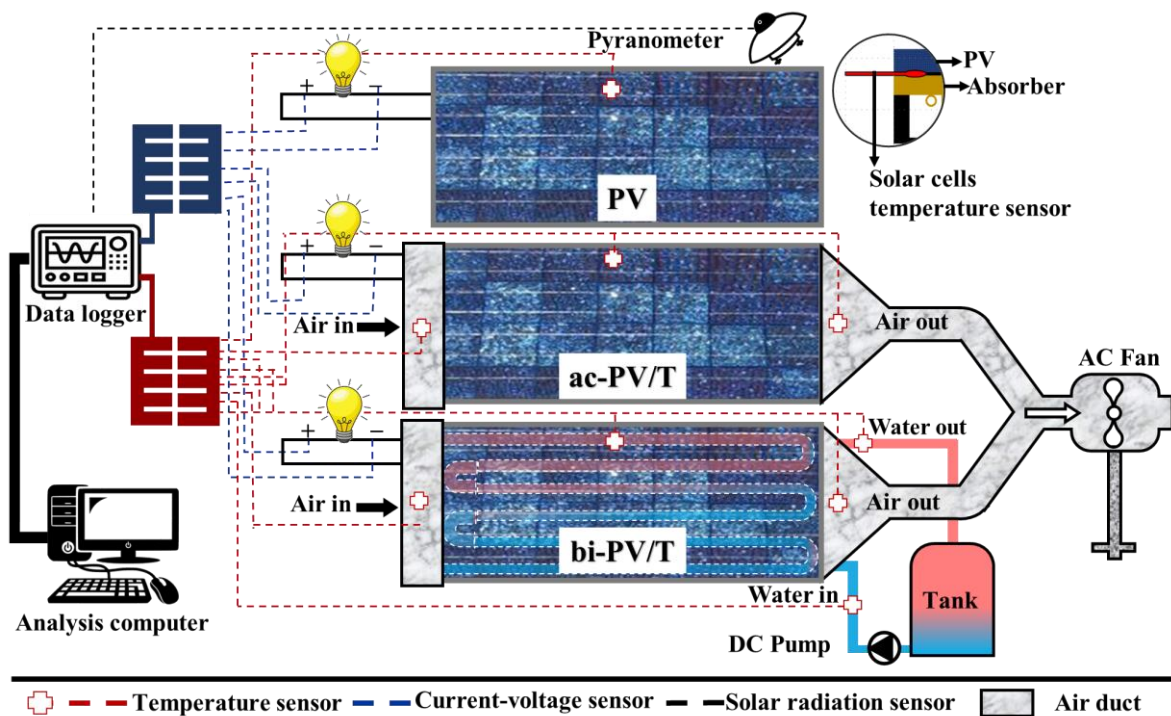






Fig. 3.31. Schematic diagram of the experiment setup and sensor placement

Table 3.9. Sensor specifications and uncertainties

Sensor model/brand	Measurement purpose	Uncertainty	Photo of the sensor
Almemo-99020FS thermocouple K-type	Temperature	$\pm 0.5\text{ }^{\circ}\text{C}$	
NTS temperature sensor B57500-M103-A005	Temperature	$\pm 0.5\%$	
DS-18B20-T	Temperature	$\pm 0.5\%$	
Pyranometer MESSKOPF-3.3	Solar radiation	$< \pm 0.5\%$	
CM11-KIPP-ZONEN Pyranometer	Solar radiation	$< \pm 0.6\%$	
Digital-YF-S402C	Water flow rate	0.02 kg/s	
ALMEMO-FVAD-35	Air speed	0.08 m/s	
MS-6252a	Digital Anemometer	0.01 m/s	
Analogue inputs within the Denkovis-smart-32-IN data logger	Instant current and voltage	$\pm 0.2\%$	

In addition to the above, this research used a high-resolution thermal camera (brand SKF-NEC-TH9260) to make the thermal images to compare the actual graphical thermal behaviour during the experimental period of the research modules. Fig. 3.32 shows the thermal camera used in this research.

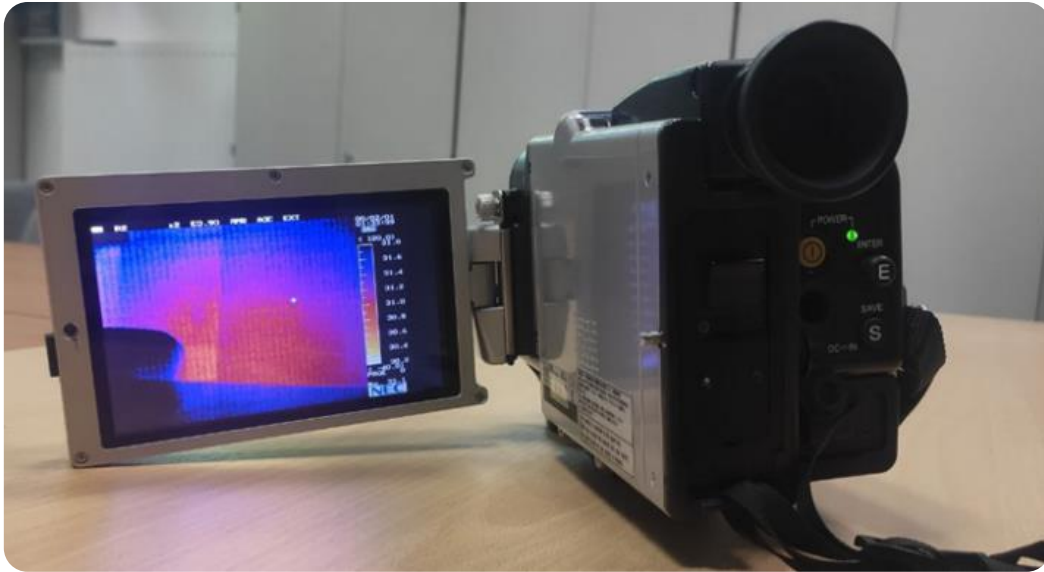


Fig. 3.32. SKF-NEC- TH9260 thermal camera

3.7. Heat transfer-thermal nodes equations

Thermodynamically, the module has several thermodynamic systems throughout its layers. Following the model of Alshibil et al. (2021), the heat transfer direction equations of the LF-PVT layers start from the ambient through glass, PV, absorber, fins, tube, air, and insulation. The neglections and assumptions of the mathematical thermal model are as follows:

- The right and left walls are well insulated; thus, they are adiabatic.
- The back side of the module is well-insulated; thus, it is an adiabatic wall.
- Glass, PV solar cells, acetoxy silicone (Tedlar), and air streams have no temperature gradients.
- The thermal conductivity of the module is constant.
- The module has entered a condition of quasi-steady state operation.
- The coefficient of heat transfer throughout the module is constant.
- Direct connection between the PV module and the new absorber.

The sky, which contains sunlight, is the first point in the heat direction throughout the layers of the LFS-PV/T module. Fig. 3.33 illustrates the nodes of the module layers and the heat-transfer mechanism between the two nodes.

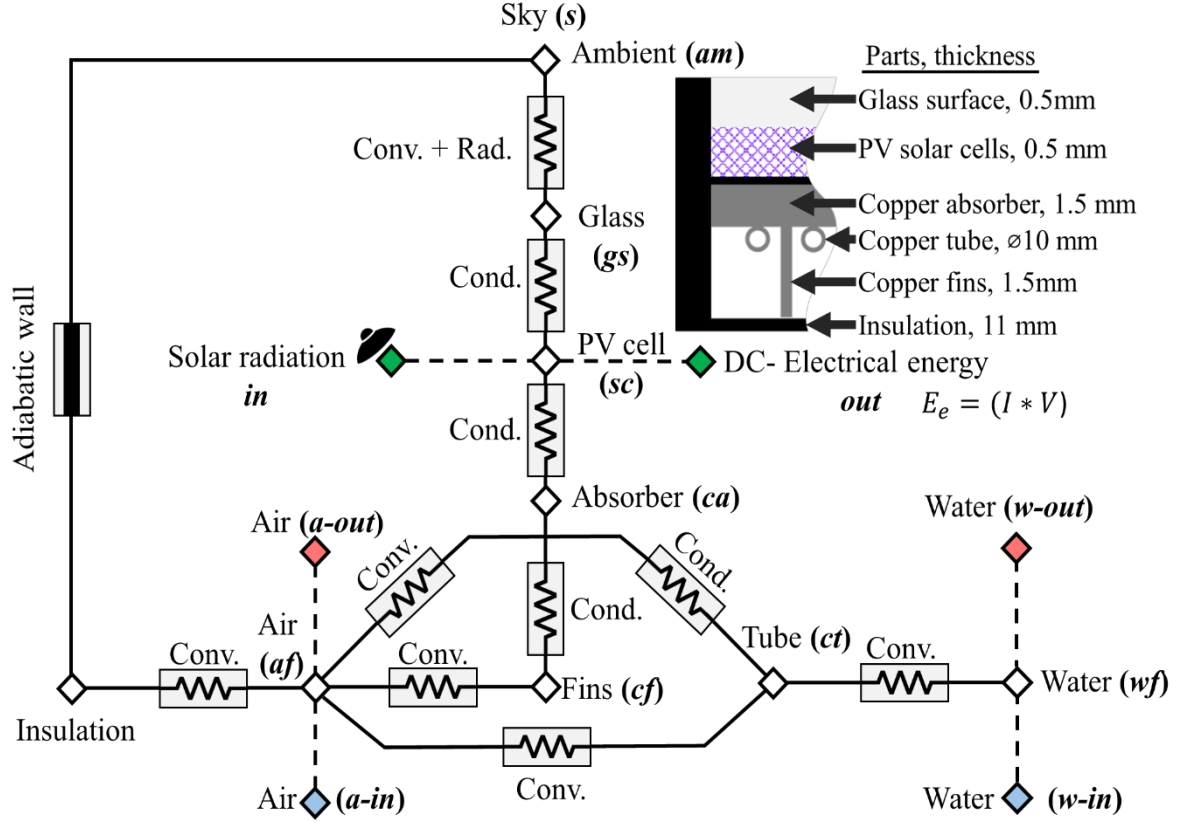


Fig. 3.331. Thermodynamic nodes of the module layers

As the first law of thermodynamics states, the following equations and figures represent the heat balance of each node, as stated in Fig. 3.34.

Glass surface node equation is (Fig. 3.34):

$$\begin{aligned} \rho_{gs} A_{gs} c p_{gs} \delta_{gs} \frac{dT_{gs}}{dt} &= E_{gs} - h_{rd,gs\sim s} A_{gs} (T_{gs} - T_{sky}) \\ &- h_{cv,gs\sim am} A_{gs} (T_{gs} - T_{am}) - h_{cd,gs\sim sc} A_{gs} (T_{gs} - T_{sc}) \end{aligned} \quad (3.19)$$

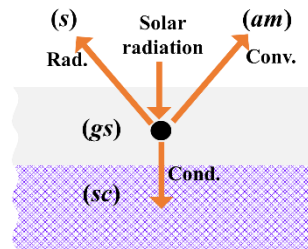


Fig. 3.34. Glass surface-node

Solar cells node equation is (Fig. 3.35):

$$\rho_{sc} A_{sc} c p_{sc} \delta_{sc} \frac{dT_{sc}}{dt} = E_{sc} + h_{cd,gs\sim sc} A_{sc} (T_{gs} - T_{sc}) - h_{cd,sc\sim ca} A_{sc} (T_{sc} - T_{ca}) - P_{el} \quad (3.20)$$

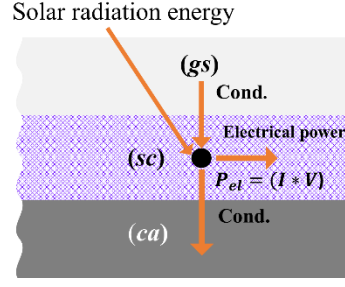


Fig. 3.35. Solar cell-node

Copper-absorber node equation is (Fig. 3.36):

$$\rho_{ca} A_{ca} c p_{ca} \delta_{ca} \frac{dT_{ca}}{dt} = h_{cd,sc \sim ca} A_{ca} (T_{sc} - T_{ca}) - h_{cd,ca \sim ct} A_{ca,ct} (T_{ca} - T_{ct}) - h_{cd,ca \sim cfi} A_{ca,cfi} (T_{ca} - T_{cfi}) - h_{cv,ca \sim af} A_{ca,af} (T_{ca} - T_{af}) \quad (3.21)$$

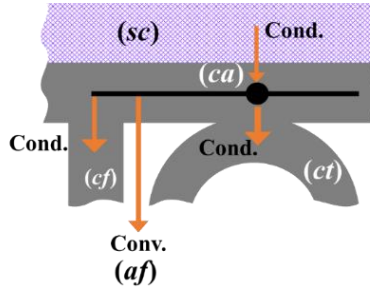


Fig. 3.36. Copper absorber-node

The air-flow node equation is (Fig. 3.37):

$$\rho_{af} A_{af} c p_{af} \delta_{af} \frac{dT_{af}}{dt} = h_{cv,ca \sim af} A_{ca,af} (T_{ca} - T_{af}) + h_{cv,cfi \sim af} A_{cfi} (T_{cfi} - T_{af}) + h_{cv,ct \sim af} A_{ct,af} (T_{ct} - T_{af}) - \dot{m}_{af} c p_{af} (T_{a-out} - T_{a-in}) \quad (3.22)$$

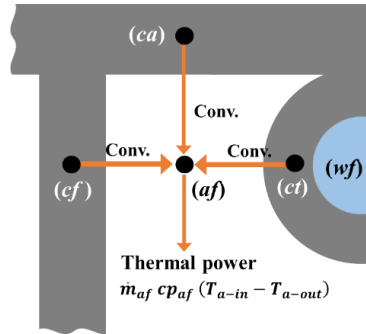


Fig. 3.37. Air flow-node

Copper-fins node equation is (Fig. 38):

$$\rho_{cf} A_{cf} c p_{cf} \delta_{cf} \frac{dT_{cf}}{dt} = h_{cd,ca \sim cf} A_{cf} (T_{ca} - T_{cf}) - h_{cv,cf \sim af} A_{cf,af} (T_{cf} - T_{af}) \quad (3.23)$$

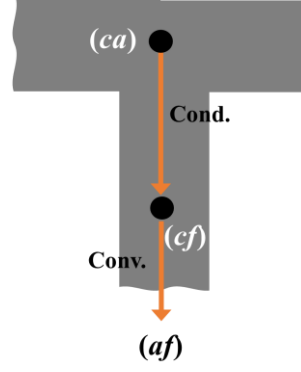


Fig. 3.38. Copper fins-node

Copper-tube node equation is (Fig. 39):

$$\rho_{ct} A_{ct} c p_{ct} \delta_{ct} \frac{dT_{ct}}{dt} = h_{cd,ca \sim ct} A_{ca,ct} (T_{ca} - T_{ct}) - h_{cv,ct \sim af} A_{ct,af} (T_{ct} - T_{af}) - h_{cv,ct \sim wf} A_{ct,wf} (T_{ct} - T_{wf}) \quad (3.24)$$

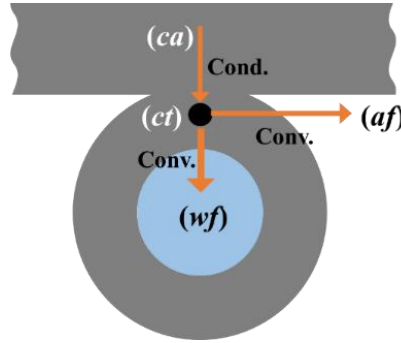


Fig. 3.39. Copper tube-node

Water flow node equation is (Fig. 40):

$$\rho_{wf} A_{wf} c p_{wf} \delta_{wf} \frac{dT_{wf}}{dt} = h_{cv,ct \sim wf} A_{ct,wf} (T_{ct} - T_{wf}) - \dot{m}_{wf} c p_{wf} (T_{w-out} - T_{w-in}) \quad (3.25)$$

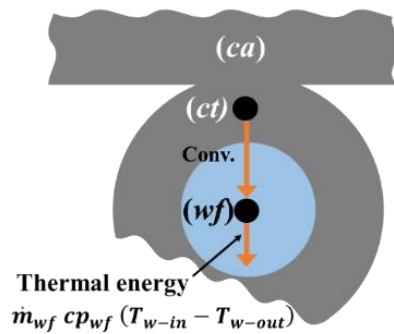


Fig.3.40. Water flow-node

The literature provided radiative, conductive, and convective heat transfer coefficient correlations and the air and water thermophysical characteristics (H. Boumaaraf et al., 2022; Gertzos et al., 2008; Rejeb et al., 2015; Zondag et al., 2002). The heat transfer coefficient h formulas for all PV/T layers are presented as follows:

Between the sky and the glass surface:

$$h_{rd,gs\sim s} = \varepsilon_g \sigma (T_g^2 + T_s^2)(T_g + T_{sky}) \quad (3.26)$$

Where T_{sky} is the sky temperature, which is indicated by Eq. 3.27:

$$T_{sky} = 0.0552 T_a^{1.5} \quad (3.27)$$

Between the glass and the ambient based on the wind speed V_w :

$$h_{cv,gs\sim am} = 2.8 + 3V_w \quad (3.28)$$

Between the solar cells and the glass surface:

$$h_{cd,gs\sim sc} = \left[\frac{\delta_g}{K_g} + \frac{\delta_{sc}}{K_{sc}} \right]^{-1} \quad (3.29)$$

Between the solar cells and the copper absorber:

$$h_{cd,sc\sim ca} = \left[\frac{\delta_{ca}}{K_{ca}} + \frac{\delta_{sc}}{K_{sc}} \right]^{-1} \quad (3.30)$$

Between the copper absorber and copper tube:

$$h_{cd,ca\sim ct} = \left[\frac{\delta_{ca}}{K_{ca}} + \frac{\delta_{ct}}{K_{ct}} \right]^{-1} \quad (3.31)$$

Between the copper absorber and copper fins:

$$h_{cd,ca\sim cfi} = \left[\frac{\delta_{ca}}{K_{ca}} + \frac{\delta_{cfi}}{K_{cfi}} \right]^{-1} \quad (3.32)$$

The convective heat transfer coefficient for the airflow within the air channel is as follows:

$$h_{cv} = \frac{Nu K_f}{D_h} \quad (3.33)$$

D_h is the hydraulic diameter indicated by:

$$D_h = \frac{4WD}{2(W + D)} \quad (3.34)$$

where D is the tube or the channel depth, and W is the width of the air channel.

Nu is the Nusselt number and some correlations were presented by Bergman et al. (2011) for forced airflow; the formulas of the Nu are listed below based on the type of flow:

For laminar flow (Reynolds number: $Re < 2300$):

$$\text{Nu} = 5.4 + \frac{0.00190 \left[\text{Re Pr} \left(\frac{D_h}{L} \right) \right]^{1.71}}{1 + 0.00563 \left[\text{Re Pr} \left(\frac{D_h}{L} \right) \right]^{1.71}} \quad (3.35)$$

where Pr is the Prandtl number.

For turbulent flow (Reynolds number: $\text{Re} > 6000$):

$$\text{Nu} = 0.116 \left(\text{Re}^{\frac{2}{3}} - 125 \right) \text{Pr}^{\frac{1}{3}} + \left[1 + \left(\frac{D_h}{L} \right)^{\frac{2}{3}} \right] \left(\frac{\mu}{\mu_w} \right)^{0.14} \quad (3.36)$$

where μ is the viscosity.

For transitional flow (Reynolds number: $2300 < \text{Re} < 6000$):

$$\text{Nu} = 0.018 \text{Re}^{0.8} \text{Pr}^{0.4} \quad (3.37)$$

3.8. Performance assessment and exergy analysis

The electrical productivity of the presented PV/T modules was evaluated against that achieved by the reference PV module. The following standard formula (Duffie and Beckman, 2013) identifies the maximum electrical power productivity:

$$P_{el} = I_{mx} V_{mx} \quad (3.38)$$

Eq. (3.39) defined the ratio of the output power as electrical power to the input power as solar radiation received by the solar cell area as the momentary electrical production efficiency (Ahmed et al., 2020):

$$\eta_{el} = \frac{P_{el}}{S A} \quad (3.39)$$

where A is the area of the PV/T module, and its value is 0.56 m^2 .

On the other hand, Zondag et al. (2003) show the electrical productivity efficiency of the PV module's solar cells as a function of the cell temperature of the PV unit:

$$\eta_{el} = \eta_{STC} (1 - \beta_{ref}(T_{sc} - T_{STC})) \quad (3.40)$$

As stated by Kumar et al. (2011), the efficiency of the cells η_{STC} based on the Standard-Test-Condition is as follows:

$$\eta_{STC} = \frac{P_{el}}{S_{STC} A} \quad (3.41)$$

The utilised thermal achievement of the PV/T modules is categorised into two heat gains, water and air, according to the type of hybrid collector. As Choi et al. (2020) reported, Eq. (3.42) verified the air heat-gain equation:

$$Q_{u,a} = \dot{m}_a c_{p_a} (T_{a-out} - T_{a-in}) \quad (3.42)$$

The rate of airflow \dot{m}_a is:

$$\dot{m}_a = \rho_a v_a A_{in,d} \quad (3.43)$$

The water heat-gain equation is:

$$Q_{u,w} = \dot{m}_w c_{p_w} (T_{w-out} - T_{w-in}) \quad (3.44)$$

The heat-gain efficiency of the PV/T modules is specified as a ratio of output energy as a heat-gain to the output energy as incident solar radiation, as Duffie and Beckman (2013) mentioned in the following equations:

The heat-gain efficiency for the AC-PV/T module is:

$$\eta_{th,ac-PV/T} = \frac{Q_{u,a}}{S A} \quad (3.45)$$

The heat-gain efficiency for the WC-PV/T module is:

$$\eta_{th,wc-PV/T} = \frac{Q_{u,w}}{S A} \quad (3.46)$$

The heat-gain efficiency for the bi-PV/T module is:

$$\eta_{th,bi-PV/T} = \frac{Q_{u,a} + Q_{u,w}}{S A} \quad (3.47)$$

Based on the second law of thermodynamics, exergy analysis is a thermodynamic approach that provides an additional and informative way to evaluate and compare processes and systems. Exergy analysis gives efficiencies, which assess how close actual behaviour is to the ideal and detects more thermodynamic losses than the energy analysis. As stated by Hassani et al. (2016), the exergy efficiency is expressed by Eq. (3.48) :

$$\eta_{ex,bi-PV/T} = \eta_{ep} + \eta_{th,air} \left[1 - \frac{T_{STC}}{T_{a,ot}} \right] + \eta_{th,water} \left[1 - \frac{T_{STC}}{T_{w,ot}} \right] \quad (3.48)$$

Besides, the exergy of the PV module is:

$$\eta_{ex,PV} = \frac{P_{el}}{\epsilon x P_i} \quad (3.49)$$

Besides, the input exergy power ($\epsilon x P_i$) of the PV module could be calculated by Eq. (3.50) (Gad et al., 2022).

$$\epsilon x P_i = S A_{PV} \left[1 - \frac{4}{3} \left(\frac{T_{am}}{T_{sun}} \right) + \frac{1}{3} \left(\frac{T_{am}}{T_{sun}} \right)^4 \right] \quad (3.50)$$

where T_{sun} is the sun's temperature, which is considered to be 5770 K (Helmi et al., 2022).

3.9. Sustainability contribution of the new PV/T module

The waste heat generated from the PV module is the first outstanding restriction of the solar system, which reduces the sustainability contribution of the building. Fig. 3.41 illustrates the wasted heat from the PV module transferring to the surrounding space. This wasted heat is considered usable heat, which would be used for other purposes later in the PV/T modules. The term 'wasted heat' refers to heat dissipating into the surroundings without being effectively utilized. However, through modifications aimed at its recovery or further investigation, this heat can be rendered useful or recoverable. The front and back surfaces of solar cells transfer the waste heat in convection and radiation forms.

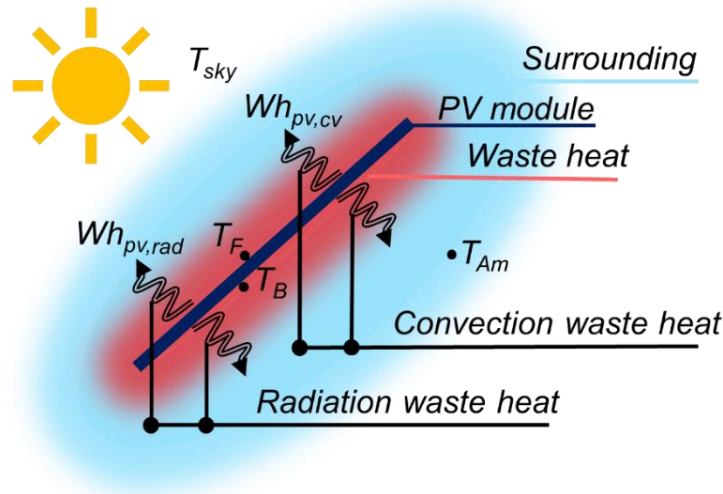


Fig. 3.41. Wasted heat from the PV module

Eq. (3.51) describes the total waste heat transferred from the PV module to the surroundings.

$$Wh_{PV} = Wh_{F,PV,cv} + Wh_{B,PV,cv} + Wh_{F,PV,rd} + Wh_{B,PV,rd} \quad (3.51)$$

where $Wh_{F,PV,rd}$ and $Wh_{F,PV,cv}$ are the radiative and convective waste heat through the front PV module surface and can be calculated by Eqs. (3.52) and (3.53) (Aste et al., 2016; Sarhaddi et al., 2010a).

$$Wh_{F,PV,cv} = h_{F,cv,PV\sim am} A_{PV} (T_F - T_{am}) \quad (3.52)$$

$$Wh_{F,PV,rd} = h_{F,rd,PV\sim sky} A_{PV} (T_F - T_{sky}) \quad (3.53)$$

where $Wh_{B,PV,rd}$ and $Wh_{B,PV,cv}$ are the radiative and convective waste heat through the back surface of the PV module and can be calculated by Eqs. (3.54) and (3.55).

$$Wh_{B,PV,cv} = h_{B,cv,PV\sim Am} A_{PV} (T_B - T_{am}) \quad (3.54)$$

$$Wh_{B,PV,rd} = h_{B,rd,PV\sim sky} A_{PV} (T_B - T_{sky}) \quad (3.55)$$

Eqs. (3.56-3.59) calculate the radiative and convective heat transfer coefficient of the front and back surfaces.

$$h_{F,cv,PV\sim am} = 2.8 + 3V_F \quad (3.56)$$

$$h_{B,cv,PV\sim am} = 2.8 + 3V_B \quad (3.57)$$

$$h_{F,rad,PV\sim sky} = \epsilon_{PV}\sigma (T_F^2 + T_{sky}^2)(T_F + T_{sky}) \quad (3.58)$$

$$h_{B,rad,PV\sim sky} = \epsilon_{PV}\sigma (T_B^2 + T_{sky}^2)(T_B + T_{sky}) \quad (3.59)$$

where:

$$T_{sky} = 0.0552 T_{am}^{1.5} \quad (3.60)$$

This unavoidable waste heat has a negative impact on net-zero energy buildings. The bi-PV/T module investigates this heat for further applications such as hot water and space heating. As shown in Fig. 3.42, the wasted heat from the PV module is transferred to the two working fluids (water and air) employed in the LFS-PV/T.

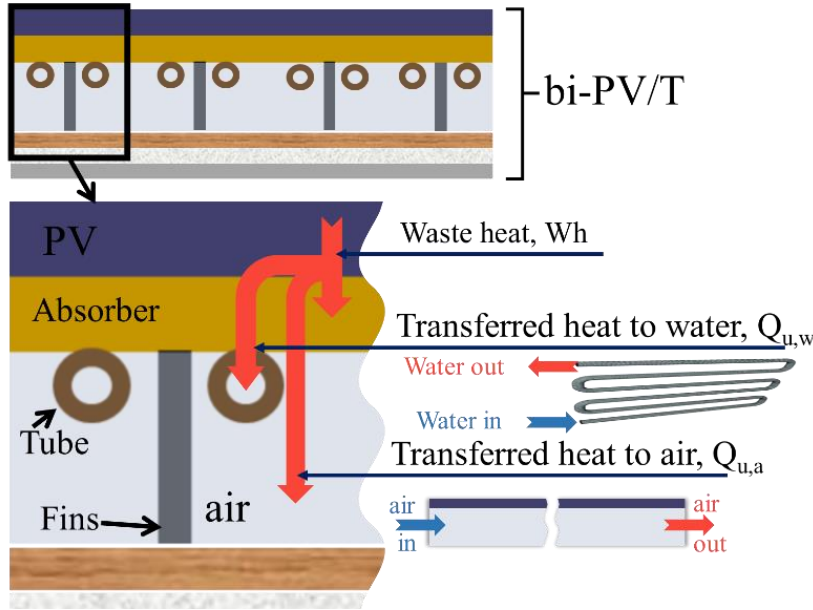


Fig. 3.42. Wasted heat from PV/T module with bi-fluid

The useful heat gained from the bi-PV/T module could be calculated for air using Eq. 3.42) and water using Eq. (3.44).

Besides, the heat losses from the front solar cell surfaces could be calculated by Eq. (3.61) as follows:

$$Wh_{PV/T} = Wh_{F,PV/T,cv} + Wh_{F,PV/T,rd} \quad (3.61)$$

All the heat loss mentioned in the previous equations is a heat loss rate, and its unit is Watt (W). Besides, the recent literature focused on the sustainability index (SI) as a factor in evaluating renewable energy systems for sustainability. The SI is a function of exergy

efficiency (Fudholi et al., 2019). Thus, the SI indicates the effectiveness of energy resources in reducing the environmental footprint and guaranteeing the sustainability of buildings. Eq. (3.62) calculates the sustainability index (Caliskan, 2017) as follows:

$$SI = \frac{1}{1 - \eta_{ex}} \quad (3.62)$$

where η_{ex} is the exergy efficiency of the systems and can be determined for the PV/T and PV modules as expressed in Eqs. (3.48) and (3.49), respectively (Gad et al., 2022; Hassani et al., 2016).

3.10. Uncertainty analysis

Because of the accuracy of the sensors and data-logging devices (see Table 3.9), an error analysis of the uncertainties in the obtained results has been performed. The uncertain test parameters are solar radiation, inlet and outlet temperature of the coolant (air and water), current and voltage. The equivalent measuring instrument uncertainty can obtain these errors.

The uncertainty analysis was examined for the module efficiencies, as stated by Holman, (2012):

$$Un_R = \left[\left(\frac{\partial R}{\partial x_1} \right)^2 Un_1^2 + \left(\frac{\partial R}{\partial x_2} \right)^2 Un_2^2 + \dots + \left(\frac{\partial R}{\partial x_n} \right)^2 Un_n^2 \right]^{1/2} \quad (3.63)$$

where Un_R is the efficiency uncertainty and x_1 to x_n are the dependent variables. Thus, the uncertainty of thermal (η_{th}) and electrical (η_{el}) efficiencies can be obtained using the following equations (3.64–3.65):

$$U_{\eta_{th}} = \left[\left(\frac{\partial \eta_{th}}{\partial T_{out}} \right)^2 (U_{T_{out}})^2 + \left(\frac{\partial \eta_{th}}{\partial T_{in}} \right)^2 (U_{T_{in}})^2 + \left(\frac{\partial \eta_{th}}{\partial G} \right)^2 (U_G)^2 \right]^{1/2} \quad (3.64)$$


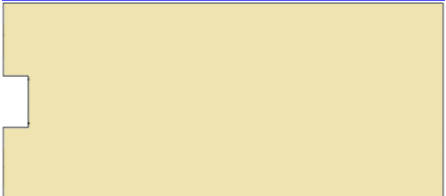
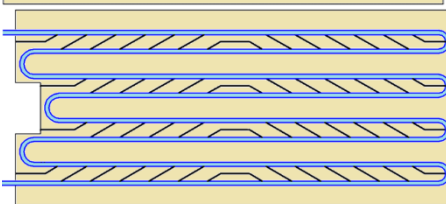
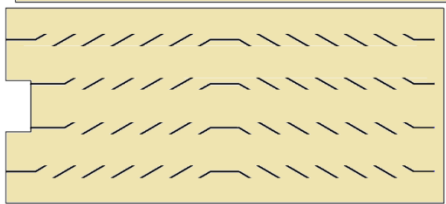

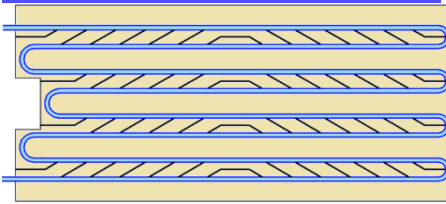
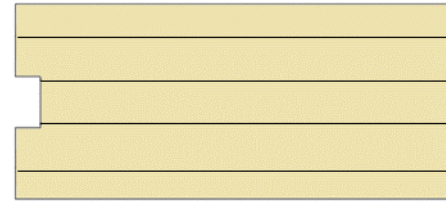
$$U_{\eta_{el}} = \left[\left(\frac{\partial \eta_{el}}{\partial I} \right)^2 (U_I)^2 + \left(\frac{\partial \eta_{el}}{\partial V} \right)^2 (U_V)^2 + \left(\frac{\partial \eta_{el}}{\partial G} \right)^2 (U_G)^2 \right]^{1/2} \quad (3.65)$$

The uncertainty analysis was conducted for all assessments described in the Results chapter. Thus, the uncertainty values of all parameters utilised in the experiments are listed in the result after each evaluation.

3.11. Experiments summary

Based on the previous subsections of the creation processes made in this research, three PV/T modules were created to achieve and fulfil the research objectives. First, the novel construction with louvered fins and serpentine tube that utilise water and air cooling at the same time; second was the classical air-cooled module without fins; the third was the water-cooled module via utilising serpentine tube connected directly to the backside of the PV module. Among these three modules, Table 3.10 lists all modification cases conducted on these modules in this research.

Table 3.10. The presented research solar modules

Case	Absorber	Fins	Tube/ fluid	Sketch of absorber	Symbol
0	None	None	None/none		PV
1	Copper absorber	None	None/air		AC-PV/T
2	Copper absorber	Louvered-fins	8.4 m Serpentine tube/ DW		LFS-PV/T
3	Copper absorber	Louvered-fins	None/air		ALF-PV/T
4	None	None	8.4 m Serpentine tube/ DW		WC-PV/T
5	Copper absorber	Louvered-fins	8.4 m Serpentine tube/ Nanofluids		LFS-PV/T-NF
6	Copper absorber	Vertical fins	None/air		AC-PV/T-V

4. RESULTS

This chapter prints the outputs of the modelling and experiment inputs to accomplish the objectives of this research regarding the performance improvement of hybrid solar collectors. The first part demonstrates the modelling approach and results of the conventional photovoltaic thermal module through TRNSYS tools. The second part presents the results of the new configuration of the photovoltaic thermal modules created in this research. The last part summarises the new scientific results achieved in this research.

4.1. Multi-functional platform of the PV/T module toward performance evaluation

TRNSYS environment held the experimental model, and the simulation results were examined to determine the relationship between solar radiation and proposed system outputs. The location was specified for Gödöllő, Hungary, with a latitude of $47^{\circ} 35' 47.65''$ N and a longitude of $19^{\circ} 21' 18.54''$ E during the simulation. The experiments have used Gödöllő as a geographical data source of TRNSYS meteorological components. The average monthly values for the measurements recorded in the experiments were used and obtained when the sun disc was visible from sunrise to sunset. Five cases were developed by TRNSYS environment to achieve this assessment; these cases are listed in the methodology chapter in Table 3. 4. Fig. 4.1 displays the solar radiation and ambient temperature for the study location in 2021. Fig. 4.2 shows the average daily sunshine time of that location during 2021.

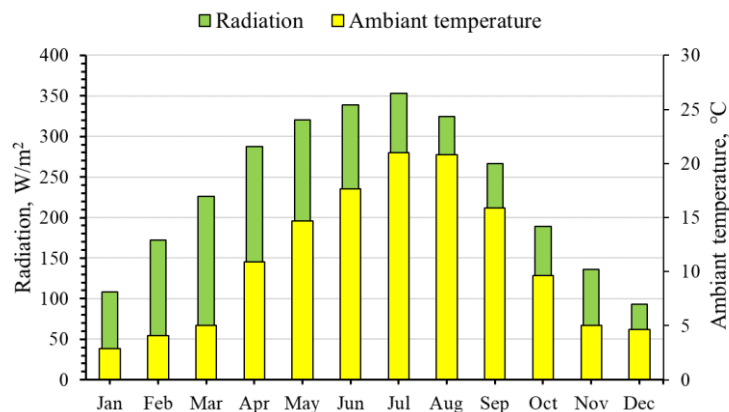


Fig. 4.1. Solar radiation and ambient temperature in Gödöllő city, Hungary

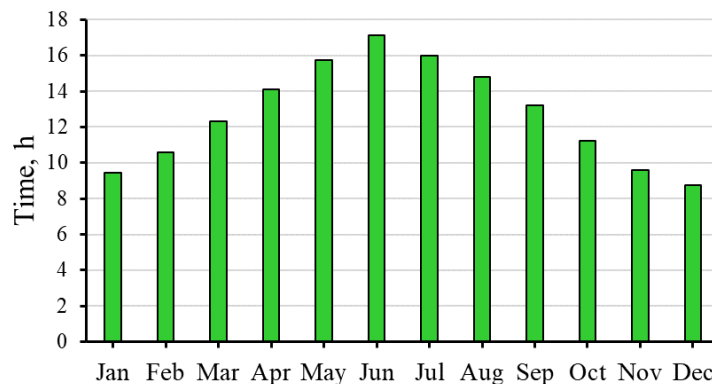


Fig. 4.2. Average daily sunshine hours in Gödöllő city, Hungary

4.1.1. Performances comparison of the PV/T with PID controller

This subsection assesses the performances of the PV/T modules with another TRNSYS model for the standalone PV module and flat plat collector (FPC). Fig. 4.3 illustrates thermal power comparisons between the basic system of this research using a PID controller PV/T-ID and the classical unit of domestic hot water as a solar flat plate collector (FPC). On the other hand, Fig. 4.4 shows electrical power comparisons between PV/T-ID and PV systems. These figures are crucial to comparing the PV/T behaviour with individual units.

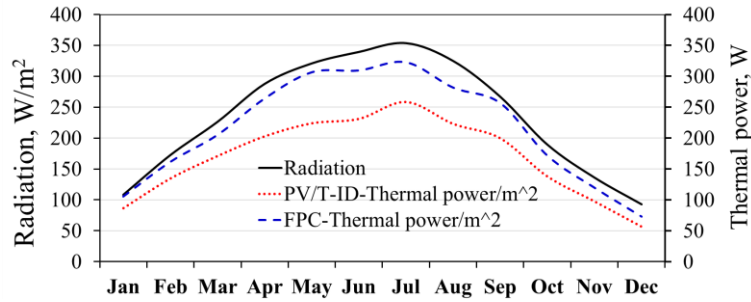


Fig. 4.3. Thermal power comparison between PV/T-ID and FPC

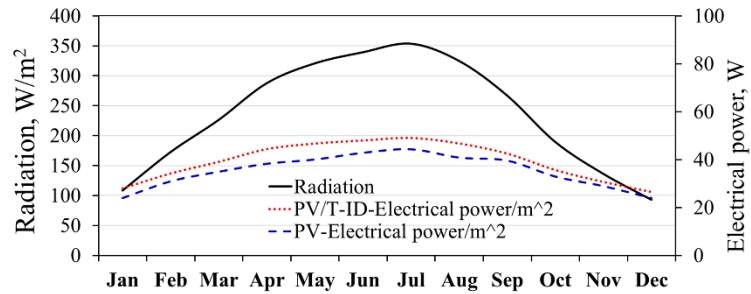


Fig. 4.4. Electrical power comparison between PV/T-ID and PV

Furthermore, the other significant factors of comparison are the thermal and electrical efficiencies. Figs. 4.5 and 4.6 illustrate the efficiency comparison of PV/T-ID with FPC and PV systems.

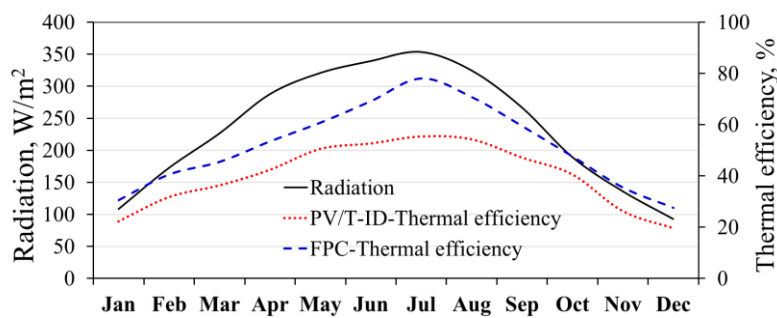


Fig. 4.5. Thermal efficiency comparison between PV/T-ID and FPC

4. Results

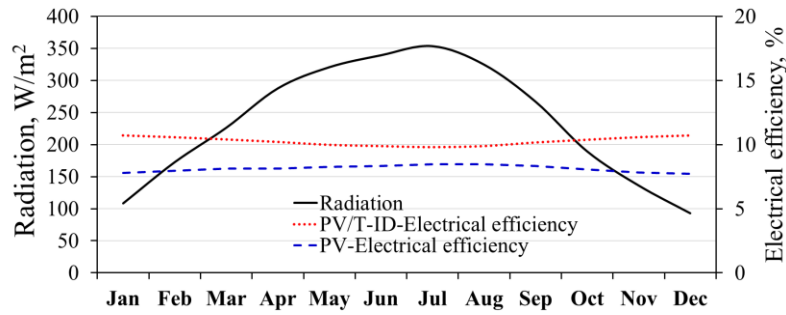


Fig. 4.6. Electrical efficiency comparison between PV/T-ID and PV

Fig. 4.3 illustrates the thermal power gain comparison between the FPC and the PV/T-ID systems. This figure demonstrates that the FPC system's thermal power gain as an individual unit has a more significant power gain. It is approximately 21% more than the case of the PV/T collector because solar radiation directly affects the collector plate. As shown in Fig. 4.4, as an average value, the electrical power of the PV/T-ID is 11% higher than that of an individual PV system as the heat is extracted from PV cells by the flat-plate collector fixed below the PV module. Moreover, based on the results in Figs. 4.5-4.6, the PV/T-ID system has a 12.5% higher electrical efficiency than the PV system. The FPC system is 22.7% more efficient than the PV/T-ID system. It is worth mentioning that the ambient temperature significantly affects the electrical behaviour of photovoltaic solar systems. Fig. 4.7 shows how the ambient temperature affects the electrical efficiency of the PV/T-ID module.

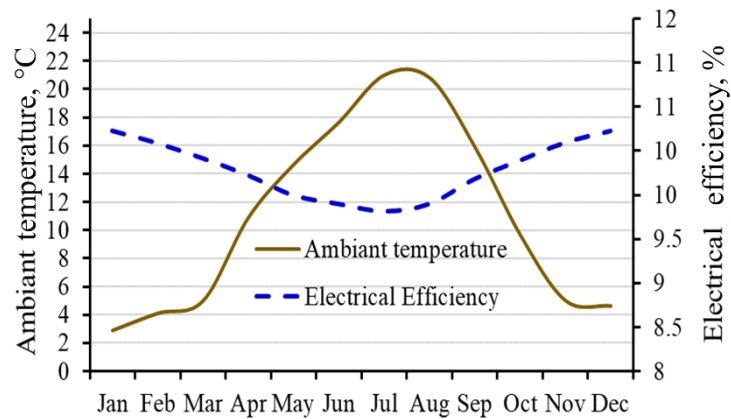


Fig. 4.7. Ambient temperature versus electrical efficiency

Based on the data charted in Fig. 4.7, for every one-degree Celsius increase in ambient temperature, the electrical efficiency of the proposed meteorological source in Gödöllő city fell by 0.21%.

The PV cell temperature is another significant factor that must be considered while evaluating any solar PV module, especially PV/T systems. Fig. 4.8 illustrates this temperature of the PV/T systems as an average value.

4. Results

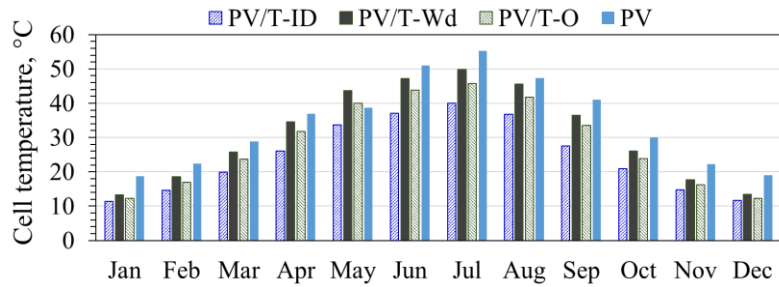


Fig. 4.8. Cell temperature of the systems

It is observed from the figure that the PV system cell temperature is higher than those in PV/T systems during this research. It means that the electrical efficiency of the PV/T systems has an efficient value since the conversion efficiency of the solar system increases when the cell temperature is decreased.

The slope of the solar panels has an essential role in their performance and how the solar modules are tilted. The simulation time was chosen for July 15. Fig. 4.9 represents the comparison of eighteen angles used in this research's basis system with 1 m² active surface, and the results were the daily average values.

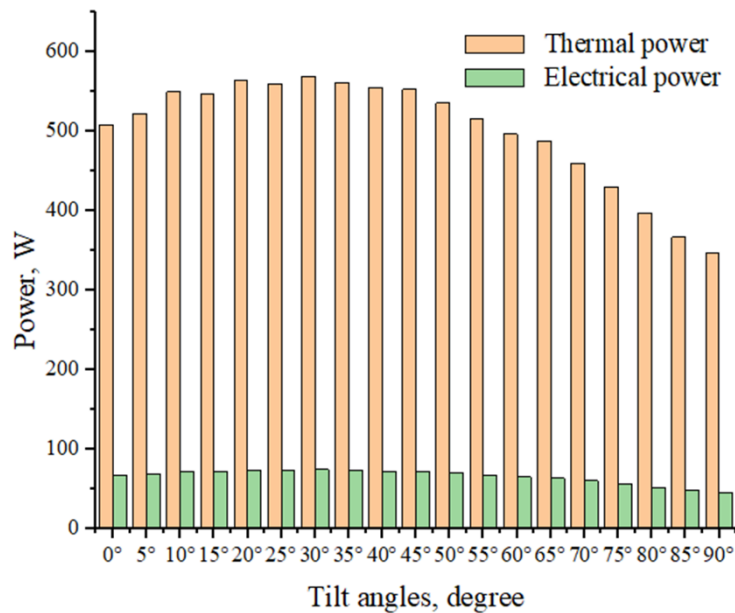


Fig. 4.9. Electrical and thermal power for the eighteen angles

As shown in Fig. 4.9, significant changes in the PV/T-ID system outputs were observed throughout changing the tilt angles. The thermal and electrical power are the highest for the systems with 20°, 25°, 30°, and 35° tilt angles. The basis system of this research, PV/T-ID, with a tilt angle of 30°, had the highest results in total thermal and electrical power.

4.1.2. Assessment of adding an ON-OFF controller

Besides the PV/T module investigated in the previous subsection, Figs. 4.10 and 4.11 indicate the impact of adding an ON-OFF controller on the PV/T performance instead of the PID controller. The results compare the primary system with a PID controller PV/T-ID and an ON-OFF controller system PV/T-O.

4. Results

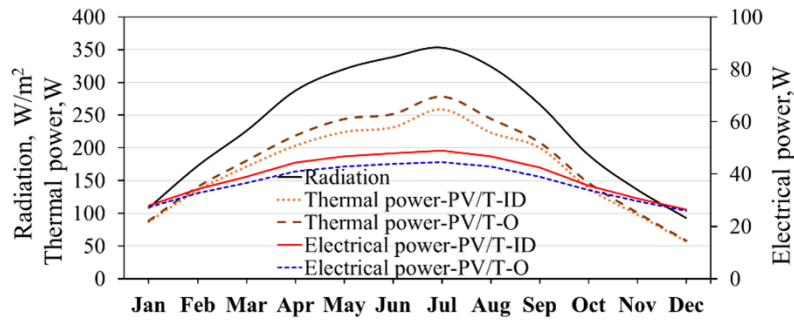


Fig. 4.10. Power comparison between PV/T-ID and PV/T-O

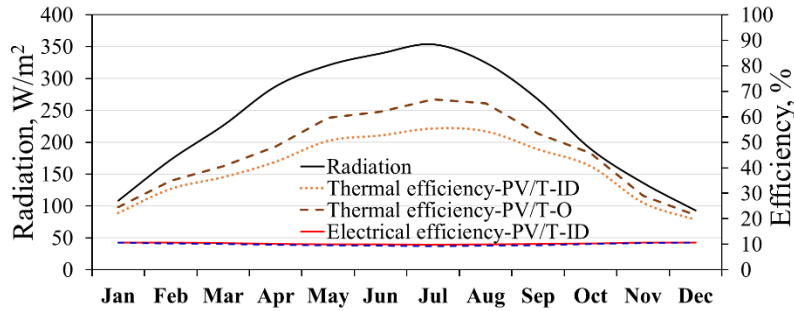


Fig. 4.11. Efficiency comparison between PV/T-ID and PV/T-O

The thermal power and efficiency of the PV/T-O system are higher than those of the PV/T-ID system by 6.1% and 13.1%, respectively. Besides, the electrical power and efficiency are high for the PV/T-ID system by 6.5% and 3%, respectively. The maximum electrical productivity was 48.5 and 45 W for the PV/T-ID and PV/T-O, respectively.

4.1.3. Daily profile of the hot water usage

The hot water usage varies in different households and periods. However, this research considered a person using 100 l of hot water throughout the day. The model consumed hot water from 7:00 am to 11:00 pm, and the consumption ended at regular intervals. Figs. 4.12 and 4.13 illustrate the effect of using a hot water profile for daily consumption by comparing the performance of the basic system, PV/T-ID, with the non-usage of the daily profile system, PV/T- Wd.

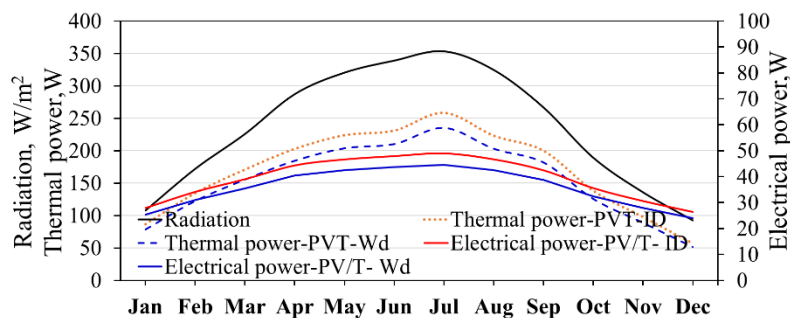


Fig. 4.12. Power comparison between PV/T-ID and PV/T-Wd

A meaningful reduction in the PV/T outputs was observed when the model did not use the daily profile of hot water. As a result, the hot water consumption affects the storage tank's thermodynamics since it changes the heat transfer line between the PV module and the FPC mounted behind it. Besides, increasing pumping power affects the entropy generation due to rising liquid friction. Additionally, the heat transfer coefficient will increase as the pumping

power grows. That ensures the enhancement in heat transfer between the pipe of the PV/T absorber and the liquid inside. Thus, this decreases the cell temperature and produces more conversion power.

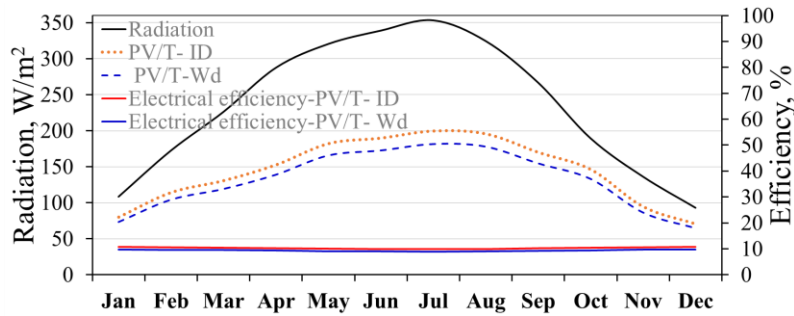


Fig. 4.13. Efficiency comparison between PV/T-ID and PV/T-Wd

4.1.4. Performance summaries of the five TRNSYS models

Based on the achievements caught from the previous outcomes for all models presented in this research mentioned in Table 3.5 that were utilised to assess the proposed PV/T system and compare it with each other, Figs. 4.14 and 4.15 show the results of each approach used for evaluation. As clearly shown in the figures above, the basic system of this research, PV/T-ID, was the most efficient system among the other two PV/T systems in terms of electrical performance, while the FPC was the most efficient in terms of thermal performance.

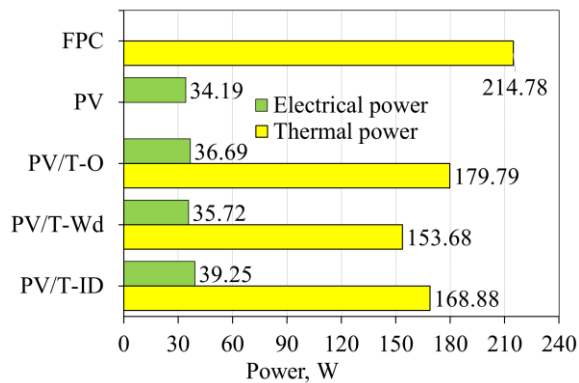


Fig. 4.14. Power comparison for study systems

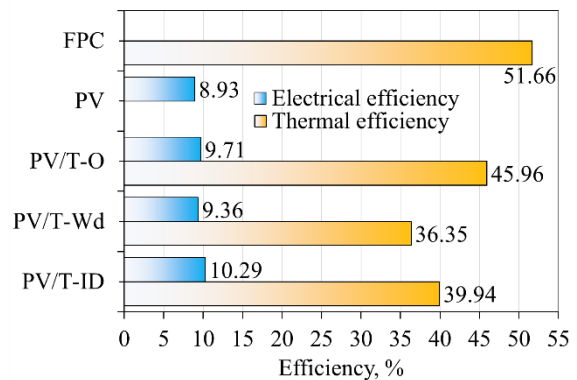


Fig. 4.15. Efficiency comparison for study systems

4.1.5. New contribution to the PID controller

Based on the literature utilising the PID controllers through the solar system and the studies that used it within their TRNSYS dynamic model, the PID controller depends on the temperature difference between stored water and the outlet temperature of the collector. And this assumption was a usual option. This research used a new consideration: changing the temperature difference used by a PID controller in a PV/T-ID system to a difference between the cell temperature and stored water with the new symbol as a PV/T-ID2 system.

Fig. 4.16 shows the performance difference between these two cases. The simulation time result for this analysis was chosen for July 15.

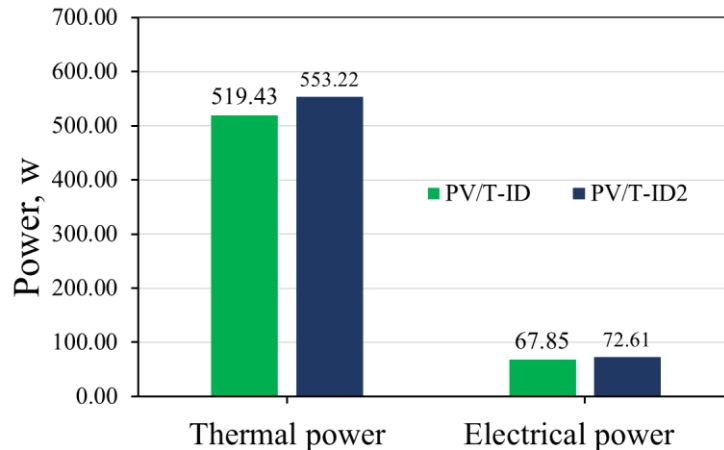


Fig. 4.16. Performance difference between PV/T-ID and PV/T-ID2

The results clarified in Fig. 4.16 indicate that the PV/T-ID2 thermal and electrical performance were more efficient than the PV/T-ID. Thus, the proper temperature difference in the PID controller is between the stored water and the PV cell temperatures. Thermal power was enhanced by 6.5%, and the electrical power was improved by 7.1% compared to the standard PID-controlled system.

Summarising the results of the TRNSYS system is as follows:

- The electrical performance of the hybrid solar collector system indicated that PID-controlled (PV/T-ID) was higher by 9% than the system without utilising a daily water profile (PV/T-Wd) and higher by 6.5% than the system that was ON-OFF controlled (PV/T-O). It means the system with regular hot water consumption was more efficient in electrical behaviour.
- The electrical performance of the PV/T-ID system was higher than that of the PV module by 10.32%. Via cell temperature decrement due to heat extraction from the PV module, which increases the solar cells' electrical efficiency.
- In contrast, the thermal performance of the hybrid solar collector system of an ON-OFF control (PV/T-O) was higher than the system of PID control (PV/T-ID) by 6.1% and higher than the system without daily water profile usage (PV/T-Wd) by 14.5%.
- The flat plate collector system's (FPC) thermal performance was higher than the PV/T-O systems by 21.4%.
- When PID and ON-OFF controllers were used, the most efficient system was the PV/T-ID if the electrical performance was preferred. In contrast, the PV/T-O system was the most efficient approach if the objective was thermal performance.
- The optimum tilt angle used in the PV/T-ID systems among eighteen values is 30° , which showed more efficient electrical and thermal performance.
- Thermal power was enhanced by 6.5%, and the electrical power was improved by 7.1% compared to the standard PID-controlled system.

4.1.6. Model validation

The model created by Kalogirou (2001) was used to validate the PV/T TRNSYS model of this research. Kalogirou used seven values of water flow rate to measure the cell and system efficiency of the PV/T system. In this research, PV/T module efficiencies based on the presented specifications of the model behaved like the Kalogirou model. As illustrated in Fig.

4.17, the model of this research matches the efficiency behaviour for the same simulation time with an average percentage variance of roughly 2.2% for both cell and system efficiency. Using the same simulation time and general configuration of the model, the results indicated in the above figures reached their maximum with a similar liquid flow rate value (25 kg/h).

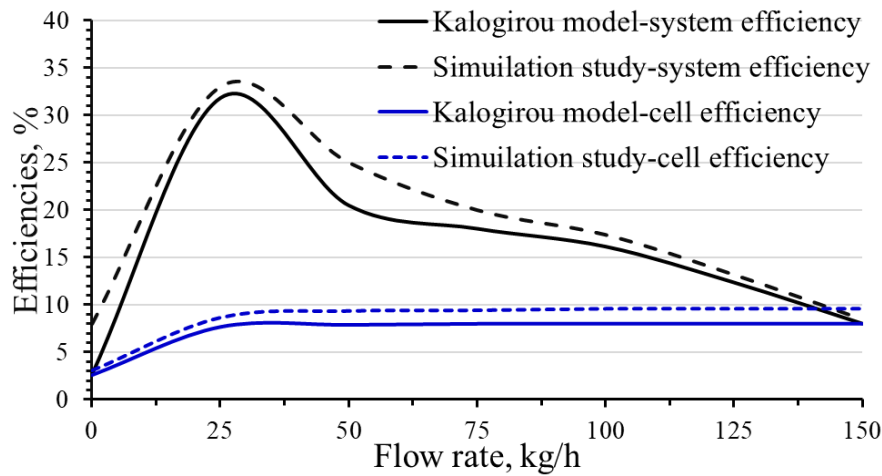


Fig. 4.17. Cell and system efficiency of the PV/T based on Kalogirou’s Model

4.2. Effect of the louvered fins

This assessment evaluates the fins configuration potentiality created and presented in this research by comparing the performance of the three different configurations of an absorber mounted to an air-cooled photovoltaic/thermal module, with louvered fins, with vertical fins and without fins absorber under steady-state circumstances. Fig. 4.18 shows these three shapes of an absorber and the dimensions regarding the areas of the parts with a height of 50 mm for both fins investigated.

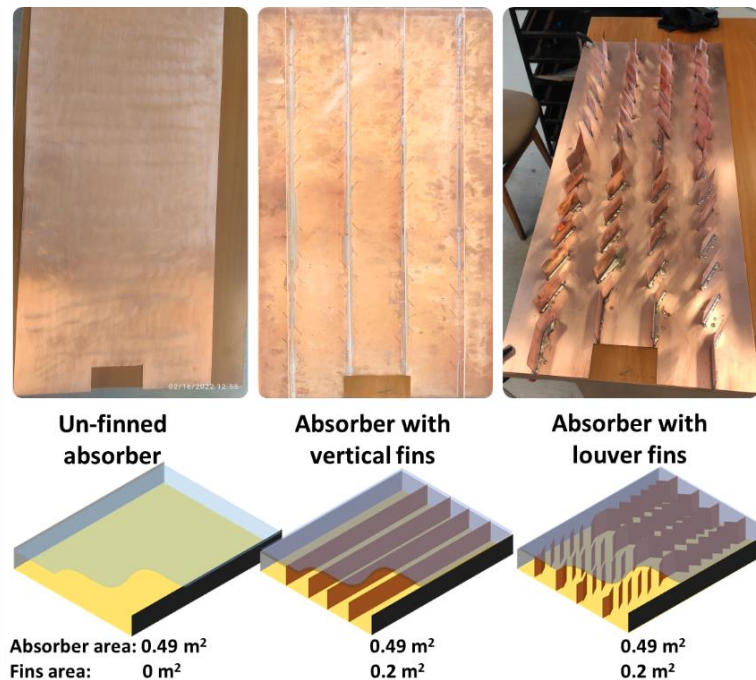


Fig. 4.18. Actual image of the proposed system of PV/T

This research was conducted under weather conditions in Gödöllő, Hungary. Fig. 4.19 describes the ambient temperature distribution during the experiment period. The maximum and average ambient temperature values are 23 °C and 21 °C, respectively. The experiments were conducted on October 17. The sky was clear, and the solar radiation distribution is illustrated in Fig. 4.20. The maximum and average solar radiation values are 906 W/m² and 821 W/m², respectively.

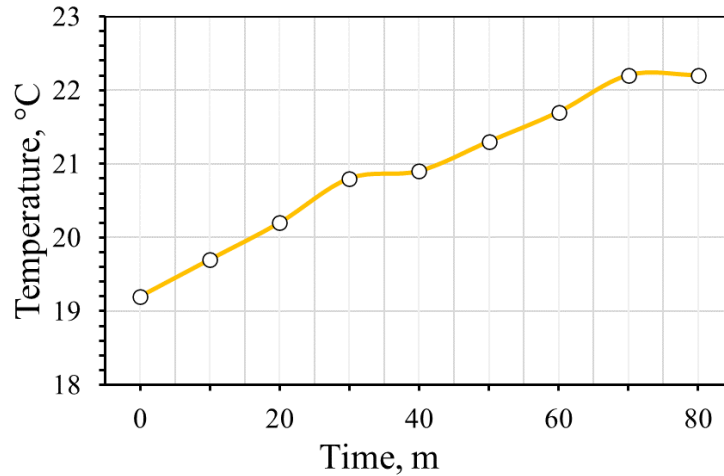


Fig. 4.19. Ambient temperature of the study site

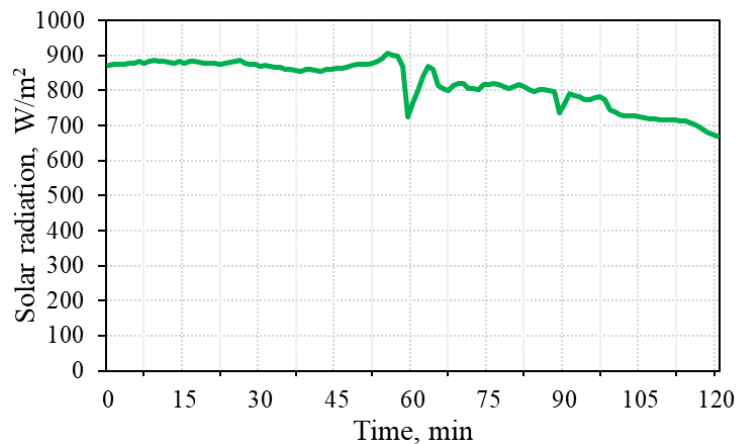


Fig. 4.20. Solar radiation distribution of the study site

The temperature difference between the inlet and outlet of the forced air flowing through the channels of the presented PV/T modules is shown in Fig. 4.21. Instantly, there was a significant increase in temperature difference ($T_{\text{out}}-T_{\text{in}}$) for the third module (louvered fins) compared to the first (un-finned) and second (vertical-fins). The first module and the second module are close to each other. By more than 48% and 56%, the third module is superior to the first and second, respectively.

4. Results

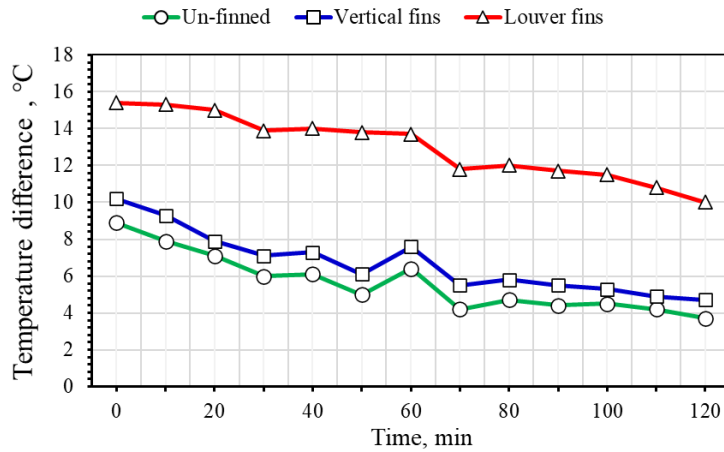


Fig. 4.21. The temperature ($T_{out}-T_{in}$) difference in time at the presented modules

As the thermal power is a function of the temperature difference between the outlet airflow rate temperature and the inlet flowrate temperature ($T_{out}-T_{in}$), based on the results specified in Fig. 4.21, Fig. 4.22 illustrates the thermal power of the three modules. The enhancement of the thermal behaviour of the PV/T module that employed the louvered fins compared to the other modules is clearly noted. The average daily value of the thermal power of the three modules is 139, 166, and 320 W for the first, second, and third modules, respectively.

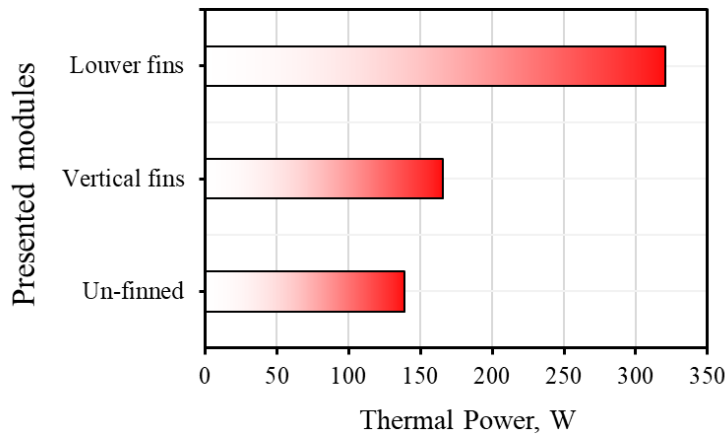


Fig. 4.22. Thermal power of the presented modules

Fig. 4.23 illustrates the thermodynamic characteristics curves of the three proposed PV/T systems for various copper absorber configurations. Thermal efficiency is obtained for the systems and plotted against the value of the $(T_m-T_a)/G$. Maximum heat yield from an air-cooled PV/T collector is shown on these curves for various absorber designs, and the inlet air temperatures varied (18, 19, 20, 21, and 22 °C). The maximum thermal efficiency achieved from the PV/T module corresponds to the use of louvered fins within an absorber. In addition, the system's efficiency is reduced when the air entering the system is at a higher temperature than when the air entering the system is at a lower temperature. As the temperature of the incoming air increases from 18 to 22 °C, the values of $(T_m-T_a)/G$ rise from 0 to 0.007 K m²/W.

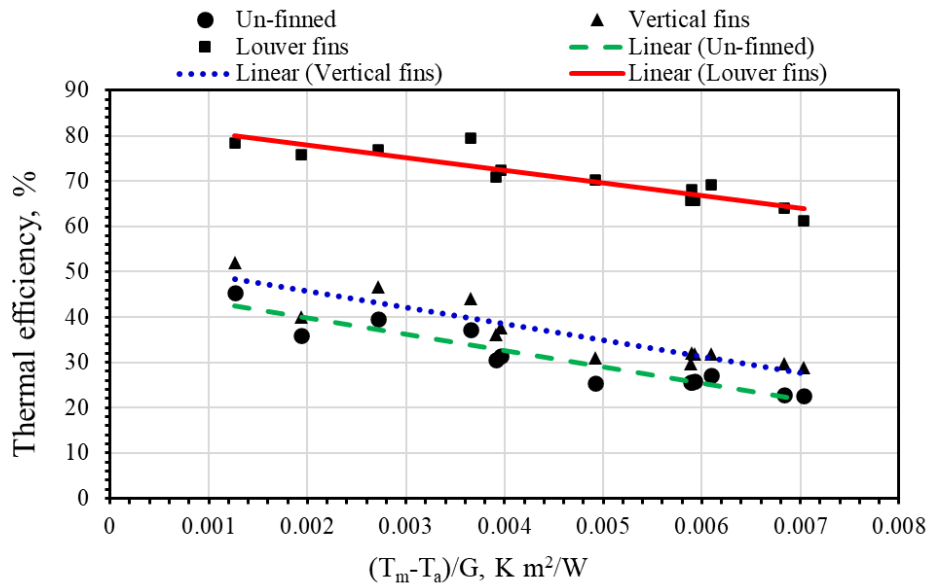


Fig. 4.23. Thermodynamics characteristic curves of the proposed PV/T systems

The performance of the three systems used in this research is clarified by the electrical and thermal efficiencies, as illustrated in Fig. 4.24; the PV/T module that employs the louvered fins has the highest performance compared to the other investigated PV/T modules. The average electrical and thermal efficiencies for the modules with louvered fins, vertical fins, and un-finned are 7.34%, 69%; 6.98%, 36.6%, and 6.53%, 33.8%, respectively.

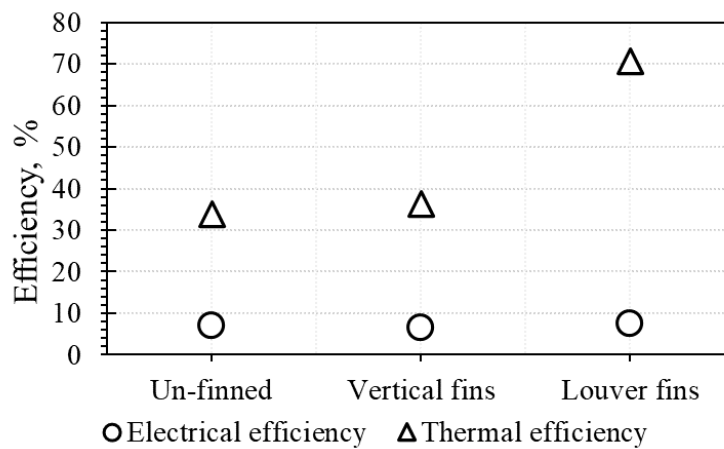


Fig. 4.24. Electrical and thermal efficiencies for presented solar PV/T systems

As a result of the heat extraction, the electrical power generation increases accordingly, with PV temperature decreasing. Fig. 4.25 illustrates the imaging of the productivity behaviour among the study modules. The average electrical power and PV temperature values for the modules with louvered fins, vertical fins, and un-finned are 36.4 W; 40.6 °C, 34 W; 45 °C and 31 W; 47 °C, respectively.

Aside from copper's high heat capacity, the low airspeed of about 0.9 m/s combined with the unique shape of the louvered fins allow for significant heat transfer from the fins to the airflow within a Reynolds number of 6312 that indicates a turbulent flow through this configuration. Thus, this leads to dramatic temperature differences between the outlet and the inlet airflow, and this difference represents the dependent value of the thermal efficiency.

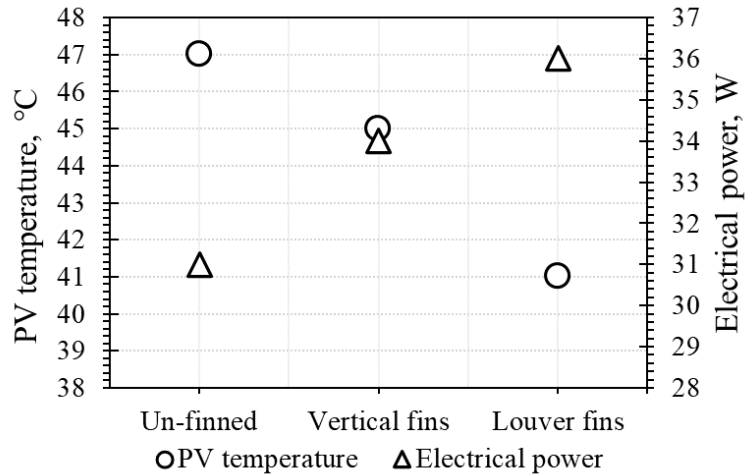


Fig. 4.25. Electrical generation versus the PV temperature of the examined modules

Besides, the thermal power, the electrical power, the thermal efficiency, and the electrical efficiency of the PV/T unit were used in the uncertainty analysis. Calculations of this method for the previous parameters are listed in Table 4.1.

Table 4.1. Values of uncertainties

Parameters	Thermal power	Electrical power	Thermal efficiency	Electrical efficiency
Values	$\pm 0.55\%$	$\pm 0.63\%$	$\pm 0.763\%$	$\pm 0.96\%$

4.3. Design of the louvered fins and serpentine tube

This research considered improving the performance of the hybrid solar panel through several scientific and practical laboratory experiments concerning changing and creating the design of the components and layers of the solar panel and changing the heat transfer fluids used in cooling. Thus, this section focuses on the results obtained from the new PV/T module. Also, investigate the potentiality of nanofluids as a high-thermal-conductivity fluid instead of distilled water. The cases examined in this section are listed in the methodology chapter in Table 3.10.


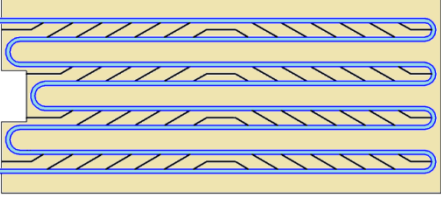
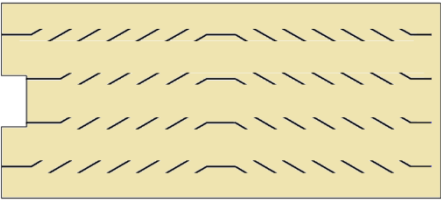
4.3.1. Temperature profile of the created PV/T module

The experimental results were collected on two clear days in June at the locations presented in Chapter 3 subsection section 3.1 at 20 and 24. June 2022. The experiments were conducted to obtain the results from the following three cases; the configurations of the case studies are detailed in Table 4.2.

- The classical unit of the hybrid solar collector uses air as the coolant (AC-PV/T),
- A new module with louvered air fins and a serpentine water tube (LFS-PV/T),
- Same case 2, but without water circulation in the serpentine tube (ALF-PV/T).

4. Results

Table 4.2. Configurations of the study cases

Case	Absorber	Fins	Serpentine tube	Sketch of absorber	Symbol
1	Copper with 1.5 mm thickness	None	None		AC-PV/T
2	Copper with 0.015 m thickness	Louvered-fins with 0.015 m thickness	8.4 m length tube with 0.01 m thickness		LFS-PV/T
3	Copper with 0.015 m thickness	Louvered-fins with 0.015 m thickness	None		ALF-PV/T

Solar irradiance is the source of heat transfer throughout the module layers. This section used the global irradiance on the tilted surface to show and determine most of the measurements. During the study period from 9:00 am to 4:00 pm, the average irradiance and surrounding temperatures (T_{sr}) were 909.4 W/m² and 30.8 °C on June 20 and 900 W/m² and 32.5 °C on June 24. The average daily values of these parameters are shown in Fig. 4.26.

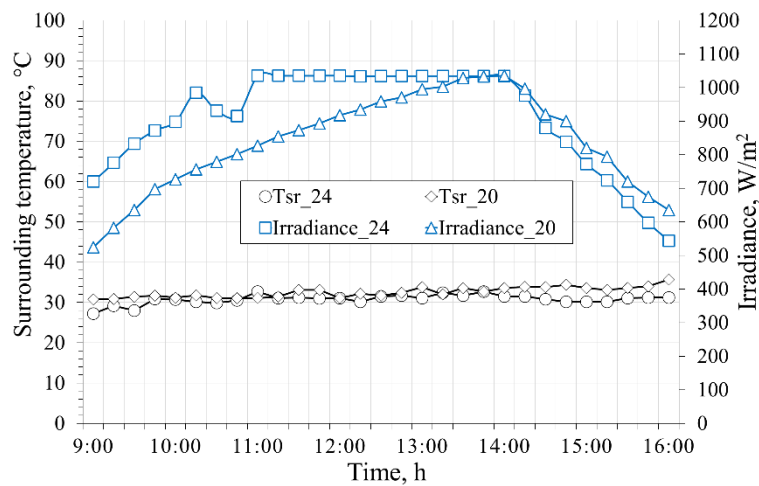


Fig. 4.26. Irradiance and surrounding temperature

This research examined the thermal behaviour of an adhesive material used to ensure direct contact between the PV modules and the new absorber by measuring the temperature between the cells and the back side of the absorber relative to the incident radiation. As illustrated in Fig. 4.27, the average temperature difference between them is less than 0.38 °C.

4. Results

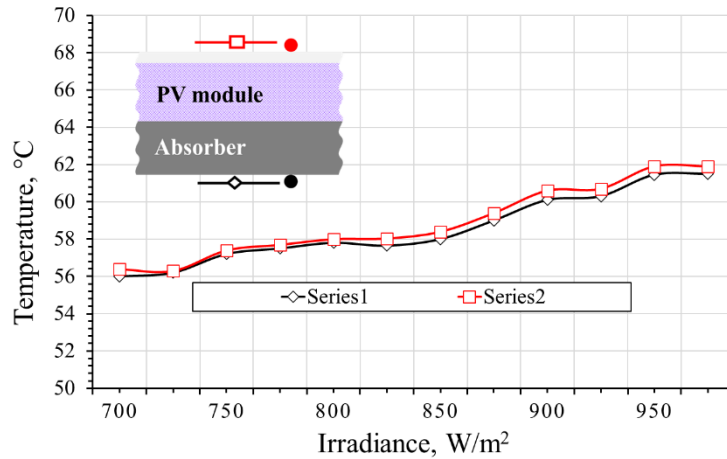


Fig. 4.27. Copper absorber back side and solar cells' surface temperatures

Fig. 4.28 indicates the surface temperature T_s of the solar cells in the three cases listed in Table 4.2 concerning the effect of global irradiance on the tilted surface S and the surrounding temperature T_{sr} .

As shown in Fig. 4.28, the curves for the three cases show a considerable and noticeable difference. The state with the lowest surface temperature was the second case (LFS-PV/T), followed by the third (ALF-PV/T) and the first (AC-PV/T). It is also clear that for the first case, the temperature difference between it and the other two cases is relatively significant when the solar radiation is greater than 1000 W/m^2 . The second case was the closest to the temperature of the surroundings compared with the other cases, which had an enormous difference. As an average of the values during the recording of the readings, the temperatures were 57.1 , 45.73 , and $38.9 \text{ }^\circ\text{C}$ for the AC-PV/T, ALF-PV/T, and LFS-PV/T modules, respectively. The solar cell surface temperature may decrease after 2:00 pm owing to the module's fixed frame (with an azimuth angle of 20° and tilt angle of 45°) and the shift position of the sun throughout the experiment. This decrease could also be attributed to the cooling methods of the modules.

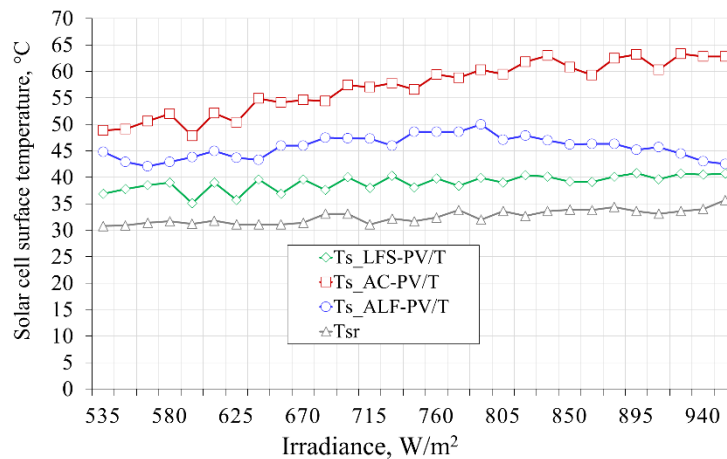


Fig. 4.28. Surface temperatures of the solar cells

In addition to the results reported in the preceding chart, this research assessed the back surface temperature T_b of the absorber plate inside the air channel for the three cases. Fig. 4.29 shows how the temperature of the back surface T_b of the absorber changes depending on the cooling method used.

4. Results

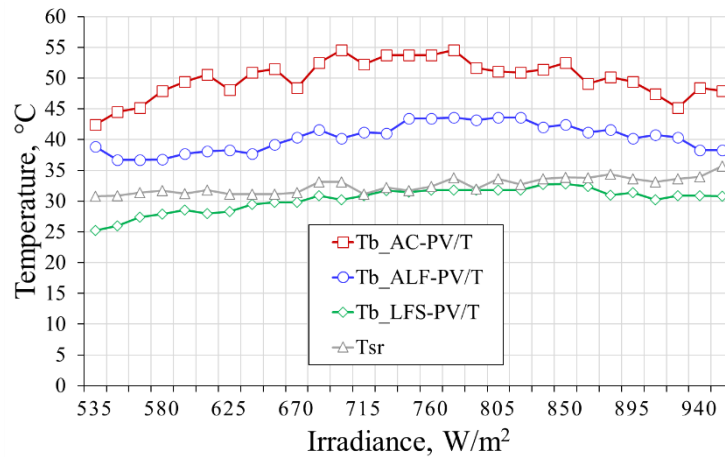


Fig. 4.29. The back surface temperature of the absorber plate

As shown in Fig. 4.29, there was a significant decrease in the back-adsorbent surface temperature for the LFS-PV/T case compared to the AC-PV/T and ALF-PV/T cases. As a result of using air fins and serpentine tubes to cool the LFS-PV/T case, the temperature of the back surface was lower than the temperature of the surrounding air. This temperature lowering shows that the design of the LFS-PV/T case is more effective at absorbing heat, as the maximum temperatures for modules LFS-PV/T, ALF-PV/T, and AC-PV/T were 32.8, 43.6, and 54.6 °C, respectively.

As an assessment of realm solar air collectors, the outlet air temperature (T_{a-out}) is a significant factor in determining consumer demand. Fig. 4.30 illustrates T_{a-out} for the three modules.

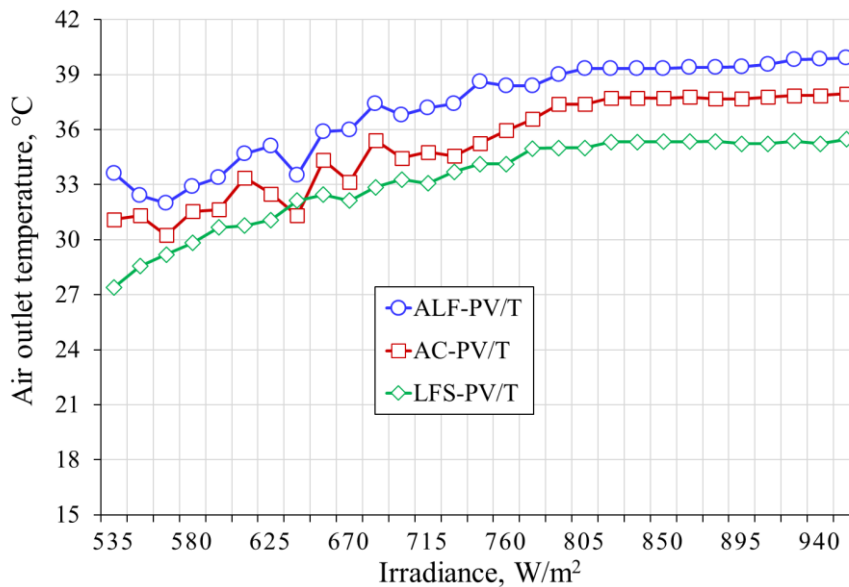


Fig. 4.30. The outlet air temperature of the systems

The increase in solar radiation dramatically affected the study modules, and the behaviour of the temperature curve shown in the above figure indicates the effectiveness of each module in transferring heat to the air passing through the air channel fixed under the solar panel. Thermodynamically, the ALF-PV/T model was significant in heat transfer owing to the new shape of the fins. As an average of the values, the temperature was 33.2 °C, 35.17 °C, and 37.15 °C for the LFS-PV/T, AC-PV/T and ALF-PV/T cases, respectively.

4.3.2. Performance achievement

Based on the result obtained from the previous analysis, Fig. 4.31 shows an overall thermal and electrical view of the modifications for the three cases. Table 4.3 lists the significant values of the cases (AC-PV/T, LFS-PV/T, ALF-PV/T) as average values.

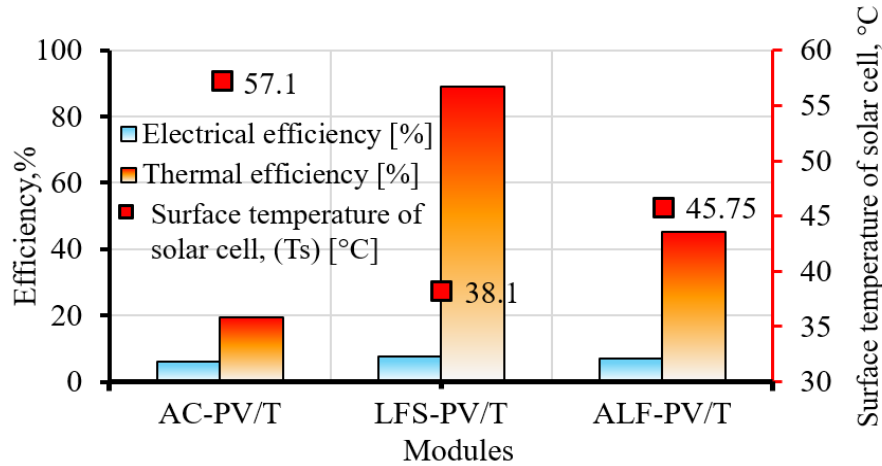


Fig. 4.31. Thermal and electrical view of the modules

Table 4.3. Average values of the research module outcomes

Module	Average values of module results						
	Electrical power [W]	Thermal power [W]	Ts [°C]	Electrical efficiency [%]	Thermal efficiency [%]	T _{a-out} [°C]	T _{w-out} [°C]
AC-PV/T	27.15	62.1	57.1	6.09	19.4	34.54	-
LFS-PV/T	34.12	559.5	38.1	7.66	89.1	32.87	32.36
ALF-PV/T	33.11	209.6	45.75	6.91	45.1	36.35	-

4.3.3. Thermal camera investigation

A TH9260- thermal camera (see Fig. 3.32) took three thermal images for all three cases during the recording period on June 20. The first image was a static situation when the systems were not working (see Fig. 4.32), the second was when the systems worked without water circulation (see Fig. 4.33), and the last was with water circulation (see Fig. 4.34).

As shown in the three thermal images (Figs. 4.32-4.34), which provide thermodynamic viewpoints of the three cases in this research and verify thermal matching with the experimental results of the new configuration that used louvered-fins and serpentine tubes, the LFS-PV/T module is the best in terms of thermal behaviour.

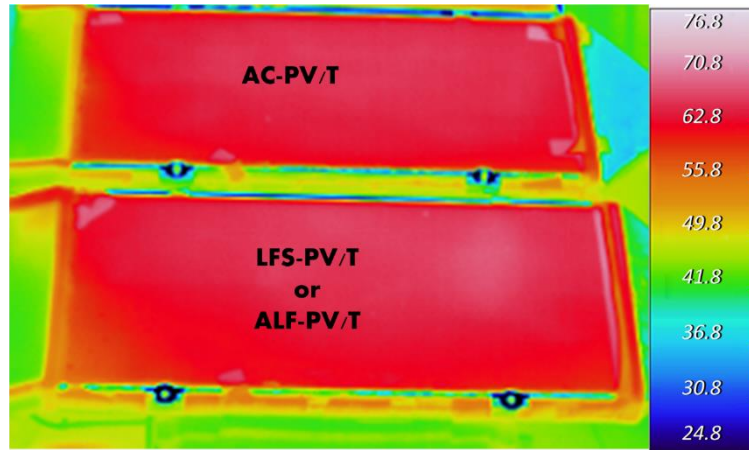


Fig. 4.32. The image of the thermal camera when the systems were not working
 Besides, the uncertainty analysis was used to accurately measure the module's efficiency. As a result, the Table 4.4 lists the uncertainty values.

Table 4. 4. Uncertainties values

Parameters	Thermal efficiency	Electrical efficiency
Values	$\pm 0.73\%$	$\pm 0.96\%$

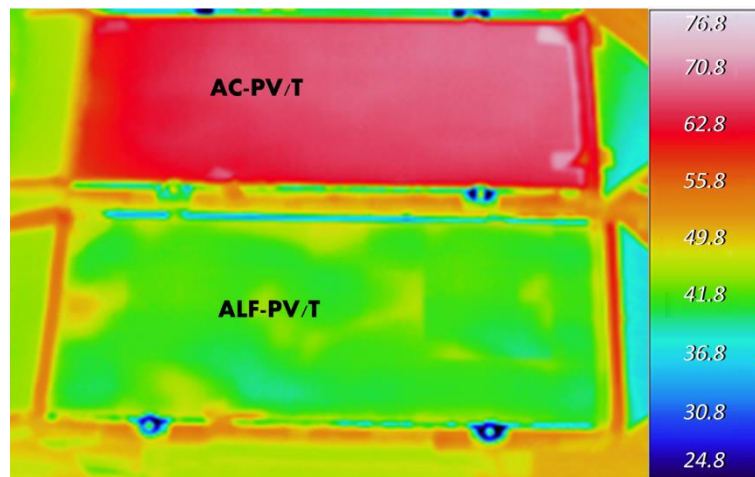


Fig. 4.33. The image of the thermal camera when the water was not circulated

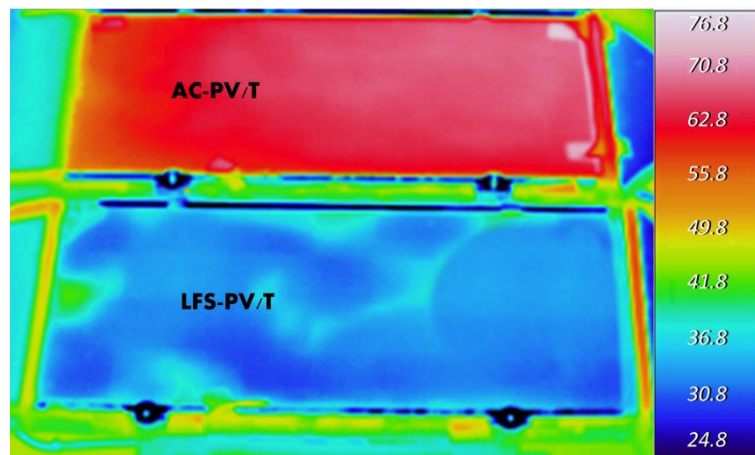


Fig. 4.34. The image of the thermal camera when the water was circulated

4.4. Correlation between solar cell temperature and solar intensity of the new PV/T

The solar cell temperature is the main effective factor in the solar energy systems performances and to make correlations to address how cell temperature is decreased as a result of the new PV/T design of this research.

So, this assessment compared an experimental performance comparison to the new PV/T (that utilised louvered fins and serpentine tube) with a classical air-cooled PV/T and the standalone PV module and the water tank was in a static state. Fig. 4.35 represents the cross-section layout (side view-inlet and outlet view) of these three modules, as named in Table 4.5.

Table 4. 5. The solar systems investigated in this research

	Module	Coolant	Symbol
1	A novel photovoltaic thermal module using louvered fins and serpentine tube	Air +water	LFS-PV/T
2	A classical photovoltaic-thermal module	Air	AC-PV/T
3	Classical photovoltaic system	NA	PV

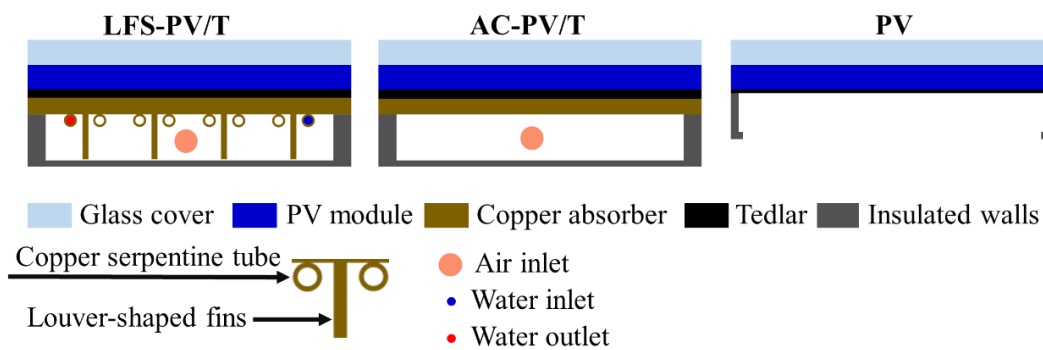


Fig. 4.35. The cross-section layout of the solar modules

This work was carried out on the outdoor experiment on July 3, 2022. The sky was mostly clear during the experiments from 10:00 to 17:00. Nonetheless, the maximum and minimum values for location environment variable quantity global solar radiation and ambient temperature during the study period were 1038.1 W/m², 31.18 °C, and 336.4 W/m², 24.7 °C, respectively (see Fig. 4.36).

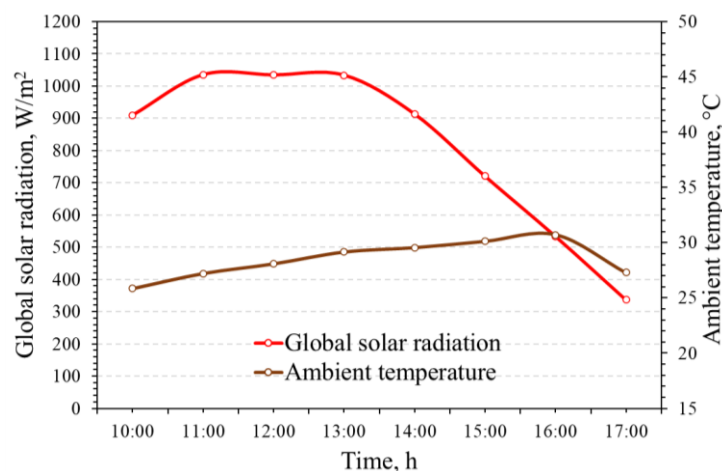


Fig. 4.36. Solar radiation and ambient temperature during a study period

4. Results

Fig. 4.37 illustrates the progression of the water and air temperatures at the input and output flow of the LFS-PV/T system throughout the experiment. This figure shows that the water leaving the system has a higher temperature than the water going into the system.

Based on the fixed flow rates of air and water, the outlet water temperature difference was higher than the air. This fact proves that water absorbs heat more than air. In contrast, Fig. 4.38 indicates the temperatures of the AC-PV/T system, in which the outlet air increased by 6.13% compared to the LFS-PV/T system. That decrease in the air outlet of the LFS-PV/T is due to the water circulation in the serpentine tube.

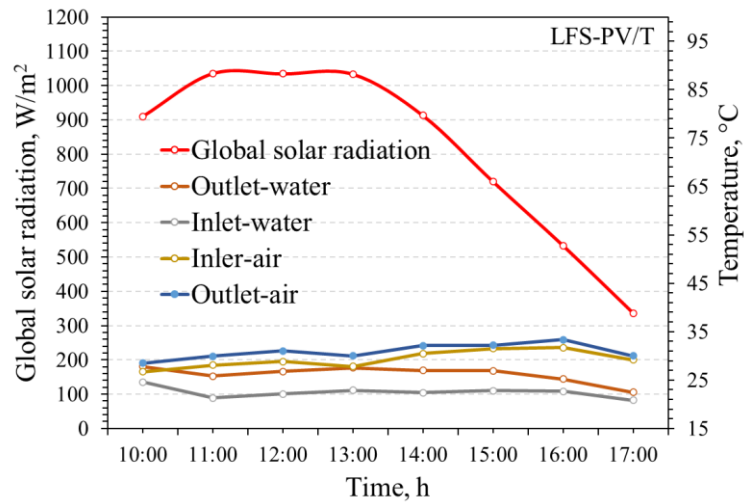


Fig. 4.37. Temperatures of LFS-PV/T module of the inlet (air and water) and outlet (air and water)

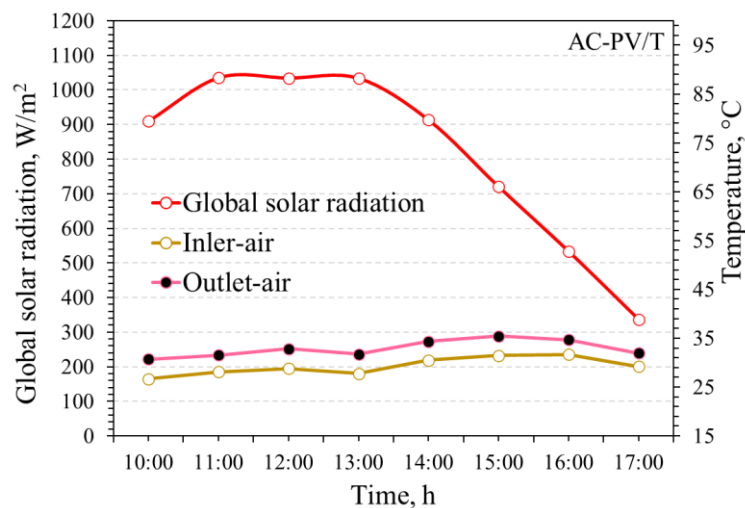


Fig. 4.38. Temperatures of an AC-PV/T system of the inlet and outlet air

The full-period PV cell temperatures for the three modules used in this research are shown in Fig. 4.39: the new hybrid LFS-PV/T system, the conventional AC-PV/T system, and the PV reference module. It is straightforward to notice that the cell temperature of the PV module (standard case) is greater than the temperature of the cells in both the LFS-PV/T and the AC-PV/T. Consequently, the idea behind the new module (LFS-PV/T) indicates that the average cell temperature dropped by 19.2 °C compared to the standard PV unit.

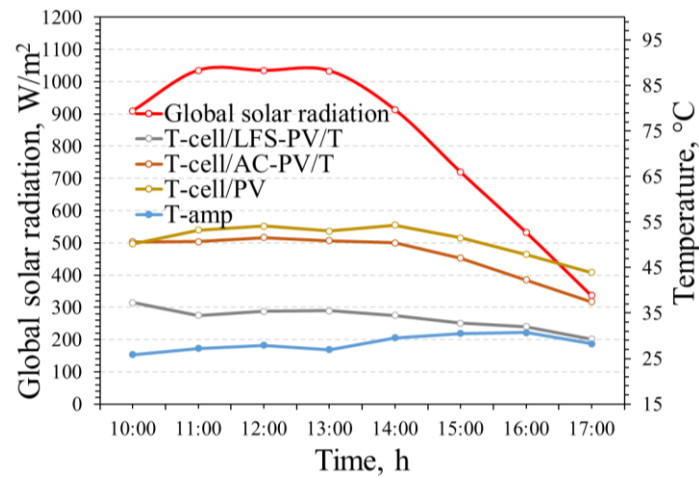


Fig. 4.39. Cell temperatures of the LFS-PV/T, AC-PV/T, and PV modules

It is clear from looking at Fig. 4.39 that the temperature of the PV cell increases gradually with the amount of direct solar energy received per unit area. This research presented a polynomial function of the temperature concerning the radiation for each of the three proposed systems. As clarified in Fig. 4.40, Table 4.6 represents the correlation formulas of each configuration used in this assessment. The solar radiation range utilised in these correlations is arranged between 350 and 1050 W/m².

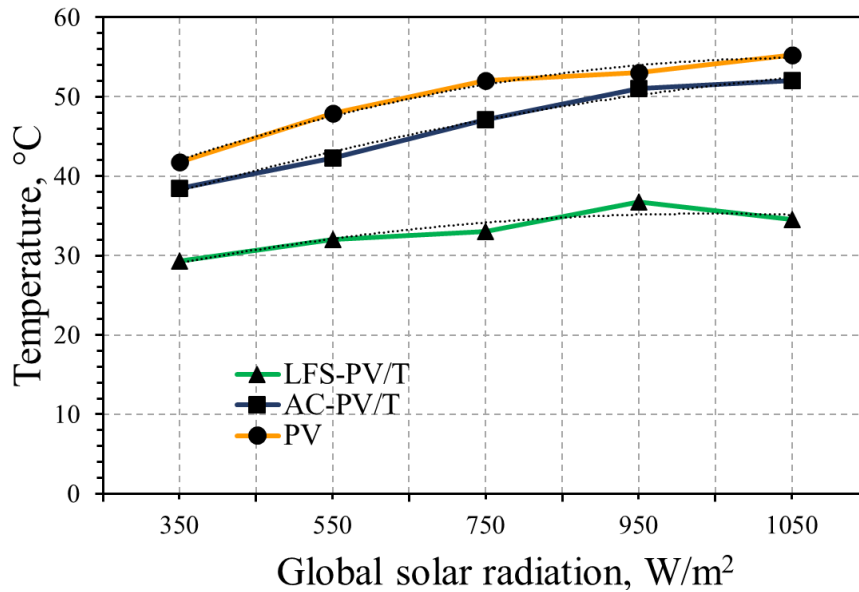


Fig. 4.40. The temperature of the modules as a function of global solar radiation

Table 4.6. Correlations formulas of the research configuration

Module	Correlations formulas
LFS-PV/T	$T_{cell} = 22.96 + 0.022 S - 9.4 \times 10^{-6} S^2$ (4. 1)
AC-PV/T	$T_{cell} = 29.91 + 0.027 S - 4.8 \times 10^{-6} S^2$ (4. 2)
PV	$T_{cell} = 28.89 + 0.046 S - 2.014 \times 10^{-5} S^2$ (4. 3)

On the other hand, this research investigates the temperature of the back side of the proposed modules. Fig. 4.41 illustrates the comparison between the cell temperature and the back sides of the modules. The average temperature difference for the LFS-PV/T, AC-PV/T, and PV was 8.3 °C, 3.25 °C, and 1.7 °C, respectively.

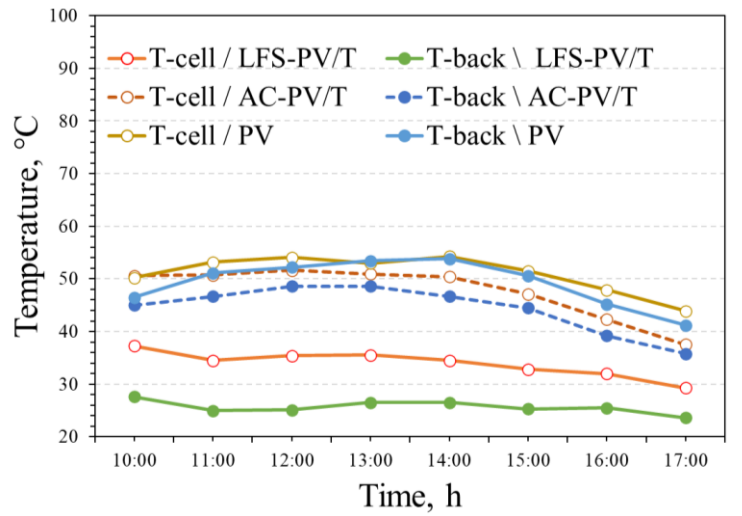


Fig. 4.41. The back and cell temperatures of the LFS-PV/T, AC-PV/T, and PV

Fig. 4.42 depicts the progress of electrical power generated by the three systems in this investigation. The modules reached a significant electrical power enhancement at 12:00. The LFS-PV/T outperformed the AC-PV/T and the PV modules by 28.53% and 13.144%, respectively. Additionally, the maximum current and voltage during the experiments were 3.15 A and 16.1 V, respectively. Based on the load applied to the modules, it was a DC 60 W lamp.

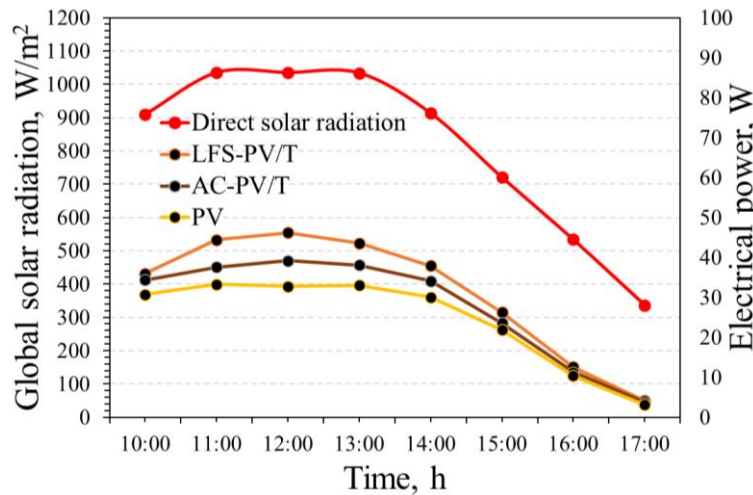


Fig. 4.42. Electrical power of the LFS-PV/T, AC-PV/T, and PV

For all the presented systems, Fig. 4.43 plots the behaviour of the electrical efficiency in time. A significant reduction in the electrical efficiency has occurred due to the decrease in the solar radiation incidence on the module surface after 15:00. Other than that, and the charts show that the electrical efficiency of new units has gone up by 27.7% compared to PV and 12.76% compared to AC-PV/T modules.

4. Results

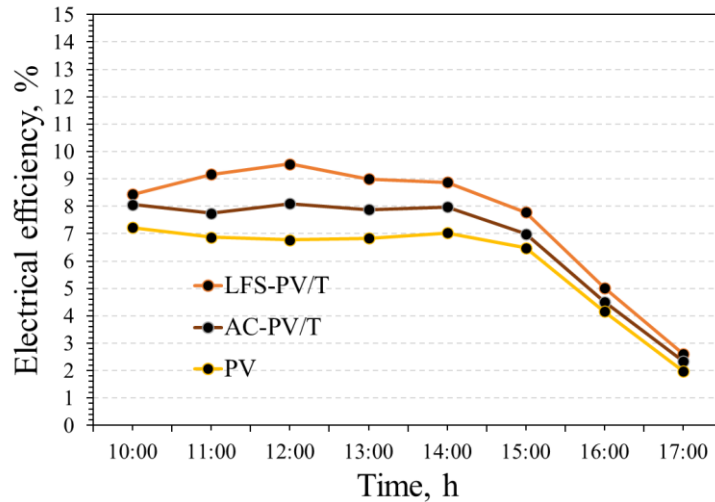


Fig. 4.43. Electrical efficiency of the LFS-PV/T, AC-PV/T, and PV

Fig. 4.44 demonstrates the hourly variants of the heat gain of the LFS-PV/T and AC-PV/T configurations. The bi-fluid unit of this research achieved a significant amount of heat gain due to the louvered fins' design. As an average useful heat-gain (H_g) gathered from the modules, the LFS-PV/T increased by 91.47% from the classical unit of the hybrid AC-PV/T.

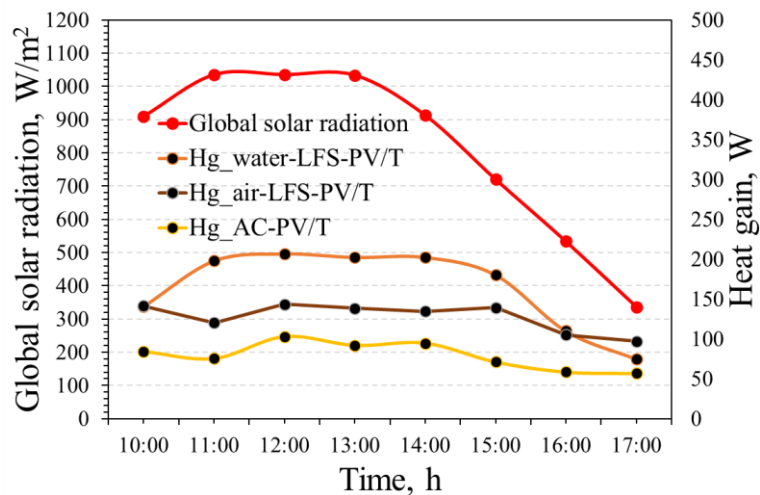


Fig. 4.44. Heat-gain gathered from the LFS-PV/T and AC-PV/T

Fig. 4.45 shows the assessed hourly variants of the heat-gain efficiency of the LFS-PV/T and AC-PV/T configurations. The average heat-gain efficiency is 66.17% and 22.3% for the conventional AC-PV/T and new LFS-PV/T systems, respectively.

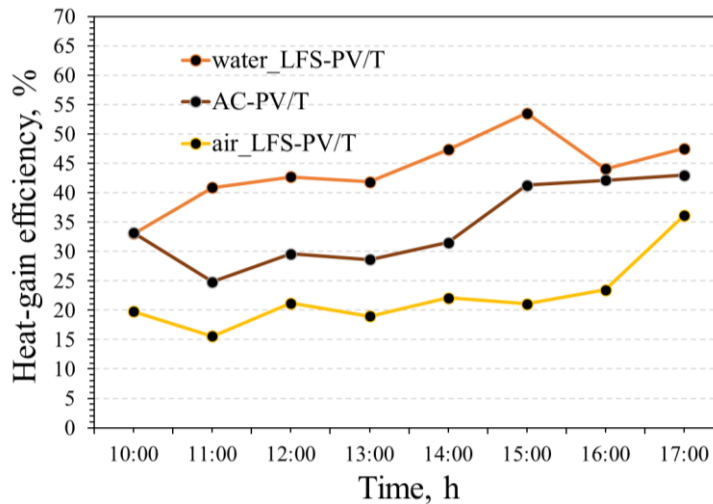


Fig. 4.45. Heat-gain efficiency of the LFS-PV/T and AC-PV/T

Besides, the uncertainty analysis was examined for the module power and efficiencies, as stated by Holman, (2012). Table 4.7 lists the uncertainties of the parameters obtained based on Eq. (3.63).

Table 4.7. The uncertainties of systems efficiencies and power

Systems	Parameters			
	Electrical power	Thermal power	Electrical efficiency	Thermal efficiency
PV	$\pm 0.536\%$	-	$\pm 0.678\%$	-
AC-PV/T	$\pm 0.536\%$	$\pm 0.654\%$	$\pm 0.678\%$	$\pm 0.687\%$
LFS-PV/T	$\pm 0.536\%$	$\pm 0.667\%$	$\pm 0.678\%$	$\pm 0.753\%$

Based on the results of these assessments, the average value of the electrical and heat-gain efficiencies values is 5.9% and 0% for the standard unit of the PV, 6.7% and 34.26% for the AC-PV/T module, 7.56%, and 66.17% for the LFS-PV/T module. Accordingly, the new configuration decreased the cell temperature by up to 19.2 °C compared to the standard PV module.

4.5. Quantifying the wasted heat toward sustainability contributions

Sustainable communities require emerging innovations to fulfil the energy needs of urban societies. Renewable energy systems are the most significant trend in net-zero energy buildings (NZEBS) that serve sustainable development. Due to their consistent power generation, standalone hybrid solar photovoltaic/thermal (PV/T) systems are currently in reasonable demand in the building sector. This section focuses on the new scientific contribution regarding the potentiality of the created LFS-PV/T module to sustainability achievement.

The experimental results in this research were obtained for a clear day on July 14, 2022, from 8:00 to 17:00 with a 3-second time step setting in the data logging system. The study considered three major climatic factors: solar radiation, ambient temperature, and wind velocity. All heat transferring throughout the layers of the examined systems was determined under a flow rate of 0.0335 kg/s and an input air velocity of 1.256 m/s. The hourly fluctuations of the weather data throughout the clear and sunny summer day are depicted in Fig. 4.46. The solar radiation

reached higher values by about 1129 W/m^2 at 13:00. The ambient temperature and wind speed ranged from $25 \text{ }^\circ\text{C}$ – $34 \text{ }^\circ\text{C}$ and 3.7 – 4.2 m/s , respectively.

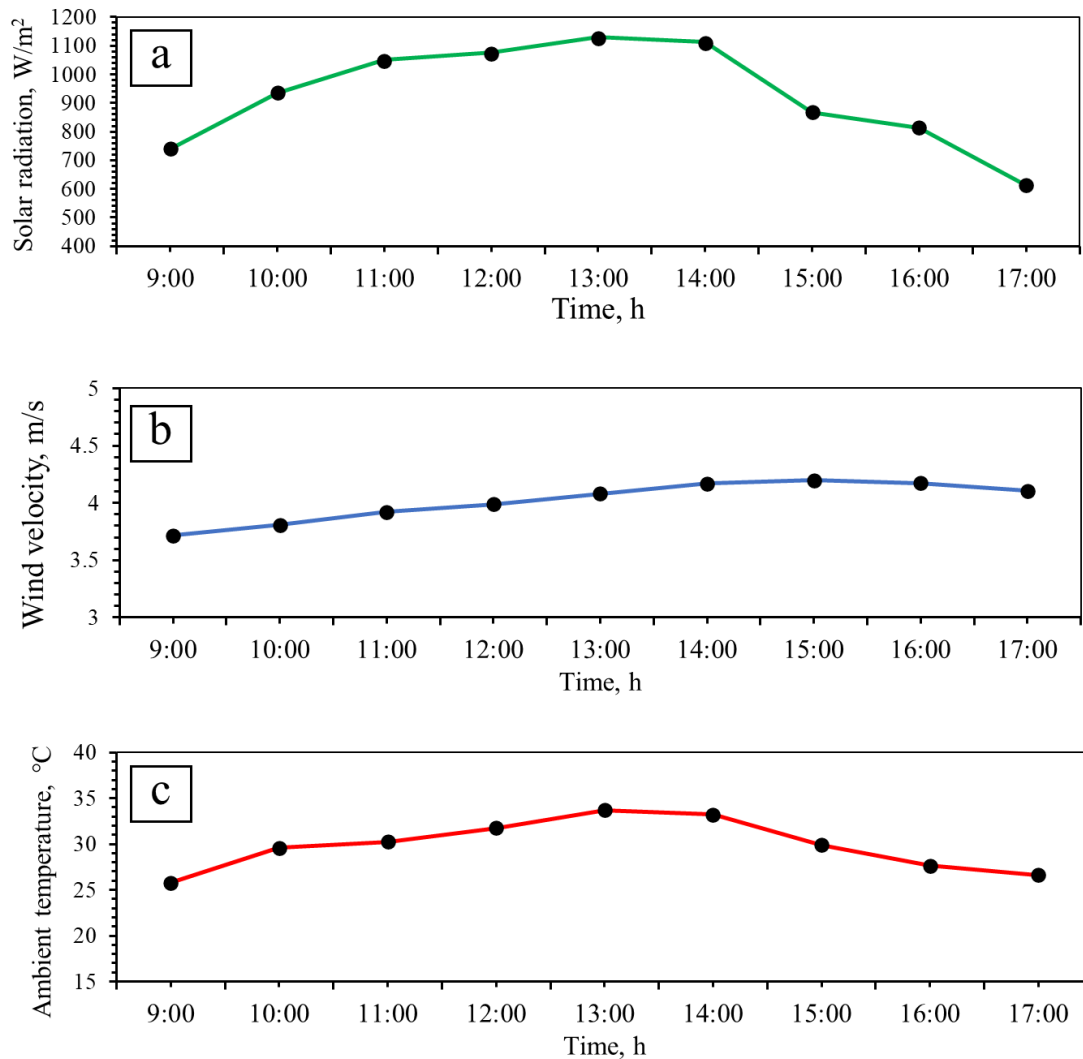


Fig. 4.46. Weather data (a) solar radiation, (b) wind speed, (c) ambient temperature

Fig. 4.47 illustrates the solar cell surface temperature trend of the LFS-PV/T and PV modules. The temperature difference between their surfaces could be noted, where this temperature difference is the dependent factor in constructing the new hybrid solar collector of this research. It can be observed that the PV module has higher temperatures compared to the LFS-PV/T, in which the front surfaced temperature reached $58.2 \text{ }^\circ\text{C}$ and $39.3 \text{ }^\circ\text{C}$ for the PV and LFS-PV/T modules, respectively.

The solar cell surface temperature increased as the solar radiation fell on the PV panels and then transferred to the backside based on the laws of thermodynamics, which state that the heat transfers from the hotter to the cooler region. Then, the heat is transferred to the surrounding area.

Fig. 4.48 illustrates the backside temperature of the PV unit, ambient temperature and the difference between the backside and ambient temperatures ΔT . The figure shows a significant temperature difference among the modules, leading to notable waste heat from the PV module to the atmosphere.

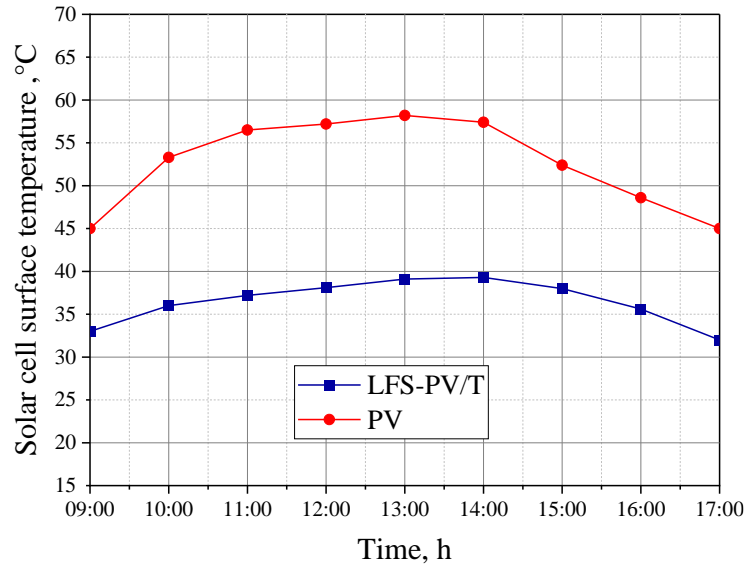


Fig. 4.47. Solar cell surface temperature trend of the LFS-PV/T and PV units

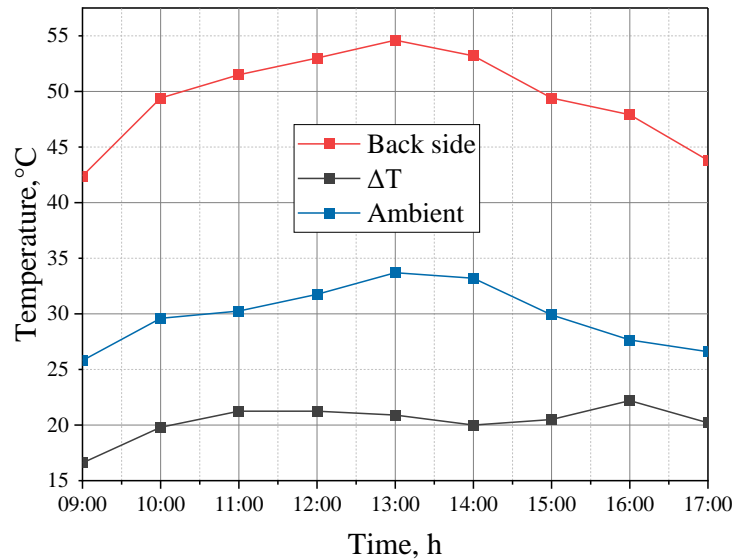


Fig. 4.48. Temperature variation of the PV module

Besides, Fig. 4.49 displays the wasted heat transferred from the PV and LFS-PV/T module surfaces due to the convection and radiation to the surroundings. The name of wasted heat is used when this heat is transferred to the surroundings as a heat loss without being utilised, but when this heat is reduced by such modifications for further investigation, then this heat is useful or recoverable. This phenomenon occurred due to the temperature difference between PV surfaces (front and back) and the ambient, which caused a significant variation between the examined modules in this research. The maximum values of the wasted heat were 213 W and 47 W for the PV and LFS-PV/T modules, respectively.

The ratio of potential useful output to potential useful input is a significant factor in comparing the performance of solar systems, represented by their exergy efficiency. Fig. 4.50 illustrates the exergy efficiency of the tested solar modules in this research. As noted in this figure, The LFS-PV/T module has a significant increment in efficiency compared to the PV module. The average exergy efficiency value for system PV and LFS-PV/T was 6% and 25%, respectively.

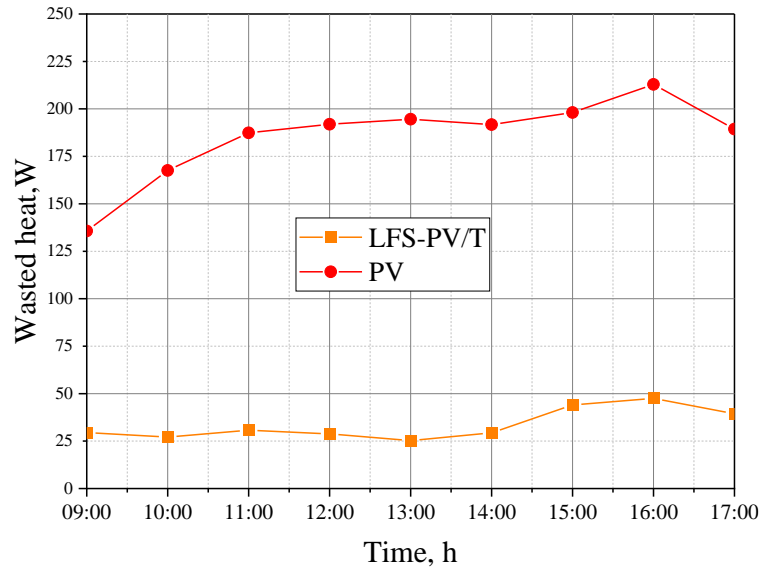


Fig. 4.49. Wasted heat generated from the PV and LFS-PV/T modules

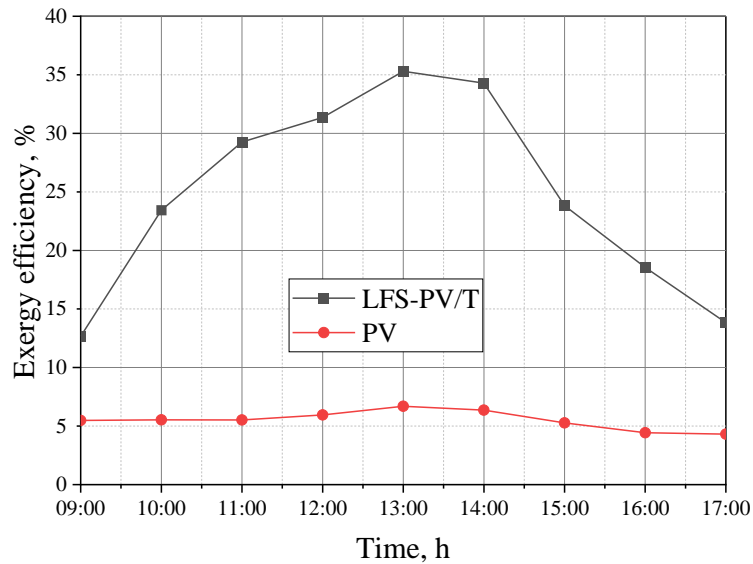


Fig. 4.50. Exergy efficiency of the tested solar modules

The sustainability index (SI), calculated based on the exergetic efficiencies of the systems (see Eq. 3.62), has recently been focused on evaluating the sustainability contribution of renewable energy systems. Fig. 4.51 shows the behaviour of the sustainability indices of the PV and LFS-PV/T modules. The SI values ranged from 1.15 and 1.6 for LFS-PV/T and between 1.03 and 1.06 for the PV module.

In parallel, Fig. 4.52 shows the actual thermal behaviour during the experimentation of the examined modules using a thermal camera. The photo taken at (13:01) shows that the temperature ranged between 15 °C and 65 °C. As clearly shown in the figure, the temperature distribution indicates an effective cooling system in the LFS-PV/T module compared with the PV module.

Consequently, the created bi-fluid PV/T module exhibited a reduction of about 77.6% in the amount of wasted heat released compared to the reference PV module.

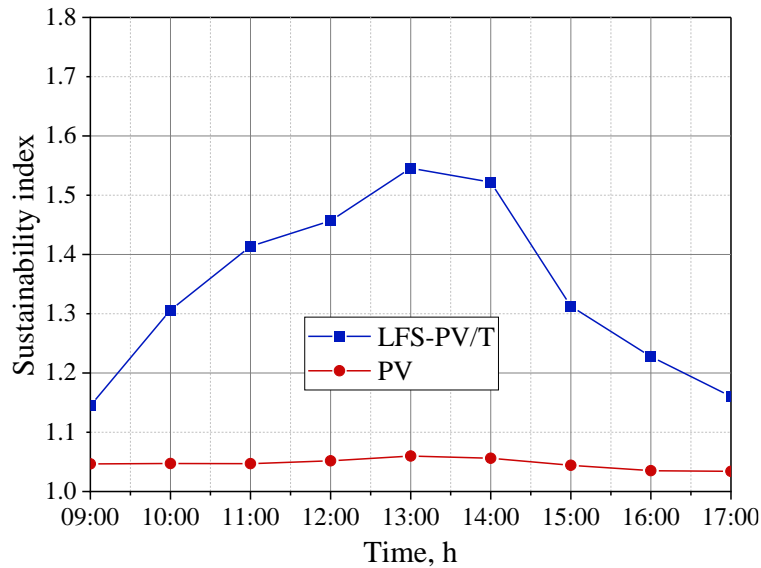


Fig. 4.51. Sustainability index of the LFS-PV/T and PV modules

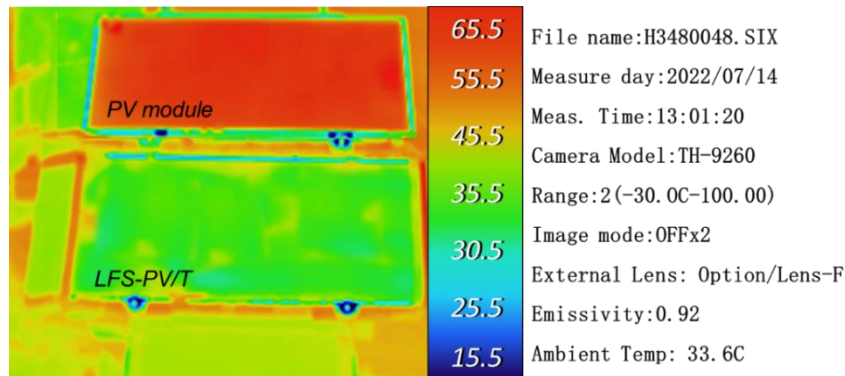


Fig. 4.52. Thermal photo of the modules

Considering all findings obtained in this research work, it can be stated that the modification verified on the PV module is remarkable compared with those conducted in the literature studies. Appendix A11 summarises the exergy efficiency and SI of the hybrid solar thermal collector as reported by various authors that utilize several techniques for PV cooling compared with the current research. As reported in the open literature, no study focused on these factors, especially with a LFS-PV/T module. Besides, data on the sustainability index regarding the PV/T modules are limited. Additionally, no studies consider the wasted heat transferred by PV modules to the surroundings could be found.

4.6. Effect of ternary nanofluid as a heat transfer fluid

Based on the experimental methodology clarified in subsection 3.5, this section presents the results obtained by the new instrument created in this research to evaluate the nanofluid. Accordingly, the efficient nanofluid was employed in the created LFS-PV/T module.

The experiments of this assessment were conducted at room temperature, and it was certified that the laboratory circumstances were the same for all experiments to ensure accurate results. The current investigation examines twenty-four nanofluid samples, categorised into four ternary and binary nanoparticles illustrated previously in section (3.5.3), each dispersed into

4. Results

six volume concentrations (ϕ), 0.05, .0.1, 0.2, 0.3, 0.4, and 0.5%. The densities (ρ) and specific heats (C) of the produced twenty-four nanofluids samples are presented in Table 4.8.

Table 4.8. Specific heat and density of the nanofluids

ϕ	MWCNTs–MgO–BN		MWCNTs–MgO		MWCNTs–BN		MgO–BN	
	ρ (kg/m ³)	C (kJ/kgk)	ρ (kg/m ³)	C (kJ/kgk)	ρ (kg/m ³)	C (kJ/kgk)	ρ (kg/m ³)	C (kJ/kgk)
0.5	1004.603	4.143	1006.215	4.138	1002.99	4.148	1006.69	4.138
0.4	1003.082	4.152	1004.372	4.148	1001.792	4.156	1004.752	4.147
0.3	1001.562	4.161	1002.529	4.157	1000.594	4.163	1002.814	4.157
0.2	1000.041	4.169	1000.686	4.167	999.396	4.171	1000.876	4.167
0.1	998.5205	4.178	998.843	4.177	998.198	4.179	998.938	4.177
0.05	997.7603	4.182	997.9215	4.182	997.599	4.183	997.969	4.182

One of the most essential properties that describes the characteristics of the nanoparticles is the scanning electron microscopy (SEM) technique. It was employed to document the microstructure and morphology of all hybrid ternary and binary nanoparticles that were created. Fig. 4.53 illustrates all the SEM images of all prepared nanoparticles: MWCNTs–MgO–BN (see Fig. 4.53d), MWCNTs–MgO (see Fig. 4.53e), MWCNTs–BN (see Fig. 4.53f), and MgO–BN (see Fig. 4.53g). As shown in the figures, the spectral images of electron-transparent samples are high-resolution at 30 kV, 5 μm and clarify the homogeneity of the prepared nanoparticles after pre-shaking and milling processes compared to original SEM images before synthesis (Fig. 4.53a-c). Besides, Fig. 4.54 illustrates the SEM images of all proposed ternary and binary hybrid nanoparticles after ball milling processes through different resolutions of 50, 20, 5, and 2 μm .

4. Results

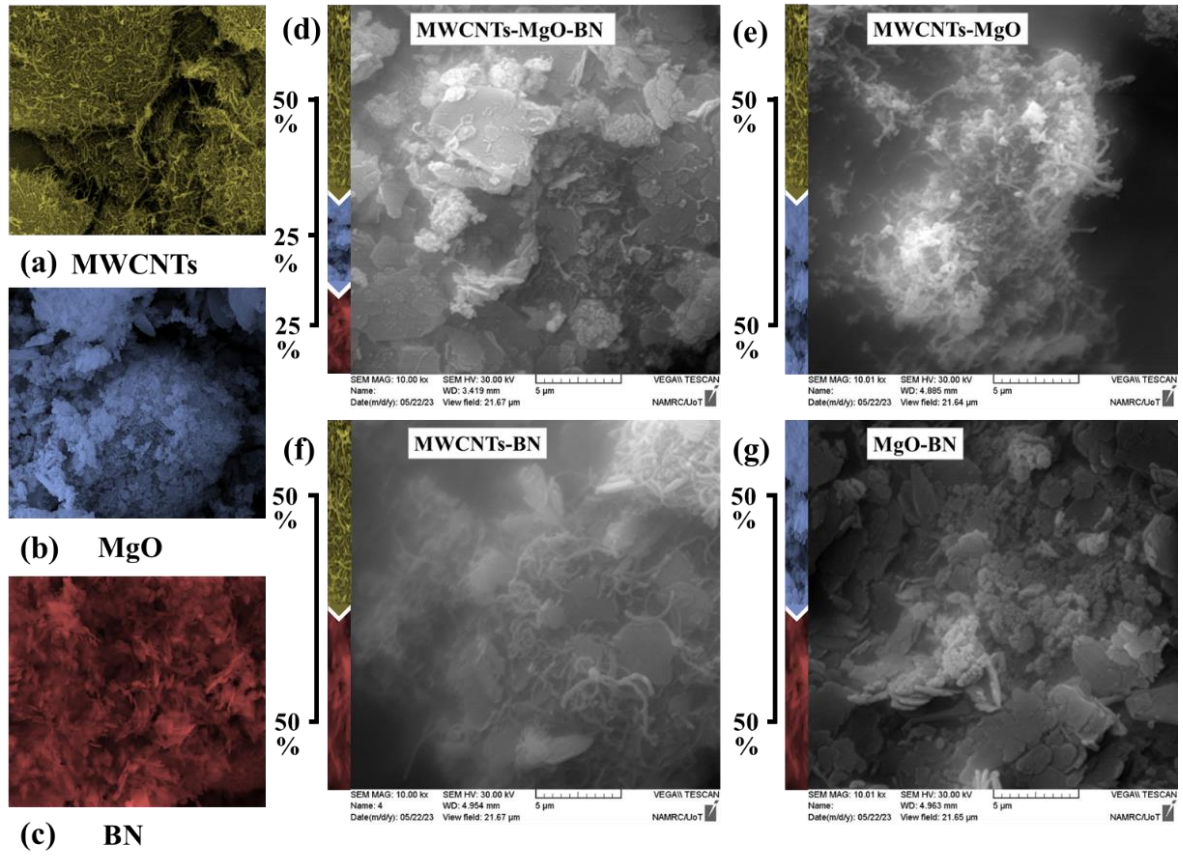


Fig. 4.53. The SEM images of the nanoparticles. a) MWCNTs, b) MgO, c) BN, d) MWCNTs–MgO–BN, e) MWCNTs–MgO, f) MWCNTs–BN, and g) MgO–BN

4. Results

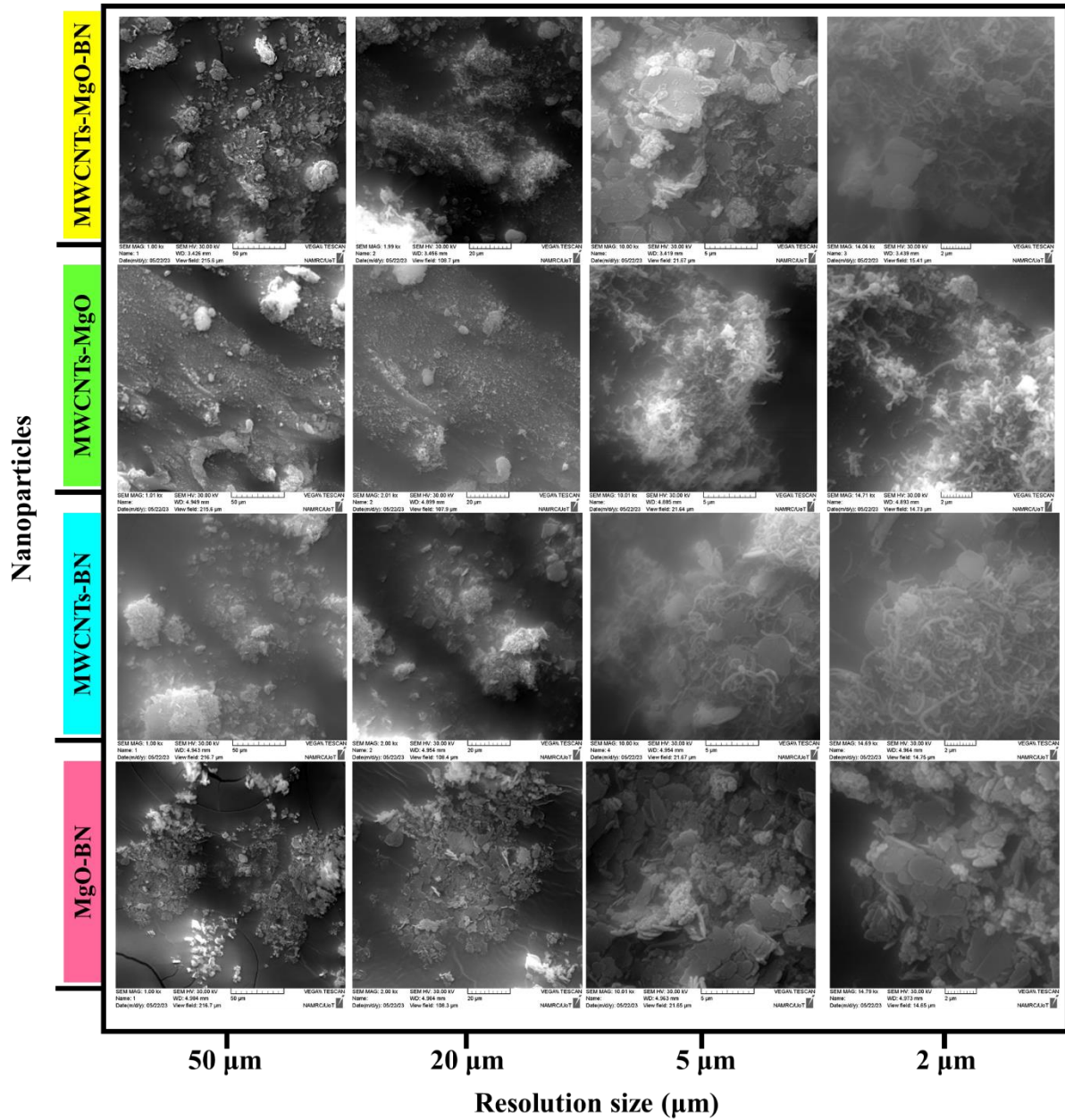


Fig. 4.54. The SEM images of the nanoparticles under different resolutions

The primary parameter assessed in the experiment for evaluating and comparing the synthesised ternary and binary hybrid nanofluids is the thermal equilibrium time (TET), as measured using the developed instrument FTET. Figs. 4.55-4.58 illustrate the TET of all proposed ternary and binary nanofluids composites.

Heat exchangers exhibit a characteristic pattern of fluid curves, wherein the width of the curves gradually decreases from an initial wide state to a narrower state, ultimately leading to a relatively constant temperature. The two fluids (water and nanofluid) utilised in the FTET instrument behave somewhat in the same trend as the heat exchanger fluids. The cold medium (nanofluid) absorbed the heat from the hot one (distilled water) until the thermal equilibrium state occurred. On the contrary, the hot medium releases heat to the cold medium until the thermal equilibrium state occurs. Fig. 4.55 illustrates the heat transfer behaviour of the water and the ternary hybrid nanofluids, MWCNTs–MgO–BN. As shown, the equilibrium point is the intersection of the boiling water temperature curve and the hotted nanofluid temperature

4. Results

curve. The equilibrium time and temperature (equilibrium points) were 189; 63, 183; 63.5, 176; 64.1, 170; 65.5, 163; 67, and 157 s; 68.5 °C for 0.05, 0.1, 0.2, 0.3, 0.4, and 0.5% volume concentrations, respectively.

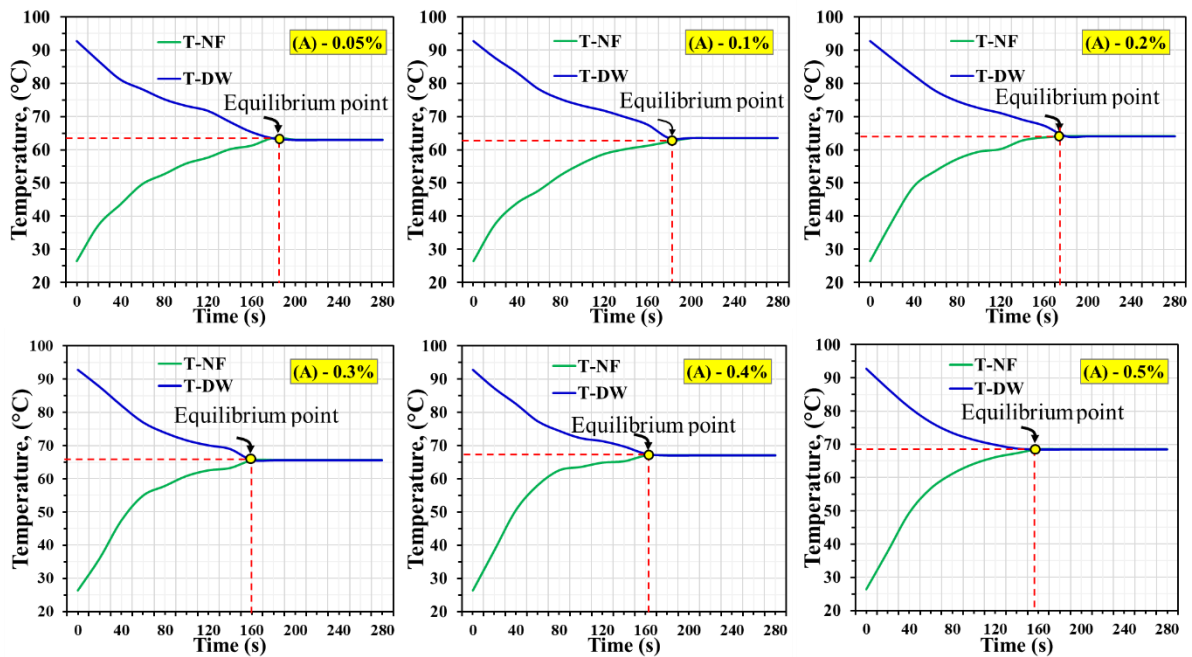


Fig. 4.55. Thermal equilibrium time and Temperatures at various volume concentrations of hybrid ternary nanofluids MWCNTs–MgO–BN

Besides, Fig. 4.56 illustrates the heat transfer behaviour of the binary hybrid nanofluids, MWCNTs–MgO. The equilibrium times and temperatures were 232; 61.35, 228; 61.79, 222; 62.45, 216; 63.12, 208; 64, and 198 s; 65 °C for 0.05, 0.1, 0.2, 0.3, 0.4, and 0.5% volume concentrations, respectively. Fig. 4.57 illustrates the heat transfer behaviour of the binary hybrid nanofluids, MWCNTs–BN. The equilibrium time and temperature were 219; 61.35, 213; 62.26, 204; 63.25, 196; 64.13, 187; 65.12, and 179 s; 66 °C for 0.05, 0.1, 0.2, 0.3, 0.4, and 0.5% volume concentrations, respectively. Fig. 4.58 illustrates the heat transfer behaviour of the binary hybrid nanofluids, MgO–BN. The equilibrium time and temperature were 259; 60.25, 255; 60.75, 245; 61.13, 243; 61.9, 238; 62.62, and 230 s; 63.5 °C for 0.05, 0.1, 0.2, 0.3, 0.4, and 0.5% volume concentrations, respectively.

Furthermore, the same test occupied for the nanofluids in the FTET instrument was conducted for the base fluid (distilled water), and the equilibrium time and temperature were 269 s and 58 °C, respectively. This test was accrued as a reference point for evaluating and comparing the distilled water, as it is a base fluid and the prepared nanofluids.

4. Results

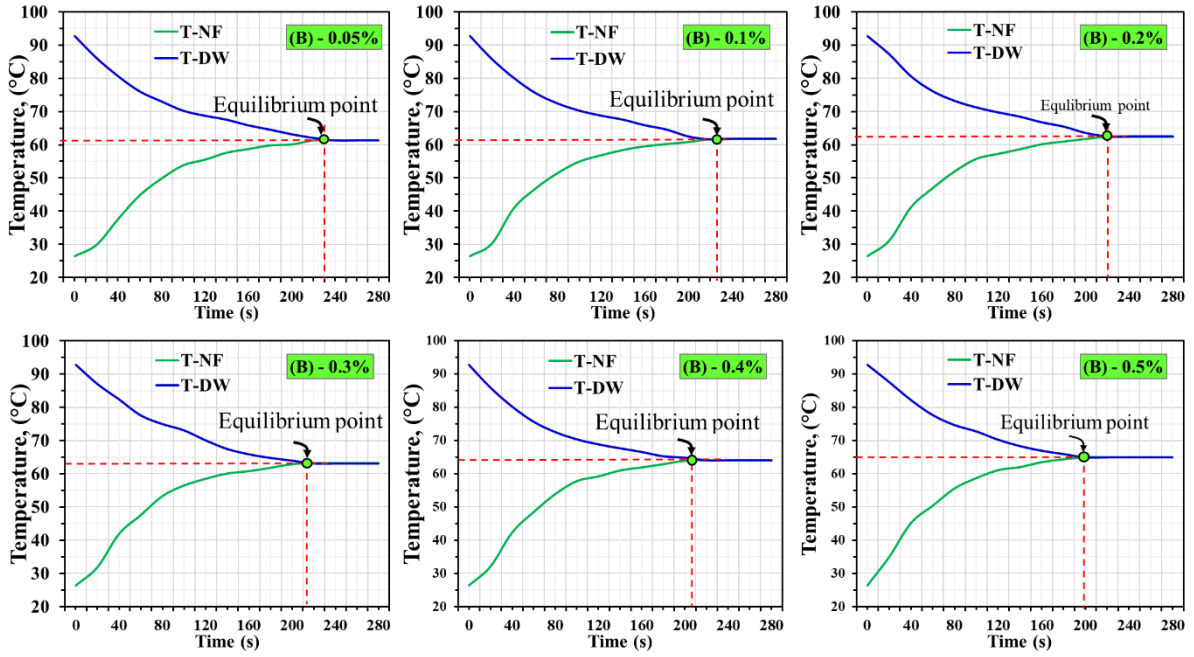


Fig. 4.56. Thermal equilibrium time and Temperatures at various volume concentrations of the binary hybrid nanofluids, MWCNTs–MgO

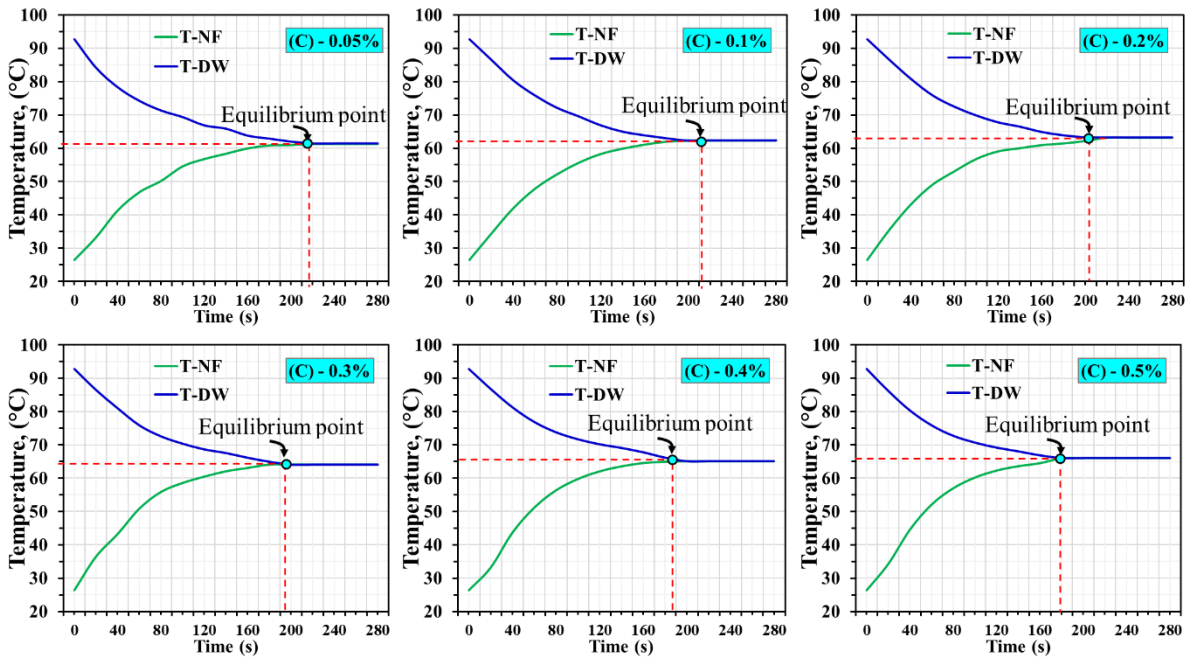


Fig. 4.57. Thermal equilibrium time and Temperatures at various volume concentrations of the binary hybrid nanofluids, MWCNTs–BN

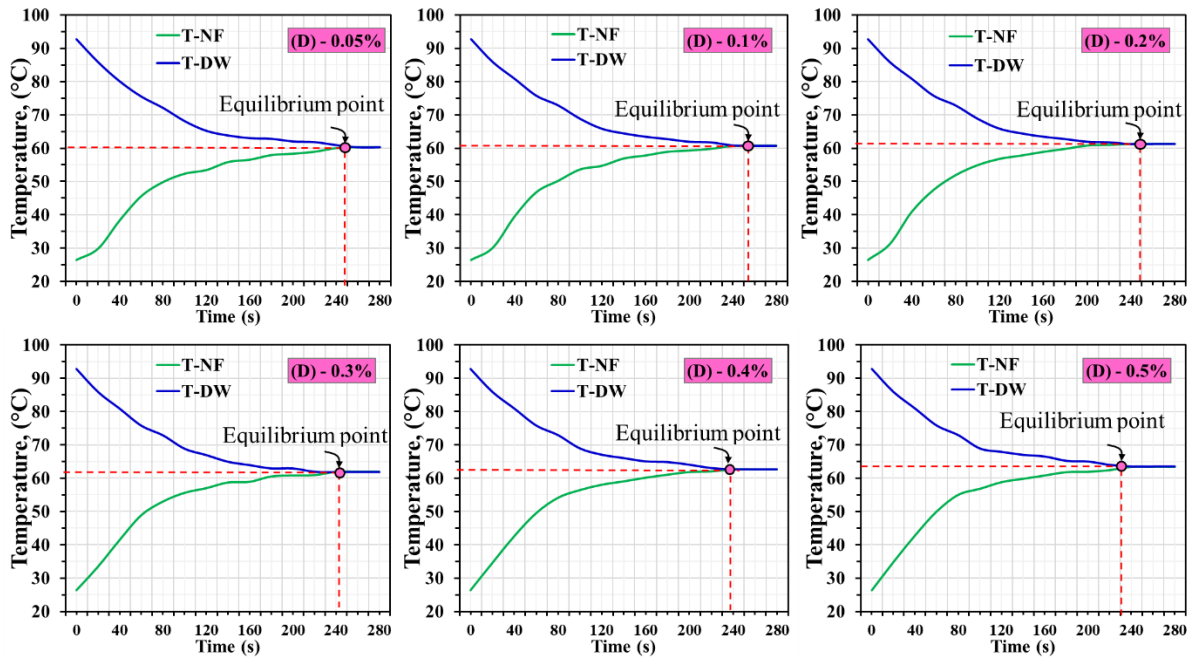


Fig. 4.58. Thermal equilibrium time and Temperatures at various volume concentrations of the binary hybrid nanofluids, MgO–BN

According to the previous results, following thermal equilibrium time, this research's other significant evaluation factor is the heat transferred to the nanofluid from the initial to thermal equilibrium states. It is calculated for all samples tested in the FTET instrument based on the temperature difference between the initial and thermal equilibrium states. This heat represents the potentiality of nanofluids compared to others. Fig. 4.59a-d specifies this heat for all the proposed particles at different volume concentrations. The maximum heat transferred to the nanofluids was 19.4, 17.7, 18.2, and 17 kJ for ternary MWCNTs–MgO–BN, binary MWCNTs–MgO, binary MWCNTs–BN, and binary MgO–BN, hybrid nanofluids, respectively. Additionally, this heat increases with the increase in the volume concentration. The heat being discussed in this context can be categorised as nano energy, emphasising the superior potential of nanofluids compared to alternative fluid mediums, which carries substantial significance within the appraisal procedure.

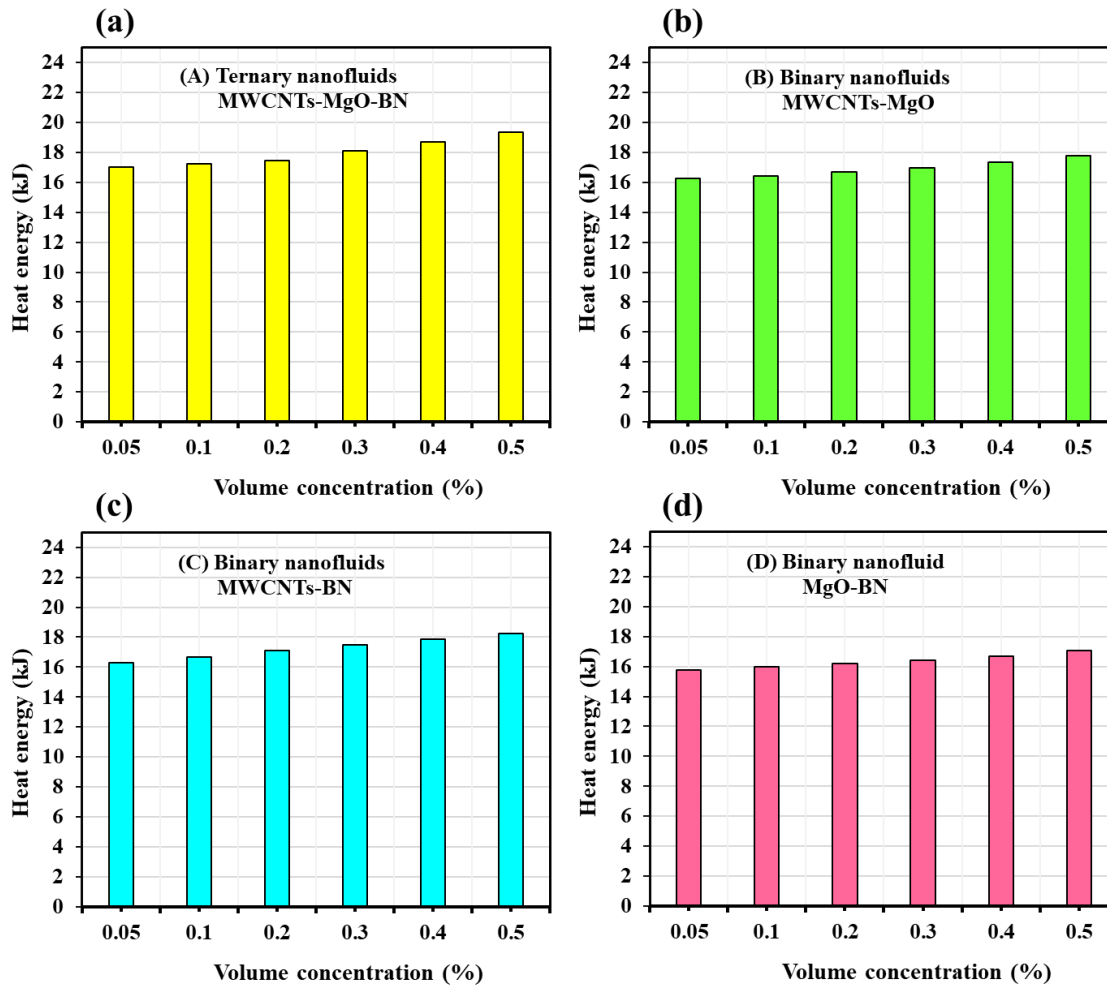


Fig. 4.59. Heat transferred to the nanofluids. a) MWCNTs–MgO–BN, b) MWCNTs–MgO, c) MWCNTs–BN, and d) MgO–BN

The more focused factor in the literature utilised to evaluate the thermal behaviour of the nanofluids is the influence of the volume concentrations. Fig. 4.60 exemplifies this factor and its effect on the equilibrium time and the thermal equilibrium temperature for the MWCNTs–MgO–BN ternary hybrid nanofluids (Fig. 4.60a), MWCNTs–MgO, binary hybrid nanofluids (Fig. 4.60b), MWCNTs–BN, binary hybrid nanofluids (Fig. 4.60c) and MgO–BN, binary hybrid nanofluids (Fig. 4.60d).

MWCNTs–MgO–BN transferred more heat than MWCNTs–MgO, MWCNTs–BN, and MgO–BN by 8.3, 5.8, and 11.8%, respectively. This heat under consideration could be classified as nano energy, highlighting the potential of nanofluids compared to other fluids. This aspect holds significant importance in the process of evaluation.

4. Results

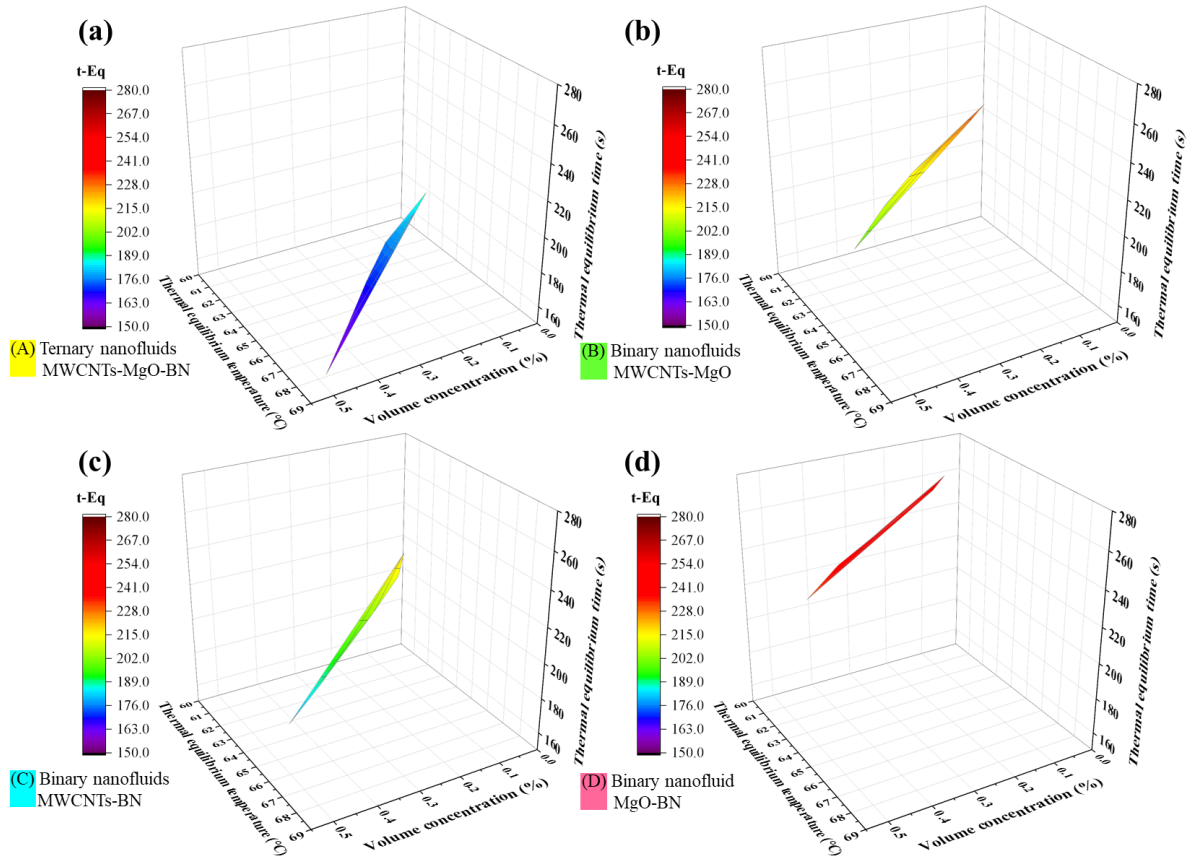


Fig. 4.60. Effect of the volume concentration. a) MWCNTs–MgO–BN, b) MWCNTs–MgO, c) MWCNTs–BN, and d) MgO–BN

As seen in the figure, the volume concentration has a significant role in heat transfer enhancement for the proposed particles. The thermal equilibrium time of the samples decreased with the increase in volume concentration, which means that the thermal conductivity of the samples is accordingly enhanced as time decreases.

The thermal potential of the composite “A” (MWCNTs–MgO–BN) clarifies that the new ternary nanofluid has a positive contribution; this would contribute efficiently to energy conversion applications due to thermal conductivity enhancement.

Regarding nanofluid potentiality in bi-fluid LFS-PV/T module and based on the results obtained via the new technique utilised by the FTET instrument, the more thermal effective nanofluid was used in the photovoltaic thermal PV/T module created in this research; the new bi-fluid PV/T module utilises a novel copper absorber with serpentine tubes and louvered fins, LFS-PV/T (Alshibil et al., 2023d)

Hybrid ternary nanofluid MWCNTs-MgO-BN with a volume concentration of 0.5% was selected to enhance the PV/T module performance and compared with water-based units and a standalone PV unit as a reference module.

Data was systematically collected between 9:00 and 15:00 on specific days in August at the solar laboratory of MATE University in Gödöllő, Hungary. Throughout the tests, the collector's tilt angle was consistently set at 43°, representing the inclination relative to the horizontal surface when the collector is oriented towards the south with a –20 azimuth angle. The solar

radiation and ambient temperature for the days were almost close in value. Fig. 4.61 illustrates the weather conditions of the study location.

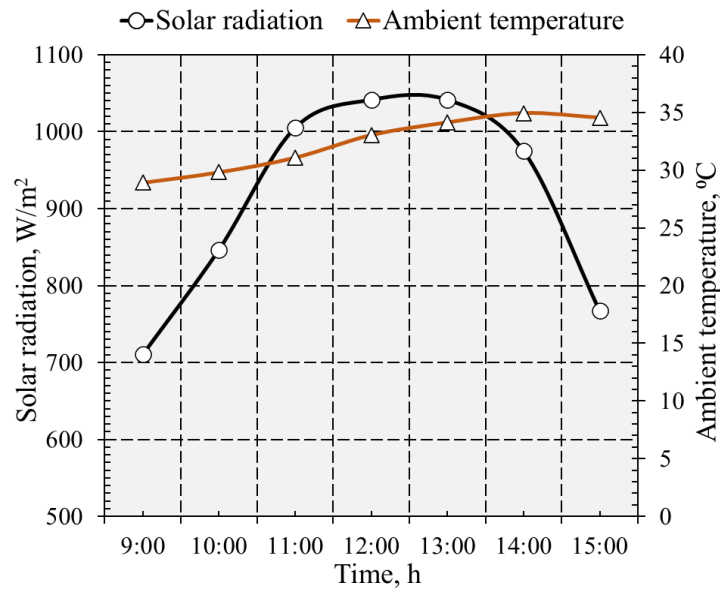


Fig. 4.61. Radiation and the ambient temperature of the study location

The direct and primary effect of radiation on the studied solar systems is more prior than the effect of the remaining variables. The maximum value of solar radiation was $1045 W/m^2$ at 12:20 pm, and the ambient temperature was measured based on the ASHRAE standard, and the maximum value was $35.7 ^{\circ}C$.

The most significant parameter to measure and evaluate is the cell temperature of the PV modules; accordingly, Fig. 4.62 displays the variation of these temperature profiles for water-cooled (LFS-PV/T) and nanofluid-cooled (LFS-PV/T-NF) modules examined in this research over test time compared to the PV module. Radiation has a dramatic effect on the surfaces of solar cells. These surfaces rise in temperature due to the radiation and their ability to transfer heat from them to their surroundings or the parts attached to them.

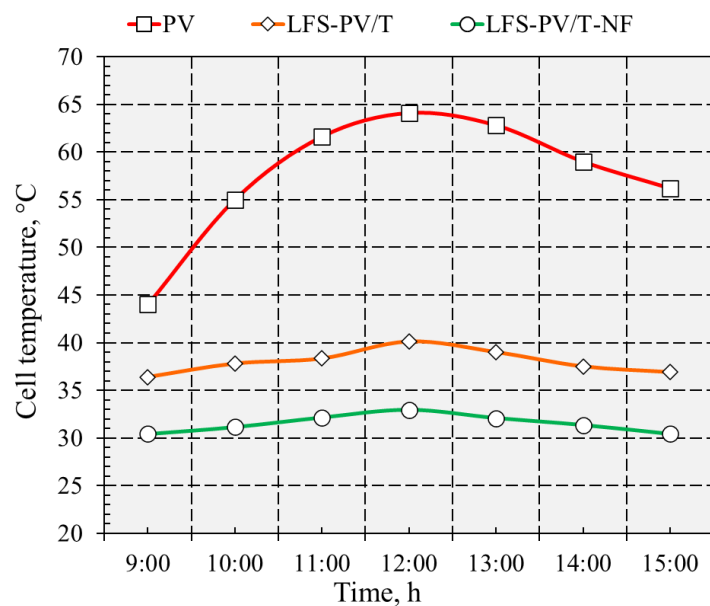


Fig. 4.62. Cell temperatures of the study modules

Consequently, the maximum temperature grasped by the PV module was about 64.8 °C. The temperature of the solar cell rises swiftly, reaching 43 °C by 9:00 am, and proceeds to increase, leaping to 64.8 °C at 12:00 pm. The elevated temperature of the photovoltaic (PV) cell results from the intense radiation levels in the research location on the selected days. The core portion of incoming sunlight is transformed into wasted thermal energy within the PV cells, resulting in an increase in their temperature.

Besides, the highest cell temperatures of the LFS-PV/T and LFS-PV/T-NF were 40 °C and 33 °C, respectively. The PV/T modules exhibit remarkable cooling efficiency, while the solar cell maintains a significantly low surface temperature, especially in the nanofluid-based unit. This effect remains consistent even when exposed to the same amount of solar radiation as the PV cell. Consequently, it is undeniable that this factor significantly impacts the system's overall performance.

Fig. 4.63 displays the mean daily fluctuations in the improvement as an augmentation in electrical efficiency relative to the reference module, which is closely correlated with the temperature of the PV surface.

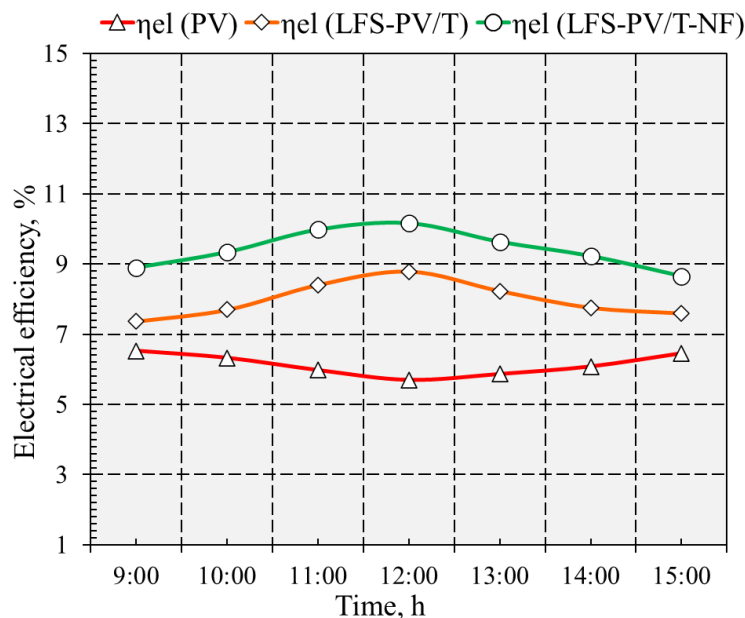


Fig. 4.63. Electrical efficiency of the studied module

Based on Fig. 4.63, the maximum electrical efficiency associated with the reference unit is achieved in the day at the highest solar irradiance at 12:00, where the maximum electrical efficiency values were 10.16%, 8.78% and 6.6% for LFS-PV/T-NF, LFS-PV/T and PV modules respectively.

The utilisation of nanofluid leads to a more substantial augmentation in voltage, which is represented in the total power generated in the PV/T modules. The electric power of the unit filled with nanofluid was greater than that of the units filled with water and standalone PV modules. As vividly elucidated in Fig. 4.63, the maximum values of the modules were 53 W, 46 W and 32 W for LFS-PV/T-NF, LFS-PV/T and PV modules, respectively.

4. Results

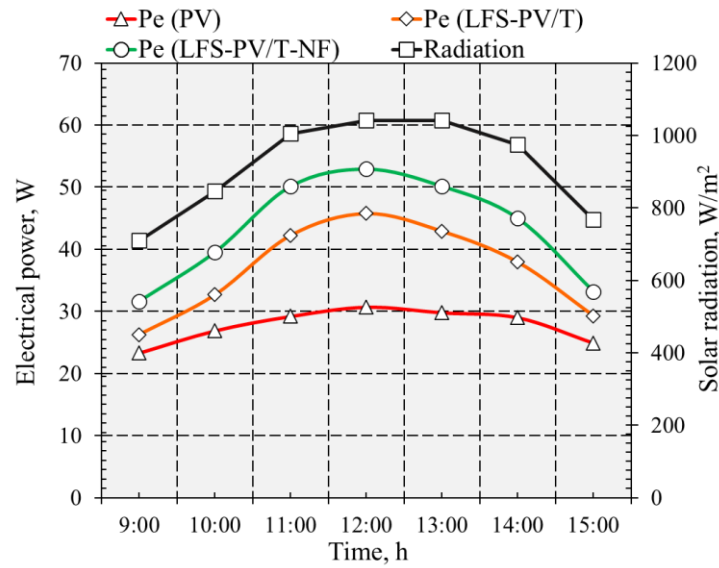


Fig. 4.64. The electrical power of the studied modules

Fig. 4.65 depicts the variations in thermal and electrical powers throughout the daily experiment (from 9:00 to 15:00) for various scenarios, including LFS-PV/T-NF, LFS-PV/T, and PV modules.

The figure demonstrates that the utilisation of nanofluids in the LFS-PV/T-NF module results in a 37.65% increase in thermal power compared to the LFS-PV/T module.

The literature has identified many phenomena as possible causes for the thermal power enhancement of the PV/T system, including Brownian motion, nanoparticle migration, sedimentation, and viscosity gradient.

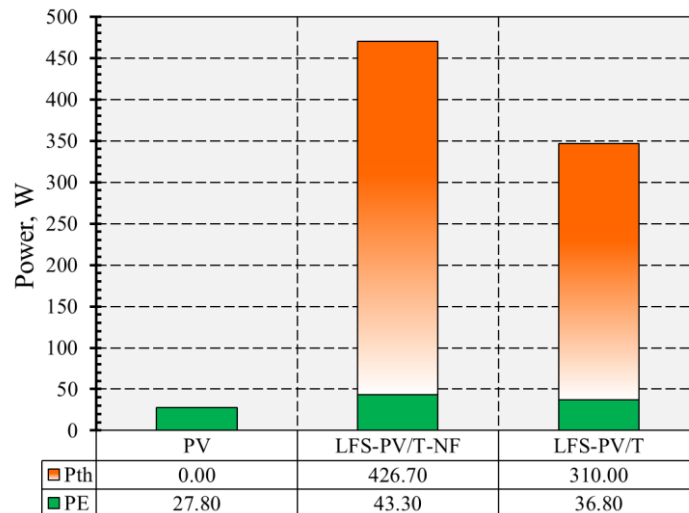


Fig. 4.65. Average electrical and thermal power values of study modules

It can be seen in Fig. 4.65 that the PV/T-W and LFS-PV/T-NF modules produce more electricity than the PV module by 32.37 and 55.75%, respectively. These findings indicate that the LFS-PV/T-NF module, which shows the highest thermal power enhancement, also exhibits the highest electrical power enhancement. This improvement is because the LFS-PV/T-NF module reduces cell surface temperature more consistently than the PV and LFS-PV/T modules.

Fig. 4.66 demonstrates the average values of electrical and thermal efficiency achieved throughout the course of daily testing. The LFS-PV/T-NF module exhibits a thermal efficiency that is 30.78% higher than that of the LFS-PV/T module. Furthermore, the average daily electrical efficiencies for the two modules, LFS-PV/T-NF and LFS-PV/T, experienced a rise of 41.7% and 20.2%, respectively, compared to the solitary PV module. Employing a nanofluid as the operational fluid leads to a more significant reduction in surface temperature than LFS-PV/T and PV modules. Thus, the use of nanofluid results in superior electrical efficiency.

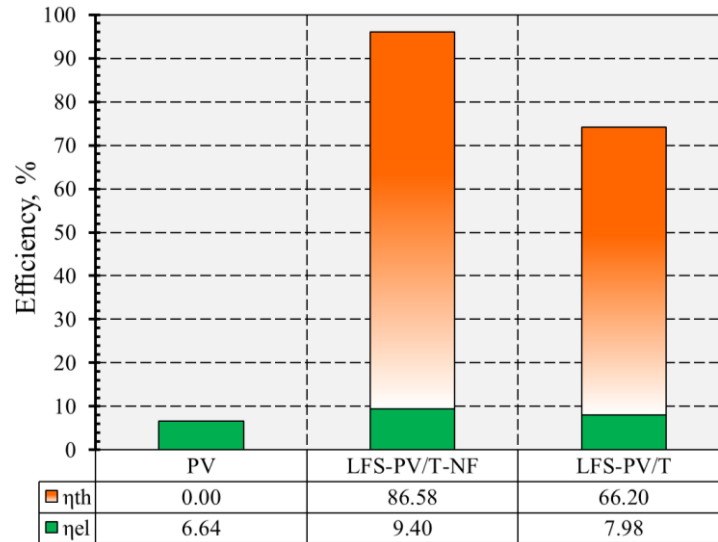


Fig. 4.66. Average electrical and thermal energy efficiency values of study modules

4.7. Thermal conductivity of the ternary nanofluids

As proved in the previous sections, MWCNT-MgO-BN ternary nanofluid is the best nanofluid among others. This assessment focuses on the results of the thermal conductivity and generates a new related correlation for further investigations.

The thermal conductivity of the ternary nanofluids was determined in the current investigation using a KD-2 Pro thermal characteristics instrument manufactured by Decagon Inc. in the United States. The margin of error for the measurements was approximately 5%. This technology utilizes the transient hot wire approach to quantify the thermal conductivity of fluids. This technique is recognised for its rapidity and reliability. The instrument was calibrated with ASHRAE society to ensure adequate accuracy before beginning the measurements.

All thermal conductivity measurements were repeated for various temperatures ranging from 25–55 °C. The measurement considered a range that was appropriate for the experiment periods, which occurred during the summer. On the other hand, if the experiment were extended for the whole year, then the measurement range should be extended and suitable for the entire year. For example, the range may be between -15 and 60 °C.

According to the results conducted in this experiment, the thermal conductivity ratio is defined as:

$$\text{Thermal conductivity ratio (kR)} = \frac{k_{tn}}{k_{bf}} \quad (4.4)$$

The graph in Fig. 4.67 displays how temperature and volume concentration in the ternary nanofluids affect the thermal conductivity ratio. The ratio changes with temperature (T) and the volume concentration (ϕ) of the nanoparticles in the base fluid. The kR of ternary nanofluids decreases with rising temperature and increases with increasing volume concentration.

Since the thermal conductivity of ternary nanofluids significantly improves with temperature, this may explain why the thermal conductivity ratio decreases as the temperature rises. The tests on thermal conductivity show that the ternary nanofluid has the best improvement, with a 20.8% rise in thermal conductivity at a temperature of 25 °C and a volume concentration of 0.5%.

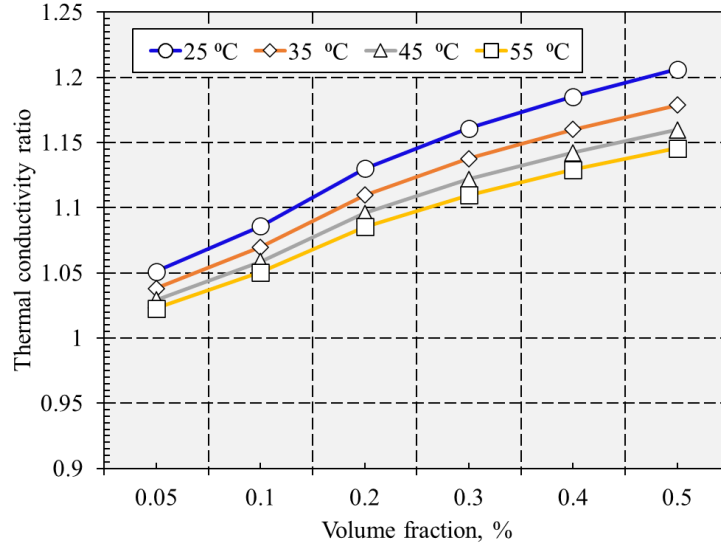


Fig. 4.67. Variants of kR with solid volume concentration and temperature

Previous literature has not investigated ternary nanofluids consisting of MWCNT-MgO-BN; hence, no correlation exists to predict the ratio of thermal conductivity between ternary nanofluids and the base fluid. This research provides a correlation derived from experimental assessments, as presented in Eq. (4.5). This correlation predicts the thermal conductivity ratio as a function of the MWCNT-MgO-BN ternary nanofluid volume fractions and temperatures. The correlation has an identical extraordinary accuracy R^2 of 0.995,

$$kR = \frac{k_{tn}}{k_{bf}} = 0.9159 + 0.95 \times \left[\frac{(\phi)^{0.332}}{(T)^{0.297}} \right] \quad (4.5)$$

Consequentially, this empirical equation can be utilised for heat transfer applications with the utmost precision.

An investigation of the deviation margin DM in the thermal conductivity ratio was conducted to assess the reliability of the correlation. The discrepancy between empirical findings and projected data could be computed in the following manner:

$$DM = \left[\frac{kR_{Ex.} - kR_{Pr.}}{kR_{Ex.}} \right] \times 100 \quad (4.6)$$

where kR_{Ex} and kR_{Pr} . Are the experimental and predicted thermal conductivity ratio.

Fig. 4.68 compares the values of the thermal conductivity ratio for the results obtained by the new correlation and the result obtained by the KD-2. As shown in the figure, the values of the DM are illustrated based on Eq. (4.6). It is evident that the majority of the data points are located either close to or directly on the equality line, indicating a lack of significant deviation.

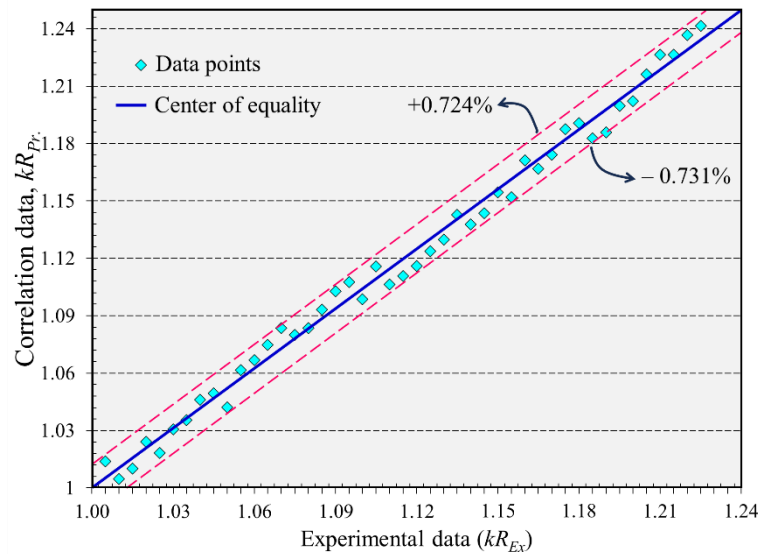


Fig. 4.68. Thermal conductivity ratio values of the correlation and KD-2

4.8. Flowrate influence

The mass flow rate is a crucial factor in the conceptualisation of PV/T solar systems. This section focuses on the influence of the flow rate of the heat transfer fluid on the performance of the created LFS-PV/T module. As the presented module utilised water and air as a working fluid, five values of water flow rates and four values of air flow rate were used, as listed in Table 4.9.

Table 4.9. Flow rates of water and airflow

Water flow rate, kg/s		Air flow rate, kg/s	
W1	0.016	A1	0.017
W2	0.02	A2	0.021
W3	0.025	A3	0.028
W4	0.03	A4	0.034
W5	0.035		

This research was conducted on several clear days in July 2023 in Gödöllő at the Solar Lab of MATE University. The method started by fixing each air flow rate and varying the water flow rate for two hours. Fig. 4.69 a-d illustrates the thermal and electrical efficiency change with flow rate values. As clarified, thermal and electrical efficiency increased with increasing air and water flow rates in the LFS-PV/T module.

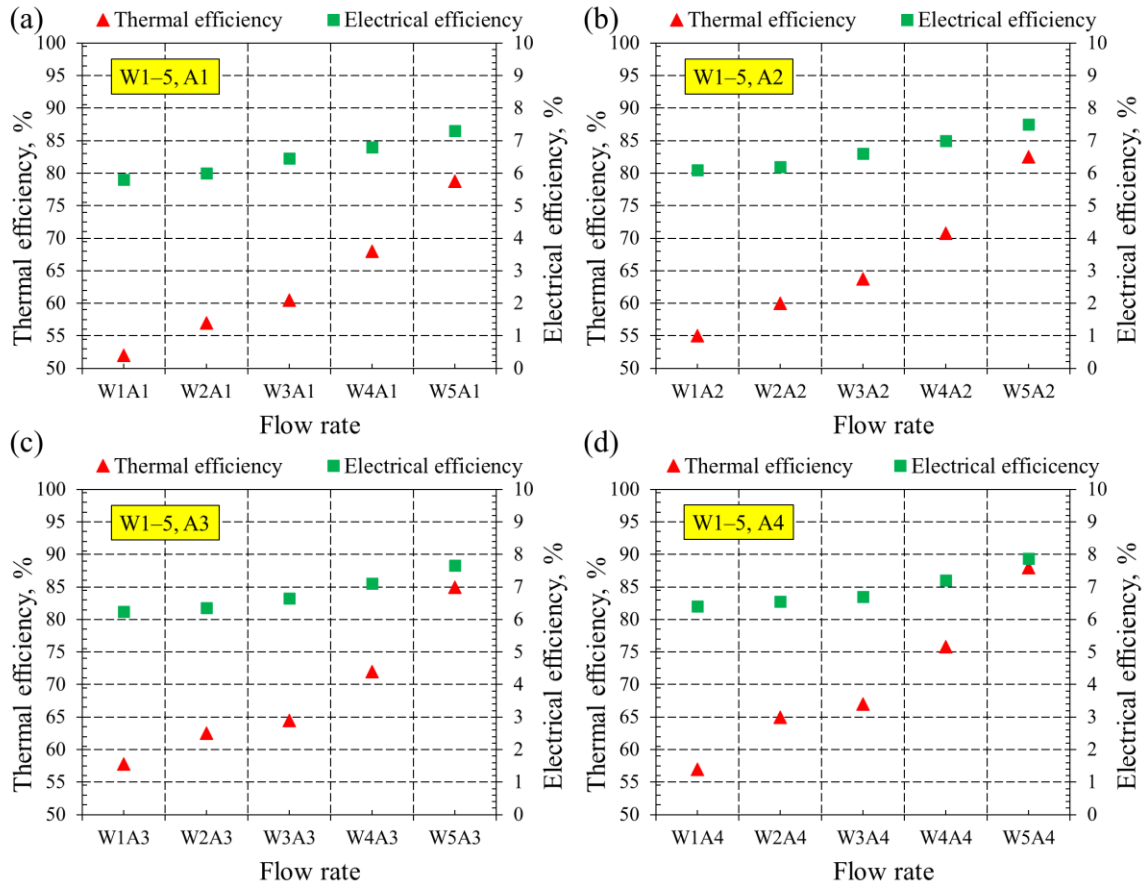


Fig. 4.69. Electrical and thermal efficiency evolution with mass flow rate varying water flow rate from W1 to W5 at the fixed air flow rate of a) 0.017 (A1), b) 0.021 (A2), c) 0.028 (A3), d) 0.034 (A4)

4.9. Water-cooled PV/T module

This assessment focuses on the new water-cooled PV/T created in this research, as described in subsection 3.4.6.2, and compares it with the new bi-fluid LFS-PV/T module and PV module. The study location was the same as in the previous experiments and was conducted on a clear day on August 15, 2023.

The dramatic parameter most literature focused on is the PV module's cell temperature; the cell temperatures were measured for the three modules investigated in this assessment. Fig. 4.70 clarified the comparison of these cell's temperatures relative to the solar radiation. The maximum solar radiation received is 1043 W/m^2 , and the maximum cell temperatures reached by the module are 42, 49, and $62 \text{ }^\circ\text{C}$ for the LFS-PVT, WC-PV/T, and PV modules, respectively.

4. Results

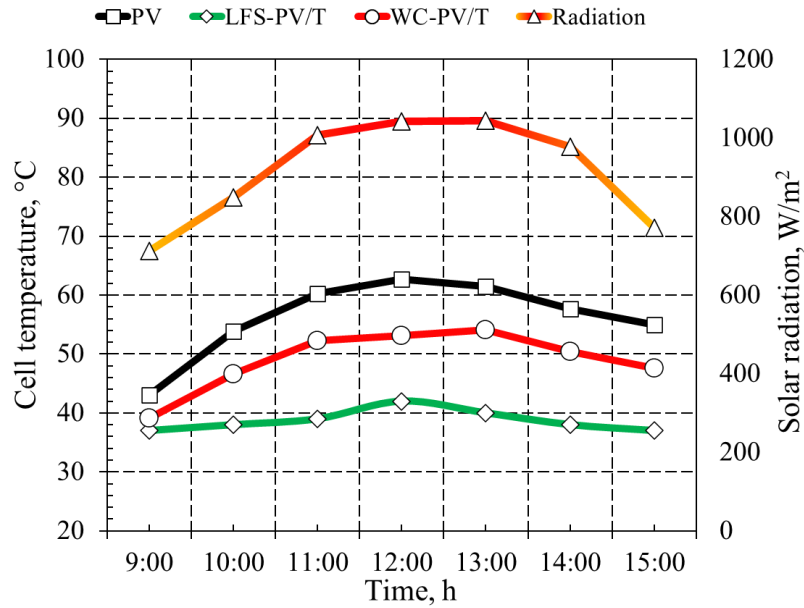


Fig. 4.70. Cells temperature of the modules

As clearly seen in the figure, the cell temperature of the LFS-PV/T is lower than that of other modules investigated in this assessment. This lowering confirms the effectiveness of the cooling method used in this module compared to the WC-PV/T.

Fig. 4.71 illustrates the electrical power of the three modules related to solar radiation. As confirmed graphically from the figures, the more electrical productivity introduced by the new bi-fluid module (LFS-PV/T), thanks to the fact stated by the literature that the decrease in the cell temperature leads to an increase in the electrical efficiency. The electrical efficiencies of the modules are graphed in Fig. 4.72.

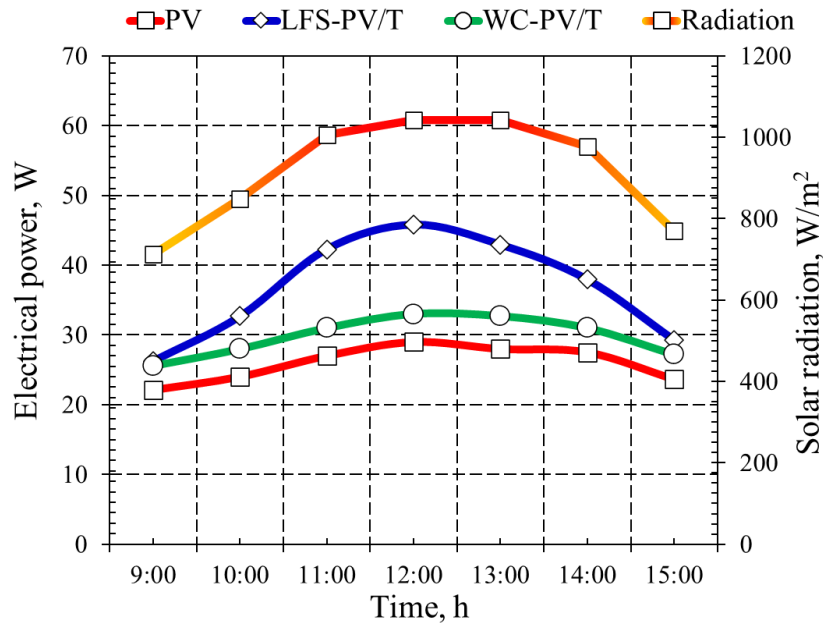


Fig. 4.71. The electrical power of the modules

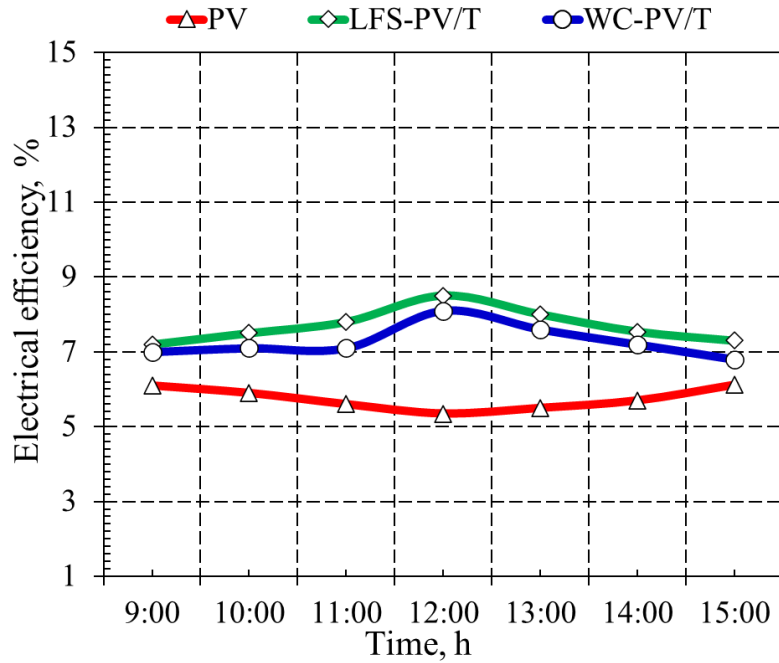


Fig. 4.72. Electrical efficiency of the modules

Besides, the thermal gain and the efficiency of the LFS-PV/T and WC-PV/T modules are illustrated in Figs 4.73 and 4.74, respectively. The figures demonstrate that the LFS-PV/T module has a better thermodynamic performance than the water-cooled module. Accordingly, the maximum heat gain obtained from the modules is 362 and 310 W for the LFS-PV/T and WC-PV/T modules, respectively.

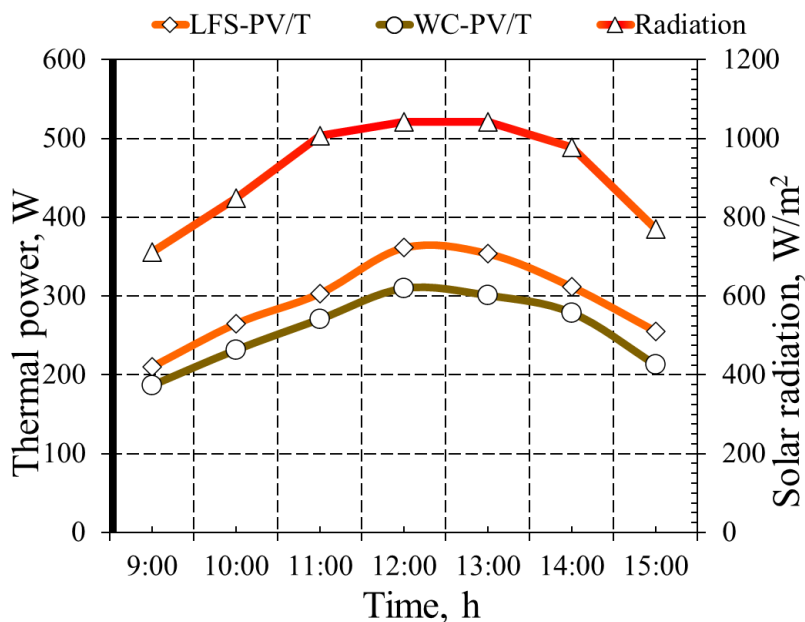


Fig. 4.73. Thermal power of the modules

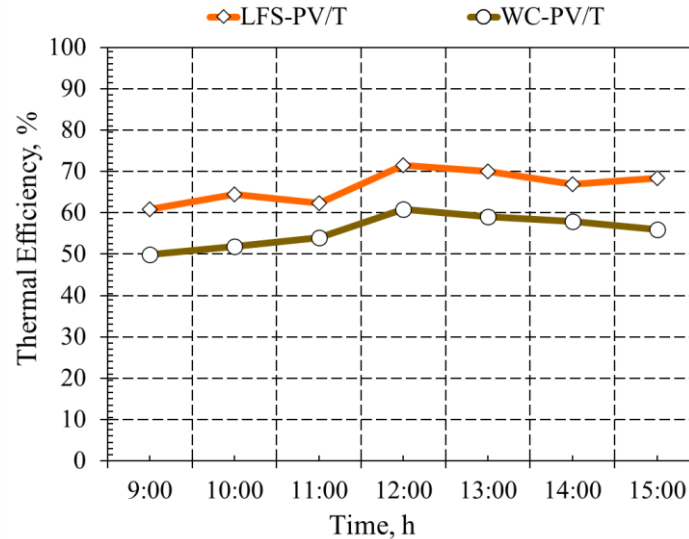


Fig. 4.74. Thermal efficiency of the modules

4.10. New scientific results

This section focuses on the new scientific contribution results achieved by the assessments conducted in this research to fulfil the objectives. The concise description of the new scientific results based on the research work are as follows:

1. Multi-functional platform of the PV/T module

Based on the new functional TRNSYS model, in order to evaluate the performance and behaviour of the PV/T module, I have developed multi-aspect approaches and several controllers. I proved that the PID controller has an effective electrical performance, and the ON-OFF controller has an effective thermal performance. Accordingly, I enhanced the electrical efficiency of PV/T that PID controlled by 6.5% compared to the ON-OFF controlled system. The maximum electrical productivity also reached 48.5 W for the PID-controlled system and 45 W for the ON-OFF-controlled system.

Additionally, based on the modifications I made to the programming code of the PID controller within the TRNSYS environment, I improved the thermal and electrical productivity of the PV/T module by 6.5% and 7.1%, respectively, compared to the standard TRNSYS PID-controlled PV/T. Accordingly, the developed model can be used to comprehensively evaluate the performance of PV/T systems in multiple circumstances. Furthermore, the findings align closely with the existing literature on measurements within the same field.

2. Effect of the louvered fins

I have developed and evaluated a novel fin configuration, a louvered fin, which proved its thermal effectiveness in the air heat exchanger. It is mounted to the copper absorber to configure air-cooled-based PV/T and compared with vertical-fins-based PV/T and no-fins PV/T modules. Furthermore, these louvered fins are first used in configuring PV/T modules.

Based on the experimental results, I have proved that the essence behind the idea of using louvered fins is to improve the thermal behaviour of the temperature distribution of the PV/T module through the path changing of an airflow caused by the louvered fin shape makes sufficient time for convective heat transfer from the fin's surfaces to the airflow. This process created a more significant difference in temperature between the inlet and the outlet, thus

enhancing the thermal performance. Examining the two fin configurations in this study, I found that the module's thermal efficiency increased by 48% and 54% when equipped with louvered fins, as compared to vertical fins and unfinned modules. The Reynolds number, recorded at 6312 throughout the experiment, signifies the onset of turbulent flow within the system's configuration. This turbulent airflow manifests intricate dynamics, fostering heightened convective heat and energy transfer mechanisms across the system.

3. Design of the louvered fins and serpentine tube

I have developed and evaluated a novel configuration of a bilateral-based (LFS-PV/T) module with a unique design of a flat-plate absorber fitted with louvered fins and a serpentine-shaped tube using water and air as coolants simultaneously. The copper alloy was utilised to create the absorber, fins, and tube.

Based on the experimental findings, I evidenced that the novel design developed uniform cooling of the PV/T module compared to the classical air-cooled PV/T module. A dramatic decrease in the surface temperature of the solar cell was achieved; the created bi-fluid PV/T module decreased the surface temperature by 31.7% compared to the air-cooled module. Accordingly, I have enhanced the thermal and electrical performances of the created module compared to the classical air-cooled module. The thermal and electrical efficiency of the two examined modules were 19.4 and 6.1% for the air-cooled module and 89.1 and 7.7% for the bilateral-based PV/T module, respectively.

PV/T systems typically entail a higher initial investment compared to individual PV modules or flat plate collectors. However, their dual functionality makes them a cost-effective investment. With reduced installation costs and space optimization, PV/T systems offer attractive returns by simultaneously generating electricity and thermal energy, making them a prudent investment choice.

4. Correlation between solar cell temperature and solar intensity of the new PV/T

Based on comparing assessments of the experimental results among the bi-fluid PV/T, air-cooled PV/T, and PV module, I have identified new proposed correlations to estimate the relation between the solar cell temperatures (T_{cell}) and the solar radiation (S) received by solar modules, thus, evaluating how solar cells temperature increases with solar radiation. The solar radiation range utilised in these correlations is arranged between 350 and 1050 W/m²:

For the bi-fluid LFS-PV/T:

$$T_{cell} = 22.96 + 0.022 S - 9.4 \times 10^{-6} S^2$$

For the air-cooled AC-PVT:

$$T_{cell} = 29.91 + 0.027 S - 4.8 \times 10^{-6} S^2$$

For the PV:

$$T_{cell} = 28.89 + 0.046 S - 2.014 \times 10^{-5} S^2$$

I found that the increase in cell temperature with solar radiation is the lowest for the new bi-fluid PV/T module created in this research. Accordingly, the new configuration of the PV/T module is well addressed in terms of how the new methodology utilised has a positive potential to decrease the cell temperature based on the correlation between the solar cell temperature and the solar intensity. Accordingly, the cell temperature decreased by 19.2 °C compared to the standard PV module.

5. Quantifying the wasted heat towards the enhancement of sustainability contributions

I have introduced a new thermodynamic mathematical model to calculate the wasted heat to the surroundings by the PV module to assess the contribution of the created bi-fluid PV/T toward sustainability through exergy analysis and sustainability index.

Based on the experimental results coupled with the thermodynamic model, I enhanced the sustainability contribution of the new PV/T. The amount of wasted heat released by the new bi-fluid PV/T module was lower by approximately 77.6% compared to the amount of wasted heat released by the PV module used as a reference. The sustainability index is the most crucial evaluation parameter focused on by scientific research to evaluate energy systems, as it is directly proportional to the conversion efficiency of the system. The sustainability index has been improved using PV/T modification, achieving 1.15–1.6 and 1.03–1.06 for the bi-fluid PV/T and the PV module, respectively. Thus, the examined design of hybrid solar collector systems has an efficient sustainability contribution and has the potential to support sustainable buildings towards net-zero energy buildings.

6. Effect of ternary nanofluid as a heat transfer fluid

I have developed a novel instrument that provides a new fluid characteristic by measuring the time required to reach a thermal equilibrium state to select the efficient fluid, where the lowest time means the highest thermal conductivity. I have examined and justified using ternary and nanofluids containing MWCNTs, MgO, and BN as heat transfer fluid.

Based on the experimental results of the proposed technique, a fluid that reaches thermal equilibrium quickly absorbs heat faster, indicating higher thermal conductivity. Accordingly, the appropriate nanofluid was ternary nanofluid MWCNTs-MgO-BN with a volume concentration of 0.5%, utilised in the bi-fluid PV/T model.

I improved the performance of the PV/T module. The nano-based PV/T module exhibits a 30.8% thermal efficiency higher than the water-based PV/T module. The average daily electrical efficiencies for the two modules experienced a rise of 41.7% and 20.2%, respectively, compared to the PV module. Employing a nanofluid leads to a more significant reduction in the surface temperature of the modules. Thus, the use of nanofluid results in superior electrical efficiency. The tested nanofluid can, therefore, be effectively used in thermal solar energy systems, including solar collectors and PV/T modules.

7. Thermal conductivity of ternary nanofluids

Based on experimental results, I have identified a new proposed correlation for MWCNTs–MgO–BN ternary nanofluids (with 0.25% GA surfactant) thermal conductivity enhancement ratios. This correlation is valid for volume concentrations ranging from 0.05% to 0.5% and temperatures ranging from 25 °C to 55 °C.

$$kR = \frac{k_{tn}}{k_{bf}} = 0.9159 + 0.95 \times \left[\frac{(\phi)^{0.332}}{(T)^{0.297}} \right].$$

According to experimental results, I have found that the thermal conductivity of 0.5% MWCNTs–MgO–BN was evaluated at 25 °C and was 20.8% higher than the thermal conductivity of the base fluid.

5. CONCLUSION AND SUGGESTIONS

An experimental analysis was conducted to evaluate the performance of hybrid solar collectors or photovoltaic thermal modules (PV/T) through dynamic modelling, novel creation, a combination of the two heat transfer fluids (water and air), the effect of the solar cells temperature, sustainability contribution and the effect of the nanofluid as high thermal conductivity heat transfer fluid under climate conditions of Gödöllő city, Hungary at Hungarian University of Agriculture and Life Sciences.

Firstly, a new element for a PV/T module was built, evaluated, and simulated using the TRNSYS tool to display the predicted performance behaviour. The main conclusion behind the points above is that the most efficient PV/T system in electrical conversion was the PV/T system with a PID controller, and the most efficient system in terms of thermal conversion was the PV/T with an ON-OFF controller.

A novel configuration of fins was employed within the copper absorber to assess the air-cooled PV/T module performance of so-called louvered fins. The new fins were evaluated by comparison with the vertical fin absorber and unfinned absorber in the air-cooled PV/T module. The enhancement result showed that the thermal efficiency of the louvered fin unit increased by 48% and 54% compared to the vertical fin and unfinned units, respectively. Thus, louvered fins have a significant potential compared to the classical vertical fins with the same surface area.

Besides, a novel design of the louvered fins and the serpentine tube was mounted directly to the copper absorber to configure a bi-fluid photovoltaic thermal module (LFS-PV/T) to enhance the performance. The thermal and electrical efficiency of the three examined systems were 19.4 and 6.1% for the AC-PV/T system, 89.1 and 7.7% for the LFS-PV/T system, and 45.1 and 6.9% for the ALF-PV/T system, respectively. The new configuration decreased the cell temperature by more than 19.2 °C compared to the standard PV module. This decrease led to the highest electrical efficiency of the LFS-PV/T module.

Based on the thermodynamic model conducted in this research, the created LFS-PV/T module makes an efficient contribution to sustainability and has the potential to support sustainable buildings towards NZEBs.

Based on the results achieved by the new fluid thermal equilibrium time instrument, it was proven that the ternary MWCNTs-MgO-BN nanofluid was efficient. Utilising this nanofluid in the LFS-PV/T presents a dramatic performance improvement. The PV/T module exhibits a 30.8% higher thermal efficiency than the LFS-PV/T module that uses water. The average daily electrical efficiency experienced a rise of 20.2% compared to the water-based module. Employing a nanofluid leads to a more significant reduction in the surface temperature of the modules. Thus, the use of nanofluid results in superior electrical efficiency.

However, the work is still open to enhance the efficiency of the PV/T system. In addition to the simulation improvements, the work still has the potential for many studies that could consider the flow rate control related to the temperature of the solar cell based on the demand for what power is needed from the PV/T module; it requires a complicated mechatronics control system.

6. SUMMARY

EFFICIENCY IMPROVEMENT OF THE HYBRID SOLAR COLLECTOR SYSTEMS

Comprehensive and detailed experimentation was conducted to analyse the thermal and electrical performance improvements of photovoltaic thermal modules. The first assessments were conducted on a conventional PV/T module installed at a solar lab of the MATE university through the TRNSYS tool, and the second experiments were conducted on a novel created PV/T module by utilising a conventional PV module available in the Solar Lab of MATE University. The creation assessments experimentally verified and evaluated a novel design of the bilateral module of a PV/T module that utilises water and air as coolants. The novel bi-fluid photovoltaic thermal module LFS-PV/T utilises copper louvered fins and serpentine tubes soldered to the copper absorber within the LFS-PV/T module. Several configurations were created to be compared with the new module to evaluate the performance improvements accordingly. A thermodynamic model was developed to assess the sustainability contribution of the new module.

Apart from the reconfiguration, another performance enhancement factor in the field of solar systems is the heat transfer fluid, and the most common and recently used in solar systems are nanofluids., which are used as heat transfer fluid. This research investigated the potentiality of the ternary nanofluids containing MWCNTs-MgO- BN to improve the efficiency of the created PV/T module. The selection and evaluation of the nanofluids were obtained based on the new FTET instrument created in this research, which indicates the efficient nanofluid based on the thermal equilibrium time.

Based on the experimentation findings, the louvered fins confirmed the effectiveness of the essence behind their shape. The thermal efficiency of the unit with louvered fins was enhanced by 48% and 54% compared to the vertical fins and unfinned units. The results between the two fin configurations examined in this research lead to the fact that the area needed by the copper vertical fins to reach the performance of the louvered fins is higher by more than half. Thus, louvered fins are better than vertical fins with the same surface area.

The path changing of an airflow caused by the louvered fin shape makes sufficient time for convection heat transfer from the fin's surfaces to the airflow. This process created a more significant difference in temperature between the inlet and the outlet, thus enhancing the thermal performance. The electrical efficiency of the examined LFS-PV/T module was improved by 27.6% compared to the PV module, and the thermal efficiency was improved by 94% compared to the classical air-cooled PV/T.

Investigating ternary MWCNTs-MgO-BN nanofluid enhances the thermal and electrical performances of the LFS-PV/T module. The nano-based modules produce more electricity than the water-based LFS-PV/T module by 23%. These findings indicate that the nano-based module, which shows the highest thermal power enhancement, also exhibits the highest electrical power enhancement.

7. ÖSSZEFOGLALÁS (SUMMARY IN HUNGARIAN)

HIBRID NAPKOLLEKTOROS RENDSZEREK HATÉKONYSÁGÁNAK NÖVELTÉSE

A kutatómunka során részletes, átfogó kísérleteket végeztem fotovillamos-termikus hibrid (PV/T) modulok hő- és villamos teljesítmény javulásának elemzésére. A vizsgálatok a MATE Napenergiás laboratóriuma területén telepített, hagyományos PV/T modul segítségével történtek, és az eredmények általánosításához TRNSYS modellt dolgoztam ki. A további vizsgálatok pedig egy hagyományos PV modul felhasználásával, saját, egyedi tervezésű és kialakítású PV/T modulon történt. A működés helyszíne itt is a MATE Napenergiás laboratórium területe volt. A gyártási értékelések alátámasztották ezen PV/T modul folyadékot és levegőt is hűtőközegként használó termikus részének újdonságot jelentő kialakítását. Az új bi-fluid (LFS-PV/T) hibrid kollektor termikus része speciális réz terelőlemezeket és szerpentin csöveket tartalmaz, amelyek réz abszorberhez vannak forrasztva. Az LFS-PV/T PV moduljával megegyező PV modulokból kiindulva számos egyéb PV/T konfiguráció is készült az új modullal való összehasonlításhoz, és hogy ennek alapján számszerűen is értékeljem a teljesítményben bekövetkező javulásokat. Az új LFS-PV/T modul fenntarthatósági hozzájárulásának felmérésére termodinamikai modellt dolgoztam ki.

Az egyedi konfiguráció mellett a termál szolár rendszerek területén másik fontos teljesítménynövelő tényező a hőhordozó közeg megválasztása. PV/T rendszerek szolárfolyadékaként napjainkban elterjedten használt hőhordozók a különböző nanofolyadékok, ehhez kapcsolódóan a kutatásom során azt vizsgáltam, hogy az MWCNTs-MgO-BN-t tartalmazó háromkomponensű nanofolyadék képes-e javítani az új PV/T modul hatékonyságát. A nanofolyadék kiválasztása és a hatékonyság értékelése egy erre a célra készített FTET műszer segítségével történt, amely a termikus egyensúlyi idő alapján adja meg a hatékonyságot.

A kísérleti eredmények alapján a speciális alakú terelőlemezekkel megvalósított bordázat a kialakításából adódóan megnövelte a hatékonyságot, a termikus hatásfok 48%-kal, illetve 54%-kal javult az áramlással párhuzamos bordák, illetve a bordázatlan egységekhez viszonyítva. A vizsgált két borda-konfiguráció közötti eredmények azt mutatják, hogy párhuzamos bordák esetén másfélszer annyi rézfelület szükséges a speciális kialakítású bordázat segítségével nyert teljesítmény eléréséhez, így az új kialakítású bordázat hatékonyabb, mint az azonos felületű párhuzamos bordák. Az új bordastruktúra a légáramlás útjának megváltoztatásával több időt biztosít a konvektív hőátadásra a bordák felületeiről a légáram felé, ami jelentősebb hőmérséklet-különbséget eredményez a bemenet és a kimenet között, így javítja a hőtelsítményt. A vizsgált LFS-PV/T modul villamos hatásfoka a PV modulhoz képest 27,6%-kal, a termikus hatásfoka pedig a klasszikus léghűtéses PV/T modulhoz képest 94%-kal javult.

A vizsgálatok alapján a háromkomponensű MWCNTs-MgO-BN nanofolyadék javítja az LFS-PV/T modul termikus és villamos teljesítményét. A nanofolyadékos modulok ugyanolyan körülmények között 23%-kal több energiát termelnek, mint a vízbázisú LFS-PV/T modulok. Az eredmények azt mutatják, hogy a vizsgált esetek közül a legnagyobb hőtelsítmény-növekedést mutató nano szolárfolyadékos modul, egyben a legnagyobb villamos teljesítménynövekedést is mutatja.

8. APPENDICES

A1: Bibliography

1. Abbas, N., Bilal, M., Amer, M., Muhammad, S., Sajjad, U., Muhammad, H., Zahra, N., Hussain, M., Badshah, M. A., and Turab, A., (2019): Applications of nanofluids in photovoltaic thermal systems: A review of recent advances, *Physica A: Statistical Mechanics and Its Applications*, 536, pp. 122513.
<https://doi.org/10.1016/j.physa.2019.122513>
2. Abdalla, A. N., and Shahsavari, A., (2023): An experimental comparative assessment of the energy and exergy efficacy of a ternary nanofluid-based photovoltaic / thermal system equipped with a sheet-and-serpentine tube collector, *Journal of Cleaner Production*, 395(January), pp. 136460.
<https://doi.org/10.1016/j.jclepro.2023.136460>
3. Abdul-Ganiyu, S., Quansah, D. A., Ramde, E. W., Seidu, R., and Adaramola, M. S., (2021): Study effect of flow rate on flat-plate water-based photovoltaic-thermal (PVT) system performance by analytical technique, *Journal of Cleaner Production*, 321, pp. 128985. <https://doi.org/10.1016/j.jclepro.2021.128985>
4. Abdullah, Lateef, A., Misha, S., Tamaldin, N., Rosli, M. A. M., and Sachit, A., (2020): Theoretical study and indoor experimental validation of performance of the new photovoltaic thermal solar collector (PVT) based water system, *Case Studies in Thermal Engineering*, 18(January), pp. 100595.
<https://doi.org/doi.org/10.1016/j.csite.2020.100595>
5. Abdullah, A. A., Attulla, F. S., Ahmed, O. K., and Algburi, S., (2022): Effect of cooling method on the performance of PV/Trombe wall: Experimental assessment, *Thermal Science and Engineering Progress*, 30(January), pp. 101273.
<https://doi.org/10.1016/j.tsep.2022.101273>
6. Abdullah, A. L., Misha, S., Tamaldin, N., Rosli, M. A. M., and Sachit, F. A., (2019): Hybrid photovoltaic thermal PVT solar systems simulation via Simulink/Matlab, *CFD Letters*, 11(4), pp. 64–78.
<https://www.akademiabaru.com/submit/index.php/cfdl/article/view/3155>
7. Aboueian, J., and Shahsavari, A., (2022): Feasibility study of improving the energy and exergy performance of a concentrating photovoltaic/thermal system by the simultaneous application of biological water-silver nanofluid and sheet-and-grooved tube collector: Two-phase mixture model, *Engineering Analysis with Boundary Elements*, 144(September), pp. 433–440.
<https://doi.org/10.1016/j.enganabound.2022.08.039>
8. Abu Bakar, M. N., Othman, M., Hj Din, M., Manaf, N. A., and Jarimi, H., (2014): Design concept and mathematical model of a bi-fluid photovoltaic/thermal (PV/T) solar collector, *Renewable Energy*, 67, pp. 153–164.
<https://doi.org/10.1016/j.renene.2013.11.052>
9. Adun, H., Adedeji, M., Dagbasi, M., Bamisile, O., Senol, M., and Kumar, R., (2021): A numerical and exergy analysis of the effect of ternary nanofluid on performance of Photovoltaic thermal collector, *Journal of Thermal Analysis and Calorimetry*, pp. 1413–1429.
<https://doi.org/10.1007/s10973-021-10575-y>

10. Adun, H., Adedeji, M., Ruwa, T., Senol, M., and Kavaz, D., (2022): Energy, exergy, economic, environmental (4E) approach to assessing the performance of a photovoltaic-thermal system using a novel ternary nanofluid, *Sustainable Energy Technologies and Assessments*, 50 (November), pp. 101804. <https://doi.org/10.1016/j.seta.2021.101804>
11. Adun, H., Kavaz, D., and Dagbasi, M., (2021): Review of ternary hybrid nanofluid: Synthesis, stability, thermophysical properties, heat transfer applications, and environmental effects, *Journal of Cleaner Production*, 328(October), pp. 129525. <https://doi.org/10.1016/j.jclepro.2021.129525>
12. Afzanizam, R., Ping, Y. J., Misha, S., Akop, M. Z., Sopian, K., Mat, S., and Saruni, N. J. A.-S., (2018): Simulation Study of Computational Fluid Dynamics on Photovoltaic Thermal Water Collector with Different Designs of Absorber Tube, *Journal of Advanced Research in Fluid Mechanics and Thermal Sciences*, 52(1), pp. 12–22.
13. Agrawal, S., and Tiwari, G. N., (2011): Energy and exergy analysis of hybrid micro-channel photovoltaic thermal module, *Solar Energy*, 85(2), pp. 356–370. <https://doi.org/10.1016/j.solener.2010.11.013>
14. Agrawal, S., and Tiwari, G. N., (2013): Enviroeconomic analysis and energy matrices of glazed hybrid photovoltaic thermal module air collector, *Solar Energy*, 92, pp. 139–146. <https://doi.org/10.1016/j.solener.2013.02.019>
15. Agrawal, S., and Tiwari, G. N., (2015): Performance analysis in terms of carbon credit earned on annualized uniform cost of glazed hybrid photovoltaic thermal air collector, *Solar Energy*, 115(2015), pp. 329–340. <https://doi.org/10.1016/j.solener.2015.02.030>
16. Ahmadinejad, M., and Moosavi, R., (2023): Energy and exergy evaluation of a baffled-nanofluid-based photovoltaic thermal system (PVT), *International Journal of Heat and Mass Transfer*, 203, pp. 123775. <https://doi.org/10.1016/j.ijheatmasstransfer.2022.123775>
17. Ahmadinejad, M., Soleimani, A., and Gerami, A., (2022): The effects of a novel baffle-based collector on the performance of a photovoltaic/thermal system using SWCNT/Water nanofluid, *Thermal Science and Engineering Progress*, 34(June), pp. 101443. <https://doi.org/10.1016/j.tsep.2022.101443>
18. Ahmadinejad, M., Soleimani, A., and Gerami, A., (2023): Performance enhancement of a photovoltaic thermal (PVT) system with sinusoidal fins: A quasi-transient energy-exergy analysis, *International Journal of Green Energy*, 20(9), pp. 978–996. <https://doi.org/10.1080/15435075.2022.2131434>
19. Ahmed, A., Khalil, O., Mustafa, M., and Ibrahim, K., (2020): Performance augmentation of a PV / Trombe wall using Al₂O₃ / Water nano-fluid: An experimental investigation, *Renewable Energy*, 157, pp. 515–529. <https://doi.org/10.1016/j.renene.2020.05.052>
20. Al-waeli, A. H. A., Chaichan, M. T., Kazem, H. A., Sopian, K., Ibrahim, A., Mat, S., and Ha, M., (2018): Comparison study of indoor /outdoor experiments of a photovoltaic thermal PV/T system containing SiC nano fluid as a coolant, 151. <https://doi.org/10.1016/j.energy.2018.03.040>
21. Al-waeli, A. H. A., Kazem, H. A., Yousif, J. H., Chaichan, M. T., and Sopian, K., (2020): Mathematical and neural network modeling for predicting and analyzing of nano fluid-nano PCM photovoltaic thermal systems performance, *Renewable Energy*, 145, pp. 963–980. <https://doi.org/10.1016/j.renene.2019.06.099>

22. Al-Waeli, A. H. A., Sopian, K., Chaichan, M. T., Kazem, H. A., Hasan, H. A., and Al-Shamani, A. N., (2017a): An experimental investigation of SiC nanofluid as a base-fluid for a photovoltaic thermal PV/T system, *Energy Conversion and Management*, 142, pp. 547–558. <https://doi.org/10.1016/j.enconman.2017.03.076>
23. Al-waeli, A. H. A., Sopian, K., Kazem, H. A., and Chaichan, M. T., (2017b): Photovoltaic/Thermal (PV/T) systems: Status and future prospects, *Renewable and Sustainable Energy Reviews*, 77(November), pp. 109–130. <https://doi.org/10.1016/j.rser.2017.03.126>
24. Alayi, R., Jahanbin, F., Aybar, H., Sharifpur, M., and Khalilpoor, N., (2022): Investigation of the Effect of Physical Factors on Exergy Efficiency of a Photovoltaic Thermal (PV/T) with Air Cooling, *International Journal of Photoenergy*, 2022, pp. 9882195. <https://doi.org/10.1155/2022/9882195>
25. Alfegi, E., Sopian, K., Othman, M. Y. H., and Yatim, B. Bin, (2009): The effect of flow rates on the performance of finned single pass, double duct photovoltaic thermal solar air heaters, *European Journal of Scientific Research*, 25(4), pp. 339–344.
26. Alfegi, M. E. A., Sopian, K., Othman, M. Y. H., and Yatim, B. Bin, (2008): Experimental Investigation of Single Pass, Double Duct Photovoltaic Thermal (PV/T) Air Collector with CPC and Fins, *American Journal of Applied Sciences*, 5(7), pp. 866–871.
27. Alktranee, M., Ahmed Shehab, M., Németh, Z., Bencs, P., and Hernadi, K., (2023): Experimental study for improving photovoltaic thermal system performance using hybrid titanium oxide-copper oxide nanofluid, *Arabian Journal of Chemistry*, 16(9), pp. 105102. <https://doi.org/10.1016/j.arabjc.2023.105102>
28. Alktranee, M., and Péter, B., (2023): Energy and exergy analysis for photovoltaic modules cooled by evaporative cooling techniques, *Energy Reports*, 9, pp. 122–132. <https://doi.org/10.1016/j.egy.2022.11.177>
29. Alshibil, A. M. A., Farkas, I., and Víg, P., (2022): Multi-aspect approach of electrical and thermal performance evaluation for hybrid photovoltaic/thermal solar collector using trnsys tool, *International Journal of Thermofluids*, 16(September), pp. 100222. <https://doi.org/10.1016/j.ijft.2022.100222>
30. Alshibil, A. M. A., Farkas, I., and Víg, P., (2023a): Evaluation of fin configurations for an air-cooled hybrid photovoltaic-thermal solar collector, *Thermal Science*, online first (00), pp. 84–84. <https://doi.org/10.2298/TSCI230116084A>
31. Alshibil, A. M. A., Farkas, I., and Víg, P., (2023b): Experimental performance comparison of a novel design of bi-fluid photovoltaic-thermal module using Louver fins, *Energy Reports*, 9, pp. 4518–4531. <https://doi.org/10.1016/j.egy.2023.03.110>
32. Alshibil, A. M. A., Farkas, I., and Víg, P., (2023c): Sustainability contribution of hybrid solar collector towards net-zero energy buildings concerning solar cells wasted heat, *Energy for Sustainable Development*, 74, pp. 185–195. <https://doi.org/10.1016/j.esd.2023.04.001>
33. Alshibil, A. M. A., Farkas, I., and Víg, P., (2023d): Thermodynamical analysis and evaluation of louver-fins based hybrid bi-fluid photovoltaic/thermal collector systems, *Renewable Energy*, 206, pp. 1120–1131. <https://doi.org/10.1016/j.renene.2023.02.105>
34. Alshibil, A. M. A., Víg, P., and Farkas, I., (2021): Heat Transfer Behaviour of Hybrid Solar Collector Module for Liquid-Based Type, G. Quaglia, A. Gasparetto, V. Petuya,

- and G. Carbone, eds., International Workshop IFToMM for Sustainable Development Goals, Springer International Publishing, Cham, 20–29.
https://doi.org/10.1007/978-3-030-87383-7_3
35. Arslan, E., Aktaş, M., and Can, Ö. F., (2020): Experimental and numerical investigation of a novel photovoltaic thermal (PV/T) collector with the energy and exergy analysis, *Journal of Cleaner Production*, 276, pp. 123255.
<https://doi.org/10.1016/j.jclepro.2020.123255>
 36. Assoa, Y. B., Menezes, C., Fraisse, G., Yezou, R., and Brau, J., (2007): Study of a new concept of photovoltaic – thermal hybrid collector, *Solar Energy*, 81(9), pp. 1132–1143.
<https://doi.org/10.1016/j.solener.2007.04.001>
 37. Aste, N., Del Pero, C., Leonforte, F., and Manfren, M., (2016): Performance monitoring and modeling of an uncovered photovoltaic-thermal (PVT) water collector, *Solar Energy*, 135, pp. 551–568. <https://doi.org/10.1016/j.solener.2016.06.029>
 38. Aste, N., Leonforte, F., and Del Pero, C., (2015): Design, modeling and performance monitoring of a photovoltaic-thermal (PVT) water collector, *Solar Energy*, 112, pp. 85–99. <https://doi.org/10.1016/j.solener.2014.11.025>
 39. Atkinson, R., Drakulic, M.R., Heikal, T.A., and Cowell, (1998): Two- and three-dimensional numerical models of flow and heat transfer over louvred fin arrays in compact heat exchangers, *International Journal of Heat and Mass Transfer*, 41(24), pp. 4063–4080. [https://doi.org/10.1016/S0017-9310\(98\)00165-3](https://doi.org/10.1016/S0017-9310(98)00165-3)
 40. Atmaca, M., and Pektemir, Z., (2019): An investigation on the effect of the total efficiency of water and air used together as a working fluid in the photovoltaic thermal systems, *Processes*, 7(8), pp. 516. <https://doi.org/10.3390/pr7080516>
 41. Bakar Abu, N. M., Othman, M., Hj, M., Manaf, N. A., and Jarimi, H., (2014): Design concept and mathematical model of a bi-fluid photovoltaic/thermal (PV/T) solar collector, *Renewable Energy*, 67, pp. 153–164.
<https://doi.org/10.1016/j.renene.2013.11.052>
 42. Bakker, M., Zondag, H. A., Elswijk, M. J., Strootman, K. J., and Jong, M. J. M., (2005): Performance and costs of a roof-sized PV/thermal array combined with a ground coupled heat pump, *Solar Energy*, 78(2), pp. 331–339.
<https://doi.org/10.1016/j.solener.2004.09.019>
 43. Baljit, S. S. S., Chan, H., Audwinto, V. A., Hamid, S. A., Fudholi, A., Zaidi, S. H., Othman, M. Y., and Sopian, K., (2017): Mathematical modelling of a dual- fluid concentrating photovoltaic- thermal (PV-T) solar collector, *Renewable Energy*, 114, pp. 1258–1271. <https://doi.org/10.1016/j.renene.2017.08.001>
 44. Baljit, S. S. S., Chan, H. Y., Zaidi, S. H., and Sopian, K., (2020): Performance study of a dual-fluid photovoltaic thermal collector with reflection and refraction solar concentrators, *International Journal of Low-Carbon Technologies*, 15(1), pp. 25–39.
<https://doi.org/10.1093/ijlct/ctz054>
 45. Bambrook, S. M., and Sproul, A. B., (2012): Maximising the energy output of a PVT air system, *Solar Energy*, 86(6), pp. 1857–1871.
<https://doi.org/10.1016/j.solener.2012.02.038>
 46. Barbu, M., Siroux, M., and Darie, G., (2021): Numerical model and parametric analysis of a liquid based hybrid photovoltaic thermal (PVT) collector, *Energy Reports*, 7, pp. 7977–7988. <https://doi.org/10.1016/j.egyr.2021.07.058>

47. Bel Haj Jrad, A., Ben Hamida, M. B., Ghnay, R., and Mhimid, A., (2017): Contribution to the study of combined adsorption-ejection system using solar energy, *Advances in Mechanical Engineering*, 9(7), pp. 1–9. <https://doi.org/10.1177/1687814017711855>
48. Bergman, T. L., Incropera, F. P., Dewitt, D. P., and Lavine, A. S., (2011): *Fundamentals of heat and mass transfer* (7th ed.) (L. Ratts, S. Dumas, and T. Kulesa, Eds.), John Wiley & Sons, 1048.
49. Bevilacqua, P., Bruno, R., Rollo, A., and Ferraro, V., (2022): A novel thermal model for PV panels with back surface spray cooling, *Energy*, 255, pp. 124401. <https://doi.org/10.1016/j.energy.2022.124401>
50. Bilbao, J. I., and Sproul, A. B., (2015): Detailed PVT-water model for transient analysis using RC networks, *Solar Energy*, 115, pp. 680–693. <https://doi.org/10.1016/j.solener.2015.03.003>
51. Bilen, K., Işık, B., Gezer, S., and Kıyık, F., (2022): Theoretical investigation of the effect of fin type on cooling in air cooled photovoltaic panels, *Journal of Polytechnic*, 25(2), pp. 711–722.
52. Bódi, S., Víg, P., and Farkas, I., (2018): Possibilities of improving PV/T system efficiency, *Hungarian Agricultural Engineering*, 7410(33), pp. 55–58. <https://doi.org/10.17676/hae.2018.33.55>
53. Bombarda, P., Di Marcoberardino, G., Lucchini, A., Leva, S., Manzolini, G., Molinaroli, L., Pedranzini, F., and Simonetti, R., (2016): Thermal and electric performances of roll-bond flat plate applied to conventional PV modules for heat recovery, *Applied Thermal Engineering*, 105, pp. 304–313. <https://doi.org/10.1016/j.applthermaleng.2016.05.172>
54. Boumaaraf, B., Boumaaraf, H., Slimani, M. E. A., Tchoketch_Kebir, S., Ait-cheikh, M. S., and Touafek, K., (2020): Performance evaluation of a locally modified PV module to a PV/T solar collector under climatic conditions of semi-arid region, *Mathematics and Computers in Simulation*, 167, pp. 135–154. <https://doi.org/10.1016/j.matcom.2019.09.013>
55. Boumaaraf, H., Boumaaraf, B., Slimani, M. E.-A., Ait-Cheikh, M. S., and Touafek, K., (2022): A comparative study on two different configurations of hybrid photovoltaic thermal collector with experimental validation and uncertainty analysis, *Environmental Progress & Sustainable Energy*, 41(1), pp. e13704. <https://doi.org/10.1002/ep.13704>
56. Caliskan, H., (2017): Energy, exergy, environmental, enviroeconomic, exergoenvironmental (EXEN) and exergoenvironomic (EXENEC) analyses of solar collectors, *Renewable and Sustainable Energy Reviews*, 69(November 2016), pp. 488–492. <https://doi.org/10.1016/j.rser.2016.11.203>
57. Cengel, Y., (2003): *Heat transfer: a practical approach* (2nd ed.), McGraw-Hill, London, 932.
58. Cengel, Y. A., (2011): *ThermodynamicsAn Engineering Approach 5th Edition* By Yunus A Cengel: *ThermodynamicsAn Engineering Approach*, Digital Designs.
59. Chandra, J., Tong, W., Chyuan, H., and Leong, K. Y., (2016): An experimental investigation on performance analysis of air type photovoltaic thermal collector system integrated with cooling fins design, *Energy & Buildings*, 130, pp. 272–285. <https://doi.org/10.1016/j.enbuild.2016.08.040>
60. Chen, H., Wang, Y., Yang, H., Badiei, A., and Li, G., (2022): Experimental investigation and exergy analysis of a high concentrating photovoltaic system

- integrated with spray cooling, *Energy Conversion and Management*, 268(April), pp. 115957. <https://doi.org/10.1016/j.enconman.2022.115957>
61. Choi, H., Kim, Y., Son, C., Yoon, J., and Choi, K., (2020): Experimental study on the performance of heat pump water heating system coupled with air type PV / T collector, *Applied Thermal Engineering*, 178(April), pp. 115427. <https://doi.org/10.1016/j.applthermaleng.2020.115427>
62. Choi, S. M., Kwon, H. G., Kim, T., Moon, H. K., and Cho, H. H., (2022): Active cooling of photovoltaic (PV) cell by acoustic excitation in single-dimpled internal channel, *Applied Energy*, 309, pp. 118466. <https://doi.org/10.1016/j.apenergy.2021.118466>
63. Çiftçi, E., Khanlari, A., Sözen, A., Aytaç, İ., and Tuncer, A. D., (2021): Energy and exergy analysis of a photovoltaic thermal (PVT) system used in solar dryer: A numerical and experimental investigation, *Renewable Energy*, 180, pp. 410–423. <https://doi.org/10.1016/j.renene.2021.08.081>
64. Daghigh, R., and Khaledian, Y., (2017): Design and fabrication of a bi-fluid type photovoltaic-thermal collector, *Energy*, 135(September), pp. 112–127. <https://doi.org/10.1016/j.energy.2017.06.108>
65. Ding, Y., Alias, H., Wen, D., and Williams, R. A., (2006): Heat transfer of aqueous suspensions of carbon nanotubes (CNT nanofluids), *International Journal of Heat and Mass Transfer*, 49(1–2), pp. 240–250. <https://doi.org/10.1016/j.ijheatmasstransfer.2005.07.009>
66. Diwania, S., Agrawal, S., Siddiqui, A. S., and Singh, S., (2019): Photovoltaic–thermal (PV/T) technology: a comprehensive review on applications and its advancement, *International Journal of Energy and Environmental Engineering*, 11(1), pp. 33–54. <https://doi.org/10.1007/s40095-019-00327-y>
67. Dubey, S., and Tay, A. A. O., (2013): Testing of two different types of photovoltaic – thermal (PVT) modules with heat flow pattern under tropical climatic conditions, *Energy for Sustainable Development*, 17(1), pp. 1–12. <https://doi.org/10.1016/j.esd.2012.09.001>
68. Dubey, S., and Tiwari, G. N., (2008): Thermal modeling of a combined system of photovoltaic thermal (PV/T) solar water heater, *Solar Energy*, 82(7), pp. 602–612. <https://doi.org/10.1016/j.solener.2008.02.005>
69. Dubey, S., and Tiwari, G. N., (2009): Analysis of PV/T flat plate water collectors connected in series, *Solar Energy*, 83(9), pp. 1485–1498. <https://doi.org/10.1016/j.solener.2009.04.002>
70. Duffie, J. A., and Beckman, (2013): *Solar Engineering of Thermal Processes (Fourth)*, John Wiley & Sons, Inc, John Wiley & Sons., Canada, 116, 910. <https://doi.org/10.1002/9781118671603>
71. Dupeyrat, P., Menezo, C., Rommel, M., and Henning, H., (2011): Efficient single glazed flat plate photovoltaic – thermal hybrid collector for domestic hot water system, *Solar Energy*, 85, pp. 1457–1468. <https://doi.org/10.1016/j.solener.2011.04.002>
72. Eid, A. F., Lee, S. ik, Hong, S. G., and Choi, W., (2022): Hybrid cooling techniques to improve the performance of solar photovoltaic modules, *Solar Energy*, 245(August), pp. 254–264. <https://doi.org/10.1016/j.solener.2022.09.026>

73. Elminshawy, N. A. S., El-Damhogi, D. G., Ibrahim, I. A., Elminshawy, A., and Osama, A., (2022): Assessment of floating photovoltaic productivity with fins-assisted passive cooling, *Applied Energy*, 325(June), pp. 119810.
<https://doi.org/10.1016/j.apenergy.2022.119810>
74. Elsafi, A. M., and Gandhidasan, P., (2015): Comparative study of double-pass flat and compound parabolic concentrated photovoltaic – thermal systems with and without fins, *Energy Conversion and Management*, 98, pp. 59–68.
<https://doi.org/10.1016/j.enconman.2015.03.084>
75. Elsayed, A. O., (2018): Numerical investigation of heat transfer from multi-bulges pins, *Case Studies in Thermal Engineering*, 12, pp. 636–643.
<https://doi.org/10.1016/j.csite.2018.08.005>
76. Erbay, L. B., Doğan, B., and Öztürk, M. M., (2017): Comprehensive Study of Heat Exchangers with Louvered Fins, 218 in S M Sohel Murshed, ed., *Heat Exchangers - Advanced Features and Applications*, IntechOpen.
77. Fan, W., Kokogiannakis, G., and Ma, Z., (2018): A multi-objective design optimisation strategy for hybrid photovoltaic thermal collector (PVT)-solar air heater (SAH) systems with fins, *Solar Energy*, 163, pp. 315–328.
<https://doi.org/10.1016/j.solener.2018.02.014>
78. Fan, W., Kokogiannakis, G., Ma, Z., and Cooper, P., (2017): Development of a dynamic model for a hybrid photovoltaic thermal collector-Solar air heater with fins, *Renewable Energy*, 101, pp. 816–834.
<https://doi.org/10.1016/j.renene.2016.09.039>
79. Faraz Ahmad, F., Said, Z., and Amine Hachicha, A., (2022): Experimental performance evaluation of closed loop mist/fog cooling system for photovoltaic module application, *Energy Conversion and Management: X*, 14(April), pp. 100226.
<https://doi.org/10.1016/j.ecmx.2022.100226>
80. Farshchimonfared, M., Bilbao, J. I., and Sproul, A. B., (2015): Channel depth, air mass flow rate and air distribution duct diameter optimization of photovoltaic thermal (PV/T) air collectors linked to residential buildings, *Renewable Energy*, 76, pp. 27–35.
<https://doi.org/10.1016/j.renene.2014.10.044>
81. Florschuetz, L. W., (1975): On heat rejection from terrestrial solar cell arrays with sunlight concentration, 11th photovoltaic specialists conference, Institute of Electrical and Electronics Engineers, New York, 318–326.
82. Florschuetz, L. W., (1979): Extension of the Hottel-Whillier model to the analysis of combined photovoltaic/thermal flat plate collectors, *Solar Energy*, 22(4), pp. 361–366.
[https://doi.org/10.1016/0038-092X\(79\)90190-7](https://doi.org/10.1016/0038-092X(79)90190-7)
83. Franklin, J. C., and Chandrasekar, M., (2019): Performance enhancement of a single pass solar photovoltaic thermal system using staves in the trailing portion of the air channel, *Renewable Energy*, 135, pp. 248–258.
<https://doi.org/10.1016/j.renene.2018.12.004>
84. Fterich, M., Chouikhi, H., and Sandoval-torres, S., (2021): Numerical simulation and experimental characterization of the heat transfer in a PV/T air collector prototype, *Case Studies in Thermal Engineering*, 27(July), pp. 101209.
<https://doi.org/10.1016/j.csite.2021.101209>

85. Fudholi, A., Zohri, M., Jin, G. L., Ibrahim, A., Yen, C. H., Othman, M. Y., Ruslan, M. H., and Sopian, K., (2018): Energy and exergy analyses of photovoltaic thermal collector with ∇ -groove, *Solar Energy*, 159, pp. 742–750.
<https://doi.org/10.1016/j.solener.2017.11.056>
86. Fudholi, A., Zohri, M., Rukman, N. S. B., Nazri, N. S., Mustapha, M., Yen, C. H., Mohammad, M., and Sopian, K., (2019): Exergy and sustainability index of photovoltaic thermal (PVT) air collector: A theoretical and experimental study, *Renewable and Sustainable Energy Reviews*, 100, pp. 44–51.
<https://doi.org/10.1016/j.rser.2018.10.019>
87. Gad, R., Mahmoud, H., Ookawara, S., and Hassan, H., (2022): Energy, exergy, and economic assessment of thermal regulation of PV panel using hybrid heat pipe-phase change material cooling system, *Journal of Cleaner Production*, 364(February), pp. 132489. <https://doi.org/10.1016/j.jclepro.2022.132489>
88. Gang, P., Huide, F., Tao, Z., and Jie, J., (2011): A numerical and experimental study on a heat pipe PV/T system, *Solar Energy*, 85(5), pp. 911–921.
<https://doi.org/10.1016/j.solener.2011.02.006>
89. Gao, Y., Wang, C., Wu, D., Dai, Z., Chen, B., and Zhang, X., (2022): A numerical evaluation of the bifacial concentrated PV-STEG system cooled by mini-channel heat sink, *Renewable Energy*, 192, pp. 716–730.
<https://doi.org/10.1016/j.renene.2022.04.153>
90. Garg, H. P., and Adhikari, R. S., (1997): Conventional hybrid photovoltaic/thermal (PV/T) air heating collectors: Steady-state simulation, *Renewable Energy*, 11(3), pp. 363–385. [https://doi.org/10.1016/S0960-1481\(97\)00007-4](https://doi.org/10.1016/S0960-1481(97)00007-4)
91. Gelis, K., Ozbek, K., Celik, A. N., and Ozyurt, O., (2022): A novel cooler block design for photovoltaic thermal systems and performance evaluation using factorial design, *Journal of Building Engineering*, 48(October 2021), pp. 103928.
<https://doi.org/10.1016/j.jobe.2021.103928>
92. Gelis, K., Ozbek, K., Ozyurt, O., and Naci Celik, A., (2023): Multi-objective optimization of a photovoltaic thermal system with different water based nanofluids using Taguchi approach, *Applied Thermal Engineering*, 219(PB), pp. 119609.
<https://doi.org/10.1016/j.applthermaleng.2022.119609>
93. Gertzog, K. P., Pnevmatikakis, S. E., and Caouris, Y. G., (2008): Experimental and numerical study of heat transfer phenomena, inside a flat-plate integrated collector storage solar water heater (ICSSWH), with indirect heat withdrawal, *Energy Conversion and Management*, 49(11), pp. 3104–3115.
<https://doi.org/10.1016/j.enconman.2008.06.005>
94. Gholampour, M., Ameri, M., and Samani, M. S., (2014): Experimental study of performance of Photovoltaic–Thermal Unglazed Transpired Solar Collectors (PV/UTCs): Energy, exergy, and electrical-to-thermal rational approaches, *Solar Energy*, 110(December), pp. 636–647. <https://doi.org/10.1016/j.solener.2014.09.011>
95. Gholampour, Maysam, and Ameri, M., (2016a): Energy and exergy analyses of Photovoltaic/Thermal flat transpired collectors: Experimental and theoretical study, *Applied Energy*, 164(15 February), pp. 837–856.
<https://doi.org/10.1016/j.apenergy.2015.12.042>

96. Gholampour, Maysam, and Ameri, M., (2016b): Energy and exergy analyses of Photovoltaic/Thermal flat transpired collectors: Experimental and theoretical study, *Applied Energy*, 164, pp. 837–856. <https://doi.org/10.1016/j.apenergy.2015.12.042>
97. Gomaa, M. R., Ahmed, M., and Rezk, H., (2022): Temperature distribution modeling of PV and cooling water PV/T collectors through thin and thick cooling cross-fined channel box, *Energy Reports*, 8, pp. 1144–1153. <https://doi.org/10.1016/j.egy.2021.11.061>
98. Gopi, S., Muraleedharan, C., and Gopi, S., (2022): Modelling and experimental studies on a double-pass hybrid photovoltaic-thermal solar air heater with vertical slats attached in the lower channel, *International Journal of Ambient Energy*, 43(1), pp. 4664–4674. <https://doi.org/10.1080/01430750.2021.1918241>
99. Gupta, A., Das, B., Biswas, A., and Mondol, J. D., (2022): Sustainability and 4E analysis of novel solar photovoltaic-thermal solar dryer under forced and natural convection drying, *Renewable Energy*, 188(April), pp. 1008–1021. <https://doi.org/10.1016/j.renene.2022.02.090>
100. Hajatzadeh Pordanjani, A., Aghakhani, S., Afrand, M., Mahmoudi, B., Mahian, O., and Wongwises, S., (2019): An updated review on application of nanofluids in heat exchangers for saving energy, *Energy Conversion and Management*, 198(July), pp. 111886. <https://doi.org/10.1016/j.enconman.2019.111886>
101. Hamdan, M. A., (2022): Performance enhancement of a photovoltaic module by passive cooling using water-based aluminum oxide nano-fluid, *Journal of Ecological Engineering*, 23(4), pp. 276–286. <https://doi.org/10.12911/22998993/146675>
102. Hamid, S. A., Othman, M. Y., Sopian, K., and Zaidi, S. H., (2014): An overview of photovoltaic thermal combination (PV/T combi) technology, *Renewable and Sustainable Energy Reviews*, 38, pp. 212–222. <https://doi.org/10.1016/j.rser.2014.05.083>
103. Han, Y., Liu, Y., Lu, S., Basalike, P., and Zhang, J., (2021): Electrical performance and power prediction of a roll-bond photovoltaic thermal array under dewing and frosting conditions, *Energy*, 237, pp. 121587. <https://doi.org/10.1016/j.energy.2021.121587>
104. Hasan, M. A., and Sumathy, K., (2010): Photovoltaic thermal module concepts and their performance analysis: A review, *Renewable and Sustainable Energy Reviews*, 14(7), pp. 1845–1859. <https://doi.org/10.1016/j.rser.2010.03.011>
105. Hassani, S., Saidur, R., Mekhilef, S., and Taylor, R. A., (2016): Environmental and exergy benefit of nanofluid-based hybrid PV/T systems, *Energy Conversion and Management*, 123, pp. 431–444. <https://doi.org/10.1016/j.enconman.2016.06.061>
106. Hazami, M., Riahi, A., Mehdaoui, F., Nouicer, O., and Farhat, A., (2016): Energetic and exergetic performances analysis of a PV/T (photovoltaic thermal) solar system tested and simulated under to Tunisian (North Africa) climatic conditions, *Energy*, 107, pp. 78–94. <https://doi.org/10.1016/j.energy.2016.03.134>
107. Hazi, A., Hazi, G., Grigore, R., and Vernica, S., (2014): Opportunity to use PVT systems for water heating in industry, *Applied Thermal Engineering*, 63(1), pp. 151–157. <https://doi.org/10.1016/j.applthermaleng.2013.11.010>
108. Hegazy, A. A., (2000): Comparative study of the performances of four photovoltaic/thermal solar air collectors, *Energy Conversion and Management*, 41(8), pp. 861–881. [https://doi.org/10.1016/S0196-8904\(99\)00136-3](https://doi.org/10.1016/S0196-8904(99)00136-3)

109. Helmi, N., Nazari, A., Bezaatpour, M., Nateghi, S., and Ghaebi, H., (2022): Investigation of energy storage in parabolic rotary trough solar collectors using various porous fins with magnetic nanoparticles, *Energy for Sustainable Development*, 70, pp. 194–204. <https://doi.org/10.1016/j.esd.2022.07.009>
110. Herrando, M., Markides, C. N., and Hellgardt, K., (2014): A UK-based assessment of hybrid PV and solar-thermal systems for domestic heating and power: System performance, *Applied Energy*, 122, pp. 288–309. <https://doi.org/10.1016/j.apenergy.2014.01.061>
111. Herrando, M., Ramos, A., Zabalza, I., and Markides, C. N., (2019): A comprehensive assessment of alternative absorber-exchanger designs for hybrid PVT-water collectors, *Applied Energy*, 235(November 2018), pp. 1583–1602. <https://doi.org/10.1016/j.apenergy.2018.11.024>
112. Hissouf, M., Feddaoui, M., Najim, M., and Charef, A., (2020): Numerical study of a covered Photovoltaic-Thermal Collector (PVT) enhancement using nanofluids, *Solar Energy*, 199(January), pp. 115–127. <https://doi.org/10.1016/j.solener.2020.01.083>
113. Holman, (2012): *Experimental Methods for Engineers (Eighth)* (Marty Lange, Ed.), McGraw-Hill, New York, 739.
114. Hooshmandzade, N., Motevali, A., Reza, S., Seyedi, M., and Biparva, P., (2021): Influence of single and hybrid water-based nanofluids on performance of microgrid photovoltaic/thermal system, *Applied Energy*, 304(May), pp. 117769. <https://doi.org/10.1016/j.apenergy.2021.117769>
115. Hossain, M. S., Kumar, L., and Nahar, A., (2021): A comparative performance analysis between serpentine-flow solar water heater and photovoltaic thermal collector under Malaysian climate conditions, *International Journal of Photoenergy*, 2021, pp. 1–9. <https://doi.org/10.1155/2021/7176506>
116. Huang, C., Sung, H., and Yen, K., (2012): Experimental study of photovoltaic/thermal (PV/T) hybrid system, *International Journal of Smart Grid and Clean Energy*, 2(2), pp. 147–151.
117. Hussain, F., Othman, M. Y. H., Sopian, K., Yatim, B., Ruslan, H., and Othman, H., (2013): Design development and performance evaluation of photovoltaic/thermal (PV/T) air base solar collector, *Renewable and Sustainable Energy Reviews*, 25, pp. 431–441. <https://doi.org/10.1016/j.rser.2013.04.014>
118. Hussien, A., Eltayesh, A., and El-Batsh, H. M., (2023): Experimental and numerical investigation for PV cooling by forced convection, *Alexandria Engineering Journal*, 64, pp. 427–440. <https://doi.org/10.1016/j.aej.2022.09.006>
119. Ibrahim, A., Othman, M. Y., Ruslan, M. H., Alghoul, M., Yahya, M., Zaharim, A., and Sopian, K., (2009): Performance of photovoltaic thermal collector (PVT) with different absorbers design, *WSEAS Transactions on Environment and Development*, 5(3), pp. 321–330.
120. Ibrahim, A., Othman, M. Y., Ruslan, M. H., Mat, S., and Sopian, K., (2011): Recent advances in flat plate photovoltaic/thermal (PV/T) solar collectors, *Renewable and Sustainable Energy Reviews*, 15(1), pp. 352–365. <https://doi.org/10.1016/j.rser.2010.09.024>

121. Jahromi, S. N., Vadiiee, A., and Yaghoubi, M., (2015): Exergy and Economic Evaluation of a Commercially Available PV/T Collector for Different Climates in Iran, *Energy Procedia*, Elsevier B.V., 75, 444–456.
<https://doi.org/10.1016/j.egypro.2015.07.416>
122. Jaiganesh, K., and Duraiswamy, K., (2013): Experimental study of enhancing the performance of pv panel integrated with solar thermal system, *International Journal of Engineering and Technology*, 5(4), pp. 3419–3426.
123. Jarimi, H., Abu Bakar, M. N., Othman, M., and Din, M. H., (2016): Bi-fluid photovoltaic/thermal (PV/T) solar collector: Experimental validation of a 2-D theoretical model, *Renewable Energy*, 85, pp. 1052–1067.
<https://doi.org/10.1016/j.renene.2015.07.014>
124. Jarimi, H., Nazari, M., Bakar, A., Manaf, N. A., Othman, M., and Din, M., (2013): Mathematical modelling of a finned bi-fluid type photovoltaic/thermal (PV/T) solar collector, *IEEE Conference on Clean Energy and Technology (CEAT)*, IEEE, Langkawi, Malaysia, 163–168.
<https://doi.org/10.1109/CEAT.2013.6775619>
125. Jha, P., Das, B., and Gupta, R., (2019): An experimental study of a photovoltaic thermal air collector (PVTAC): A comparison of a flat and the wavy collector, *Applied Thermal Engineering*, 163(August), pp. 114344.
<https://doi.org/10.1016/j.applthermaleng.2019.114344>
126. Jha, P., Das, B., and Gupta, R., (2020): Performance of air-based photovoltaic thermal collector with fully and partially covered photovoltaic module, *Applied Thermal Engineering*, 180(July), pp. 115838.
<https://doi.org/10.1016/j.applthermaleng.2020.115838>
127. Jha, P., Das, B., and Gupta, R., (2022): Energy matrices evaluation of a conventional and modified partially covered photovoltaic thermal collector, *Sustainable Energy Technologies and Assessments*, 54(August), pp. 102610.
<https://doi.org/10.1016/j.seta.2022.102610>
128. Joseph, A., and Thomas, S., (2022): Energy, exergy and corrosion analysis of direct absorption solar collector employed with ultra-high stable carbon quantum dot nanofluid, *Renewable Energy*, 181, pp. 725–737.
<https://doi.org/10.1016/j.renene.2021.09.079>
129. Joshi, A. S., Tiwari, A., Tiwari, G. N., Dincer, I., and Reddy, B. V., (2009): Performance evaluation of a hybrid photovoltaic thermal (PV/T) (glass-to-glass) system, *International Journal of Thermal Sciences*, 48(1), pp. 154–164.
<https://doi.org/10.1016/j.ijthermalsci.2008.05.001>
130. Joshi, S. S., Dhoble, A. S., and Jiwanapurkar, P. R., (2016): Investigations of different liquid based spectrum beam splitters for combined solar photovoltaic thermal systems, *Journal of Solar Energy Engineering, Transactions of the ASME*, 138(2), pp. 1–7.
<https://doi.org/10.1115/1.4032352>
131. Kalateh, M. R., Kianifar, A., and Sardarabadi, M., (2022): Energy, exergy, and entropy generation analyses of a water-based photovoltaic thermal system, equipped with clockwise counter-clockwise twisted tapes: An indoor experimental study, *Applied Thermal Engineering*, 215(June), pp. 118906.
<https://doi.org/10.1016/j.applthermaleng.2022.118906>

132. Kalogirou, S. A., (2001): Use of TRNSYS for modelling and simulation of a hybrid PV – thermal solar system for Cyprus, *Renewable Energy*, 23(2), pp. 247–260. [https://doi.org/10.1016/S0960-1481\(00\)00176-2](https://doi.org/10.1016/S0960-1481(00)00176-2)
133. Kalogirou, S. A., (2014): *Solar Energy Engineering Processes and Systems* (2nd ed.), Solar Energy Engineering, Elsevier, 816. <https://doi.org/10.1016/b978-0-12-374501-9.00014-5>
134. Kamthania, D., Nayak, S., and Tiwari, G. N., (2011): Performance evaluation of a hybrid photovoltaic thermal double pass facade for space heating, *Energy and Buildings*, 43(9), pp. 2274–2281. <https://doi.org/10.1016/j.enbuild.2011.05.007>
135. Karthik, P., Kumaresan, V., and Velraj, R., (2015): Experimental and parametric studies of a louvered fin and flat tube compact heat exchanger using computational fluid dynamics, *Alexandria Engineering Journal*, 54(4), pp. 905–915. <https://doi.org/10.1016/j.aej.2015.08.003>
136. Kazem, H. A., (2019): Evaluation and analysis of water-based photovoltaic/thermal (PV/T) system, *Case Studies in Thermal Engineering*, 13(December 2018), pp. 100401. <https://doi.org/10.1016/j.csite.2019.100401>
137. Kazem, H. A., Al-waeli, A. H. A., Chaichan, M. T., and Sopian, K., (2021): Numerical and experimental evaluation of nanofluids based photovoltaic/thermal systems in Oman: Using silicone-carbide nanoparticles with water-ethylene glycol mixture, *Case Studies in Thermal Engineering*, 26(March), pp. 101009. <https://doi.org/10.1016/j.csite.2021.101009>
138. Kazem, H. A., Chaichan, M. T., Al-Waeli, A. H. A., and Sopian, K., (2021): Comparison and evaluation of solar photovoltaic thermal system with hybrid collector: An experimental study, *Thermal Science and Engineering Progress*, 22(January), pp. 100845. <https://doi.org/10.1016/j.tsep.2021.100845>
139. Kenfack, A. Z., Nematchoua, M. K., Simo, E., Mfoundikou, M. N., Fosso, J. V. K., Babikir, M. H., and Chara-Dackou, V. S., (2023): Exergetic optimization of some design parameters of the hybrid photovoltaic/thermal collector with bi-fluid air/ternary nanofluid (CuO/MgO/TiO₂), *SN Applied Sciences*, 5(8), pp. 226.
140. Kern, Jr., and M. C. R., (1978): Combined photovoltaic and thermal hybrid collector systems, 13th IEEE Photovoltaic Specialists' Conference, Washington, 1–5.
141. Kianifard, S., Zamen, M., and Nejad, A. A., (2020): Modeling, designing and fabrication of a novel PV/T cooling system using half pipe, *Journal of Cleaner Production*, 253, pp. 119972. <https://doi.org/10.1016/j.jclepro.2020.119972>
142. Klein SA et al., (2006): TRNSYS reference manual, Standard Component Library Overview, 3–93 in TRNSYS 16, a TRaNsient SYstem Simulation program, University of Wisconsin, Madison, retrieved from internet: <http://sel.me.wisc.edu/trnsys>.
143. Kouravand, A., Kasaeian, A., Pourfayaz, F., and Vaziri Rad, M. A., (2022): Evaluation of a nanofluid-based concentrating photovoltaic thermal system integrated with finned PCM heatsink: An experimental study, *Renewable Energy*, 201(P1), pp. 1010–1025. <https://doi.org/10.1016/j.renene.2022.11.025>
144. Kumar, R., and Rosen, M. A., (2011): Performance evaluation of a double pass PV/T solar air heater with and without fins, *Applied Thermal Engineering*, 31(8–9), pp. 1402–1410. <https://doi.org/10.1016/j.applthermaleng.2010.12.037>

145. Lalović, B., Kiss, Z., and Weakliem, H., (1986): A hybrid amorphous silicon photovoltaic and thermal solar collector, *Solar Cells*, 19(2), pp. 131–138. [https://doi.org/10.1016/0379-6787\(86\)90038-4](https://doi.org/10.1016/0379-6787(86)90038-4)
146. Lebbi, M., Touafek, K., Benchatti, A., Boutina, L., Khelifa, A., Taher, M., and Hassani, S., (2021): Energy performance improvement of a new hybrid PV / T Bi-fluid system using active cooling and self-cleaning: Experimental study, *Applied Thermal Engineering*, 182, pp. 1–15. <https://doi.org/10.1016/j.applthermaleng.2020.116033>
147. Leu, J., Liu, M., Liaw, J., and Wang, C., (2001): A numerical investigation of louvered fin-and-tube heat exchangers having circular and oval tube configurations, *International Journal of Heat and Mass Transfer*, 44(22), pp. 4235–4243. [https://doi.org/10.1016/S0017-9310\(01\)00081-3](https://doi.org/10.1016/S0017-9310(01)00081-3)
148. Li, S., Zhou, Z., Liu, J., Zhang, J., Tang, H., Zhang, Z., Na, Y., and Jiang, C., (2022): Research on indirect cooling for photovoltaic panels based on radiative cooling, *Renewable Energy*, 198(August), pp. 947–959. <https://doi.org/10.1016/j.renene.2022.08.020>
149. Liang, Y. Y., Liu, C. C., Li, C. Z., and Chen, J. P., (2015): Experimental and simulation study on the air side thermal hydraulic performance of automotive heat exchangers, *Applied Thermal Engineering*, 87, pp. 305–315. <https://doi.org/10.1016/j.applthermaleng.2015.05.018>
150. Mahmood, D. M. N., and Aljubury, I. M. A., (2022): Experimental investigation of a hybrid photovoltaic evaporative cooling (PV/EC) system performance under arid conditions, *Results in Engineering*, 15(August), pp. 100618. <https://doi.org/10.1016/j.rineng.2022.100618>
151. Maleki, A., Haghighi, A., and Mahariq, I., (2021): Machine learning-based approaches for modeling thermophysical properties of hybrid nano fluids: A comprehensive review, *Journal of Molecular Liquids*, 322, pp. 114843. <https://doi.org/10.1016/j.molliq.2020.114843>
152. Manssouri, O., El Fouas, C., Hajji, B., Rabhi, A., Tina, G. M., and Gagliano, A., (2020): Modeling and performances assessments of PV/T bifluid hybrid collector: Three cooling modes operation case, 4th International Conference on Electrical and Information Technologies ICEIT, 0–5. <https://doi.org/10.1109/ICEIT48248.2020.9113233>
153. Manssouri, O. El, Hajji, B., Tina, G. M., Gagliano, A., and Aneli, S., (2021): Electrical and Thermal Performances of Bi-Fluid PV/Thermal Collectors, *Energies*, 14(6), pp. 1663. <https://doi.org/10.3390/en14061633>
154. Mao, J. N., Chen, H. X., Jia, H., Wang, Y. Z., and Hu, H. M., (2013): Effect of air-side flow maldistribution on thermal-hydraulic performance of the multi-louvered fin and tube heat exchanger, *International Journal of Thermal Sciences*, 73, pp. 46–57. <https://doi.org/10.1016/j.ijthermalsci.2013.06.001>
155. Nabil, T., and Mansour, T. M., (2022): Augmenting the performance of photovoltaic panel by decreasing its temperature using various cooling techniques, *Results in Engineering*, 15(August), pp. 100564. <https://doi.org/10.1016/j.rineng.2022.100564>
156. Nahar, A., Hasanuzzaman, M., and Rahim, N. A., (2017): A 3D comprehensive numerical investigation of different operating parameters on the performance of a

- photovoltaic thermal system with pancake collector, *Journal of Solar Energy Engineering, Transactions of the ASME*, 139(3), pp. 031009.
<https://doi.org/10.1115/1.4035818>
157. Nayak, S., and Tiwari, G. N., (2008): Energy and exergy analysis of photovoltaic/thermal integrated with a solar greenhouse, *Energy and Buildings*, 40(11), pp. 2015–2021. <https://doi.org/10.1016/j.enbuild.2008.05.007>
158. Nualboonrueng, T., Tuenpusa, P., Ueda, Y., and Akisawa, A., (2012): Field experiments of PV-Thermal collectors for residential application in Bangkok, *Energies*, 5(4), pp. 1229–1244. <https://doi.org/10.3390/en5041229>
159. Okbaz, A., Pınarbas, A., and Bahadır, A., (2020): Experimental investigation of effect of different tube row-numbers, fin pitches and operating conditions on thermal and hydraulic performances of louvered and wavy finned heat exchangers, *International Journal of Thermal Sciences*, 151, pp. 106256.
<https://doi.org/10.1016/j.ijthermalsci.2019.106256>
160. Okbaz, A., Pınarbas, A., Bahadır, A., and Hilmi, M., (2018): An experimental, computational and flow visualization study on the air-side thermal and hydraulic performance of louvered fin and round tube heat exchangers, *International Journal of Heat and Mass Transfer*, 121, pp. 153–169.
<https://doi.org/10.1016/j.ijheatmasstransfer.2017.12.127>
161. Ömer, F. C., Arslan, E., Koşan, M., Demirtaş, M., Aktaş, M., and Aktekeli, B., (2022): Experimental and numerical assessment of PV-TvsPV by using waste aluminum as an industrial symbiosis product, *Solar Energy*, 234(February), pp. 338–347.
<https://doi.org/10.1016/j.solener.2022.02.008>
162. Othman, Mohd, Y., Yatim, B., Sopian, K., and Bakar, M. N. A., (2007): Performance studies on a finned double-pass photovoltaic-thermal (PV/T) solar collector, *Desalination*, 209(1–3), pp. 43–49. <https://doi.org/10.1016/j.desal.2007.04.007>
163. Othman, M. Y. H., Hussain, F., Sopian, K., Yatim, B., and Ruslan, H., (2013): Performance study of air-based photovoltaic-thermal (PV/T) collector with different designs of heat exchanger, *Sains Malaysiana*, 42(9), pp. 1319–1325.
164. Othman, M. Y., Hamid, S. A., Tabook, M. A. S., Sopian, K., Roslan, M. H., and Ibrahım, Z., (2016): Performance analysis of PV/T Combi with water and air heating system: An experimental study, *Renewable Energy*, 86, pp. 716–722.
<https://doi.org/10.1016/j.renene.2015.08.061>
165. Othman, Mohd, H., Yatim, B., Sopian, K., Nazari, M., and Bakar, A., (2005): Performance analysis of a double-pass photovoltaic/thermal (PV/T) solar collector with CPC and fins, *Renewable Energy*, 30(13), pp. 2005–2017.
<https://doi.org/10.1016/j.renene.2004.10.007>
166. Othman, Yatim, B., Sopian, K., and Bakar, M. N. A., (2006): Double-Pass Photovoltaic-Thermal Solar Air Collector with Compound Parabolic Concentrator and Fins, *Journal of Energy Engineering*, 132(3), pp. 116–120.
[https://doi.org/10.1061/\(asce\)0733-9402\(2006\)132:3\(116\)](https://doi.org/10.1061/(asce)0733-9402(2006)132:3(116))
167. Özakin, A. N., and Kaya, F., (2020): Experimental thermodynamic analysis of air-based PVT system using fins in different materials: Optimization of control parameters by Taguchi method and ANOVA, *Solar Energy*, 197, pp. 199–211.
<https://doi.org/10.1016/j.solener.2019.12.077>

168. Pathak, M. J. M., Sanders, P. G., and Pearce, J. M., (2014): Optimizing limited solar roof access by exergy analysis of solar thermal, photovoltaic, and hybrid photovoltaic thermal systems, *Applied Energy*, 120, pp. 115–124.
<https://doi.org/10.1016/j.apenergy.2014.01.041>
169. Pounraj, P., Prince Winston, D., Kabeel, A. E., Praveen Kumar, B., Manokar, A. M., Sathyamurthy, R., and Christabel, S. C., (2018): Experimental investigation on Peltier based hybrid PV/T active solar still for enhancing the overall performance, *Energy Conversion and Management*, 168(April), pp. 371–381.
<https://doi.org/10.1016/j.enconman.2018.05.011>
170. Nanda, K., Venkatachalapathy, S., Kalidoss, P., and Chaupal, P., (2023): Experimental Investigation with ANN Modeling of Thermal Conductivity and Viscosity of a Ternary Nanofluid at Different Mixing Ratios and Volume Concentrations, *Journal of Molecular Liquids*, 383(May), pp. 122006.
<https://doi.org/10.1016/j.molliq.2023.122006>
171. Rahman, M. M., Hasanuzzaman, M., and Rahim, N. A., (2017): Effects of operational conditions on the energy efficiency of photovoltaic modules operating in Malaysia, *Journal of Cleaner Production*, 143, pp. 912–924.
<https://doi.org/10.1016/j.jclepro.2016.12.029>
172. Raina, G., Sinha, S., Saini, G., Sharma, S., Malik, P., and Thakur, N. S., (2022): Assessment of photovoltaic power generation using fin augmented passive cooling technique for different climates, *Sustainable Energy Technologies and Assessments*, 52(PB), pp. 102095. <https://doi.org/10.1016/j.seta.2022.102095>
173. Raju, M., Sarma, R. N., Suryan, A., Nair, P. P., and Nižetić, S., (2022): Investigation of optimal water utilization for water spray cooled photovoltaic panel: A three-dimensional computational study, *Sustainable Energy Technologies and Assessments*, 51(December), pp. 101975. <https://doi.org/10.1016/j.seta.2022.101975>
174. Raza, M. Q., Nadarajah, M., and Ekanayake, C., (2016): On recent advances in PV output power forecast, *Solar Energy*, 136, pp. 125–144.
<https://doi.org/10.1016/j.solener.2016.06.073>
175. Rejeb, O., Dhaou, H., and Jemni, A., (2015): A numerical investigation of a photovoltaic thermal (PV/T) collector, *Renewable Energy*, 77, pp. 43–50.
<https://doi.org/10.1016/j.renene.2014.12.012>
176. Salem, M. R., Ali, R. K., and Elshazly, K. M., (2017): Experimental investigation of the performance of a hybrid photovoltaic/thermal solar system using aluminium cooling plate with straight and helical channels, *Solar Energy*, 157, pp. 147–156.
<https://doi.org/10.1016/j.solener.2017.08.019>
177. Salman, A. H. A., Hilal, K. H., and Ghadhban, S. A., (2022): Enhancing performance of PV module using water flow through porous media, *Case Studies in Thermal Engineering*, 34(January), pp. 102000. <https://doi.org/10.1016/j.csite.2022.102000>
178. Santbergen, R., Rindt, C. C. M., Zondag, H. A., and van Zolingen, R. J. C., (2010): Detailed analysis of the energy yield of systems with covered sheet-and-tube PVT collectors, *Solar Energy*, 84(5), pp. 867–878.
<https://doi.org/10.1016/j.solener.2010.02.014>
179. Sardouei, M. M., Morteza pour, H., and JAFARI NAEIMI, K., (2018): Temperature distribution and efficiency assessment of different PVT water collector designs, *Sādhanā*, 43(84), pp. 1–13. <https://doi.org/10.1007/s12046-018-0826-x>

180. Sarhaddi, F., Farahat, S., Ajam, H., and Behzadmehr, A., (2010): Exergetic performance assessment of a solar photovoltaic thermal (PV/T) air collector, *Energy and Buildings*, 42(11), pp. 2184–2199. <https://doi.org/10.1016/j.enbuild.2010.07.011>
181. Sarhaddi, F., Farahat, S., Ajam, H., Behzadmehr, A., and Adeli, M. M., (2010): An improved thermal and electrical model for a solar photovoltaic thermal (PV/T) air collector, *Applied Energy*, 87(7), pp. 2328–2339. <https://doi.org/10.1016/j.apenergy.2010.01.001>
182. Sathe, T. M., and Dhoble, A. S., (2017): A review on recent advancements in photovoltaic thermal techniques, *Renewable and Sustainable Energy Reviews*, 76, pp. 645–672. <https://doi.org/10.1016/j.rser.2017.03.075>
183. Selimefendigil, F., and Şirin, C., (2022): Energy and exergy analysis of a hybrid photovoltaic/thermal-air collector modified with nano-enhanced latent heat thermal energy storage unit, *Journal of Energy Storage*, 45, pp. 103467. <https://doi.org/10.1016/j.est.2021.103467>
184. Shahirah, N., Rukman, B., Fudholi, A., Farhana, N., and Razali, M., (2019): Energy and Exergy Analyses of Photovoltaic-Thermal (PV/T) System with TiO₂/Water Nanofluid Flow, *International Conference on Sustainable Energy and Green Technology 2018 11–14 December 2018, Kuala Lumpur, Malaysia*, IOP Publishing, 268, 012075. <https://doi.org/10.1088/1755-1315/268/1/012075>
185. Shahsavar, A., and Ameri, M., (2010): Experimental investigation and modeling of a direct-coupled PV/T air collector. <https://doi.org/10.1016/j.solener.2010.07.010>
186. Shahsavar, A., Ameri, M., and Gholampour, M., (2012): Energy and exergy analysis of a photovoltaic-thermal collector with natural air flow, *Journal of Solar Energy Engineering, Transactions of the ASME*, 134(1), pp. 1–10. <https://doi.org/10.1115/1.4005250>
187. Shrivastava, A., Prakash Arul Jose, J., Dilip Borole, Y., Saravanakumar, R., Sharifpur, M., Harasi, H., Abdul Razak, R. K., and Afzal, A., (2022): A study on the effects of forced air-cooling enhancements on a 150 W solar photovoltaic thermal collector for green cities, *Sustainable Energy Technologies and Assessments*, 49, pp. 101782. <https://doi.org/10.1016/j.seta.2021.101782>
188. Shyam, Tiwari, G. N., Fischer, O., Mishra, R. K., and Al-Helal, I. M., (2016): Performance evaluation of N-photovoltaic thermal (PVT) water collectors partially covered by photovoltaic module connected in series: An experimental study, *Solar Energy*, 134, pp. 302–313. <https://doi.org/10.1016/j.solener.2016.05.013>
189. Singh, A. P., Akshayveer, Kumar, A., and Singh, O. P., (2019): Strategies for effective cooling of photovoltaic panels integrated with solar chimney, *Materials Today: Proceedings*, 39, pp. 1950–1954. <https://doi.org/10.1016/j.matpr.2020.08.440>
190. Singh, D. K., (2020): Free convection with MWCNT/water nanofluid having varying aspect ratio of MWCNT nanoparticle in thermally undulated enclosures, *International Journal of Mechanical Sciences*, 178(March), pp. 105626. <https://doi.org/10.1016/j.ijmeosci.2020.105626>
191. Singh, S., Agarwal, S., Tiwari, G. N., and Chauhan, D., (2015): Application of genetic algorithm with multi-objective function to improve the efficiency of glazed photovoltaic thermal system for New Delhi (India) climatic condition, *Solar Energy*, 117, pp. 153–166. <https://doi.org/10.1016/j.solener.2015.04.025>

192. Slimani, M. E. A., Amirat, M., Bahria, S., Kurucz, I., Aouli, M., and Sellami, R., (2016): Study and modeling of energy performance of a hybrid photovoltaic/thermal solar collector: Configuration suitable for an indirect solar dryer, *Energy Conversion and Management*, 125, pp. 209–221. <https://doi.org/10.1016/j.enconman.2016.03.059>
193. Slimani, M. E. A., Sellami, R., Said, M., and Bouderbhal, A., (2021): A novel hybrid photovoltaic/thermal bi-fluid (air/water) solar collector: an experimental investigation, *Proceedings of the 4th International Conference on Electrical Engineering and Control Applications*, *Lecture Notes in Electrical Engineering* 682, 682, 697–709. https://doi.org/10.1007/978-981-15-6403-1_47
194. Slimani, M. E., SELLAMI, R., AMIRAT, M., and Mahrane, A., (2019): Study of hybrid photovoltaic/thermal collector provided with finned metal plates: a numerical investigation under real operating conditions, *International Conference on Advanced Electrical Engineering (ICAEE)*, IEEE, Algiers, Algeria, 1–6. <https://doi.org/10.1109/ICAEE47123.2019.9015175>
195. Sultan, S. M., Tso, C. P., Ervina, E. M. N., and Abdullah, M. Z., (2022): Cost and time effective performance evaluation methods for photovoltaic module cooling techniques: Analytical and experimental study, *Applied Energy*, 326(August), pp. 119940. <https://doi.org/10.1016/j.apenergy.2022.119940>
196. Sundar, L. S., Sharma, K. V., Singh, M. K., and Sousa, A. C. M., (2017): Hybrid nanofluids preparation, thermal properties, heat transfer and friction factor – A review, *Renewable and Sustainable Energy Reviews*, 68(Part1), pp. 185–198. <https://doi.org/10.1016/j.rser.2016.09.108>
197. Sutanto, B., Indartono, Y. S., Wijayanta, A. T., and Iacovides, H., (2022): Enhancing the performance of floating photovoltaic system by using thermosiphon cooling method: Numerical and experimental analyses, *International Journal of Thermal Sciences*, 180(October 2021), pp. 107727. <https://doi.org/10.1016/j.ijthermalsci.2022.107727>
198. Tabatabaian, M., Tivy, W., and Bibby, C., (2012): Design and development of a hybrid photovoltaic-thermal/PVT system, *Proceedings of the ASME 2012 6th International Conference on Energy Sustainability ES2012*, ASME, San Diego, California, USA, 919–930. <https://doi.org/10.1115/ES2012-91258>
199. Tiwari, A., and Sodha, M. S., (2006a): Performance evaluation of hybrid PV/thermal water/air heating system: A parametric study, *Renewable Energy*, 31(15), pp. 2460–2474. <https://doi.org/10.1016/j.renene.2005.12.002>
200. Tiwari, A., and Sodha, M. S., (2006b): Performance evaluation of solar PV/T system: An experimental validation, *Solar Energy*, 80(7), pp. 751–759. <https://doi.org/10.1016/j.solener.2005.07.006>
201. Tiwari, A., and Sodha, M. S., (2007): Parametric study of various configurations of hybrid PV/thermal air collector: Experimental validation of theoretical model, *Solar Energy Materials and Solar Cells*, 91(1), pp. 17–28. <https://doi.org/10.1016/j.solmat.2006.06.061>
202. Tonui, J. K., and Tripanagnostopoulos, Y., (2007a): Air-cooled PV/T solar collectors with low-cost performance improvements, *Solar Energy*, 81(4), pp. 498–511. <https://doi.org/10.1016/j.solener.2006.08.002>

203. Tonui, J. K., and Tripanagnostopoulos, Y., (2008): Performance improvement of PV/T solar collectors with natural air flow operation, *Solar Energy*, 82(1), pp. 1–12. <https://doi.org/10.1016/j.solener.2007.06.004>
204. Tonui, J. K., and Tripanagnostopoulos, Y. A., (2007b): Improved PV/T solar collectors with heat extraction by forced or natural air circulation, *Renewable Energy*, 32(4), pp. 623–637. <https://doi.org/10.1016/j.renene.2006.03.006>
205. Touafek, K., Khelifa, A., Adouane, M., Khettaf, E. H., and Embarek, A., (2013): Experimental study on a new conception of hybrid PV/T collector, 14th International Conference on Sciences and Techniques of Automatic Control & Computer Engineering-STA'2013, IEEE, Sousse, Tunisia, 140–145. <https://doi.org/10.1109/STA.2013.6783120>
206. Tripanagnostopoulos, Y., Tzavellas, D., Zoulia, I., and Chortatou, M., (2001): Hybrid PV/T systems with dual heat extraction operation, *Proceeding of the 17th European PV solar energy conference.*, Munich, Germany, 2515–2518.
207. Tripanagnostopoulos, Y., Nousia, T., and Souliotis, M., (2000): Low-cost improvements to building integrated air cooled, P. H. H. Scheer, B. McNelis, W. Palz, H.A. Ossenbrink, ed., *Proceedings of 16th European PV Solar Energy Conference*, Routledge, Glasgow, UK, 1874 – 1899. <https://doi.org/10.4324/9781315074405>
208. Tripanagnostopoulos, Y., (2007): Aspects and improvements of hybrid photovoltaic/thermal solar energy systems, *Solar Energy*, 81(9), pp. 1117–1131. <https://doi.org/10.1016/j.solener.2007.04.002>
209. Tripanagnostopoulos, Y., Nousia, T., Souliotis, M., and Yianoulis, P., (2002): Hybrid photovoltaic/thermal solar systems, *Solar Energy*, 72(3), pp. 217–234. [https://doi.org/10.1016/S0038-092X\(01\)00096-2](https://doi.org/10.1016/S0038-092X(01)00096-2)
210. Tyagi, V. V., Kaushik, S. C., and Tyagi, S. K., (2012): Advancement in solar photovoltaic/thermal (PV/T) hybrid collector technology, *Renewable and Sustainable Energy Reviews*, 16(3), pp. 1383–1398. <https://doi.org/10.1016/j.rser.2011.12.013>
211. Valiente-Blanco, I., Lopez-Pascual, D., Diaz-Villar, P., Mallol-Poyato, R., Barragan, A., Ocaña, M., Granello, G., and Diez-Jimenez, E., (2022): Efficiency improvement of photovoltaic solar modules by cooling using an underground heat exchanger, *Journal of Solar Energy Engineering*, 144(6), pp. 61015.
212. Vallejo, J. P., Prado, J. I., and Lugo, L., (2022): Hybrid or mono nanofluids for convective heat transfer applications. A critical review of experimental research, *Applied Thermal Engineering*, 203(December 2021), pp. 117926. <https://doi.org/10.1016/j.applthermaleng.2021.117926>
213. Vivek Raman, G. N. T., (2009): A comparison study of energy and exergy performance of a hybrid photovoltaic double-pass and single-pass air collector, *International Journal of Energy Research*, 33(6), pp. 553–630. <https://doi.org/10.1002/er>
214. Wahab, A., Khan, M. A. Z., and Hassan, A., (2020): Impact of graphene nanofluid and phase change material on hybrid photovoltaic thermal system: Exergy analysis, *Journal of Cleaner Production*, 277, pp. 123370. <https://doi.org/10.1016/j.jclepro.2020.123370>
215. Widyolar, B., Jiang, L., Brinkley, J., Hota, S. K., Ferry, J., Diaz, G., and Winston, R., (2020): Experimental performance of an ultra-low-cost solar photovoltaic-thermal

- (PVT) collector using aluminum minichannels and nonimaging optics, *Applied Energy*, 268(October 2019), pp. 114894. <https://doi.org/10.1016/j.apenergy.2020.114894>
216. Wolf, M., (1976): Performance analyses of combined heating and photovoltaic power systems for residences, *Energy Conversion*, 16(1–2), pp. 79–90. [https://doi.org/10.1016/0013-7480\(76\)90018-8](https://doi.org/10.1016/0013-7480(76)90018-8)
217. Wu, S. Y., Zhang, Q. L., Xiao, L., and Guo, F. H., (2011): A heat pipe photovoltaic/thermal (PV/T) hybrid system and its performance evaluation, *Energy and Buildings*, 43(12), pp. 3558–3567. <https://doi.org/10.1016/j.enbuild.2011.09.017>
218. Xu, P., Zhang, X., Shen, J., Zhao, X., He, W., and Li, D., (2015): Parallel experimental study of a novel super-thin thermal absorber based photovoltaic/thermal (PV/T) system against conventional photovoltaic (PV) system, *Energy Reports*, 1, pp. 30–35. <https://doi.org/10.1016/j.egy.2014.11.002>
219. Yadav, A. K., and Chandel, S. S., (2013): Tilt angle optimization to maximize incident solar radiation: A review, *Renewable and Sustainable Energy Reviews*, 23, pp. 503–513. <https://doi.org/10.1016/j.rser.2013.02.027>
220. Yang, L., Du, K., and Zhang, Z., (2020): Heat transfer and flow optimization of a novel sinusoidal minitube filled with non-Newtonian SiC/EG-water nanofluids, *International Journal of Mechanical Sciences*, 168(November 2019). <https://doi.org/10.1016/j.ijmecsci.2019.105310>
221. Yazdanifard, F., and Ameri, M., (2018): Exergetic advancement of photovoltaic/thermal systems (PV/T): A review, *Renewable and Sustainable Energy Reviews*, 97, pp. 529–553. <https://doi.org/10.1016/j.rser.2018.08.053>
222. Yazdanifard, F., Ebrahimnia-Bajestan, E., and Ameri, M., (2016): Investigating the performance of a water-based photovoltaic/thermal (PV/T) collector in laminar and turbulent flow regime, *Renewable Energy*, 99, pp. 295–306. <https://doi.org/10.1016/j.renene.2016.07.004>
223. Yildirim, M. A., Cebula, A., and Sułowicz, M., (2022): A cooling design for photovoltaic panels – Water-based PV/T system, *Energy*, 256(October), pp. 124654. <https://doi.org/10.1016/j.energy.2022.124654>
224. Yoon, S., Seo, J., Choi, M., and Lee, B. J., (2022): Enhanced photovoltaic efficiency through radiative cooling augmented by a thermosyphon effect, *Energy Conversion and Management*, 268(August), pp. 116046. <https://doi.org/10.1016/j.enconman.2022.116046>
225. Yunus Khan, T. M., Soudagar, M. E. M., Kanchan, M., Afzal, A., Banapurmath, N. R., Akram, N., Mane, S. D., and Shahapurkar, K., (2020): Optimum location and influence of tilt angle on performance of solar PV panels, *Journal of Thermal Analysis and Calorimetry*, 141(1), pp. 511–532. <https://doi.org/10.1007/s10973-019-09089-5>
226. Zapałowicz, Z., and Zeńczak, W., (2022): Seawater cooling of PV modules mounted on ships in Świnoujście/Poland harbour, *Heliyon*, 8(8), pp. E10078. <https://doi.org/10.1016/j.heliyon.2022.e10078>
227. Zhao, J., Song, Y., Lam, W. H., Liu, W., Liu, Y., Zhang, Y., and Wang, D., (2011): Solar radiation transfer and performance analysis of an optimum photovoltaic/thermal system, *Energy Conversion and Management*, 52(2), pp. 1343–1353. <https://doi.org/10.1016/j.enconman.2010.09.032>

228. Zhao, Yan, Meng, T., Jing, C., Hu, J., and Qian, S., (2020): Experimental and numerical investigation on thermal performance of PV- driven aluminium honeycomb solar air collector, *Solar Energy*, 204(May), pp. 294–306.
<https://doi.org/10.1016/j.solener.2020.04.047>
229. Zhao, Yulong, Gong, S., Zhang, C., Ge, M., and Xie, L., (2022): Performance analysis of a solar photovoltaic power generation system with spray cooling, *Case Studies in Thermal Engineering*, 29(December), pp. 101723.
<https://doi.org/10.1016/j.csite.2021.101723>
230. Zhou, J., Zhu, Z., Zhao, X., Yuan, Y., Fan, Y., and Myers, S., (2020): Theoretical and experimental study of a novel solar indirect-expansion heat pump system employing mini channel PV/T and thermal panels, *Renewable Energy*, 151, pp. 674–686.
<https://doi.org/10.1016/j.renene.2019.11.054>
231. Zhou, Z., Tkachenko, S., Bahl, P., Tavener, D., de Silva, C., Timchenko, V., Jiang, J. Y., Keevers, M., and Green, M., (2022): Passive PV module cooling under free convection through vortex generators, *Renewable Energy*, 190, pp. 319–329.
<https://doi.org/10.1016/j.renene.2022.03.133>
232. Žižak, T., Domjan, S., Medved, S., and Arkar, C., (2022): Efficiency and sustainability assessment of evaporative cooling of photovoltaics, *Energy*, 254(Part A), pp. 124260. <https://doi.org/10.1016/j.energy.2022.124260>
233. Zohri, M., Bakti, L. D., and Fudholi, A., (2018a): Exergy assessment of Photovoltaic thermal with V-groove collector using theoretical study, *Telkomnika*, 16(2), pp. 550–557. <https://doi.org/10.12928/TELKOMNIKA.v16i2.8433>
234. Zohri, M., Hadisaputra, S., Fudholi, A., Air, D. S., With, H., and Fins, S., (2018b): Exergy and energy analysis of photovoltaic thermal (PV/T) with and without fins collector, *ARNP Journal of Engineering and Applied Sciences*, 13(3), pp. 803–808.
235. Zondag, H. A., de Vries, D. W., van Helden, W. G. J., van Zolingen, R. J. C., and van Steenhoven, A. A., (2003): The yield of different combined PV-thermal collector designs, *Solar Energy*, 74(3), pp. 253–269.
[https://doi.org/10.1016/S0038-092X\(03\)00121-X](https://doi.org/10.1016/S0038-092X(03)00121-X)
236. Zondag, H. A., De Vries, D. W., Van Helden, W. G. J., Van Zolingen, R. J. C., and Van Steenhoven, A. A., (2002): The thermal and electrical yield of a PV-thermal collector, *Solar Energy*, 72(2), pp. 113–128.
[https://doi.org/10.1016/S0038-092X\(01\)00094-9](https://doi.org/10.1016/S0038-092X(01)00094-9)
237. Zubeer, S. A., and Ali, O. M., (2022): Experimental and numerical study of low concentration and water-cooling effect on PV module performance, *Case Studies in Thermal Engineering*, 34(September), pp. 102007.
<https://doi.org/10.1016/j.csite.2022.102007>

A2: Publications related to the dissertation*Refereed papers in foreign languages:*

1. **Alshibil A.M.A.**, Víg P., Farkas I. (2020): Transient simulation of a hybrid solar collector system, Mechanical Engineering Letters, Gödöllő, Hungary, 20, pp. 101-106. HU ISSN 2060-3789
2. **Alshibil A.M.A.**, Víg P., Farkas I. (2021): Performance evaluation of a hybrid solar collector in two different climates, European Journal of Energy Research, 1(2), pp. 17-20. <https://doi.org/10.24018/ejenergy.2021.1.2.11>
3. **Alshibil A.M.A.**, Víg P., Farkas I. (2022): Multi-aspect approach of electrical and thermal performance evaluation for hybrid photovoltaic/thermal solar collector using TRNSYS tool, International Journal of Thermofluids, 16, pp. 100222. <https://doi.org/10.1016/j.ijft.2022.100222> (Scopus: D1)
4. **Alshibil A.M.A.**, Víg P., Farkas I. (2023): Thermodynamical analysis and evaluation of louver-fins based hybrid bi-fluid photovoltaic/thermal collector systems, Renewable Energy, 206 (April 2023), pp. 1120-1131. <https://doi.org/10.1016/j.renene.2023.02.105> (Scopus: D1, IF = 8.7)
5. **Alshibil A.M.A.**, Víg P., Farkas I. (2023): Sustainability contributions of hybrid solar collector toward net-zero energy buildings concerning solar cells wasted heat, Energy for Sustainable Development, 74 (June 2023), pp. 185-195. <https://doi.org/10.1016/j.esd.2023.04.001> (Scopus: D1, IF = 5.5)
6. **Alshibil A.M.A.**, Víg P., Farkas I. (2023): Experimental performance comparison of a novel design of bi-fluid photovoltaic-thermal module using louver fins, Energy Reports, 9 (December 2023), pp. 4518-4531. <https://doi.org/10.1016/j.egy.2023.03.110> (Scopus: Q1, IF = 5.2)
7. **Alshibil A.M.A.**, Víg P., Farkas I. (2023): Evaluation of fin configurations for an air-cooled hybrid photovoltaic-thermal solar collector, Thermal Science journal, online first (00), pp. 84. <https://doi.org/10.2298/TSCI230116084A> (IF = 1.7)
8. **Alshibil A.M.A.**, Víg P., Farkas I. (2024): Thermal equilibrium time as a novel characteristic of nanofluids evaluation: an experimental investigation of a MWCNTs+MgO+BN/distilled-water ternary nanofluid, Journal of Molecular Liquids, x(x), pp. x-x. <https://doi.org/xxxxxxxxxxxxx> (Scopus: D1, IF = 6) (under review)
9. **Alshibil A.M.A.**, Víg P., Farkas I. (2023): Performance enhancement attempts on the photovoltaic/thermal module and the sustainability achievements: a review, Energy, x(x), pp. x-x. <https://doi.org/xxxxxxxxxxxxx> (Scopus: D1, IF = 9) (under review)
10. **Alshibil A.M.A.**, Víg P., Farkas I. (2024): Experimental comparison of glazed and unglazed hybrid solar modules considering power productivity and cell temperature, Journal of Electrical Engineering & Technology, x(x), pp. x-x. <https://doi.org/xxxxxxxxxxxxx> (IF = 1.9) (under review)
11. **Alshibil A.M.A.**, Víg P., Erdélyi V., Tóth J., Farkas I. (2024): Performance assessments of direct contact serpentine tube based photovoltaic thermal module: an experimental comparison, Journal of Engineering and Sustainable Development, x(x), pp. x-x. <https://doi.org/xxxxxxxxxxxxx> (under review)

Refereed papers in Hungarian language:

12. Víg P, **Alshibil A.M.A.**, Farkas I.: Hibrid napkollektorok és alkalmazásaik, Mezőgazdasági Technika, LX. Évf., 2021. Február, 2-5. O. ISSN 0026 1890

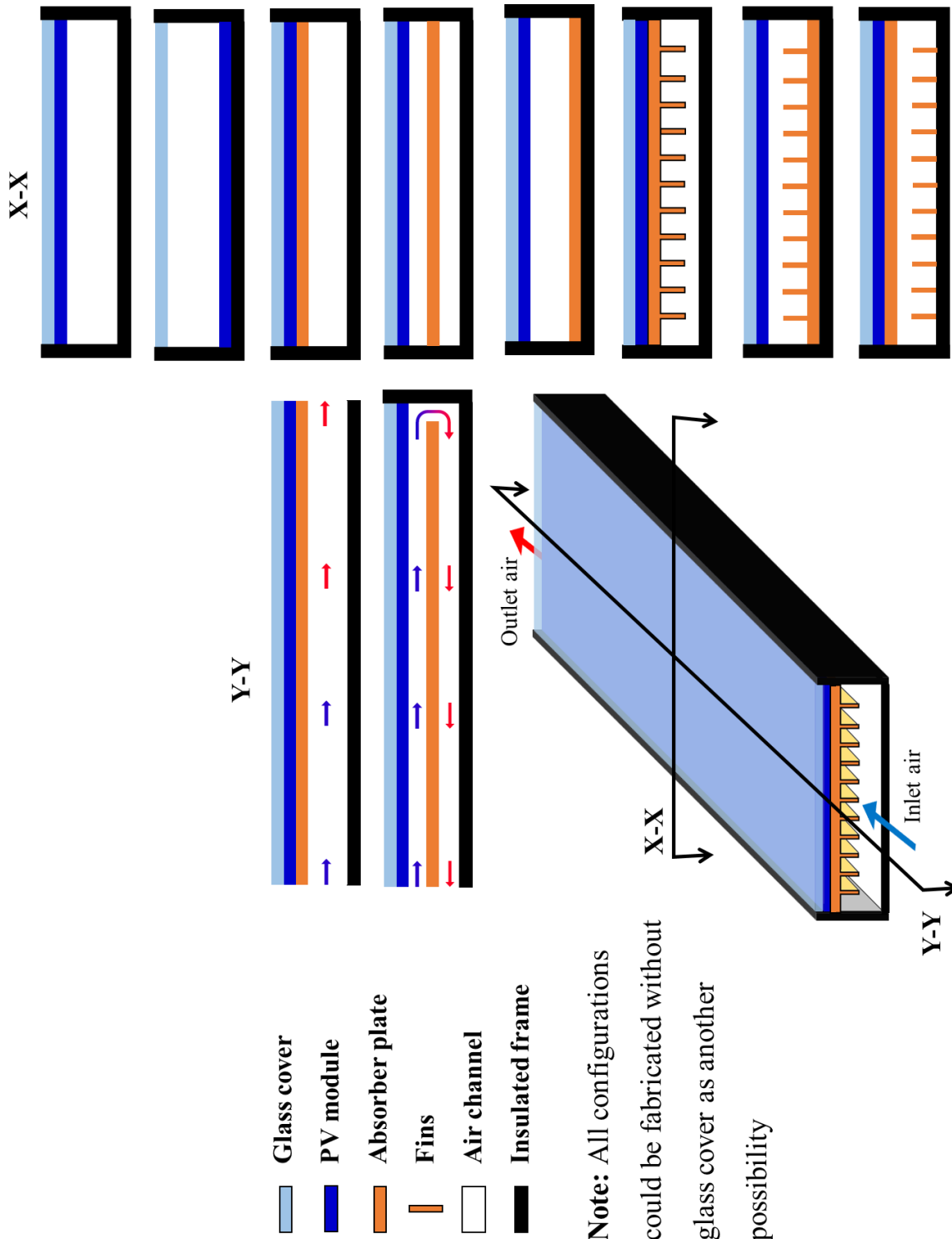
International conference proceedings

13. **Alshibil A.M.A.**, Víg P., Farkas I. (2021): Heat transfer behaviour of hybrid solar collector module for liquid-based type, Proceedings of I4SDG Workshop 2021, IFToMM for Sustainable Development Goals, Springer, Cham, November 25-26, 2021, pp. 20-29. ISBN 978-3-030-87383-7.
14. **Alshibil A.M.A.**, Víg P., Farkas I. (2021): Seasonal performance evaluation of hybrid solar collectors in a hot climate area, Proceedings of the 3rd Faculty of Industrial Technology International Congress, Bandung, Indonesia, October 28-29, 2021, pp. 136-140. ISSN: 2962 – 1798.

International conference abstracts

15. **Alshibil A.M.A.**, Víg P., Farkas I.: Efficiency improvement of the hybrid solar collector systems, Book of Abstracts, 25th Workshop on Energy and Environment, Gödöllő, Hungary, November 28-29, 2019, p. 10., ISBN 978-963-9483-95-8
16. **Alshibil A.M.A.**, Farkas I., Víg P.: Improvement attempts for the efficiency of hybrid solar collectors, Book of abstracts, 19th International Workshop for Young Scientists, (BioPhys Spring 2020), Prague, Czech Republic, May 19-21, 2020, p. 32. ISBN: 978-83-89969-64-4
17. **Alshibil A.M.A.**, Víg P., Farkas I.: TRNSYS simulation of a flat plate-based hybrid solar collector system, Book of Abstracts, 26th Workshop on Energy and Environment, Gödöllő, Hungary, December 10-11, 2020, p. 18. ISBN 978-963-269-928-8
18. **Alshibil A.M.A.**, Víg P., Farkas I.: Modelling and control of hybrid solar collector systems, Book of Abstracts, 20th International Workshop for Young Scientists (BioPhys Spring 2021), Lublin, Poland, May 18, 2021, p. 17., ISBN 978-83-89969-68-2
19. **Alshibil A.M.A.**, Víg P., Farkas I.: Thermal and electrical behaviour of a hybrid solar collector under tropical climate, International Conference on Efficiency, Solar and Thermal Energy for the Human Comfort, Gödöllő, Hungary, July 9, 2021, p. 31-32., ISBN 978-963-269-958-5
20. **Alshibil A.M.A.**, Víg P., Farkas I.: Glass cover effects on the hybrid solar collector systems performance, Book of Abstracts, 27th Workshop on Energy and Environment, Gödöllő, Hungary, December 8-9, 2021, p. 12., ISBN 978-963-269-972-1
21. **Alshibil A.M.A.**, Víg P., Farkas I.: Comparative study of an air-based hybrid photovoltaic thermal module in different absorber configurations, Book of Abstracts, 28th Workshop on Energy and Environment, Gödöllő, Hungary, December 8-9, 2022, p. 19-20., ISBN 978-963-623-016-6
22. **Alshibil A.M.A.**, Víg P., Farkas I.: Performance comparison of the hybrid photovoltaic thermal modules enhanced by water and glycol as a coolant, Book of Abstracts, 22nd International Workshop for Young Scientists (BioPhys Spring 2023), Gödöllő, Hungary, June 15-16, 2023, p. 17., ISBN 978-963-623-054-8
23. **Alshibil A.M.A.**, Víg P., Farkas I.: Experimental performance assessment of serpentine copper tube-based photovoltaic thermal module, Book of Abstracts, 29th Workshop on Energy and Environment, Gödöllő, Hungary, December 7-8, 2023, p. 23-24., ISBN 978-963-623-079-1

A3: Graphical summary of air-cooled PV/T configurations



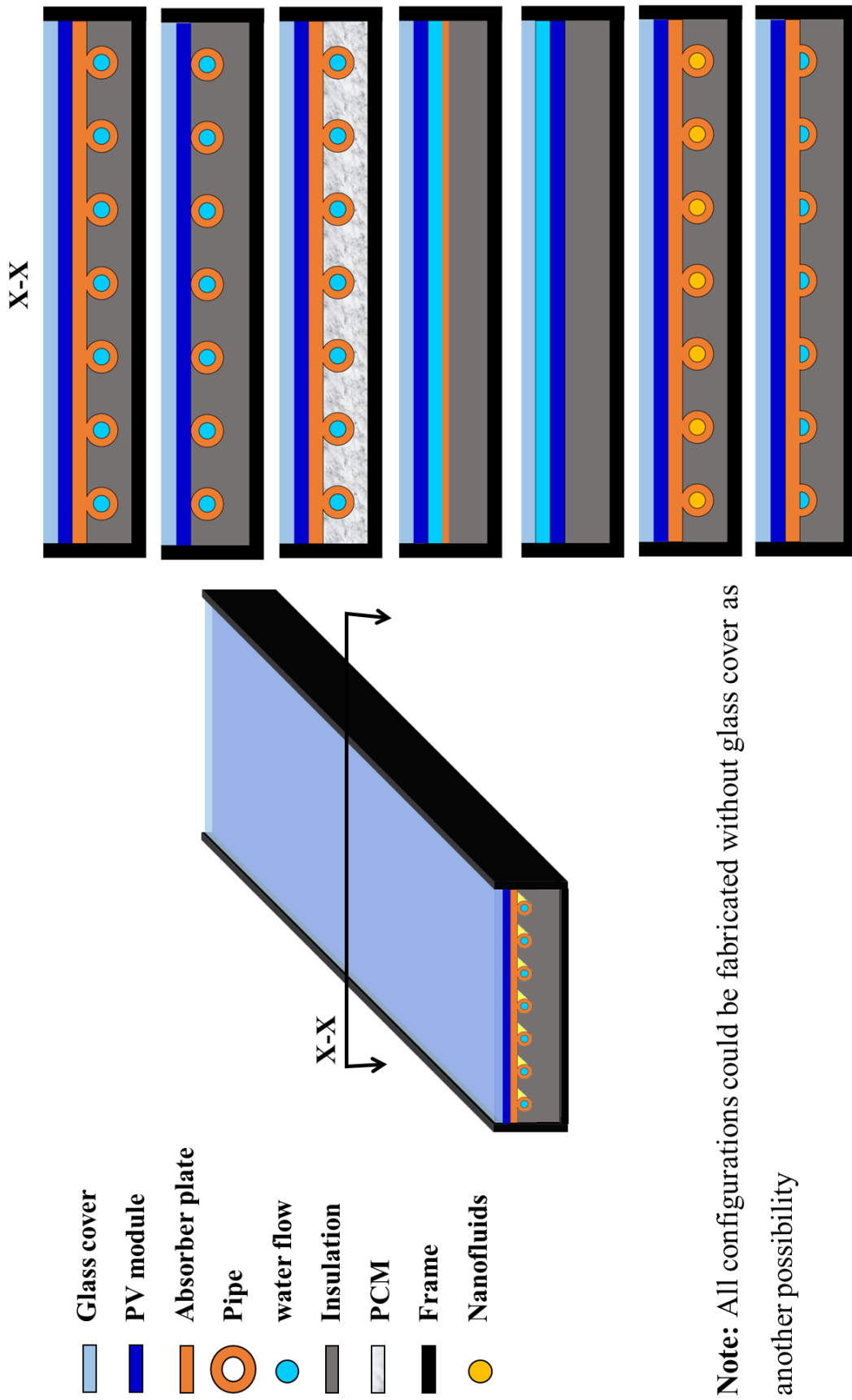
A4: Summary of recent studies conducted on the PV/T modules

Ref	Study	Place	PV cell	Cooling Methods	Heat removal technique	Heat Transfer Fluid	Electrical Conversion Efficiency Enhancement
(Ömer et al., 2022)	Ex. Nu.	N/A	M	Natural	Aluminium slag	Air	16.87%
(Abdullah et al., 2022)	Ex.	Hawija, Iraq	P	Forced	Fan at rear HE at rear	Air Water	0.8% 13.19%
(Alayi et al., 2022)	Nu.	N/A	P	Natural	Air cooling	Air	N/A
(Yildirim et al., 2022)	Nu.	N/A	M	Forced	Cooling box	Water	17.79%
(Eid et al., 2022)	Ex. Nu.	Kyonggi, South Korea	P	Mixed	Thermoelectric	Water	11.23%
(Yoon et al., 2022)	Nu.	N/A	N/A	Forced	Radiative	Water	6.4%
(Bevilacqua et al., 2022)	Ex.	Rende, Italy	P	Forced	Spray cooling	Water	7.8%
(Choi et al., 2022)	Ex.	N/A	P	Forced	dimple internal channel	Air	N/A
(Li et al., 2022)	Ex.	N/A	M	Natural	Radiative	Water	1.59%
(Salman et al., 2022)	Ex. Nu.	N/A	P	Forced	Porous media at the rear	Water	7.02%
(Sutanto et al., 2022)	Ex. Nu.	Bandung, Indonesia	P	Natural	Thermosiphon	Water	7.86%
(Zapałowicz and Zeńczak, 2022)	Nu.	N/A	M	Forced	Seawater cooling	Water	N/A
(Zhou et al., 2022)	Nu.	N/A	N/A	Natural	Vortex generator	Air	N/A
(Zubeer and Ali, 2022)	Ex. Nu.	Duhok, Iraq	P	Forced	Water flowing on the front face	Water	17.7%
(Gao et al., 2022)	Nu.	N/A	M	Forced	Heat sink	Water	14.59%
(Hussien et al., 2023)	Ex. Nu.	Benha, Egypt	M	Forced	Blowers Fans	Air	3.9% 7%
(Mahmood and	Ex.	Baghdad, Iraq	M	Natural	Evaporative	Water	9.7%

8. Appendices

Aljubury, 2022)							
(Sultan et al., 2022)	Ex. Nu.	N/A	M	Mixed	Fan cooling	Air	N/A
(Bilen et al., 2022)	Nu.	N/A	N/A	Natural	Fins	Air	11.5%
(Hamdan, 2022)	Ex.	Dhahran, Saudi Arabia	P	Natural	Fins with nano-coating	Air	2.88%
(Nabil and Mansour, 2022)	Ex.	Ismailia, Egypt	P	Forced	Fan Serpentine tube Nozzle at front	Air Water Water	2.29% 2.46% 6.84%
(Žižak et al., 2022)	Ex.	Zurich	M	Forced	Evaporative cooling	Water	9.6%
(Faraz Ahmad et al., 2022)	Ex.	Sharjah, UAE	M	Forced	Mist/fog cooling	Water	13.54%
(Yulong Zhao et al., 2022)	Nu.	N/A	N/A	Forced	Spray	Water	7.3%
(Raina et al., 2022)	Ex.	New Delhi, India	N/A	Natural	Fin augmented	Air	5.47%
(Singh et al., 2019)	Nu.	N/A	M	Natural	Solar chimney	Air	N/A
(Chen et al., 2022)	Ex. Nu.	N/A	M	Forced	Spray	Water	4.1%
(Elminshawy et al., 2022)	Ex.	Port Said, Egypt	P	Natural	Floating cooling with fin assisted	Water	22.24%
(Raju et al., 2022)	Ex. Nu.	N/A	M	Forced	Water spraying	Water	15.73%
(Valiente-Blanco et al., 2022)	Ex. Nu.	Henares, Spain	P	Forced	Underground heat exchanger	Water	9.8%
P: Poly-crystalline silicon, M: Multi-crystalline silicon, N/A: None mentioned, Ex.: Experimental, Nu.: Numerical							

A5: Graphical summary of water-cooled PV/T configurations

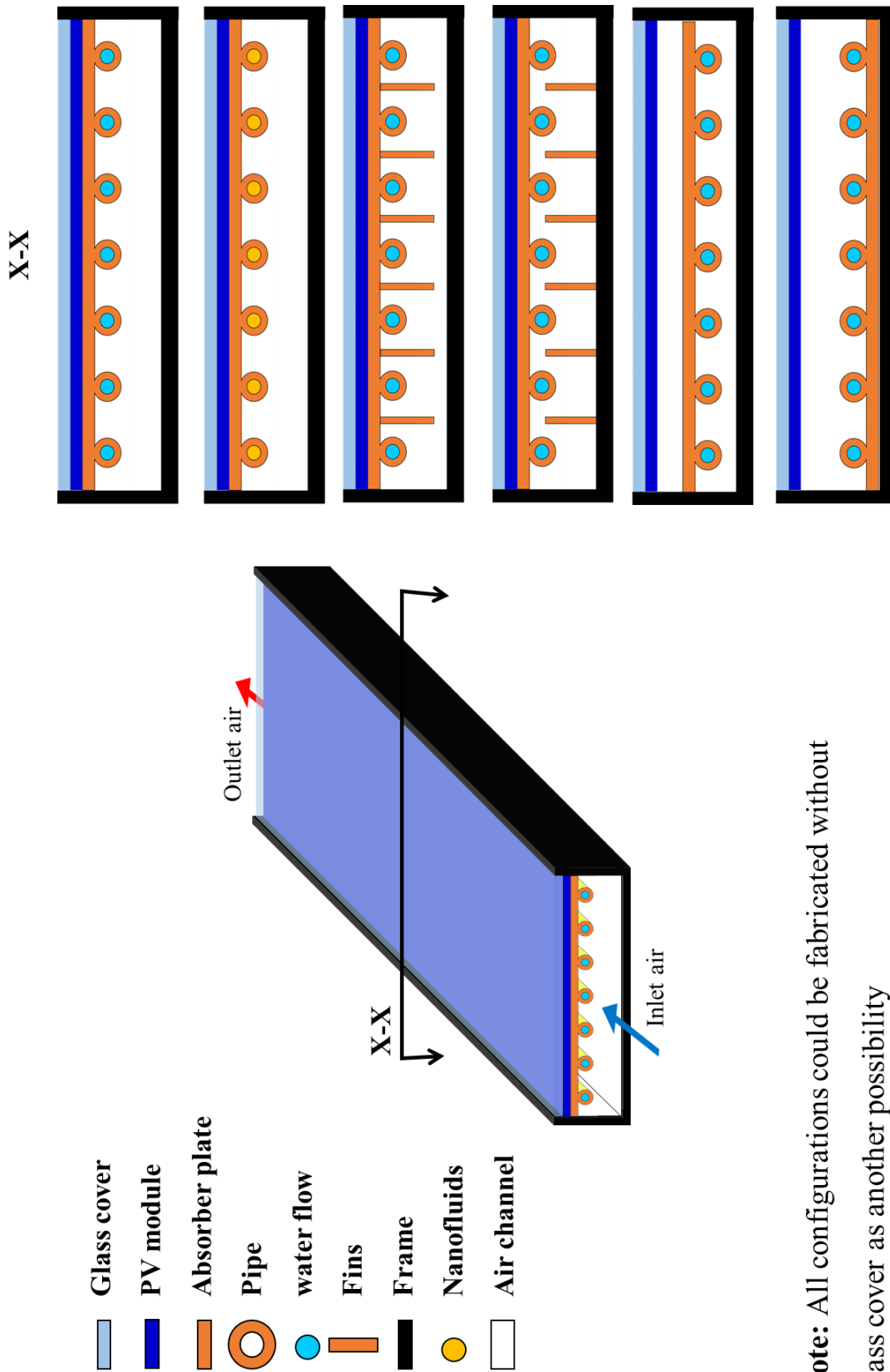


A6: Summary of exergy efficiency obtained from previous studies

Reference	Study	Type of PV	Technique for enhancement	Exergy efficiency
(Nayak and Tiwari, 2008)	Ex.	S	Integrated into a greenhouse	4%
(Sarhaddi et al., 2010)	Nu.	N/A	Airflow duct	10.75%
(Gang et al., 2011)	Nu.	S	Absorber with heat pipes	6.8%
	Ex.			
(Wu et al., 2011)	Nu.	N/A	Heat pipe	10.26%
(Jahromi et al., 2015)	Nu.	N/A	Commercialized PV/T	9.6%
(Gholampour and Ameri, 2016b)	Ex.	M	Flat transpired collectors	8.66%
(Hazami et al., 2016)	Nu.	S	Classical type of water-based PV/T with TRNSYS model	14.8%
	Ex.			
(Salem et al., 2017)	Ex.	M	Absorber plate with straight and helical channels	13.5%
(Fudholi et al., 2018)	Ex.	M	∇-groove air channel	13.26%
(Wahab et al., 2020)	Ex.	S	Nanofluid+ PCM	14.62%
(Abdul-Ganiyu et al., 2021)	Ex.	S	A flow rate of working fluid	12.75%
(Selimefendigil and Şirin, 2022)	Ex.	M	PCM enhanced by nanoparticles	15.44%
(Alktranee and Péter, 2023)	Ex.	M	Evaporative cooling by cotton wicks immersed into water	7.8%

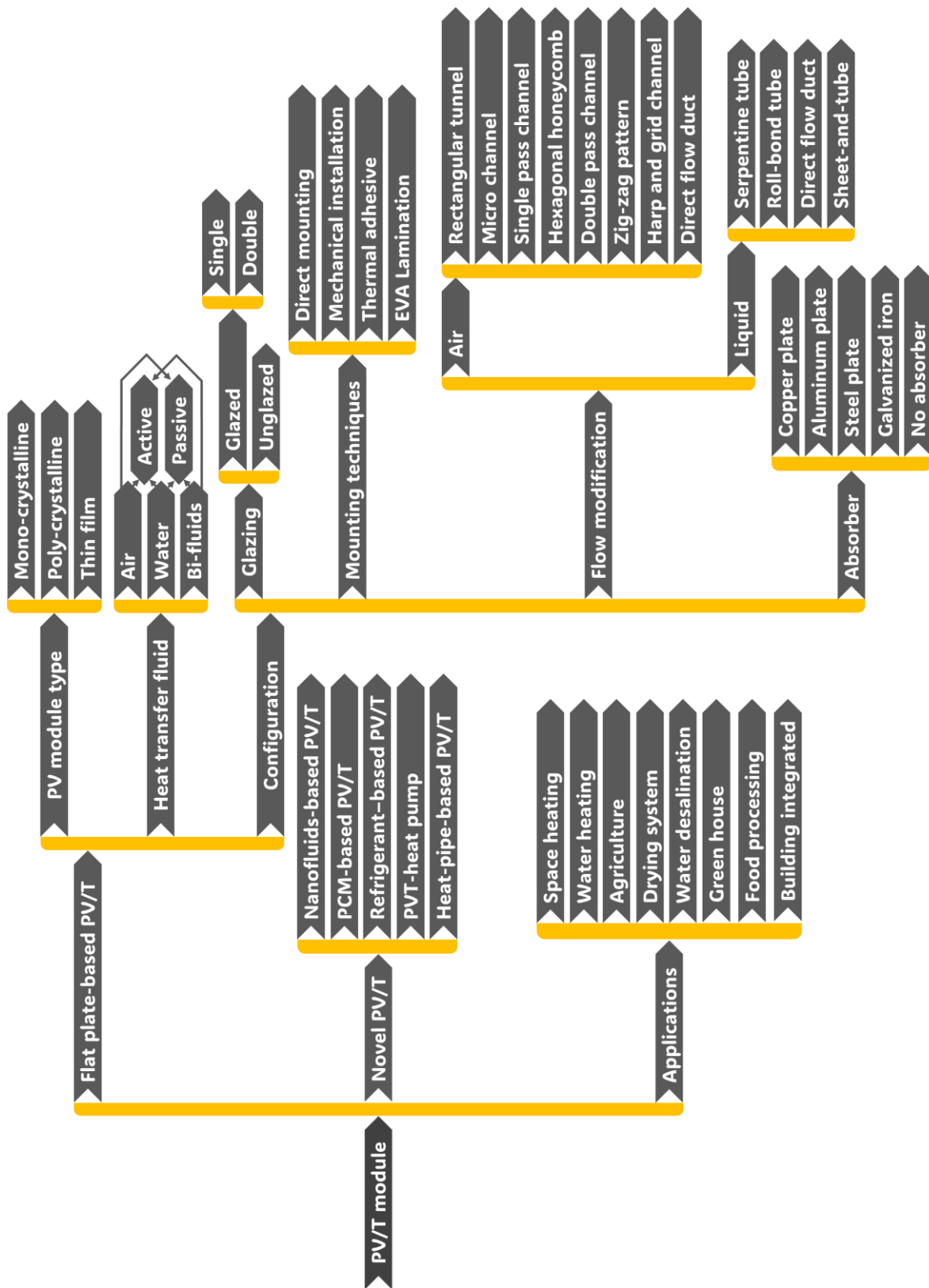
P: Poly-crystalline silicon, M: Multi-crystalline silicon, N/A: None mentioned, Ex.: Experimental, Nu.: Numerical

A7: Graphical summary of bi-PV/T configurations






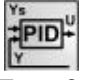







Note: All configurations could be fabricated without glass cover as another possibility

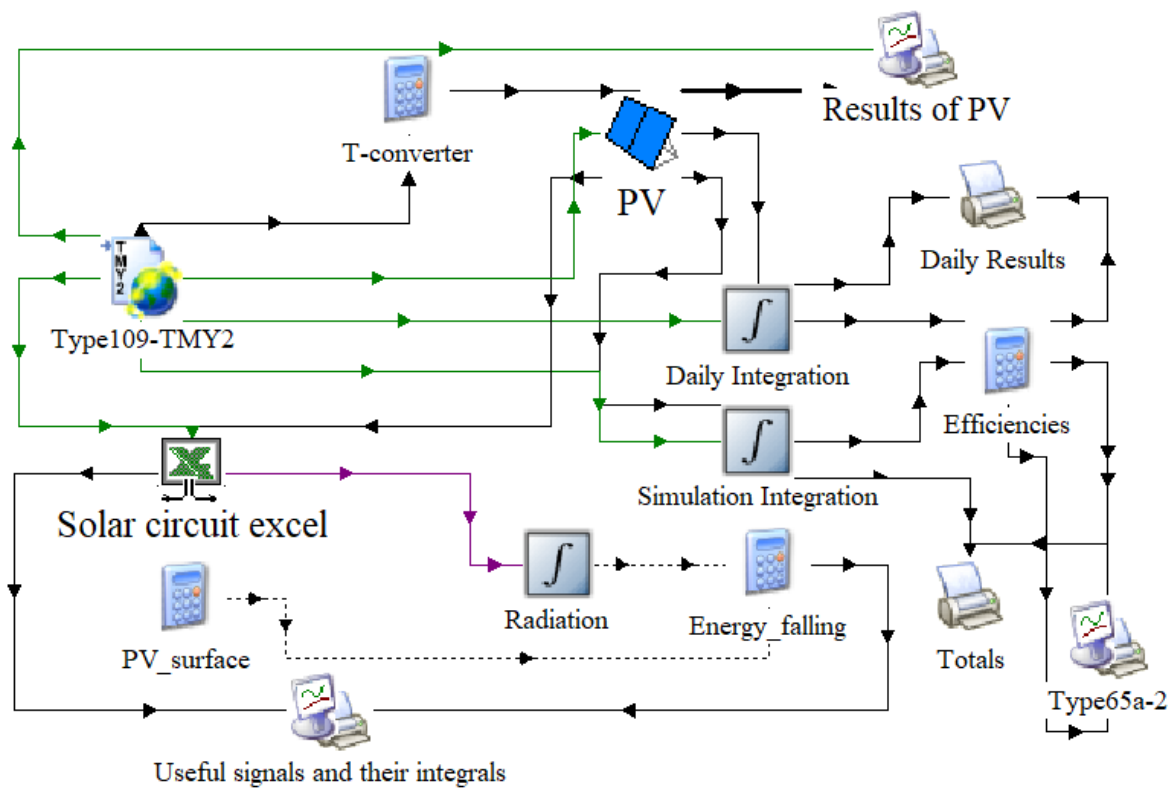
A8: Hierarchical chart of the classification of the PV/T modules



A9: Description of TRNSYS model elements

Model icons	Describes
 Type500	PV/T module
 Type4c	Hot water-storage tank
 Type 110	water-pump/ variable speed
 Type11g	T- joint of water
 Type11b	Tempering control valve
 Type23	PID-Temperature controller
 Type2b	ON-OFF-Temperature controller
 Type14b	Profile of water-consumption (water draw)
 Climate-source	Equation calculator
 Climate-source	Weather source
 Type 65a	Results Monitoring

A10: TRNSYS model of the PV system



A11: Summary of exergy efficiency and sustainability index obtained in the previous studies and current research

Reference	Type of Study	Type of PV	Technique for enhancement	Exergy efficiency	SI
(Nayak and Tiwari, 2008)	Exp	S-cry	Integrated into a greenhouse	4%	N/A
(Sarhaddi, et al., 2010)	Nu	N/A	Airflow duct	10.75	N/A
(Gang et al., 2011)	Nu	S-cry	Absorber with heat pipes	6.8%	N/A
(Wu et al., 2011)	Exp	N/A	Heat pipe	10.26%	N/A
(Jahromi et al., 2015)	Nu	N/A	Commercialized PV/T	9.6%	N/A
(Gholampour and Ameri, 2016b)	Exp	M-cry	Flat transpired collectors	8.66%	N/A
(Hazami et al., 2016)	Nu	S-cry	Classical type of water-based PV/T with TRNSYS model	14.8%	N/A
(Salem et al., 2017)	Exp	M-cry	Absorber plate with straight and helical channels	13.5%	N/A
(Fudholi et al., 2018)	Exp	M-cry	∇-groove air channel	13.26%	N/A
(Wahab et al., 2020)	Exp	S-cry	Nanofluid+ PCM	14.62%	1.153–1.17
(Abdul-Ganiyu et al., 2021)	Exp	S-cry	A flow rate of working fluid	12.75	N/A
(Selimefendigil and Şirin, 2022)	Exp	M-cry	PCM enhanced by nanoparticles	15.44%	1.14–1.18
(Alktraneé and Péter, 2023)	Exp	M-cry	Evaporative cooling by cotton wicks immersed into water	7.8%	N/A
Current research	Exp	M-cry	Absorber with fins and tube	35.3%	1.15–1.6

S-cry: Single-crystalline silicon, M-cry: Multi-crystalline silicon, N/A: None mentioned, Exp: Experimental, Nu: Numerical

9. ACKNOWLEDGEMENT

This thesis work was supported financially by the Stipendium Hungaricum Scholarship Program and the Mechanical Engineering Doctoral School at the Hungarian University of Agriculture and Life Sciences (MATE), Gödöllő, Hungary.

First and foremost, Alhamdulillah – Praise be to God – for every blessing, I ask God all the best, seek refuge with God from all evil, and ask forgiveness from God for every sin. God thank for giving me the strength, persistence, patience, boldness, and assurance to finish this work.

I would like to express my genuine appreciation to my supervisors, Prof. Dr István Farkas and Dr. Piroska Víg, for their support, inspiration, patience, and eagerness. Their direction and exhortation have propelled me to produce productive methodologies in accomplishing the goals of their examination. Without his exertion, I would not have the capacity to convey this examination to a culmination. I greatly appreciate your excellent assistance and spiritual support during my experiment. I will never forget when we were together to help me finish my work.

Great thanks to Dr. István Seres and Dr. János Buzás for helping with my laboratory work.

Special thanks to any member of the Mechanical Engineering workshop for their help in the soldering process of my experiments.

From the depths of my heart, I would like to thank my family, parents, wife, brothers, kids (Bassam, Abbas, Qabas), and sisters for empowering me with their unlimited love and support. I have dearly treasured their encouragement and moral support and realize how lucky I am to have them. Additionally, I thank all my friends for helping bolster me and urging me to do my best.

I am profoundly grateful for my cherished children, Bassam, Abbas, and Qabas. Their presence infuses my life with boundless joy and purpose, illuminating each day with love and meaning.

At last, however, not finally, I would like to express my genuine appreciation to HUNGARY, my second nation, for its boundless support and generosity...

Gödöllő, January 2024

Ahssan M. A. Alshibil